



Wi-Fi Denial of Service Attack on Wired Analog RF Channel Emulator

A Major Qualifying Project Report
Submitted to the Faculty
of the

WORCESTER POLYTECHNIC INSTITUTE

in partial fulfillment of the requirements for the

Degree of Bachelor of Science
in

Electrical and Computer Engineering
by

Sheila Werth

Jeffrey Peter Wyman

Project Number: MQP-AW1-12LL

Date: 10/17/2012

Sponsoring Organization:
MIT Lincoln Laboratory

Project Advisors:

Professor Alexander M. Wyglinski

This work was sponsored by the Department of Defense Research and Engineering under contract number FA8721-05-C-0002. Opinions, interpretations, conclusions and recommendations are those of the authors and are not necessarily endorsed by the United States Government.

Abstract

This report presents the design and implementation of an analog wireless channel emulator to examine various denial of service attacks in multiple mobile scenarios. The scenarios emulated in this project involve three node topologies of wireless interferers (Wi-Fi radios), including a software defined radio that transmits one of three denial of service (DoS) waveforms. The testbed was functional and met the original specifications. Results from mobile experiments show a clear distinction in performance among the three DoS waveforms depending on the node topology; a digital waveform using binary phase shift keying (BPSK) is most effective at reducing total network throughput at close range while sweep waveforms exhibit minor throughput reduction from a greater distance.

Acknowledgements

We would like to extend our gratitude to the many people that helped to support this project effort:

MIT Lincoln Laboratory, Group 63

Kenneth Hetling, PhD

James Vian, PhD

William O'Connell

Frank Bieberly

Robert Elliot

Jonathan Chisum, PhD

Todd Brick

Catherine Holland

Carl Fossa, PhD

Worcester Polytechnic Institute

Prof. Alexander Wyglinski

Prof. Ted Clancy

Executive Summary

Emergency response and communications during a major disaster have become increasingly important over the past decade. In cases such as the L.A. earthquake in 1994, the earthquake and tsunami in Indonesia, or Hurricane Katrina, the communications infrastructure was overwhelmed [1] and prevented local law enforcement and emergency personnel from coordinating rescues and conveying vital information [2]. The damage to the network is not always physical; often there is major disruption from network congestion [3]. Many networks are not designed to handle high volumes and the powerful human need to communicate during a disaster can overwhelm even the most sophisticated networks [4].

The FCC sponsors emergency communication systems such as the Nationwide Wireless Priority Service (WPS) that allows emergency telephone calls to avoid network congestion, and the Government Emergency Telecommunications Service (GETS). However, the effectiveness of these systems has been questioned [6], and the FCC has recently allocated portions of its Public Safety spectrum for shared commercial use [7]. If these resources become unavailable during a crisis, emergency responders may prefer to use high-speed wireless internet services [5] which are equally subject to network congestion. A standard resolution of how emergency responders and local law enforcement may clear the channel for high-priority use has not yet been proposed.

There is currently not enough exclusive spectrum for emergency responders to reliably communicate during a crisis. Additionally, recent laws regulating public safety spectrum for commercial use suggest it may be especially vulnerable to congestion. For these reasons it is critical for emergency personnel to have the capacity to silence interfering emitters during disasters so that appropriate response measures may be coordinated. Experimenting with and validating denial of service techniques over open air-waves could potentially disrupt user services and violate FCC regulations.

A controllable test platform is needed to investigate the reallocation of spectrum resources in a contested communications environment. The team designed, built, and calibrated a testbed for this purpose. Several key specifications were determined early on to ensure that the testbed met current and future testing needs.

- **Wideband:** 2-8GHz Bandwidth
- **4-Node Support:** three interfering nodes and one emergency responder
- **Motion Emulation:** real time emulation of changing nodal geometries
- **Computer control :** for analog channel emulator and radio hardware

A concept diagram of the testbed is shown in Figure 1. The testbed features an analog RF channel emulator (Yellow) which emulates mobility of radio nodes via programmable attenuators. Radio hardware includes three miniature computers equipped with Wi-Fi 802.11b/g radios (Blue) and a software defined radio called a Universal Software Radio Peripheral (USRP, Red). The entire system, including the channel emulator, radio nodes, and USRP, is computer controlled.

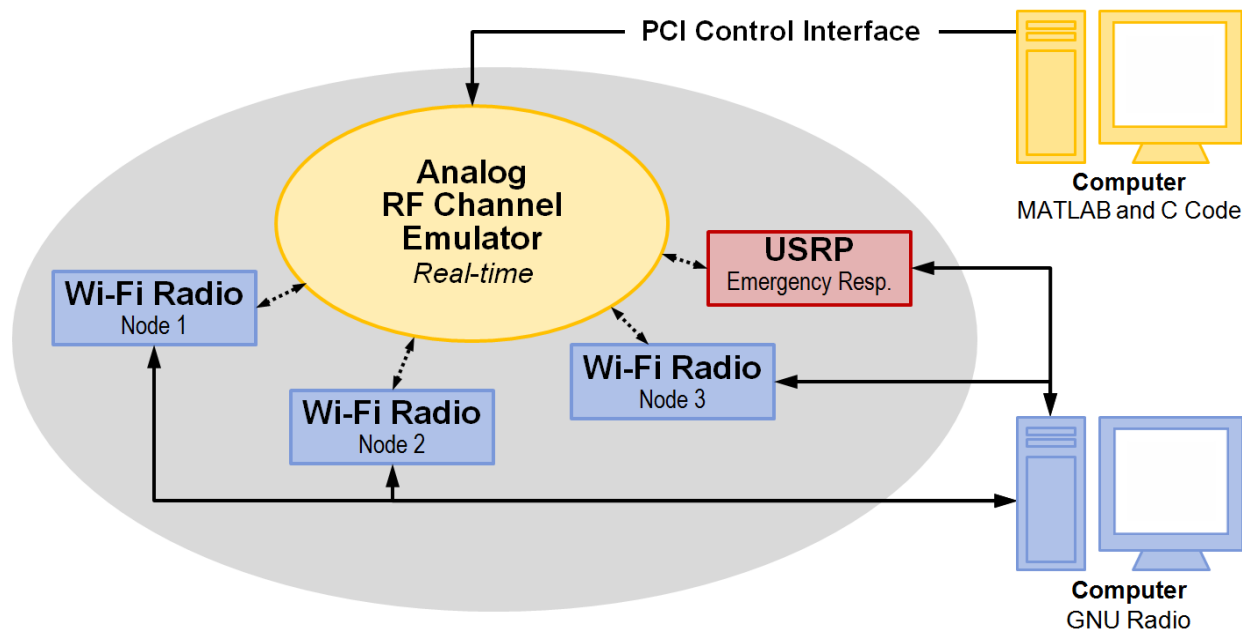


Figure 1: Testbed Concept Diagram. Real-time Analog RF Channel Emulator (Yellow). Wireless Interferers (Blue). Emergency Responder (Red).

The testbed enables emulation of different mobile scenarios in a controlled laboratory setting. For the purpose of this project, the team was interested in scenarios involving a single emergency responder node (the USRP) moving through a cluster of interfering emitters (the three Wi-Fi radios). The RF channel emulator allowed the team to experiment with several different denial of service (DoS) techniques implemented by the emergency responder node. These different methods were analyzed for effectiveness, efficiency, and overall performance.

In order to ensure that the testbed met specifications and was representative of a time-varying RF channel, the team conducted a variety of tests on the parts and the system as a whole. S-parameters were measured across the band for each part. Switching speed was measured for the attenuators. When the testbed was assembled, loss was measured throughout the system for each of the twelve possible routes through the system and calibrated to make sure that variation between those routes was minimal. A photograph of the assemble system is shown below in Figure 4.

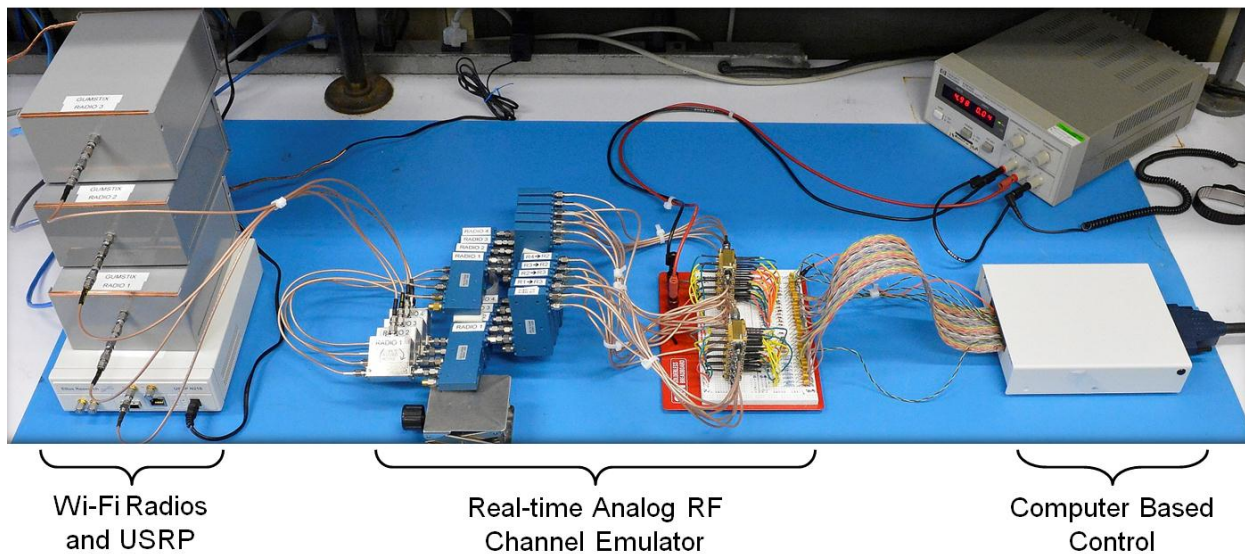
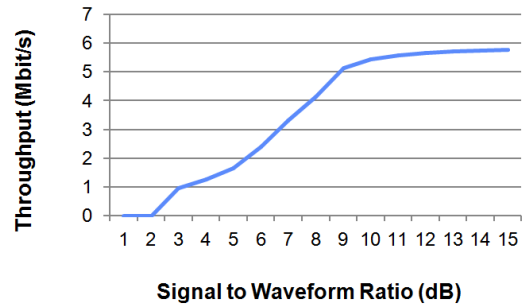
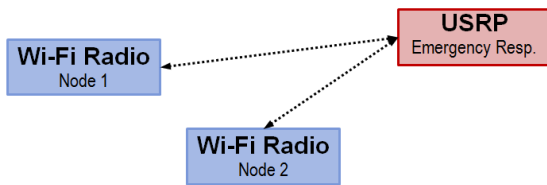


Figure 4: Assembled Testbed. Wi-Fi Radios & USRP (Left), Real-time Analog RF Channel Emulator (Middle), Computer Based Control (Right). All components are controlled through one central computer (not shown).

To further confirm that the testbed would produce reasonable results, measurements taken on a stationary two node network, similar to one described in the literature [7], were compared to measurements taken on the four radio testbed. Comparing the four node team testbed with the previously described two radio configuration served as a verification and validation of the procedures and equipment used during the course of this project. Results from this comparison are shown in Figure 3.

Two Node Testbed



Four Node Testbed

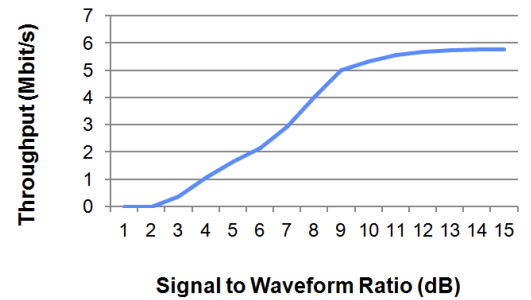
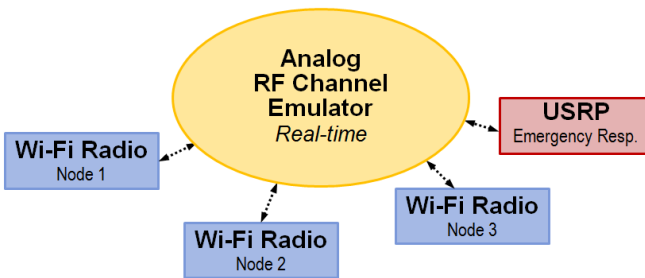


Figure 3: Verification and Validation: Comparison of Throughput vs. SWR between Two Node Testbed (Top) and Four Node Testbed with Channel Emulator (Bottom). Both testbed results are comparable to published research [7].

The experiment in Figure 3 (top) was designed to mimic an experiment from published research; it examines the effect of modulated waveforms on throughput where two nodes exchange traffic while one node injects a waveform with variable power. In this case, the waveform is binary phase shift keying (BPSK); increasing the signal to waveform ratio (SWR) will decrease throughput as shown in Figure 3. This test was repeated on the four node testbed; all values correlate with results from the two radio network within a small margin of error and serve as a validation of testbed operation.

Once the testbed had been built, tested, and validated, a series of three mobile node scenarios, along with three different denial of service waveforms, were selected for investigation on the testbed. Each waveform was implemented on each of the three mobile scenarios. For simplicity, wireless nodes were made stationary while the emergency responder traversed a straight path at a constant velocity. The three different denial of service waveforms include digital, pulse, and sweep. Figure 5 displays the results of one experimental mobile scenario repeated for each denial of service waveforms; (A) displays total network throughput over time when subject to a

jammer waveform, (B) illustrates the position of each stationary node with the start and stop location of the emergency responder.

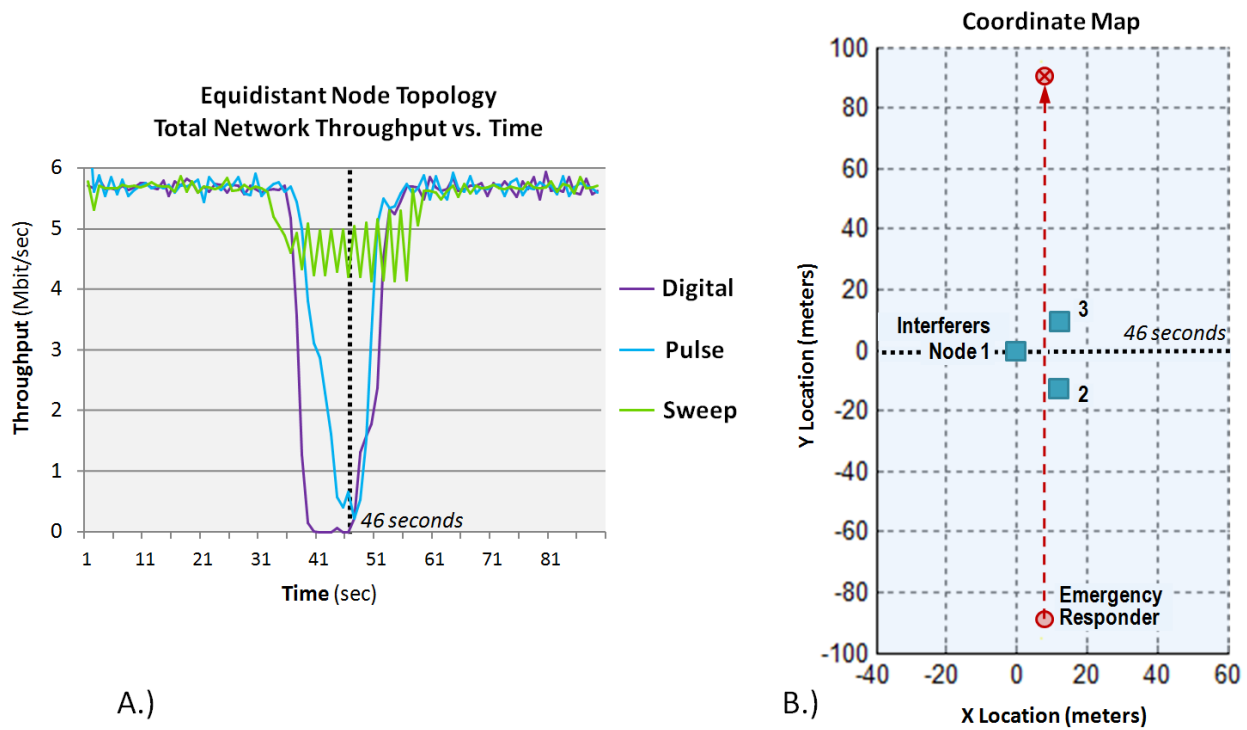


Figure 5: Comparison of performance among different jamming techniques in a mobile, Equidistant node topology. Graph of Total Network Throughput vs. Time of Digital, Pulse, and Sweep jamming (Left). Coordinate Grid (Right) of Wireless interferers (Blue) and Emergency Responder (Red) start and stop location.

According to the results in Figure 5 the team was able to conclude that digital jamming (Purple) is the most optimal technique at close range in this node topology, while sweep jamming (Green) is suited for long range, indicated by the premature drop in throughput and late recovery in (A). For all of the different jamming waveforms, throughput is at the lowest when the emergency responder node enters the cluster of interfering emitters and improves as it moves away.

In the process of completing this project, a few critical areas were identified for improvement and future consideration, including the robustness of the testbed setup, different mobile scenarios, and potentially more effective and efficient denial of service attacks. Expanding the testbed to support as many as six nodes and widening the bandwidth down to 30MHz could increase the value of the channel emulator as a test asset. An FPGA could also be used to produce more accurate digital signals to control the attenuators in a more reliable way. In terms of the denial of service attack, an investigation into the performance of MAC layer waveforms or

“Protocol” techniques may point toward an attractive, efficient substitute to the power consuming RF or PHY layer waveforms. Continuing to develop and improve denial of service techniques could enable emergency responders to more effectively communicate during a crisis.

In summary, all specifications for the RF channel emulator were met. The testbed allowed the team to conduct several experiments that investigated the performance of various denial of service waveforms used by an emergency responder against wireless interferers in an emulated mobile environment.

Table of Contents

ABSTRACT	2
ACKNOWLEDGEMENTS	3
EXECUTIVE SUMMARY	4
LIST OF FIGURES	12
LIST OF TABLES	19
LIST OF ACRONYMS	20
1 INTRODUCTION	1
1.1 MOTIVATION.....	1
1.2 PROBLEM STATEMENTS	2
1.3 PROPOSED SOLUTION.....	2
1.4 REPORT ORGANIZATION	4
2 OVERVIEW OF RF CHANNELS, WIRELESS NETWORKS, AND SECURITY	6
2.1 THE RF CHANNEL.....	6
<i>Important aspects of RF channel</i>	6
<i>Creating experimental channel conditions</i>	11
2.2 WIRELESS COMMUNICATION & SECURITY	21
<i>Brief Tutorial in Wireless Communications and 802.11b/g</i>	21
PHY Layer	24
MAC Layer	35
<i>Different types of jamming and attacks</i>	40
3 METHODS	45
3.1 CHANNEL EMULATOR DESIGN PROCESS	45
<i>Original Design Ideas and Assessment</i>	46
<i>Final Design</i>	50
3.2 ATTENUATOR CONTROL.....	52
3.3 CHANNEL EMULATOR CONSTRUCTION AND PRELIMINARY TESTING	55
3.4 PHY LAYER JAMMING.....	58
<i>Validating the Testbed against Previous Experiments</i>	59
<i>Mobile PHY Layer Jamming on the RF Channel Emulator</i>	60
3.5 MAC LAYER JAMMING.....	68
<i>Original Idea: Reactive Beacon Frame Injection</i>	68
4 RESULTS	72
4.1 CHANNEL EMULATOR: TESTING AND VALIDATION	72
<i>Assembled RF Testbed</i>	79
<i>Testing and measurements on the assembled system</i>	82
4.2 WI-FI MOBILE JAMMING EXPERIMENTS.....	95
4.2.1 MAC Layer Mobile Jamming	112

5	CONCLUSIONS AND FUTURE WORK	113
6	REFERENCES.....	116
7	APPENDIX	120
	<i>MATLAB Code: Calculate Programmable Attenuator Values</i>	<i>123</i>
	<i>MATLAB Code: Generate ASCII Characters.....</i>	<i>125</i>
	<i>C Code: Write to NI-PCI Card</i>	<i>126</i>
	<i>Datasheet: Krytar Coupler.....</i>	<i>129</i>

List of Figures

- Figure 1: Proposed solution, computer controlled RF testbed with real-time channel emulation, Universal Software Radio Peripheral (USRP) and commercially available Wi-Fi Radios 3
- Figure 2: Channel model considering sources of interference [13]. This model includes a scaled and delayed signal, multipath fading, narrowband noises and broadband noises. 7
- Figure 3: Obstacles cause electromagnetic waves to reflect and travel different paths of varying lengths. The Red path, path 1, is the line of site path while the Blue path, path 2, is the result of reflected signal power. Signal power traveling path two travels a greater distance and thus experiences greater delay. The sum of the power from both paths is a signal that is distorted due to multipath effects. 9
- Figure 4: (A) Noiseless time domain 60Hz signal. (B) Noiseless 60 Hz frequency domain signal. (C) 60 Hz time domain signal with AWGN (Blue) and noiseless 60Hz time domain signal. (D) Noisy 60 Hz signal in the frequency domain, the noise floor is shown in red. 11
- Figure 5: The real world radio communications scenario, shown on top, can be modeled using a wireless, miniaturized, configuration with attenuators (middle). The concept of a wired testbed is at the bottom of the image. A wired testbed involves radios that are connected to each other using coaxial cable and RF components, like the attenuator shown, to model channel response. 13
- Figure 6: Noise generators can be used to add noise to a channel emulator. This noise generator, or ‘noise brick’, is manufactured by Noisecom Incorporated..... 14
- Figure 7: The indoor testing facility at Rutgers University [21] is open for use to members of the research community who write their own code. Each yellow box is one of 400 stationary radio nodes. 15
- Figure 8: In the EWANT testbed, antennas can be rearranged on metallic table top with holes to create unique geometries. By switching between antennas, mobility can be emulated. .. 16
- Figure 9: The connectivity of a wired testbed created at Queensland Laboratory in Australia supports up to 5 nodes [19]. The channel response is created by programmable attenuators placed between radios, shown in red. 17
- Figure 10: 3 x 3 RF Matrix Switch [22]. Inputs are split three ways, scaled using programmable attenuators, and recombined so that each output receives power from each of the three inputs..... 18
- Figure 11: Elektrobit PropSim F32, radio channel emulator [24]. The F32 model has the capacity to support as many as 32 distinct RF channels with 16 bidirectional nodes. This channel emulator can also emulate fading. 19
- Figure 12: Open System Interconnection Architecture (OSI) Protocol Stack, a product of the International Organization for Standardization for characterizing layers of communication systems [27]. 22
- Figure 13: Input and Output using spread sequence (sequence shown is called Barker code), The Data bit is transformed into Spread bits using the spread sequence. 25
- Figure 14: Map of Barker Code Sequence at 1 Mbit/sec with DBPSK [29]. Each bit is modified by an 11-bit sequence..... 25

Figure 15: Amplitude of DSSS Signal (Blue) vs. Narrowband Jammer (Red) before despreading [30]. Note: signals are simplified and do not represent actual DSSS or jamming signals.	26
Figure 16: Amplitude of DSSS Signal (Blue) vs. Narrowband Jammer (Red) after despreading. The Despread signal is now at higher amplitude than the jammer's signal.....	26
Figure 17: Amplitude of Original Signal (Blue) vs. Processed Jammer (Red) after applying a band-pass filter. This is the overall result of using a DSSS modulation scheme against a narrowband interferer.....	27
Figure 18: Multipath signals bouncing off the environment. Signals suffer decay and arrive late at the receiver.....	28
Figure 19: Transmitted Signal (A) with two symbols, Ideal Received Signal (B), Realistic Received Signal (C) with multiple, decayed, overlapping received symbols from ISI....	29
Figure 20: Transmitted signal with high bit-rate transmission (low symbol duration) (Left). Received signal with increased ISI (Right).	29
Figure 21: Using multiple carriers to send data (FDM). Advantages: Increased data rate and resistance to ISI using guard bands. Disadvantages: inefficient use of bandwidth.	30
Figure 22: Using overlapping carriers to send data (OFDM). Advantages: greatly increased data rate, resistance to ISI using guard bands, and efficient use of bandwidth. Disadvantages: sensitive to carrier frequency offset or drift.....	31
Figure 23: Fourier transform of square, time domain signal into Sinc pulse in frequency domain. The bandwidth ΔT is inversely related to the spacing Δf	31
Figure 24: N=5 Overlapping OFDM tones. Each tone is orthogonal if the spacing between frequencies is equal to $1/NT$. Note: minimal interference at sampling points (multiples of the symbol rate).....	32
Figure 25: Two received symbols using DBPSK (Blue). Inter-Symbol Interference from multipath signal (Red).....	33
Figure 26: Two received symbols using DBPSK (Blue) and multipath signals (Red). The guard interval avoids Inter-Symbol Interference by delaying the start of the next symbol.....	33
Figure 27: Two received symbols using DBPSK (Solid Blue) with a Cyclic Prefix (Dashed Blue) added to avoid ISI. The cyclic extension is taken from the tail end of the symbol and added to the front.	34
Figure 28: Alternate view of the transmitted signal using Cyclic Prefix. The received signal avoids ISI.	34
Figure 29: Differences between Access Point (Central Server or Point Coordination) and Ad-hoc Networks (Mesh or Distributed Coordination).	35
Figure 30: IEEE 802.11 MAC Access Method using Inter-frame Spacings and the Exponential Backoff Algorithm [14, p. 530].	37
Figure 31: IEEE 802.11 Medium Access Control Logic [14, p. 528]. All clients will check the medium to see if it's idle before attempting to transmit in order to avoid collisions.	38
Figure 32: Hidden Node Problem: Nodes A & C cannot hear each other and attempt to transmit to Node B at the same time, causing a collision in the receiver of Node B.....	39
Figure 33: Implementation of the RTS/CTS mechanism in 802.11 with NAV activation, SIFS/DIFS interval, and contention window [28, p. 462].	40

Figure 34: Jamming Attacks at MAC & PHY Layer. Techniques are listed by intelligence required.	41
Figure 35: Chart of Effectiveness vs. Efficiency of PHY (RED) and MAC (BLUE) layer attacks. Note: All attacks are subjective.	43
Figure 36: Basic structure of analog channel emulator with key parts (A) Circulator (B) Power Splitter/Combiner and (C) Programmable Attenuator. This diagram shows a channel emulator that supports only three radio nodes.	46
Figure 37: Six-way splitter composed of cascaded two and three-way splitters. This design was not ultimately used because it was too lossy.	48
Figure 38: Five two-way splitters cascaded to create a six-way splitter. This design was not ultimately used because it did not provide enough isolation.	49
Figure 39: Four-way splitter created from three cascaded couplers. This design is not very lossy and provides enough isolation between paths.	51
Figure 40: The team decided to focus on a four node channel emulator that works from 2 to 8GHz. Each 4-way splitter/combiner is composed of three cascaded couplers.	52
Figure 41: Original ringing suppressing circuit with PCI Card (Left) and Programmable Attenuator (Right). This circuit worked well enough when there were fewer attenuators.	54
Figure 42: Final ringing suppressing circuit with added buffer capacitors placed within close proximity to data lines, and twisted pair cables (paired with GND) for each data signal. Note: Twisted Pair cable is not an inductor.	55
Figure 43: Two-tone test setup. From left to right: Signal Generators, Isolators, Power Divider, Device Under Test (DUT), Spectrum Analyzer. The two-tone test helps to identify third order nonlinearities of a RF device.	56
Figure 44: Two Radio Network consisting of Attenuators, Circulators, and Power Dividers. Radios are Gumstix computers with Wi-Fi 802.11b/g. Jammers used are: USRPN210, Signal Generators, or Noise Generators.	60
Figure 45: Simplified diagram of connections between radio nodes and RF Channel Emulator. Each node can vary their distance between every other node.	61
Figure 46: Equidistant node topology. All nodes are the same distance from each other and can exchange data with all other nodes. The jammer will approach the network at a rate of 2 meter/sec.	62
Figure 47: Realistic picture of Wi-Fi scenario. Three Wi-Fi emitters (Blue) within 15 meters of another. All (Blue) nodes can exchange data at the same rate. The Emergency Responder (Red) approaches the network and passes through while attempting to regain spectrum. Note: not to scale.	63
Figure 48: Map of Equidistance Node scenario. Three Wi-Fi emitters (Blue) within 15 meters of another; each can exchange data at the same rate. The Emergency Responder (Red) approaches the network and passes through while attempting to regain spectrum. Note: not to scale.	64
Figure 49: Hidden Node topology. R1 (Left) and R3 (Right) cannot communicate directly with each other. R2 can communicate with both nodes. The jammer moves toward this network at a rate of ~2 meters/sec.	65

Figure 50: Map of Hidden Node topology. Three Wi-Fi emitters (blue, R1, R2, and R3, from left to right). R1 cannot communicate with R3 and vice versa. The Emergency Responder (Red) approaches the network and passes through, attempting to regain spectrum. Note: not to scale.	66
Figure 51: Distant Node topology. Each node starts equidistant from other nodes and moves away from the network in the opposite direction. The jammer approaches the network at a rate of 2 meters/sec.....	67
Figure 52: Map of Distant Node topology. Three Wi-Fi emitters. R1 cannot communicate with R3 and vice versa. The Emergency Responder (Red) approaches the network and passes through, attempting to regain spectrum. Note: not to scale.	68
Figure 53: Reactive Beacon Frame Injection attack on IEEE 802.11b/g. The attack injects a manipulated beacon frame that seems as though it came from the target client. Subsequent packets sent to that client are then using the wrong network parameters, resulting in dropped packets and/or weakened security.	69
Figure 54: Major attenuation states, adjusted to insertion loss, DC to 8GHz. Insertion loss is shown in blue. Attenuation states are relatively flat across the band.	73
Figure 55: A tone being fed through the attenuator while it steps through different attenuation settings. The blue image on the left shows an instance of the attenuator latching the wrong state. Note: blue/grey portion of image have been inverted to improve visibility.	74
Figure 56: Isolation between -3dB ports of two different couplers. This measurement was taken from 2 to 8GHz with the vector network analyzer.	75
Figure 57: Coupler return loss, measured from 2 to 8GHz. Return loss for each of the -3dB ports shown in red and blue. Return loss for sum port shown in black.	76
Figure 58: Coupler insertion loss from sum port to both -3dB ports for two different couplers. Each of the two blue lines correspond to the loss measurement between the sum port and one of the -3dB ports while the two red lines are the same for the other coupler measured. This measurement was taken from 2 to 8GHz.....	77
Figure 59: Circulator insertion loss (top) and isolation (bottom), measured from 2 to 8GHz with network analyzer.....	78
Figure 60: Return loss of DiTom circulator, measured from 2 to 8GHz with network analyzer. Each different color represents one of the three different ports of the device.....	78
Figure 61: Assembled RF Analog Testbed. Radio hardware is on the far left, with circulators and couplers towards the middle. Attenuators are on the breadboard with the PCI breakout board on the far right.....	79
Figure 62: Circulators and cascaded couplers in final channel emulator configuration. The transmit and receive sides of the circulators are circled in green.	80
Figure 63: Programmable attenuators with ringing suppression circuit on breadboard	80
Figure 64: SCB-68 NI breakout board closed (top) and open (bottom). Wires from this board are each twisted with a ground wire and connected to the attenuators on the breadboard.	81
Figure 65: analysis throughout the system, based upon measured loss in each individual part at 2.4GHz. Expected loss through the system is 21dB.	83
Figure 66: Gain through the system on all twelve paths, before (left) and after calibration (right). Colored lines correspond to 12 distinct paths through emulator.	84

Figure 67: Spectrum of two tones combined, before entering the channel emulator	85
Figure 68: Two tones through the system, attenuators set to insertion loss	86
Figure 69: Two tones through the system, attenuators set to 16dB setting	86
Figure 70: Two tones through the system, attenuators set to 31.5dB setting	87
Figure 71: Pulse Jamming tests: Throughput vs. Pulse length & period in Two Radio (A) testbed at 11Mbit/sec (DSSS), 9Mbit/sec (OFDM), and on the Four Radio testbed (B) at 11Mbit/sec (DSSS), 9Mbit/sec (OFDM).	88
Figure 72: Sweep Jamming tests: Throughput vs. SJR & Sweep time in Two Radio testbed (A) at 11Mbit/sec (DSSS), 9Mbit/sec (OFDM), and on the Four Radio testbed (B) at 11Mbit/sec (DSSS), 9Mbit/sec (OFDM). Results are in Mbit/sec. Signal to Jammer Ratio (SJR) and sweep time are varied.....	89
Figure 73: Differences in performance of Two Radio Testbed vs. Four Radio Testbed when subject to Sweep and Pulse waveforms.	90
Figure 74: Digital Jamming tests: Throughput vs. SJR on the Two Radio testbed using MATLAB (A) and Four Radio testbed using GNURadio (B) using 11 Mbit/sec DSSS and 9 Mbit/sec OFDM.	91
Figure 75: Digital Jamming tests (Corrected): Throughput vs. SJR on the Two Radio testbed using MATLAB (A) and Four Radio testbed using MATLAB (B) using 11 Mbit/sec DSSS and 9 Mbit/sec OFDM.....	92
Figure 76: Spectrum of OFDM (9 Mbit/sec, 802.11g) signal (A) and with the addition of a Digital jammer (B). The graph in (A) shows a typical flat, OFDM signal modulation. The graph in (B) shows the OFDM modulation changing to a DSSS-like signal when a Digital jammer is introduced.	93
Figure 77: Spectrum of DSSS (11 Mbit/sec, 802.11b) signal (A) and with the addition of a Digital jammer (B). The graph in (A) shows a typical DSSS signal modulation. The graph in (B) shows the DSSS modulation changing to an OFDM-like signal when a Digital jammer is introduced.	94
Figure 78: Flow of data in mobile experiments. All mobile data shown in graphs are transmitted in one direction by the prior node.	95
Figure 79: Equidistant node topology in a mobile environment: Throughput vs. Time (A), and Coordinate Grid of Radios and Jammer (B). A Digital jamming node passes between three clients (Rx 1, 2, 3) that are equally spaced (15 meters from each node).	96
Figure 80: Correlation between Jammer attenuation (distance) and Throughput between nodes for Digital Jammer in Equidistant Node Topology. Total Network Throughput vs. Time (A), Attenuation vs. Time of programmable attenuators (B), Throughput vs. SJR of Digital Jammer in previous PHY layer experiment (C).....	97
Figure 81: Equidistant node topology in a mobile environment: Throughput vs. Time (A), and Coordinate Grid of Radios and Jammer (B). A Pulse jamming node passes between three clients (Rx 1, 2, 3) that are equally spaced (15 meters from each node).	98
Figure 82: Correlation between Jammer attenuation (distance) and Throughput between nodes for Pulse Jammer in Equidistant Node Topology. Total Network Throughput vs. Time (A), Attenuation vs. Time of programmable attenuators (B), Throughput vs. Pulse Length vs. Pulse Period of Pulse Jammer in previous PHY layer experiment (C).	99

Figure 83: Equidistant node topology in a mobile environment: Throughput vs. Time (A), and Coordinate Grid of Radios and Jammer (B). A Sweep jamming node passes between three clients (Rx 1, 2, 3) that are equally spaced (15 meters from each node).	100
Figure 84: Correlation between Jammer attenuation (distance) and Throughput between nodes for Sweep Jammer in Equidistant Node Topology. Total Network Throughput vs. Time (A), Attenuation vs. Time of programmable attenuators (B), Throughput vs. Sweep Time vs. SJR of Sweep Jammer in previous PHY layer experiment (C).....	102
Figure 85: Hidden node topology in a mobile environment: Throughput vs. Time (A), and Coordinate Grid of Radios and Jammer (B). A Digital jamming node passes between three clients (Rx 1, 2, 3) that are spaced apart laterally as to emulate a hidden node (Rx 1 and Rx 3 cannot communicate with each other).....	103
Figure 86: Hidden node topology in a mobile environment: Throughput vs. Time (A), and Coordinate Grid of Radios and Jammer (B). A Pulse jamming node passes between three clients (Rx 1, 2, 3) that are spaced apart laterally as to emulate a hidden node (Rx 1 and Rx 3 cannot communicate with each other).....	104
Figure 87: Hidden node topology in a mobile environment: Throughput vs. Time (A), and Coordinate Grid of Radios and Jammer (B). A Sweep jamming node passes between three clients (Rx 1, 2, 3) that are spaced apart laterally as to emulate a hidden node (Rx 1 and Rx 3 cannot communicate with each other).....	105
Figure 88: Distant node topology in a mobile environment: Throughput vs. Time (A), and Coordinate Grid of Radios and Jammer (B). A Digital jamming node passes between three clients (Rx 1, 2, 3); Rx 3 is isolated and can only communicate with Rx 2 from a longer distance.	106
Figure 89: Distant node topology in a mobile environment: Throughput vs. Time (A), and Coordinate Grid of Radios and Jammer (B). A Pulse jamming node passes between three clients (Rx 1, 2, 3); Rx 3 is isolated and can only communicate with Rx 2 from a longer distance.	107
Figure 90: Distant node topology in a mobile environment: Throughput vs. Time (A), and Coordinate Grid of Radios and Jammer (B). A Sweep jamming node passes between three clients (Rx 1, 2, 3); Rx 3 is isolated and can only communicate with Rx 2 from a longer distance.	108
Figure 91: Comparison of performance among different jamming techniques in a mobile, Equidistant node topology. Graph of Total Network Throughput vs. Time of Digital, Pulse, and Sweep jamming.	109
Figure 92: Comparison of performance among different jamming techniques in a mobile, Hidden node topology. Graph of Total Network Throughput vs. Time of Digital, Pulse, and Sweep jamming.....	110
Figure 93: Comparison of performance among different jamming techniques in a mobile, Distant node topology. Graph of Total Network Throughput vs. Time of Digital, Pulse, and Sweep jamming.....	111
Figure 94: Effects on throughput from Digital Jamming. Results from published work [7] (top), results from two node testbed (bottom).	121
Figure 95: Effects on throughput from Pulse Jamming. Results from published work [7] (left), results from two node testbed (right).	122

Figure 96: Effects on throughput from Sweep Jamming. Results from published work [34] (left), results from two node testbed (right)..... 122

List of Tables

Table 1: Project deliverables are divided into thresholds and objectives. Deliverables pertain to both the channel emulator and the Wi-Fi DoS portions of the project	4
Table 2: Comparison of different channel emulators and testbeds. Testbeds can be wired or wireless and include a variety of different mechanisms for motion emulation.	20
Table 3: Definitions of Inter-frame Spacings and their role in the MAC Layer [14].	36
Table 4: PHY Layer Jamming Definitions.	41
Table 5: MAC Layer Jamming Definitions.	42
Table 6: Design attempts for RF channel emulator. The two original design attempts did not meet specifications.....	50
Table 7: The testbed was channelized into two separate frequency bands, 30MHz - 3GHz and 2 - 8GHz, with two separate sets of parts.....	51
Table 8: List of equipment used in PHY layer attacks by name, model, and specifications.	58
Table 9: The twelve 'paths' in the channel emulator. Each path has its own programmable attenuator.....	82
Table 10: List of 802.11 Standards [14].	120

List of Acronyms

ACK	Acknowledgement
AP	Access Point
AWGN	Additive White Gaussian Noise
DBPSK	Differential Binary Phase Shift Keying
BER	Bit Error Rate
BPSK	Binary Phase Shift Keying
BW	Bandwidth
CDMA	Code Division Multiple Access
CSMA/CA	Carrier Sense Multiple Access / Collision Avoidance
CTS	Clear to Send
dB	Decibel
DCF	Distributed Coordinate Function
DIFS	Distributed Coordinate Function Inter-Frame Spacing
DoS	Denial of Service
DSSS	Direct Sequence Spread Spectrum
FDM	Frequency Division Multiplexing
FHSS	Frequency Hopping Spread Spectrum
FTP	File Transfer Protocol
HTTP	Hyper-Text Transfer Protocol
ICI	Inter-Carrier Interference
IEEE	Institute of Electrical and Electronics Engineer
IFS	Inter-Frame Spacing
IMAP	Internet Message Access Protocol
IP	Internet Protocol
ISI	Inter-Symbol Interference
ISO	International Standards Organization
JSR	Jammer to Signal Ratio
LAN	Local Area Network
MAC	Medium Access Control
MIMO	Multiple Input Multiple Output
NAV	Network Allocation Vector
NFS	Network File System
OFDM	Orthogonal Frequency Division Multiplexing
OSI	Open Systems Interconnection
PCF	Point Coordinate Function
PHY	Physical
PIFS	Point Coordinate Function Inter-Frame Spacing
PLCP	PHY Layer Convergence Protocol
PMD	PHY Layer Medium Dependent Protocol
POP	Post Office Protocol
RF	Radio Frequency
RTS	Request to Send
SIFS	Short Inter-Frame Spacing
SJR	Signal to Jammer Ratio
SMA	Sub-Miniature Version A

SMTP
SNR
TCP
UDP
UHF
USRP
WEP
WLAN
WPA

Simple Mail Transfer Protocol
Signal to Noise Ratio
Transmission Control Protocol
User Datagram Protocol
Ultra-High Frequency
Universal Software Radio Peripheral
Wired Equivalency Privacy
Wireless Local Area Network
Wi-Fi Protected Access

1 Introduction

1.1 Motivation

Emergency response and communications during a major disaster have become increasingly important over the past decade. In cases such as the L.A. earthquake in 1994, the earthquake and tsunami in Indonesia, or in Hurricane Katrina, the communications infrastructure was overwhelmed [1] and prevented local law enforcement and emergency personnel from coordinating rescues and conveying vital information [2]. The damage to the network is not always physical; often there is major disruption from network congestion [3]. Many networks are not designed to handle high volumes and are approaching their maximum capacity; growth in mobile video traffic is expected to double within the next 2 years [8], and the powerful human need to communicate during a disaster can overwhelm even the most sophisticated networks [4].

Crisis readiness is becoming increasingly important as communication technologies become more complex, interdependent, and vulnerable [9]. Although damage to physical network infrastructures may be unavoidable, network congestion can be just as detrimental [4], [10], [11]. Creating fully resilient networks is nearly impossible with evolving technologies, protocols, and the rapid increase in usage and demand for high speed internet and mobile video services. Communications is not only important during a disaster, but after; the internet in particular provides a backbone for financial and banking operations to support the recovery of local communities [12].

The FCC sponsors emergency communication systems such as the Nationwide Wireless Priority Service (WPS) that allows emergency telephone calls to avoid network congestion, and the Government Emergency Telecommunications Service (GETS). However, the effectiveness of these systems has been questioned [5], and the FCC has recently allocated portions of its Public Safety spectrum for shared commercial use [6]. If these resources become unavailable during a crisis, emergency responders may prefer to use high-speed wireless internet services [4] which are equally subject to network congestion. A standard resolution of how emergency responders and local law enforcement may clear the channel for high-priority use has not yet been proposed.

In this paper we introduce the problems of network congestion facing the future of communications during a crisis and the availability of this resource to emergency responders. Our team presents a prototype testbed, including a real-time channel emulator, and focuses on demonstrating a practical solution to network congestion in an emulated, mobile environment using commercial 802.11 Wi-Fi devices and programmable radios.

1.2 Problem Statements

There is currently not enough exclusive spectrum for emergency responders to reliably communicate during a crisis. Popularity and demand in wireless communication has surged in recent years, increasing susceptibility to network congestion. Additionally, recent laws regulating public safety spectrum for commercial use suggest it may be especially vulnerable to congestion. This problem presents a key question that frames our project:

How can we efficiently and effectively clear network congestion to reallocate the spectrum for emergency responders?

In order to address this question, we examine the solution space for ownership in a contested communications environment.

1.3 Proposed Solution

Our team proposes a denial of service (DoS) technique that is capable of removing Wi-Fi interferers from the channel so that authorized personnel can regain this resource. If effective, this method could be used by emergency responders to efficiently and effectively clear congested networks to re-establish communications by authorized personnel. However, experimenting with and validating this technique across open air-waves would disrupt user services and violate FCC regulations; thus a computer controlled testbed, including a real-time RF channel emulator that uses commercially available Wi-Fi radios and a Universal Software Radio Peripheral (USRP), will be designed for this purpose. The basic structure of this testbed solution is shown in Figure 1.

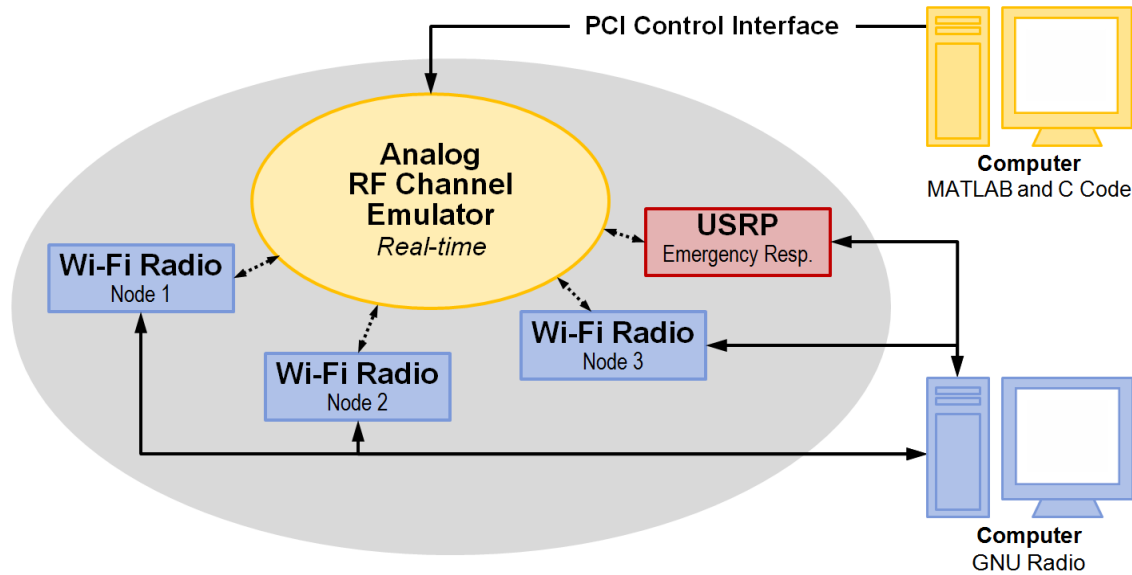


Figure 1: Proposed solution, computer controlled RF testbed with real-time channel emulation, Universal Software Radio Peripheral (USRP) and commercially available Wi-Fi Radios

The task of (1) developing a technique to clear channel bandwidth, and (2) creating an analog channel emulator to validate that technique, was divided into several key deliverables. These deliverables are composed of *thresholds* and *objectives*. Thresholds represent the most fundamental accomplishments that the team will deliver upon completion of the project. Objectives are milestones that the team will achieve only once the thresholds have been accomplished, time permitting. The thresholds and objectives target both the channel emulator and the Wi-Fi DoS portion of the project. The thresholds and objectives, as they pertain to the two main areas of focus, are shown in Table 1.

As displayed in Table 1, the most basic requirements for the channel emulator included: support for 2 to 8GHz of bandwidth, variable attenuators to simulate changing geometries, and support for four radio nodes. It was required that this channel emulator be built and tested by completion of the project. Time allowing, this channel emulator could have been scaled up to support six radios on a 30MHz to 8GHz bandwidth. Testing of the channel emulator components and the assembled system was required to validate the channel emulator.

Table 1: Project deliverables are divided into thresholds and objectives. Deliverables pertain to both the channel emulator and the Wi-Fi DoS portions of the project

	Thresholds	Objectives
Channel Emulator	Support for 4 nodes .	Support for 6 nodes .
	Wideband (2-8GHz).	Coverage for 30MHz to 8GHz.
	Real-time (variable attenuator to simulate changing nodal geometries).	
Wi-Fi DoS Attack	Validate the channel emulator by repeating existing Wi-Fi attacks .	“Reactive Beacon Frame Injection” attack in the MAC layer .
	Examine results of the same Wi-Fi attacks using different mobile scenarios .	

In order to meet threshold requirements in the Wi-Fi Denial of Service (DoS) portion of the project, known PHY (Physical) layer jamming techniques were repeated and documented, first on a simple two radio network for validation, then on the channel emulator. Repeating known attacks and validating consistency in the results was an important way to ensure functionality in the channel emulator. Once the accuracy of the testbed had been confirmed, the mobility feature of the channel emulator was used to repeat the same PHY layer attacks in three different mobile configurations of nodes. Lastly, the team did preliminary testing of a MAC (Medium Access Control) layer attack on the testbed. The proposed MAC layer attack was called “Reactive Beacon Frame Injection”, where beacon frames were injected with false information, intended to disrupt transmissions between other clients.

1.4 Report Organization

This report will document background information pertaining to the project topic, the process and methods, and subsequently the results, discussion, the conclusion. Chapter two will be an overview of RF channels, wireless networks, and Wi-Fi security. The important attributes of an RF channel and different ways that these characteristics have been recreated in various types of channel emulators will be covered. In addition, wireless network basics and Wi-Fi protocol and

security will be outlined. Chapter 3 will detail the methods used to design, build, and test the analog channel emulator along with the techniques for both PHY and MAC layer jamming. Finally, the results of the group's measurements on the testbed, PHY layer jamming, and the Reactive Beacon Frame Injection will be presented in chapter 4, discussed in chapter 5, and put into context in chapter 6.

2 Overview of RF Channels, Wireless Networks, and Security

In order to successfully build an analog RF channel emulator and demonstrate a DoS attack, background research was necessary in many areas. Our team isolated several key areas for further investigation. In particular, the team was interested in the different characteristics that define realistic RF channels and how these conditions can be, and have been, recreated in different types of channel emulators and testbeds. The ability to create a realistic analog channel emulator depends upon a thorough understanding of the RF channel and how it has been emulated by researchers in the past. An in-depth knowledge of Wi-Fi, in particular the MAC and PHY layers of IEEE 802.11, is instrumental in isolating and exploiting any weaknesses. In order to create a new DoS attack, the team also conducted a literature review of different types of Wi-Fi denial of service attacks that have already been tested. This chapter will review these topics as they pertain to our project goals.

2.1 The RF Channel

In an ideal world, transmitted RF power would arrive at the receiver unscathed. In reality, the signal is scaled, delayed, and distorted in a variety of ways. Understanding all of the factors that can impact signal integrity is crucial to successful radio communications. Being able to emulate and recreate some of these characteristics and effects to allow for accurate testing is of equal importance. This section describes the basic attributes of an RF channel and then reviews some of the different techniques for recreating these conditions for wireless network testing.

Important aspects of RF channel

An RF channel describes the path between a transmitter and a receiver. In an ‘ideal’ channel, the signal is the same at the receiver as it is at the transmitter with the exception of a small delay and attenuation. However, this model of a channel neglects some of the many other types of interferences and distortions that could alter or corrupt the signal on its way the receiver [13, p. 11]. Some of these impairments include multipath, signal fading, and various noise sources. Figure 2 shows one channel model that includes some of the different types of distortion and interference.

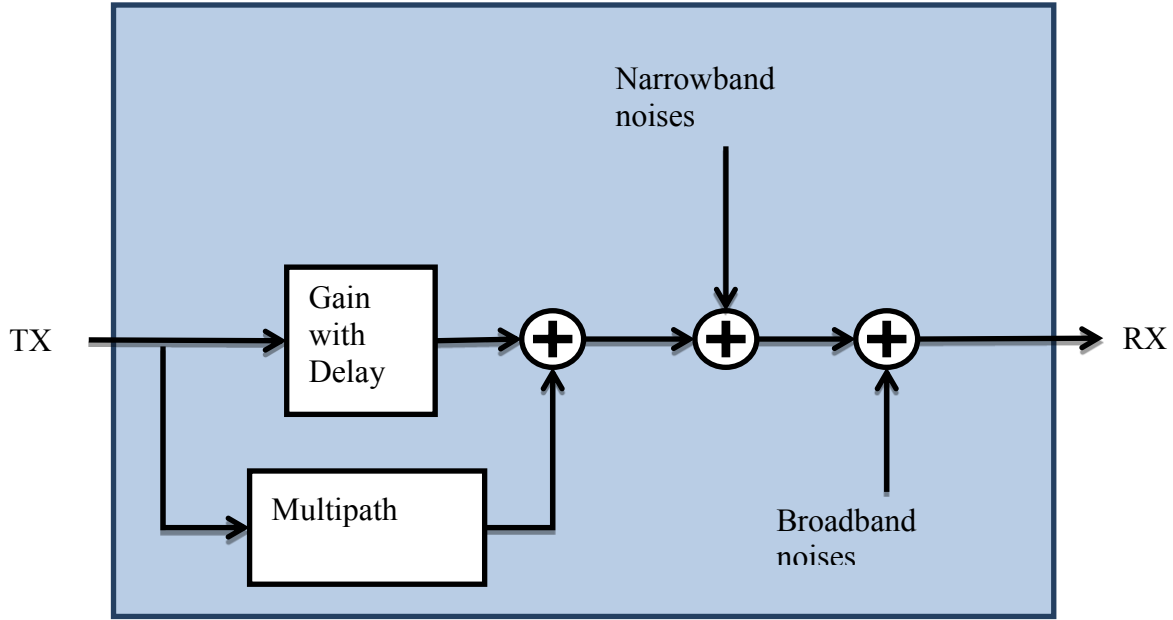


Figure 2: Channel model considering sources of interference [13]. This model includes a scaled and delayed signal, multipath fading, narrowband noises and broadband noises.

Free space path loss

In the real world, radios communicating over different distances experience varying amounts of attenuation based upon their physical separation. Radios that are located within a small distance of each other are subject to less attenuation while radios that are positioned greater distances from each other face greater amounts of attenuation. Free Space Path Loss (FSPL) is the attenuation of signal power with increased distance between transmitter (TX) and receiver (RX) due to the spreading of the signal over a greater area [14, pp. 129-131]. Free space path loss does not take into account diffraction (the spreading or bending of waves in the presence of obstacles) or reflection (change in propagation direction due to encountering a different medium). Free space path loss is also the ratio of transmit power (P_T) over power received (P_R):

$$FSPL = \frac{P_T}{P_R} = \left(\frac{4\pi d}{\lambda}\right)^2 = \left(\frac{4\pi d f}{c}\right)^2 \quad (2.1)$$

where λ and f are the wavelength [meters] and frequency [Hz] of the carrier signal respectively, d is the distance in meters between the transmitter and receiver, and c is the speed of light. As shown in the equation above, FSPL is proportional to the square of the carrier frequency as well as the square of the distance between the two radios. The correlation between distance and

attenuation has to do with the spreading of electromagnetic energy through space with increased distance. The frequency dependency, however, does not actually arise from path loss effects. Instead, this correlation has to do with the receiving antenna's ability to collect electromagnetic energy. Assuming constant transmit power, greater values of d correspond to greater values of $\frac{P_T}{P_R}$ which in turn reflects larger amounts of loss or attenuation between transmitting and receiving radios. Rewriting this equation in terms of decibels, we get:

$$FSPL_{dB} = 10 \log_{10} \left(\left(\frac{4\pi d}{\lambda} \right)^2 \right) = 20 \log_{10} \left(\frac{4\pi d}{\lambda} \right) \quad (2.2)$$

Note that these equations do not take into account the antenna gain. For a setup with a transmitting antenna gain G_T and a receiving antenna gain G_R , the free space path loss is given by:

$$FSPL = \frac{P_T}{P_R} = \frac{(4\pi d)^2}{G_T G_R \lambda^2} = \frac{(\lambda d)^2}{A_T A_R} \quad (2.3)$$

where A_T is the effective area of the transmitting antenna while A_R is the effective area of the receiving antenna. Expressed as a decibel value:

$$FSPL_{dB} = 20 \log_{10}(d\lambda) - 10 \log_{10}(A_T A_R) \quad (2.4)$$

This equation implies that at greater distances the signal experiences greater attenuation. Without antenna gains to compensate, radios communicating at higher frequencies also experience greater attenuation.

Multipath

Multipath arises from differing path lengths that result from reflections off of interfering obstacles located between the transmitter and receiver. Reflections of varying magnitude take different paths that correspond to slightly different arrival times resulting in either reinforcement or cancellation of the signal at the receiver. Figure 3 displays the concept of differing path lengths from the same source to receiver due to collision with reflective surfaces. The delays and signal magnitude associated with each of the paths in the diagram will determine, to some extent, the quality of the signal received at receiver.

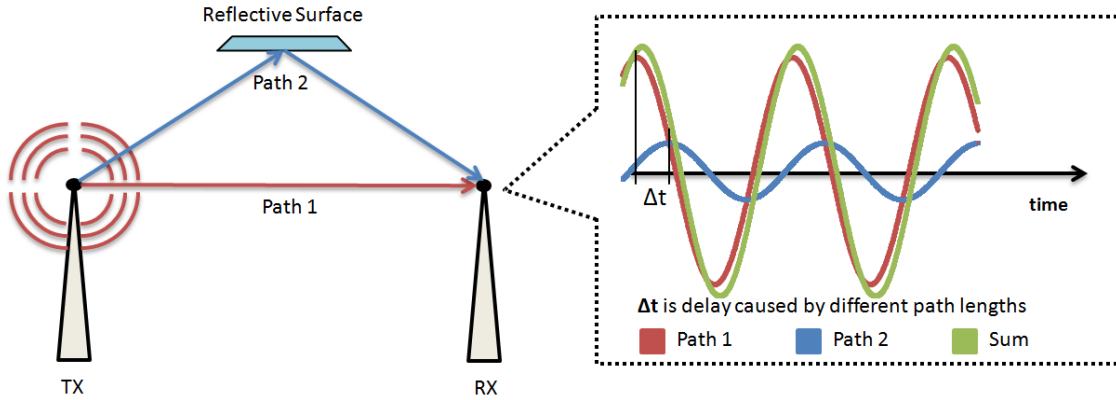


Figure 3: Obstacles cause electromagnetic waves to reflect and travel different paths of varying lengths. The Red path, path 1, is the line of site path while the Blue path, path 2, is the result of reflected signal power. Signal power traveling path two travels a greater distance and thus experiences greater delay. The sum of the power from both paths is a signal that is distorted due to multipath effects.

In the case of the diagram shown above, the signal power at the receiver is composed of power from the line of site path (path 1) and power from the reflected path (path 2). The graph to the right shows what the waveforms might look like at the receiver. Because power travelling path 2 (Blue) travels a greater distance, it arrives at the receiver some time delay Δt after signal power traveling along path 1 (Red) arrives. As a result, the sum of the two received signals (Green) is a slightly distorted version of the original signal. This scenario displays the concept of multipath, but in reality, many more paths can exist creating even greater distortion. The signal at the receiver in any given time can be expressed as the sum of the scaled and delayed reflections arriving at the receiving radio [13, p. 62]. If $s(t)$ represents the transmitted signal then the received signal $rx(t)$ is given by:

$$rx(t) = h_1s(t - \Delta_1) + h_2s(t - \Delta_2) + \dots + h_Ns(t - \Delta_N) \quad (2.5)$$

where h_n is the magnitude of the signal Δ_n is the time delay, and N is the total number of delays. Physically, this means that the received signal, as shown in Figure 2Figure 3, is composed of not only the power from the line of site propagation but also signal power from any reflected path that might exist. Electromagnetic energy propagating along the reflected paths arrive some time delay Δ_n after the line of site propagation arrives. This time delay is based upon the length of the path traveled. Summing all of the different scaled and delayed reflections that arrive at the receiver can result in a signal that is distorted to some degree. If this distortion is severe enough, it can interfere with signal integrity.

Noise

There are a variety of ways that noise can be introduced in a channel. Types of noise can generally be divided into two types: narrowband and broadband. Noises that occupy a very small range of frequencies constitute narrowband noises while noises that span a large range of frequencies are broadband noises. Other transmitters utilizing the same channel are one possible source of narrowband noise. When narrowband noises exist outside the frequency band of interest, they can be filtered out relatively easily, but when they are in-band, they pose more of a challenge. Broadband noises can come from a variety of sources including thermal noise and atmospheric sources.

Additive White Gaussian Noise (AWGN) refers to wideband noise that exists at a constant spectral density with amplitude determined by a Gaussian distribution. The spectral density of AWGN is given in units of power per hertz of bandwidth. One type of AWGN is thermal noise, cause by tiny random motions of electrons [13]. This type of temperature dependent noise exists in any electrical component as well as in all transmission media [14, pp. 86-87]. The thermal noise power N [W], that exists in bandwidth B [Hz], in any given component is given by

$$N = N_0 B = (kT)B \text{ [W]} \quad (2.6)$$

where $N_0 \left[\frac{W}{1 \text{ Hz}} \right]$ is the noise power density and k is Boltzmann's constant. Because thermal noise is inherent in any media and component and cannot be completely removed, it is a fundamental limitation of communication systems.

Impulse noise is a potentially broadband, sudden, form of interference. Impulse noise can come from a variety of sources that are often located within the proximity of an RF system. Some possible sources of impulse noise are car ignitions, poor insulation on high voltage lines, and lightning [15]. As shown in Figure 2, these different types of noise are combined with the signal additively.

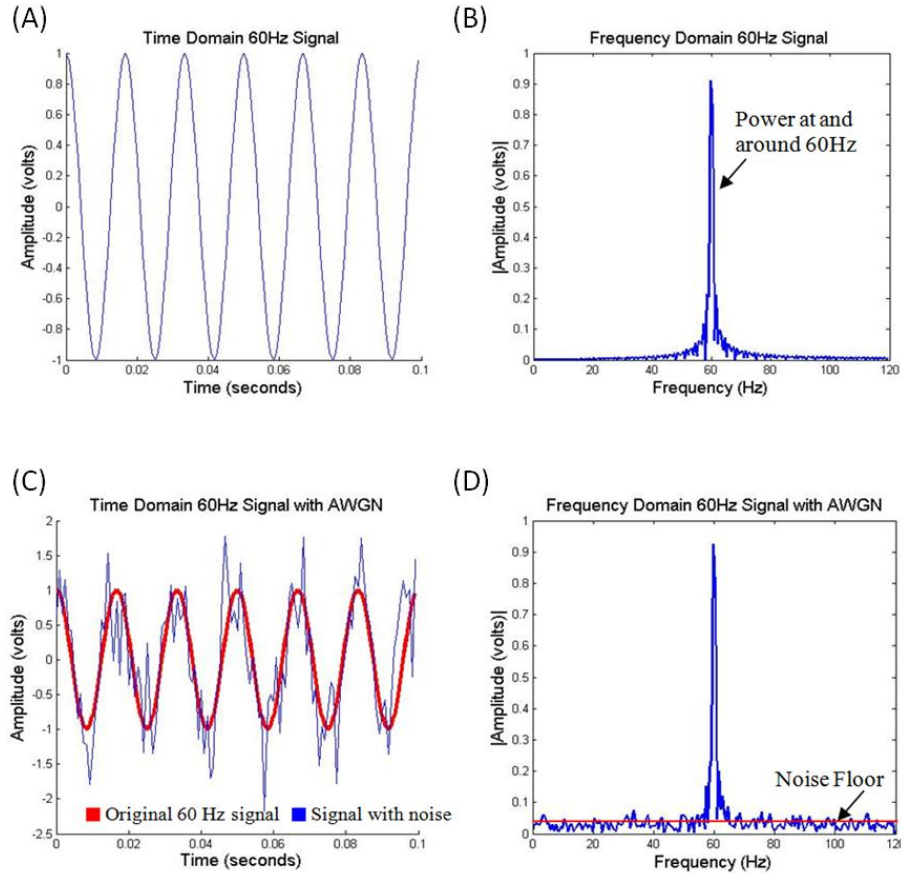


Figure 4: (A) Noiseless time domain 60Hz signal. (B) Noiseless 60 Hz frequency domain signal. (C) 60 Hz time domain signal with AWGN (Blue) and noiseless 60Hz time domain signal. (D) Noisy 60 Hz signal in the frequency domain, the noise floor is shown in red.

Figure 4 (A) shows a 60 Hz time domain signal without any type of distortion or noise added to it. This same signal is shown in Figure 4 (B) in the frequency domain, with the signal power concentrated at and around 60 Hz. Figure 4 (C) is the same 60 Hz time domain signal, this time with AWGN. The red trace shows the original unaltered signal while the blue signal shows the signal with AWGN. In the frequency domain [Figure 4 (D)] this noisy signal still has the majority of its power located at 60 Hz, however there is noise power located at other frequencies as well. The sum of all unwanted signal power and noise is the *noise floor*, shown in red in Figure 4 (D).

Creating experimental channel conditions

In order to examine the functionality of different types of wireless networks and the impacts of varying certain network parameters, experimenters need to be able to reliably create and/or

control certain channel conditions. Different techniques exist to allow for wireless network testing in an experimental channel. These include software based channel simulation, channel emulators, wireless radio testbeds, and wired testbeds. These different test environments perform differently in terms of experiment repeatability, ease and extent of control, adaptability, and cost [16]. For the purpose of this report, ‘channel emulator’ refers to a system where radios remain stationary while radio signals are altered to simulate a RF channel changing with time [17, p. 3].

Software simulation

Software based channel simulators can model a variety of different channel conditions. While channel simulators can be adapted widely to a wide array of different types of experiments, they are limited in their ability to accurately replicate the complexity of a channel. According to experimenters at the University of Colorado Boulder, software simulations offer relatively good estimation results but fall short when it comes to accurately representing the physical layer [18]. They can sometimes also neglect communication between different layers of the protocol. In their work, these authors have noticed specific inconsistencies between simulation and hardware results.

Ray tracing is one simulation technique that is commonly used in software based simulation. As electromagnetic waves propagate through a wireless channel, they can encounter certain environmental characteristics and objects that cause the wave to change direction. Ray tracing is a method that approximates the traveling wave as a set of small ‘rays’ that travel in a straight lines across small sections of distance. Each ray is moved in a straight line over that small distance and then the direction of propagation is calculated again for the next small section. For a radio channel, this method can be used for simulating the effects of multipath. For an isotropic source, for example, radiation could be modeled as a large amount of rays coming directly out of the source. When one of these rays encounters a reflective surface, it changes direction accordingly. The sum of rays that arrive at the receiver at any given time is the resulting distorted signal. While software based simulation is extremely useful for some types of testing, testbeds that connect to actual radio hardware offer additional accuracy in the PHY layer.

Wireless testbeds

In the real world, radios generally communicate over a given distance, through air, using antennas. This real world scenario is shown in the top part of Figure 5. Testing radios in this type of setting requires large amounts of space and is often complicated, difficult to control, and not very repeatable. Furthermore, proper permissions need to be obtained from the FCC in order to use certain bandwidths at certain broadcast powers. For this reason, this type of testing is not always feasible and alternatives in a controlled laboratory setting are needed. In the context of this report, wireless radio testbeds refer to testbeds that involve an arrangement of nodes where physical antennas remain as part of the system. This is an important distinction from wired testbeds where antennas are removed and replaced with coaxial cables. Both types of testbeds along with the real world scenario that they represent are portrayed in Figure 5. Real world distances can be mimicked in a much smaller laboratory environment by placing attenuators between the output of the radio and the antennas as shown in the middle section of Figure 5. This causes the magnitude of the transmitted and received signal to be smaller, as it would be if the radios were communicating over a greater distance.

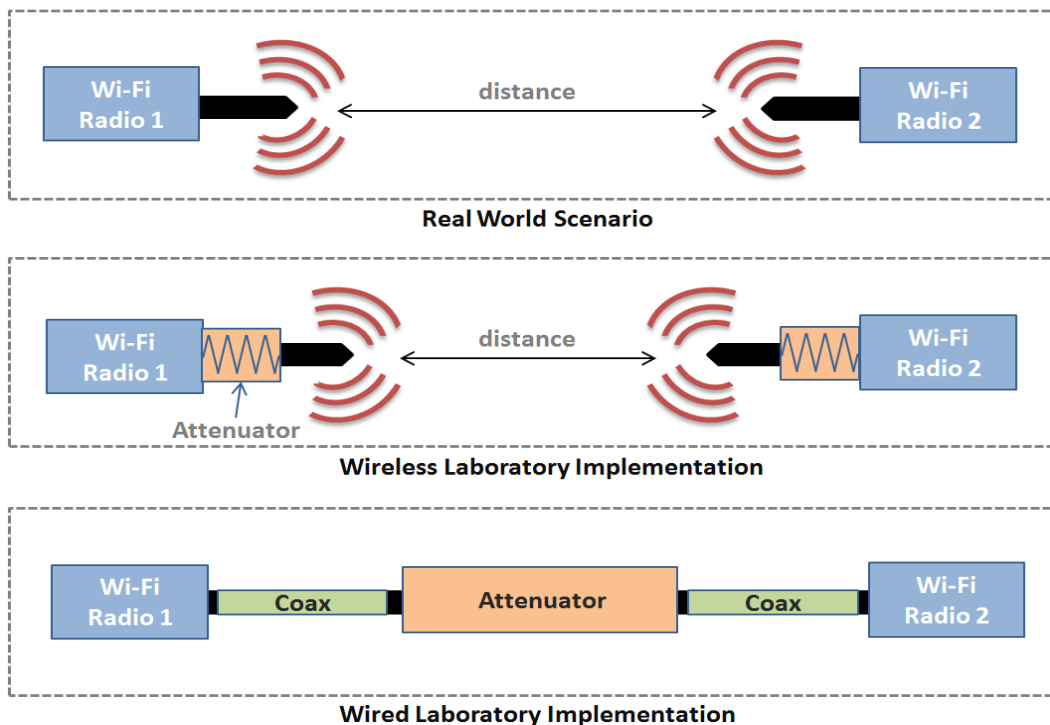


Figure 5: The real world radio communications scenario, shown on top, can be modeled using a wireless, miniaturized, configuration with attenuators (middle). The concept of a wired testbed is at the bottom of the image. A wired testbed involves radios that are connected to each other using coaxial cable and RF components, like the attenuator shown, to model channel response.

The channel can be further modified by introducing noise generators [19]. Noise generators, or ‘noise bricks’, give experimenters another degree of control over the channel that is being emulated. An RF noise generator is shown below in Figure 6.



Figure 6: Noise generators can be used to add noise to a channel emulator. This noise generator, or ‘noise brick’, is manufactured by Noisecom Incorporated.

While wireless testbeds can sometimes create useful and realistic experimental conditions, implementing them comes with some unique challenges, such as achieving repeatability [20]. Fading and external sources of interference tend to vary with time and are extremely difficult to control, even in the laboratory. In some wireless testbeds, system mobility can be achieved only through actually physically moving nodes. For example, the Miniaturized Wireless Network Testbed (MiNT), created by researchers at Stony Brook University, achieves node mobility by mounting nodes on iRobot’s Roomba, a vacuum cleaning robot.

One of the better known wireless network testbeds is the Open Access Research Testbed for Next-Generation Wireless Networks (ORBIT), located at Rutgers University. This testbed is accessible to members of the research community who can write their own code to run custom experiments remotely on the radio grid. ORBIT currently houses 400 radio nodes indoors. A picture of some of these nodes is in Figure 7.



Figure 7: The indoor testing facility at Rutgers University [21] is open for use to members of the research community who write their own code. Each yellow box is one of 400 stationary radio nodes.

Despite the impressive utility of ORBIT, it does not exist without limitation. For example, all nodes in ORBIT are stationary. For this reason, the only way to change network topology is by either including or excluding specific nodes from the configuration. Orbit also faces the same challenges as any other wireless testbed in terms of controlling experiment reproducibility.

A smaller scale and less expensive testbed called The Emulated Wireless Ad Hoc Network Testbed (EWANT) was created at the University of Colorado at Boulder [18]. This testbed is significantly scaled down in size and is capable of simulating node mobility. Attenuators situated between antennas and Wi-Fi cards allow a large scale setup to exist in a much smaller location. In order to create mobility, the RF signal is multiplexed four ways and terminated in four separate antennas. A switch enables selection between the four unique antenna outputs. The antennas in EWANT are arranged in different configuration on a metallic tabletop with holes as shown in Figure 8. Antennas can be moved to different holes to represent different node geometries.

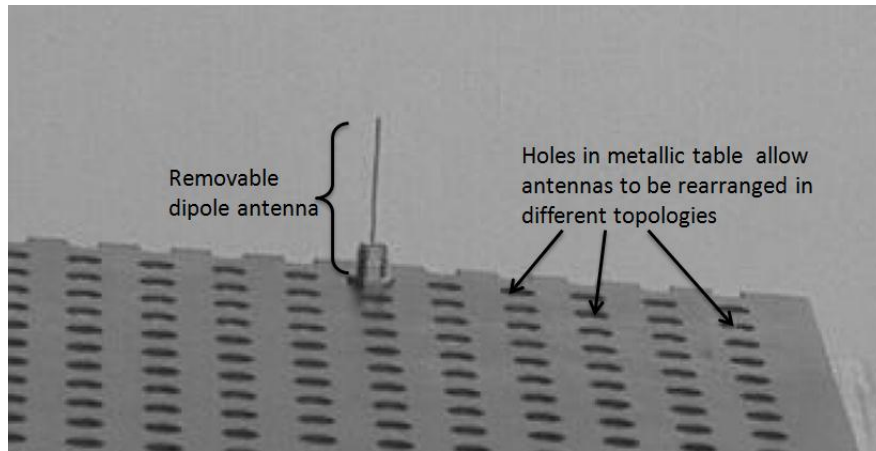


Figure 8: In the EWANT testbed, antennas can be rearranged on metallic table top with holes to create unique geometries. By switching between antennas, mobility can be emulated.

Because each radio is connected to a switch that can select from one of four differently placed antennas, limited mobility can be emulated. When the switch selects a different transmitting antenna, it is as if the radio has ‘moved’, albeit rather suddenly.

Wired Testbeds

Wired testbed configurations generally involve physically connecting radios with a network of coax cables and a combination of passive and active components that create realistic and controllable channel conditions. The key benefit to wired testbeds is their repeatability. Unlike wireless testbeds, where many of the external conditions are difficult to control, wired testbeds exist in a smaller, much more controllable, and thus far more repeatable environment. Despite the high costs of creating an adaptable wired testbed, they can offer a repeatable and realistic test setting.

One interesting realization of a wired channel emulator was created by engineers in Queensland Laboratory in Australia. With this particular implementation, ten programmable signal attenuators, power splitter/combiners, and coaxial cables, connect up to five wireless nodes [19]. Different attenuation levels are programmed using a national instrument PCI card. The authors varied the nature of the ‘channel’ by changing attenuation setting in the ten attenuators. A diagram from their paper is in Figure 9. Radio nodes are represented in blue and attenuators in red. Black lines indicate connectivity. In this configuration, changing the attenuation value between any pair of nodes changes the emulated ‘distance’ between them. Greater attenuation

values correspond to greater distances while smaller attenuation values emulate radios within close proximity of each other. By varying the attenuation values between all of the nodes simultaneously, the creators of this system mimic the changing geometry of a system of nodes, all moving with respect to one another.

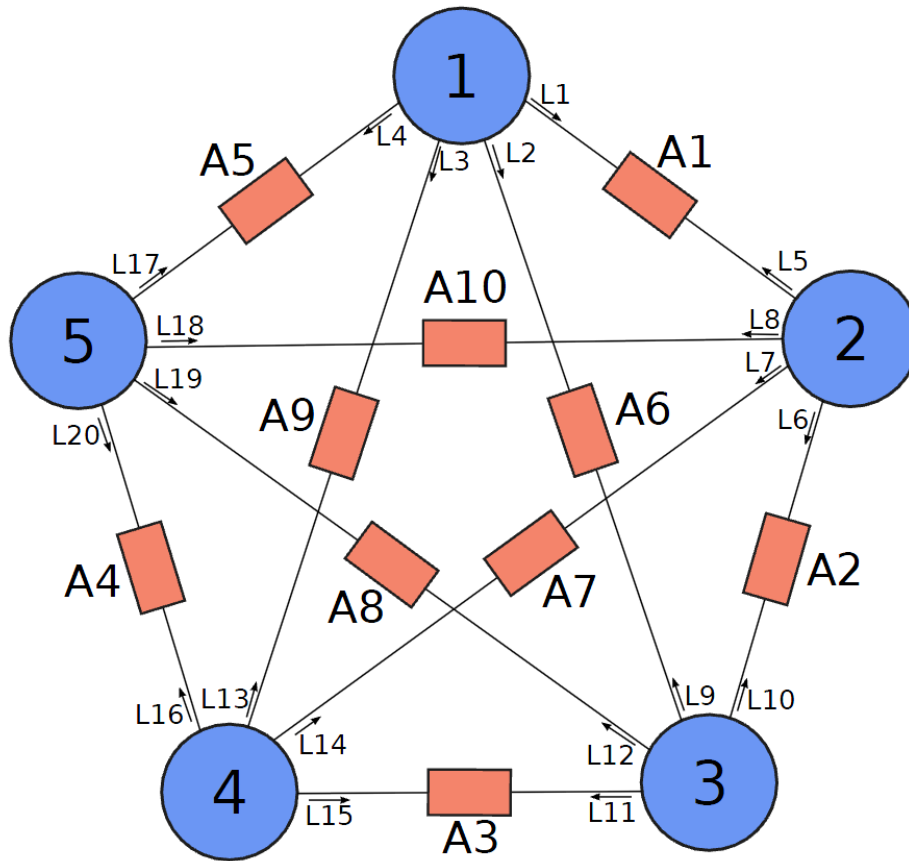


Figure 9: The connectivity of a wired testbed created at Queensland Laboratory in Australia supports up to 5 nodes [19]. The channel response is created by programmable attenuators placed between radios, shown in red.

A similar testbed, called MeshTest, was created by the Laboratory for Telecommunications Sciences to support as many as twelve nodes [20]. Researchers who created this testbed used an RF matrix switches to route and attenuate signals between the different nodes. An example of a 3 x 3 RF matrix switch is shown in Figure 10, with three inputs, three outputs, and nine attenuators.

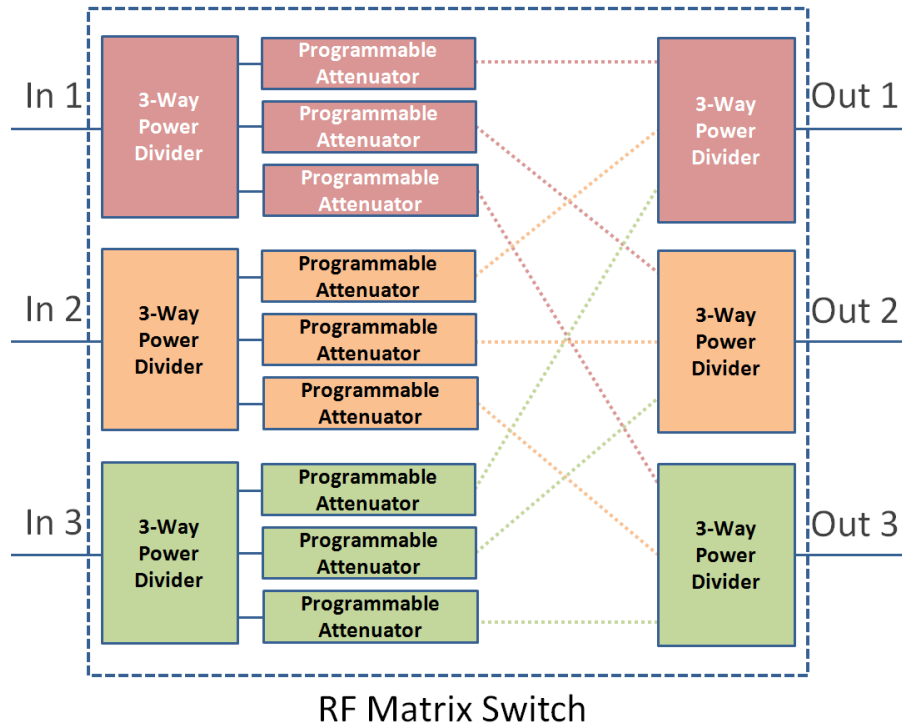


Figure 10: 3 x 3 RF Matrix Switch [22]. Inputs are split three ways, scaled using programmable attenuators, and recombined so that each output receives power from each of the three inputs.

The RF matrix switch shown in Figure 10 works by splitting the power from each input three ways. Each RF path is then connected to a programmable attenuator and power from each of the three inputs is combined into each of the three outputs using a 3-way divider to combine the signals. The programmable attenuators allow the user to control the magnitude of each input at each of the three outputs. In MeshTest, this configuration allows the user to control the signal power between all of the radio pairs.

For this type of connectivity, the number of attenuators needed is equivalent to the number of inputs multiplied by the number of outputs. For MeshTest, programmable attenuators supported attenuation values from 0-127dB. According to authors, the values programmed into the attenuators can be expressed in a matrix L , where the number of rows and columns is the same as the number of nodes. The multiplicative attenuation from node i to node j is given by element $l_{i,j}$ in the matrix L . Different values in matrix L represent different physical configurations and distances between radios in the channel. Adjusting the attenuator values rapidly can mimic channel conditions for a mobile group of nodes. To increase usability, creators of this testbed

developed a GUI that allows the user to define starting, interim, and ending locations for the nodes as well as certain timing intricacies.

A second class of wired channel emulators utilize FPGA based signal processing rather than programmable attenuators to emulate motion and to mimic more complicated channel conditions. These types of channel emulators can model multipath, fading, as well as path loss. Radios that comprise a network under test are plugged directly into this device. The RF signal from each of these nodes is then downconverted and sampled by an ADC. The resulting signals are then sent to a channel simulating FPGA board where signals can be attenuated, filtered, and combined. Finally, the signals pass through a DAC, are upconverted, and sent to recipient radios. The CMU Wireless Emulator is one example of this type of channel emulator from academia [23]. This emulator is capable of supporting up to 15 nodes with 210 independent channels. In this case, the channel simulator board is a Virtex 2 Pro FPGA. This emulator is somewhat similar to the commercially available Elektrobit Prosim F32 channel emulator shown in Figure 11.



Figure 11: Elektrobit Prosim F32, radio channel emulator [24]. The F32 model has the capacity to support as many as 32 distinct RF channels with 16 bidirectional nodes. This channel emulator can also emulate fading.

This emulator has the capacity for up to 32 distinct RF channels, supports 16 bidirectional nodes, and offers up to 128 fading channels. Operating frequency range for the Prosim is 30 to 2700MHz with a signal bandwidth of up to 40MHz. All of the different types of channel

emulators and testbeds discussed in this section, including the Elektrobot Prosim, are summarized in Table 2 [17].

Table 2: Comparison of different channel emulators and testbeds. Testbeds can be wired or wireless and include a variety of different mechanisms for motion emulation.

Name	Mobility Mechanism	Wireless or Wired	Maximum Number of Nodes	Wireless Medium Modeling
MiNT (Miniaturized Wireless Network Testbed)	Robots (iRobot's Roomba)	Wireless	8	IEEE 802.11
ORBIT (Open-access Research Testbed for Next-Generation Wireless Networks)	Antenna switching	Wireless	400	IEEE 802.11, Bluetooth,
EWANT (Emulated Wireless Ad-hoc Network Testbed)	Antenna switching	Wireless	4	IEEE 802.11
MeshTest (Laboratory-based wireless testbed for large topologies)	Programmable attenuators	Wired	12	IEEE 802.11
Queensland Lab Testbed (For wireless mesh networks [13])	Programmable attenuators	Wired	5	IEEE 802.11
CMU Wireless Emulator	FPGA channel simulator board	Wired	15 (210 independent channels)	IEEE 802.11 (2.4GHz, 90MHz BW)
Elektrobot Prosim F32	FPGA	Wired	16 (128 fading channels)	30 to 2700MHz (40MHz BW)

In summary, the testbeds reviewed were either wired (connected by RF components and coax) or wireless (transmitting over air using antennas). Wireless testbeds can be miniaturized using attenuators, but they still use antennas to communicate, such as the MiNT, EWANT and ORBIT testbeds. Wired testbeds replace antennas with coaxial cables and other RF hardware that mimics certain channel conditions, as in the MeshTest, Queensland Lab, CMU emulator, and the Elektrobit Prosim testbeds. A variety of different techniques, including robots, antenna switching, and programmable attenuators can be used to emulate a changing geometry of radio nodes. These testbeds offer a platform for testing different aspects of wireless communications and security.

2.2 Wireless Communication & Security

This section will cover a small portion of the broad field of communications, more specifically, the IEEE 802.11b and 802.11g wireless standards. By popular demand, Wi-Fi has seen explosive growth over the past 15 years, so much that developers have had a difficult time anticipating problems in security. The first wireless security & encryption protocol built in 1999 (WEP, or Wired Equivalent Privacy), was publicly compromised only 2 years later [25] and subsequently deprecated with the replacement WPA (Wi-Fi Protected Access) in 2002, leading to the now prevalent WPA2 in 2004 [26]. As this paper may show, staying ahead of the curve of wireless security is a complex and difficult process; predicting and accounting for every possible weakness is nearly impossible.

Brief Tutorial in Wireless Communications and 802.11b/g

Communication between computers requires an agreed upon architecture and protocol. The ISO (International Standard Organization) developed the OSI (Open System Interconnection Architecture) to support development and operation of communications. Figure 12 illustrates the OSI protocol stack.

Breaking up the protocol into separate layers simplifies each operation. Devices can specialize in one layer while ignoring details on lower layers. Each subsequent layer facilitates the transfer of information to other programs, computers, or networks. It helps to imagine network protocols as stripping off (or adding back) layers of an onion. For example, when sending an e-mail, the application layer would be responsible for identifying the sender and receiver. After the

presentation layer encodes the data with ASCII characters (or the specified coding scheme), a session may be initiated (by the Session layer) where a conversation between two computers is opened.

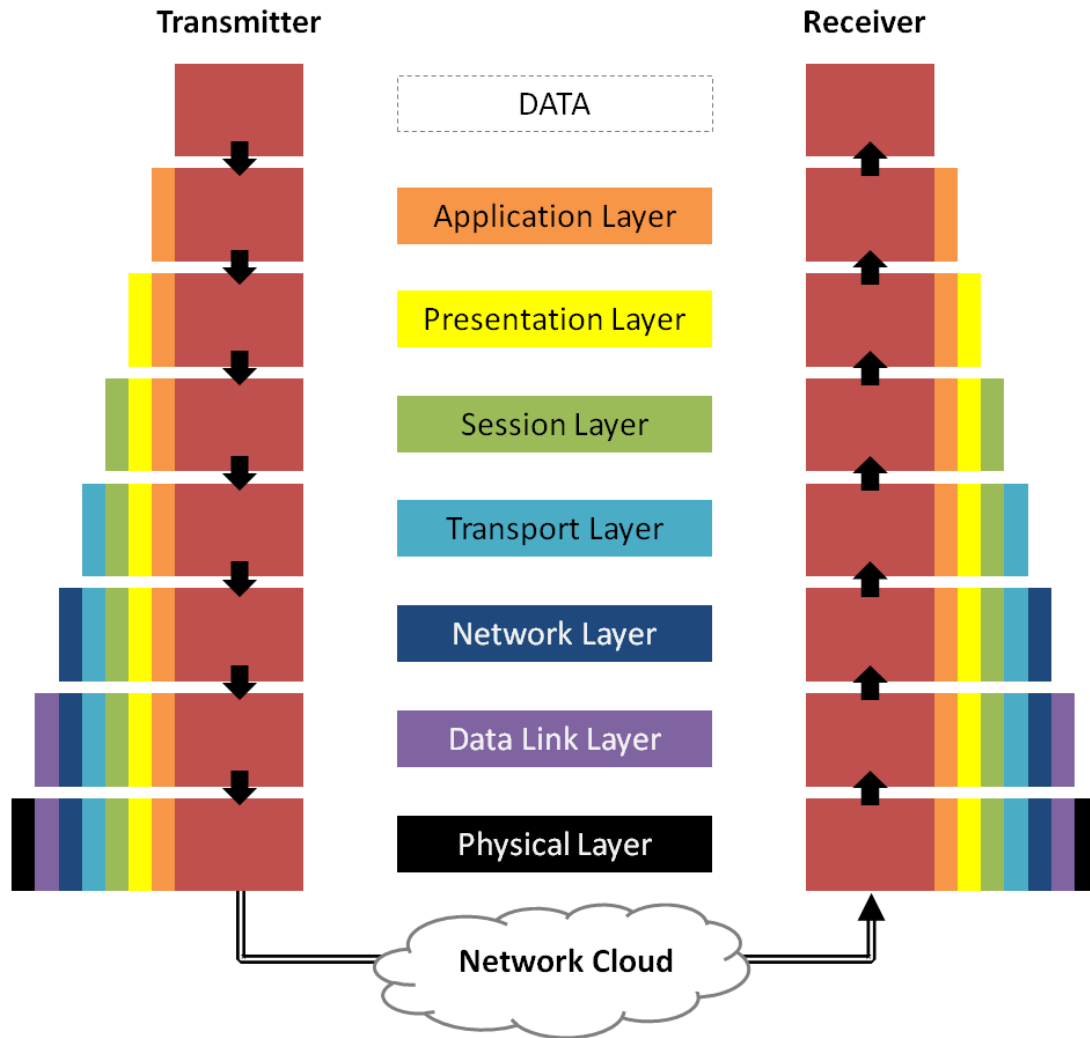


Figure 12: Open System Interconnection Architecture (OSI) Protocol Stack, a product of the International Organization for Standardization for characterizing layers of communication systems [27].

The message would then get divided into a TCP (Transmission Control Protocol) packet by the Transport layer, which ensures end-to-end delivery. The Network layer then adds network addressing and routing information in order to open and maintain network connections. Access and control of the medium is negotiated by the Data Link layer. Finally, the Physical layer then modulates the data into a bit stream that is transferred over the medium to another client.

The IEEE 802 standard, built upon the OSI model, provided a framework for wireless communication, which requires a slightly modified protocol to account for mobility and security. Motivation for wireless communication standards began in the 1980's to support factory environments [28]. The IEEE 802.11 standard became the first and only WLAN (Wireless Local Area Network) standard to successfully secure a market. This 2,500 page document specifies the protocol for PHY (Physical: RF and modulation schemes) and MAC (Medium Access Control) layers of a communication architecture.

The main objectives of the 802.11 standard were to provide a mechanism that could allow overlapping networks, include conditions that handle interference from radios and microwave ovens, eliminate "hidden terminal" problems, support time-bounded services, and maintain privacy and secure access [28]. Table 10 in the Appendix lists 802.11 standards and their scope. The following list describes layers implemented in the 802.11 protocol stack [14]:

- **Upper layers** are not defined in 802.11 and are assumed to use the IEEE 802 standard, or the network's supported variation, consisting of Internet, Transport, and Application layers.
 - The **Application layer** transfers information specific to an application such as websites (HTTP), file transfers (FTP), e-mail (SMTP/IMAP/POP), and secure logins/connections (SSH, Telnet). Many varieties of TCP/IP protocols implemented in the application layer exist, including NFS (Network File System), and WHOIS (remote directory access).
 - The **Transport layer** provides error and flow control with ensured delivery, using TCP and UDP (User Datagram Protocol). TCP messages constitute the majority of information sent over applications such as email and websites, while video and other streaming information typically utilize UDP.
 - The **Network layer** uses IPv4 or IPv6 and provides ICMP (Ping), and packet forwarding and routing. Host addressing (IP address) and resolution also included. Note that IP datagrams do not require acknowledgments, which are implemented in the Transport layer or Data Link layer.

- The **Data Link layer** is the logical interface to network hardware including the MAC layer. Channel access, coordination, and reliable data delivery are key components to this layer, explained in more detail in the MAC Layer section.
- The **Physical layer** is responsible for modulating and representing signals over a medium. In 802.11b/g, this layer modulates bits into Direct Sequence Spread Spectrum (DSSS) at 5.5 & 11 Mbps or Orthogonal Frequency Division Multiplexing (OFDM) at up to 54 Mbps, respectively. This layer is explained further in the following section.

The 802.11 standard only specifies operation within the MAC and PHY layer. The MAC layer is divided into two sublayers: the MAC sublayer controls roaming access, power management, and connection management, and the MAC-*Management* sublayer provides an access mechanism and reassembles packets. The PHY layer contains three sublayers: PHY Layer Convergence Protocol (PLCP), used for carrier sensing and packet formation, PHY Medium Dependent Protocol (PMD), used to specify modulation and coding, and PHY Layer Management Sublayer, used to control channel tuning and similar options [28].

PHY Layer

The Physical layer of the 802.11 protocol stack dictates the transmission of raw bits over a medium. Each version of the 802.11 standard (a, b, etc., listed in Table 10) includes variations of PHY layer implementations and technologies. These modulation schemes have their own advantages and disadvantages in certain environments.

Direct Sequence Spread Spectrum (DSSS) is a modulation technique used in 802.11b which spreads each bit of a signal into smaller pulses using a *spreading code*. This technique sacrifices bandwidth (data rate) by spreading information out in frequency, which increases performance against narrowband noise and multipath propagation [28]. The spread bits are then modulated and transmitted across a medium, shown in Figure 13.

Input	Output
1	+1, -1, +1, +1, -1, +1, +1, +1, -1, -1, -1
0	-1, +1, -1, -1, +1, -1, -1, -1, +1, +1, +1

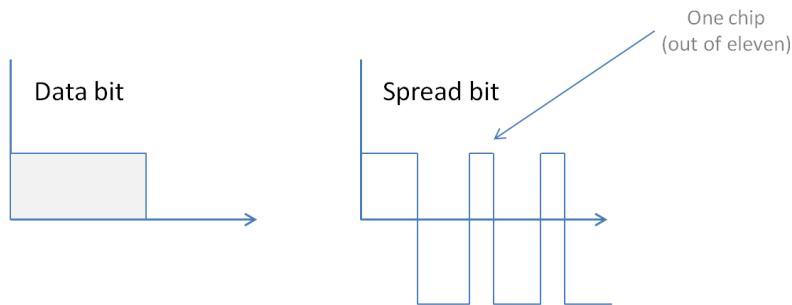


Figure 13: Input and Output using spread sequence (sequence shown is called Barker code), The Data bit is transformed into Spread bits using the spread sequence.

The spreading code used in 802.11 is called the *Barker code*, which is also shown as the example sequence in Figure 13. It has low cross-correlation properties, allowing a more uniform spectrum and increased performance against noise [29]. At 1 Mbps, each bit is spread into an eleven ‘chip’ sequence, which is then modulated using Differential Binary Phase Shift Keying (DBPSK), as in Figure 14.

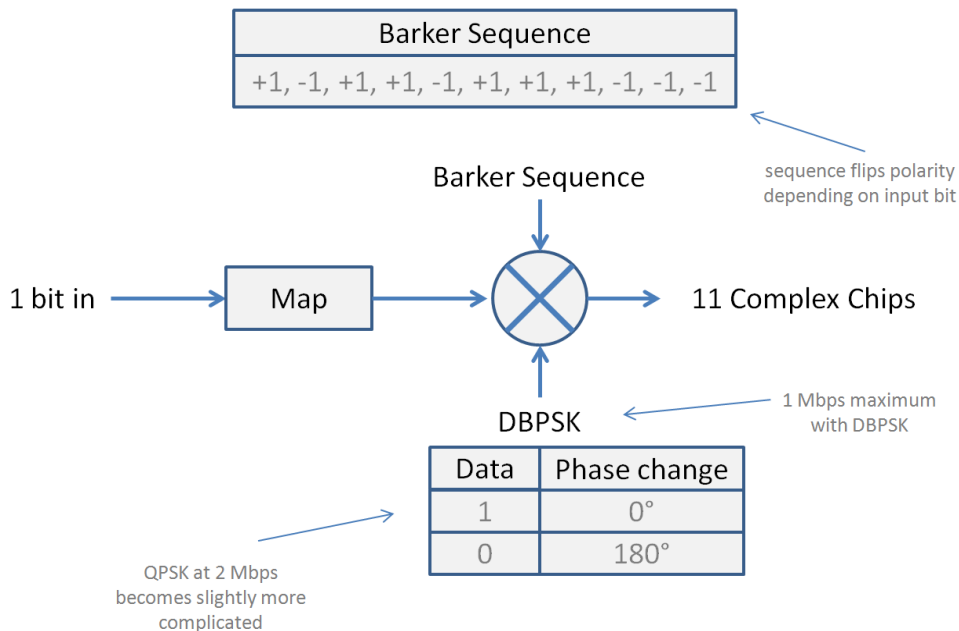


Figure 14: Map of Barker Code Sequence at 1 Mbit/sec with DBPSK [29]. Each bit is modified by an 11-bit sequence.

Data sent at 2 Mbps is possible using Differential Quadrature Phase Shift Keying (DQPSK), which simply adds a 90° phase change to DBPSK. Figure 15 illustrates the effect of a narrowband jammer on a DSSS signal before despreading.

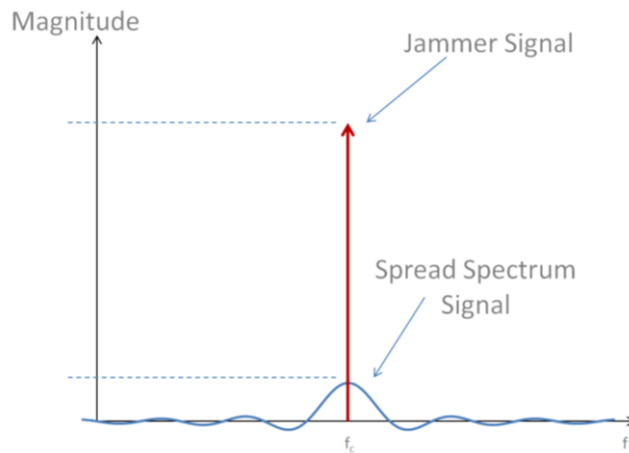


Figure 15: Amplitude of DSSS Signal (Blue) vs. Narrowband Jammer (Red) before despreading [30]. Note: signals are simplified and do not represent actual DSSS or jamming signals.

For demonstration purposes, the signals are over-simplified. Figure 15 shows a narrowband interferer (jammer, Red) with much larger signal amplitude than the DSSS signal (Blue). In some cases the DSSS signal is even beneath the noise floor, an ideal characteristic in covert military applications. Figure 16 illustrates the effect of despreading both signals.

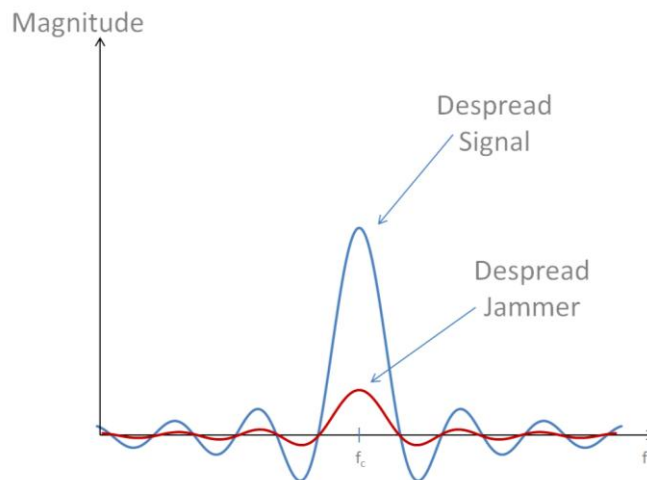


Figure 16: Amplitude of DSSS Signal (Blue) vs. Narrowband Jammer (Red) after despreading. The Despreading signal is now at higher amplitude than the jammer's signal.

After despreading the signal, the jammer is minimized (the Barker code contributes to the efficiency of this operation). The end result, after applying a band-pass filter in Figure 17, is a transmitted signal with much greater amplitude than the jammer, despite the difference in power.

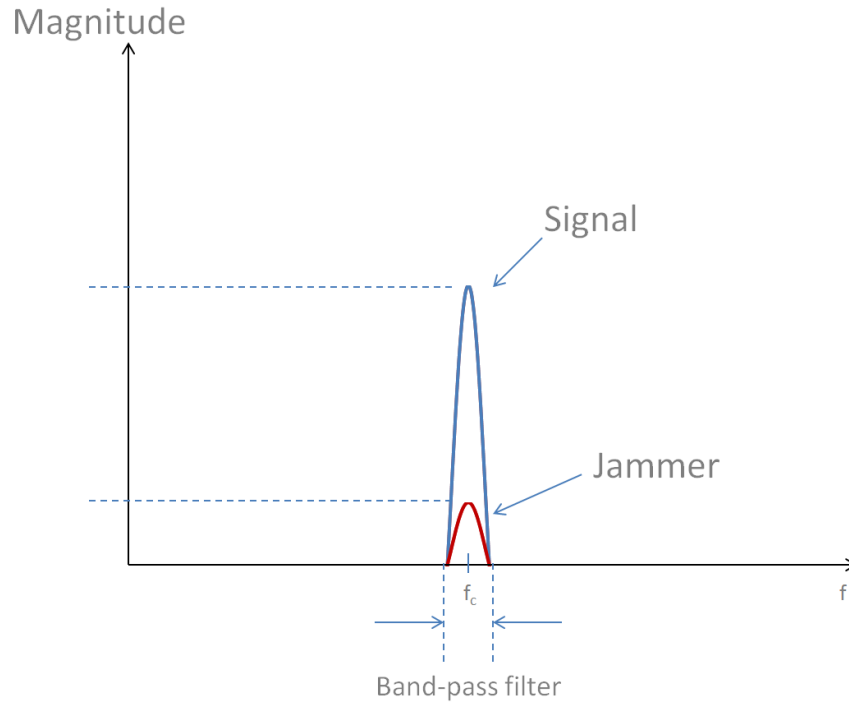


Figure 17: Amplitude of Original Signal (Blue) vs. Processed Jammer (Red) after applying a band-pass filter. This is the overall result of using a DSSS modulation scheme against a narrowband interferer.

This effect against jammers and avoidance to detection helps to explain why DSSS was first developed by the military. It is worth noting that the military developed cryptographic techniques to deploy the spreading code, as an adversary with this knowledge could effectively jam the network by modulating their jammer with the spreading code [31].

Orthogonal Frequency Division Multiplexing (OFDM), used in 802.11g, enables higher throughput (up to 54Mbps). OFDM does well against narrowband interference, frequency-selective fading, and multi-path distortion, while maintaining high spectral efficiency. To help illustrate the effectiveness of this technique, multipath fading and inter-symbol interference are described in the following paragraphs.

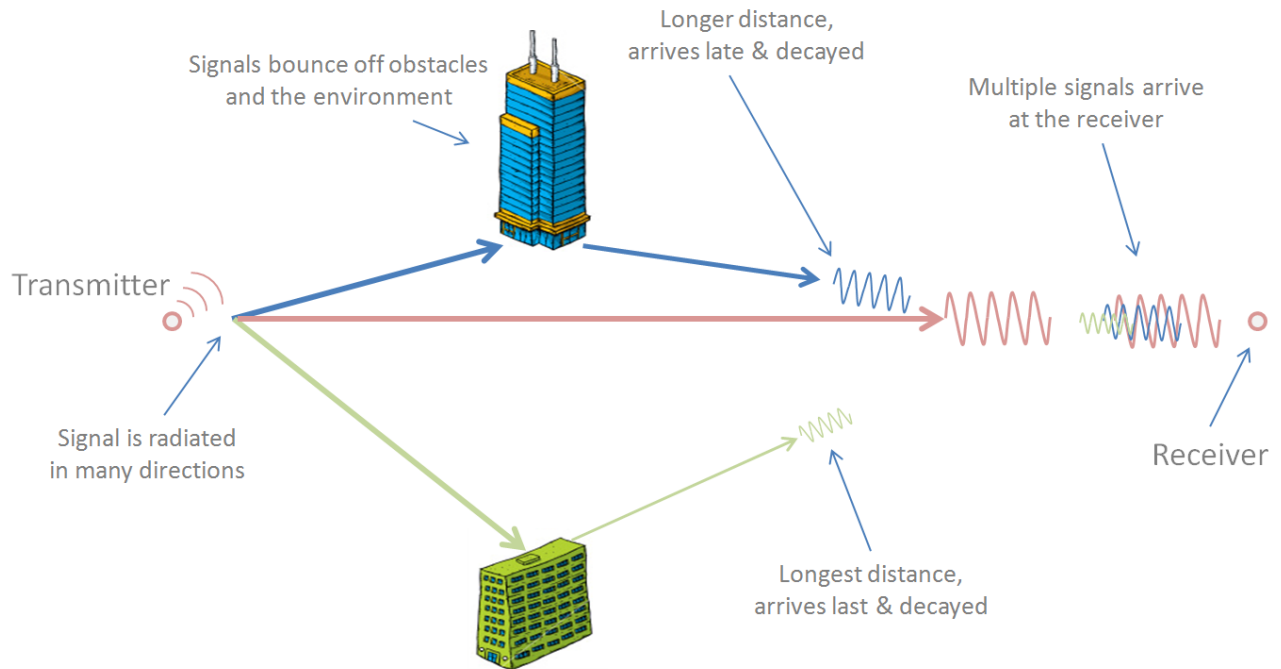


Figure 18: Multipath signals bouncing off the environment. Signals suffer decay and arrive late at the receiver.

Multipath fading is common in any real-world application of wireless communication. The original transmitted signal (Red) will follow multiple paths (Green and Blue), bounce off the environment, and arrive at the receiver delayed in time and decayed in amplitude. Figure 19 shows the transmission of two signals at the transmitter (A), the ideal received signal (exactly the same as the transmitted signal, B), and the realistic scenario of multiple signals arriving at the receiver due to inter-symbol interference (C).

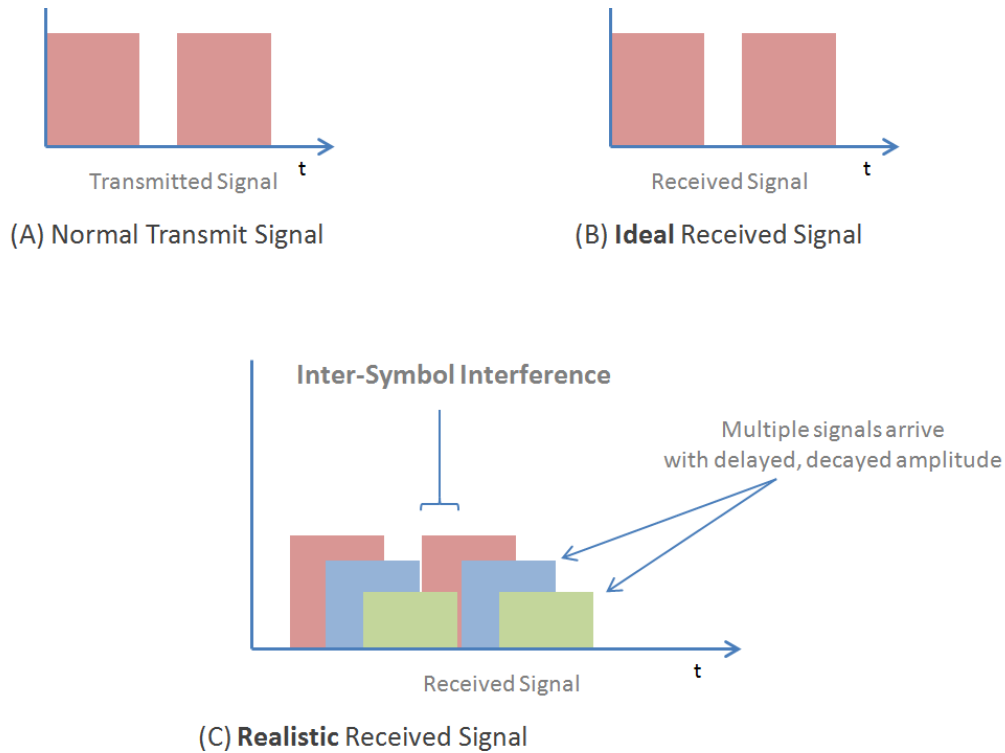


Figure 19: Transmitted Signal (A) with two symbols, Ideal Received Signal (B), Realistic Received Signal (C) with multiple, delayed, decayed, overlapping received symbols from ISI.

In Figure 19 (C), the delayed received signal of the first bit (Green) overlaps into the second bit (Red), an effect called *inter-symbol interference* (ISI). If the two signals were spaced far enough apart, their multipath equivalents would not affect the following signal. This problem worsens when attempting high data-rate transmissions, as in Figure 20.

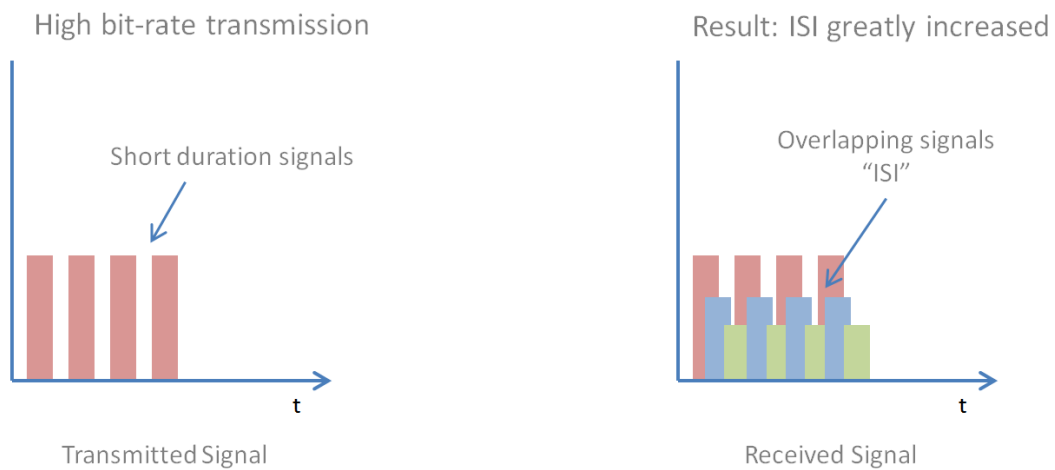


Figure 20: Transmitted signal with high bit-rate transmission (low symbol duration) (Left). Received signal with increased ISI (Right).

In order to squeeze more data into a shorter amount of time, the duration between each symbol is shortened. This shortening causes the effects of inter-symbol interference to intensify, as the travel time of multipath signals does not change with data-rate.

OFDM addresses this issue in a few ways; dividing carriers into sub-carriers with lower data rates, using guard intervals between bands and symbols, and the addition of cyclic prefixes. Figure 21 demonstrates the use of multiple carriers to send data.

OFDM encodes data with low rates on multiple carrier frequencies. This process diminishes intersymbol interference (ISI). For example, when increasing the data rate, digital signals are modulated with shorter durations. This makes them more susceptible to noise or other impairments. However, dividing these carriers into subcarriers allows a high overall data rate while maintaining a low data rate per carrier.

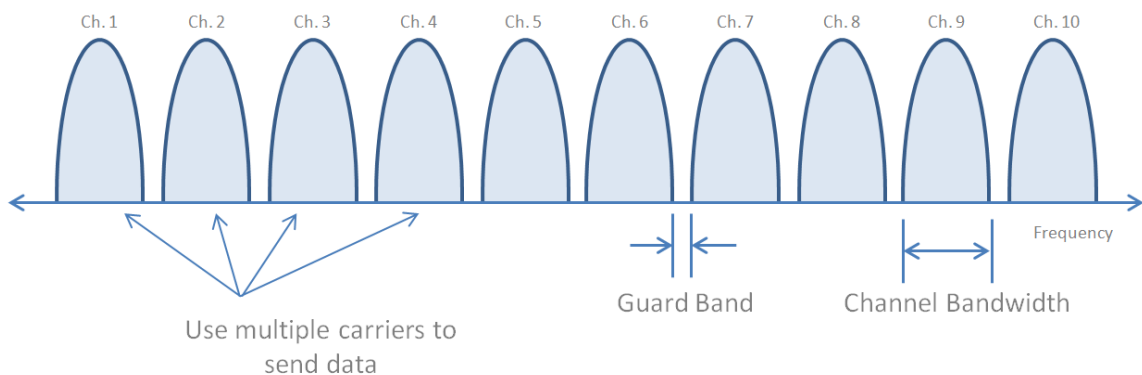


Figure 21: Using multiple carriers to send data (FDM). Advantages: Increased data rate and resistance to ISI using guard bands. Disadvantages: inefficient use of bandwidth.

By dividing one channel into many, each individual channel can use a lower data rate, but will sum to the original, high-speed data rate. The lower data rates imply longer durations between symbols and help to diminish ISI. However, this model, also known as Frequency Division Multiplexing (FDM) is not bandwidth efficient. The introduction of orthogonal frequencies allows a more efficient use of bandwidth.

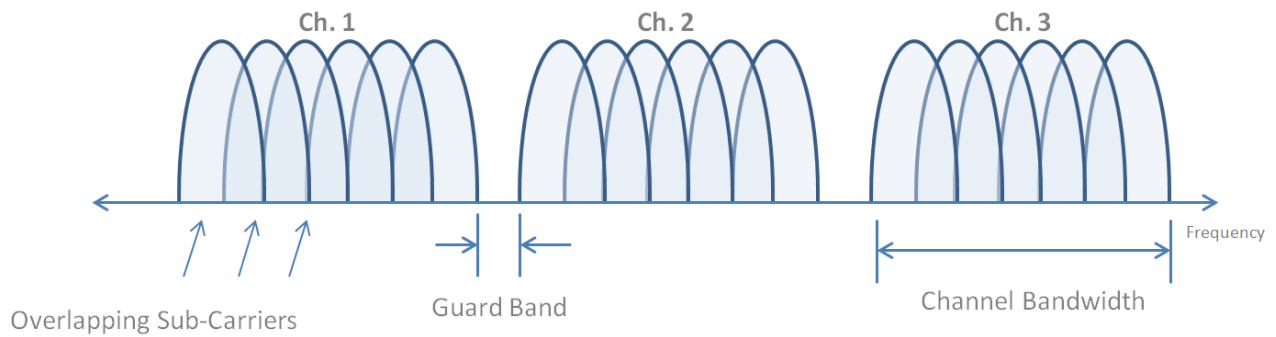


Figure 22: Using overlapping carriers to send data (OFDM). Advantages: greatly increased data rate, resistance to ISI using guard bands, and efficient use of bandwidth. Disadvantages: sensitive to carrier frequency offset or drift.

Figure 22 demonstrates efficient use of bandwidth using OFDM sub-carriers for each channel. IEEE 802.11a/g uses 52 sub-carriers (48 for data, 4 for pilot tones) [26]. This feature can be explained by first examining the Fourier transform of a simple square signal in time, shown in Figure 23.

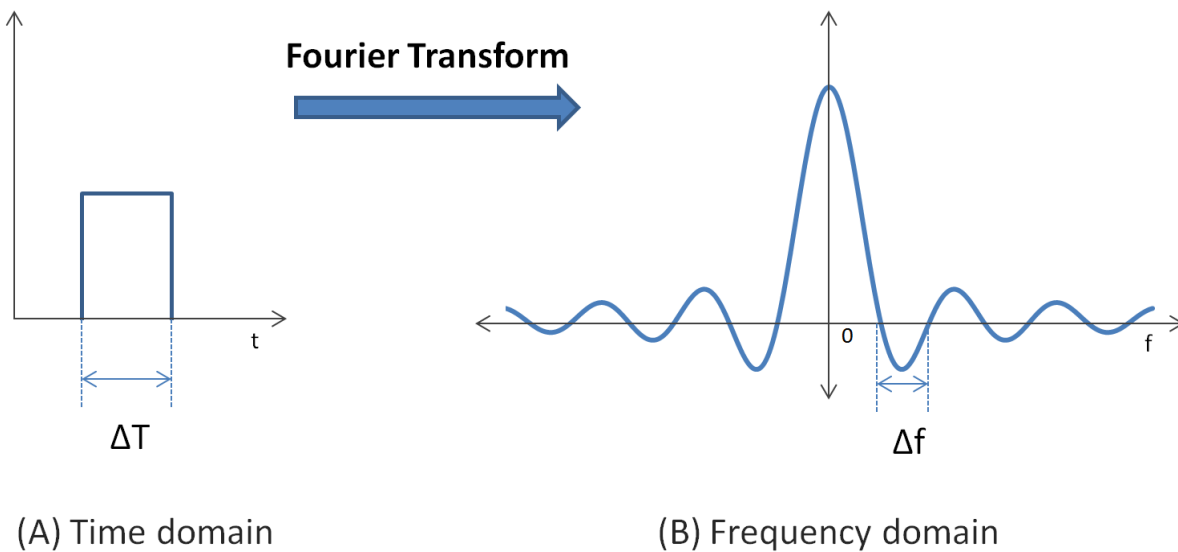


Figure 23: Fourier transform of square, time domain signal into Sinc pulse in frequency domain. The bandwidth ΔT is inversely related to the spacing Δf .

A square signal in time is a $Sinc(x) = \frac{\sin(x)}{x}$ function in frequency. Sinc pulses will intersect at equally spaced points if they are spaced apart by Δf . When utilizing this feature, each sub-carrier is spaced such that, when sampled, it has no interference from the other frequencies. Figure 24 illustrates this orthogonality with multiple overlapping sinusoids.

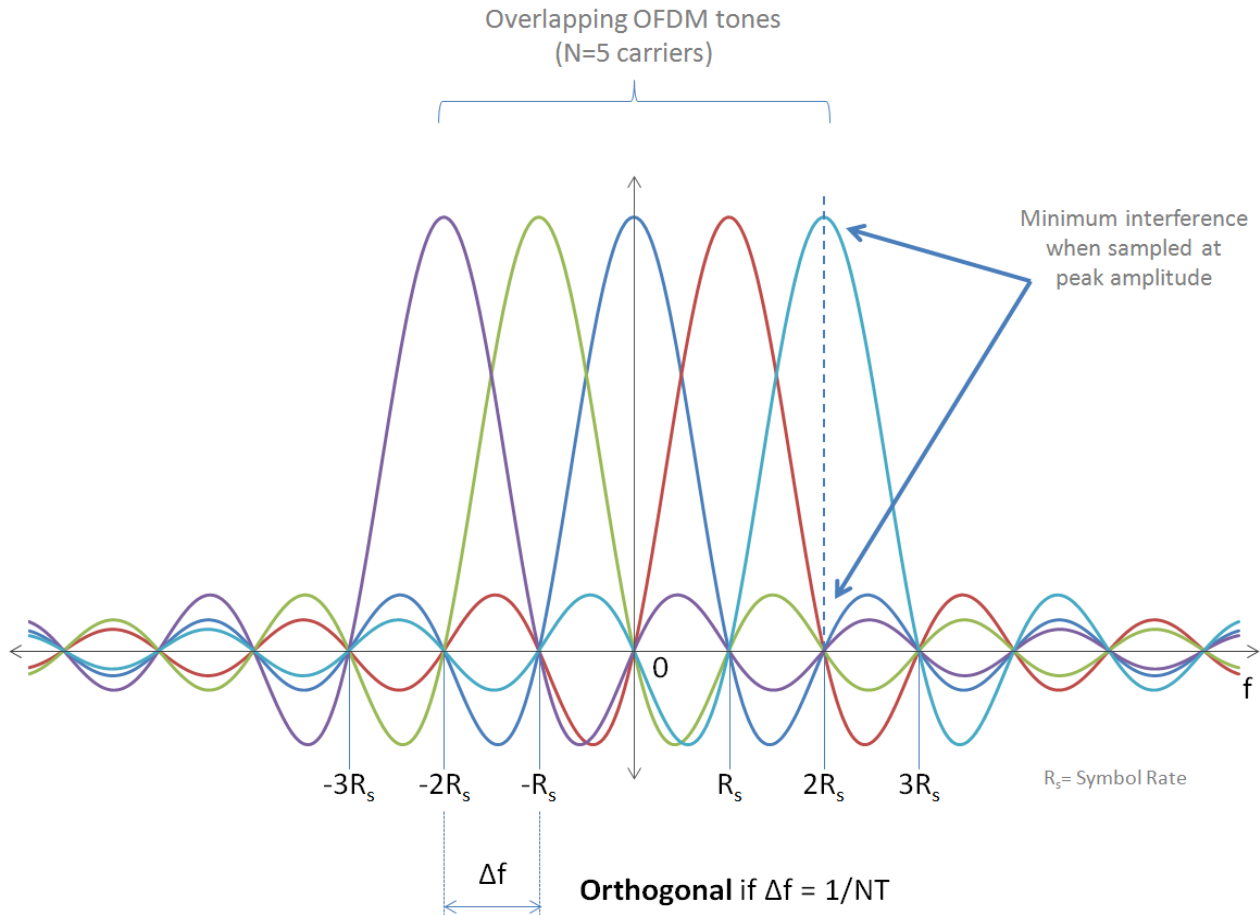


Figure 24: N=5 Overlapping OFDM tones. Each tone is orthogonal if the spacing between frequencies is equal to $1/NT$. Note: minimal interference at sampling points (multiples of the symbol rate).

The symbol duration ΔT is inversely related to the spacing Δf ; in other words, increasing the data rate (shortening ΔT) requires an increase in carrier spacing. Hence, a trade-off exists between data rate and spectral efficiency (higher data rates require increased carrier spacing, consuming more bandwidth).

These methods increase spectral efficiency, but inter-symbol interference is still an issue. To reiterate the problem, consider Figure 25; it starts with the transmission of two symbols using DBPSK (Blue), with a faded multipath symbol (Red) indicating inter-symbol interference (gray).

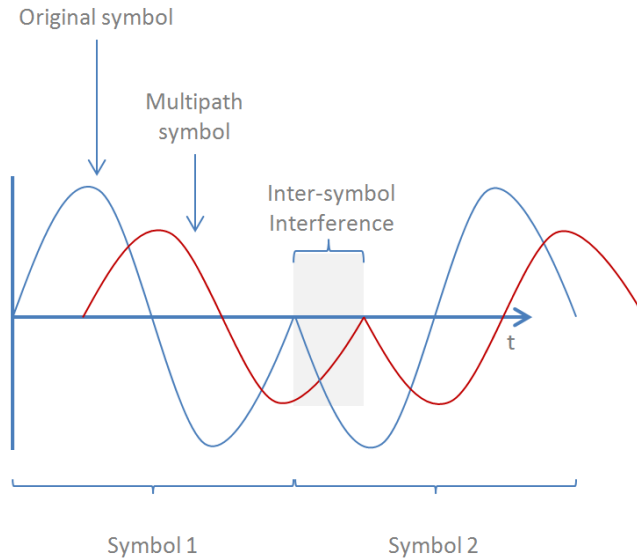


Figure 25: Two received symbols using DBPSK (Blue). Inter-Symbol Interference from multipath signal (Red).

The specific interval of interference is highlighted in gray. The multipath delay spread is a direct result of the environment and has nothing to do with modulation or symbol rate. Therefore, the most direct solution would be to shift the next symbol back in time (delay) so that the multipath signal does not affect the next symbol. This technique is implemented in Figure 26.

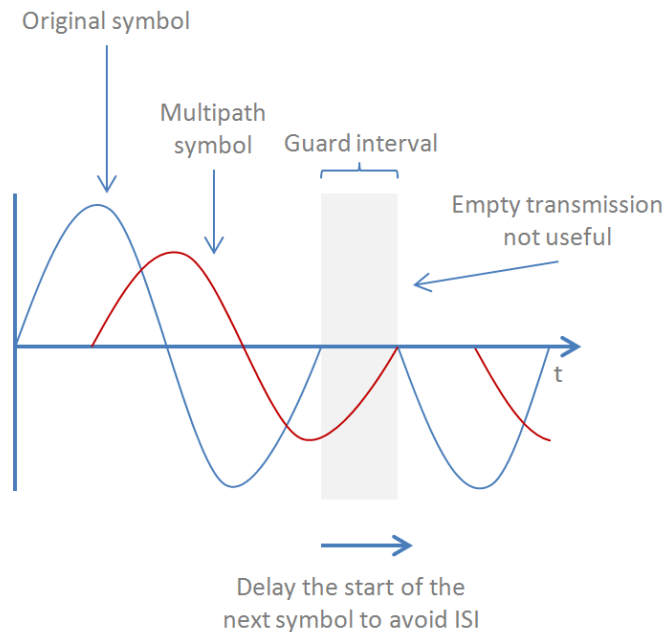


Figure 26: Two received symbols using DBPSK (Blue) and multipath signals (Red). The guard interval avoids Inter-Symbol Interference by delaying the start of the next symbol.

Notice that the next symbol does not start until the end of the multipath symbol, thus ISI has been eliminated. However, an empty transmission in time is not technically applicable in most hardware (which outputs continuous signals) and could cause disruptions and desynchronization in the receiver. A solution to this problem is to fill the guard interval with the tail of the symbol, depicted in Figure 27.

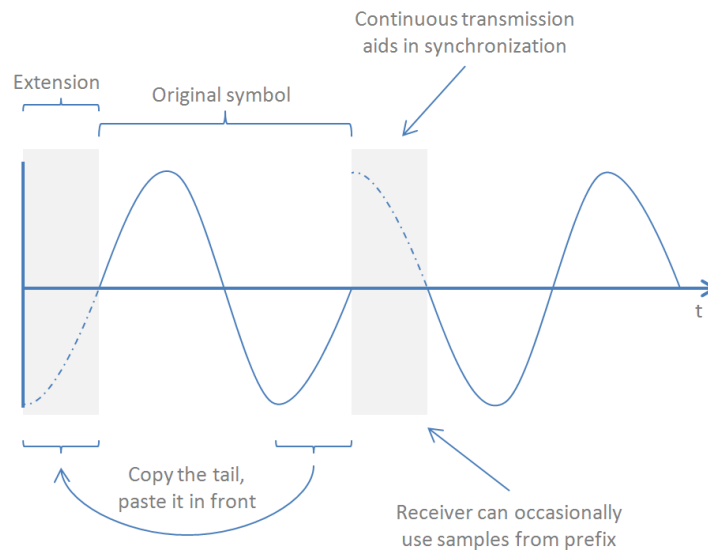


Figure 27: Two received symbols using DBPSK (Solid Blue) with a Cyclic Prefix (Dashed Blue) added to avoid ISI. The cyclic extension is taken from the tail end of the symbol and added to the front.

This technique eliminates ISI by including a tail of the symbol to fill the guard interval, and allows the beginning of symbols to become corrupted without affecting demodulation. Figure 28 shows an alternative view of the transmitted symbol using cyclic extensions.

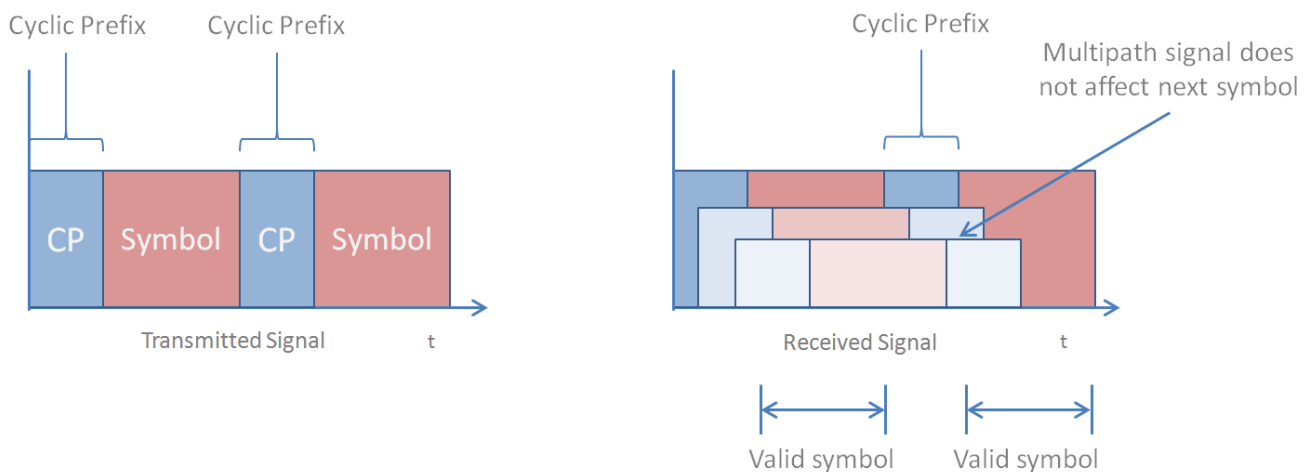


Figure 28: Alternate view of the transmitted signal using Cyclic Prefix. The received signal avoids ISI.

OFDM will typically use 0.8 μ S for the cyclic prefix, based on the maximum delay spread of the environment, and not necessarily to every sub-carrier [26]. The one drawback with this method is the loss in data rate used to include the redundant information (the cyclic prefix). OFDM is also implemented in the latest 802.11n standard with Multiple Input Multiple Output (MIMO), achieving longer range and increased data rates (up to 600 Mbps) via multiple antennas [32].

MAC Layer

Nearly every form of wireless communication includes a MAC layer or protocol (Medium Access Control). In wireless communication, only one person can talk at a time on the same channel. The MAC Layer defines the rules on how clients share the channel equally while minimizing interference, in addition to accounting for reliable delivery and security. In the most basic sense, the MAC layer is the protocol that dictates when and who gets to use the “talking stick.” In Wi-Fi, this is implemented in two main fashions: a Distributed Coordinate Function (DCF), and a Point Coordinate Function (PCF, implemented *on top of* the DCF). PCF is used in Access Point (AP) mode, where there exists a server or “leader” who takes control and organizes the network. DCF is used in Ad-hoc mode, where there is no formal structure or leader and all users rely on a protocol of how to share the medium with each other. A four node example of the two basic network configurations is shown in Figure 29.

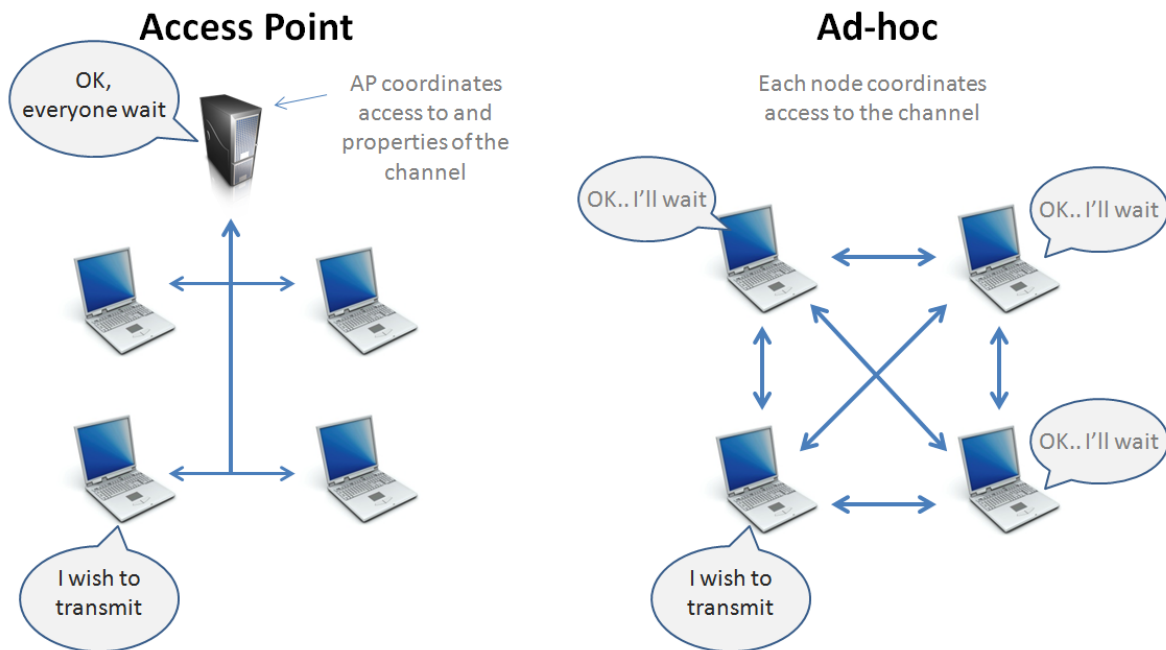


Figure 29: Differences between Access Point (Central Server or Point Coordination) and Ad-hoc Networks (Mesh or Distributed Coordination).

In each scenario in Figure 29, one node attempts to transmit (bottom left node). In AP networks, the point coordinator (PCF) issues the NAV signal to all other nodes, allowing the one client to transmit. The AP will also issue contention-free periods (NAV signals) to stop all other terminals and poll other stations in a semi-periodic fashion [28]. Ad-hoc networks rely on a set of rules to allow each user a fair chance at using the medium, and decide when to transmit and when to be silent based on those rules.

At the heart of the DCF is the Carrier Sense Multiple Access (CSMA) protocol. This is a process by which the channel is sensed (virtually and physically) before attempting to transmit. A critical component of CSMA is a priority schema, where three different Inter-frame Spacings (IFS), described in Table 3, exist for different types of packets,

Table 3: Definitions of Inter-frame Spacings and their role in the MAC Layer [14].

Name	Definition
IFS	Inter-frame Spacing. The amount of time to wait to transmit after the medium has been sensed as busy.
SIFS	Short IFS. The shortest duration (highest priority) to wait to transmit. This is used in Acknowledgement (ACK), Clear to Send (CTS), and Poll Response messages.
PIFS	Point Coordination Function IFS. This is used in Access Point mode by the central controller when issuing polls or to take precedence over DIFS.
DIFS	Distributed Coordinate Function IFS. The longest duration (lowest priority), used for all ordinary traffic.

The IFS between transmissions allow specific packets to have priority over others. The SIFS primarily allows some room for receivers to respond before others begin transmitting, such as when a receiver sends an ACK to confirm delivery to the transmitter, or when a receiver signals others that a transmission is about to begin (CTS). The PIFS is used by an Access Point or “point coordinator” to maintain priority control of the channel. All other traffic must wait the duration of DIFS before attempting to transmit. Figure 30 demonstrates the use of IFS and a backoff window, explained in the following paragraph.

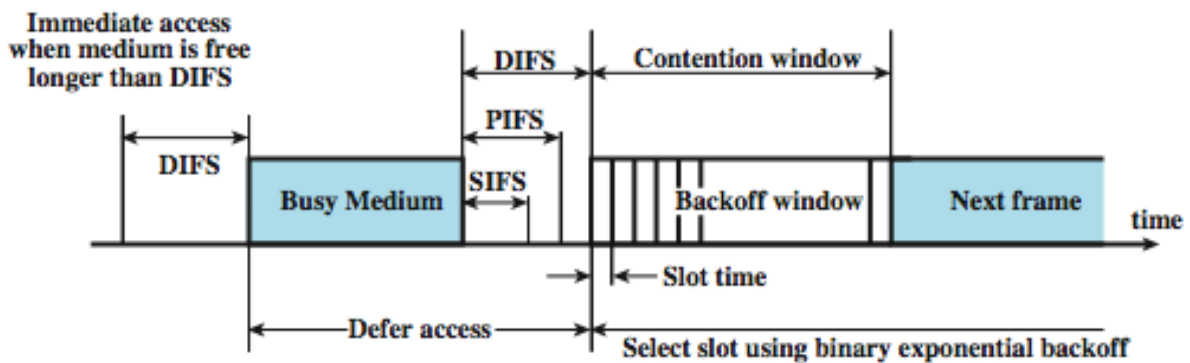


Figure 30: IEEE 802.11 MAC Access Method using Inter-frame Spacings and the Exponential Backoff Algorithm [14, p. 530].

If one or more radios transmit while the medium is busy, a collision can occur. To reduce the probability of collisions and provide equal opportunity for transmission, each radio uses an *exponential backoff algorithm*. The algorithm attempts to space out repeated transmissions in a populated network [28]. This involves choosing a random number and, while the medium is free, waiting that number of time slots before attempting to transmit. If the medium is sensed as busy, the timer freezes until the channel is idle again. Further collisions cause the timer to increase exponentially.

As shown in Figure 30, after waiting DIFS, any client is allowed to transmit if the medium is free. Once a transmission is detected, all clients activate their Network Allocation Vector (NAV, an indicator of a busy channel) signal for the duration of the transmission. The receiving client will wait the duration of SIFS and return an ACK, CTS or Poll Response message if necessary. If an Access Points needs to take control of the medium after transmission, it will wait the duration of PIFS. Other clients will wait the duration of DIFS before attempting to transmit. At this point, if one client is unable to gain access to the medium or notices a collision with another client, it will begin counting its backoff timer while the medium is idle, then when the timer reaches zero it will attempt to retransmit. A general overview of this process is shown in Figure 31.

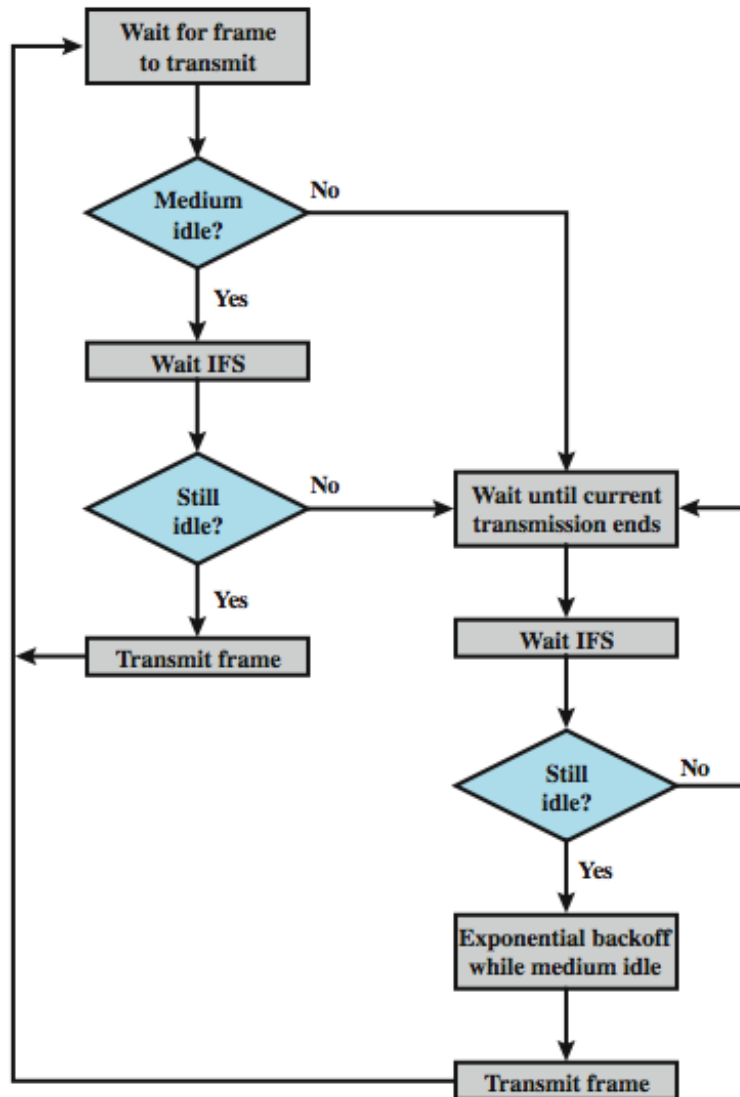


Figure 31: IEEE 802.11 Medium Access Control Logic [14, p. 528]. All clients will check the medium to see if it's idle before attempting to transmit in order to avoid collisions.

A client attempting to transmit will first check if the medium is being used. If it is clear, it will wait one IFS and check the medium once more before transmitting a frame. If the medium is busy, it will wait until the transmission ends (the duration is usually announced beforehand by the transmitting client), then it will wait one IFS before checking the medium again. If the medium is still busy, it begins counting a random backoff counter.

A common problem in early wireless technology was the “Hidden Node,” illustrated in Figure 32. Nodes A and B can communicate with each other, as well as B and C, but node A cannot

communicate with node C. Both nodes A and C have no way of knowing if the other is transmitting, and if both transmit to node B at the same time, their transmissions will collide.

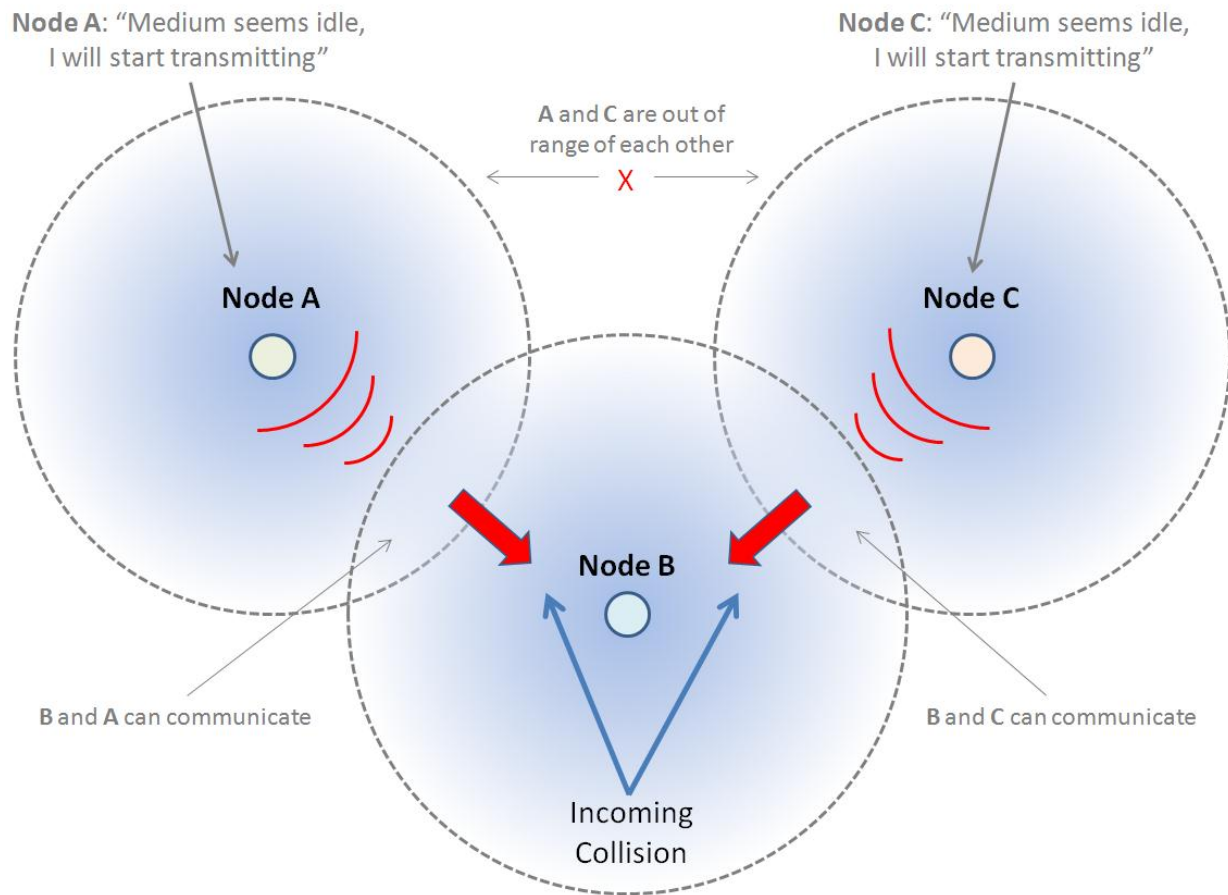


Figure 32: Hidden Node Problem: Nodes A & C cannot hear each other and attempt to transmit to Node B at the same time, causing a collision in the receiver of Node B.

The solution to this problem is Carrier Sense Multiple Access / Collision Avoidance (CSMA/CA). This involves sending a “Request to Send” (RTS) and “Clear to Send” (CTS) notification before sending and receiving transmissions, shown in Figure 33. In the above scenario, if node A attempts to transmit to node B, it first sends a RTS packet. Then, if node B is available, it will send a CTS packet containing the duration of the transmission, giving permission for node A to continue. Node C will then hear the CTS packet and wait until the end of the transmission.

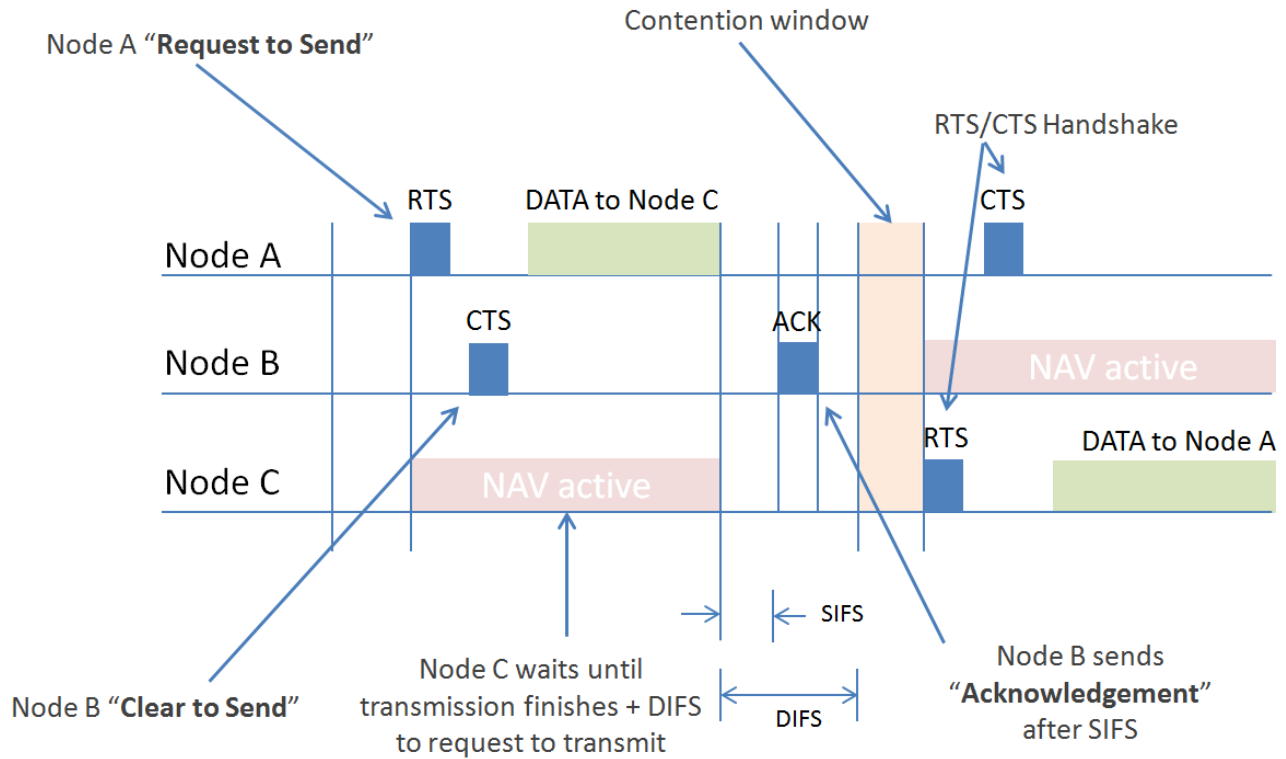


Figure 33: Implementation of the RTS/CTS mechanism in 802.11 with NAV activation, SIFS/DIFS interval, and contention window [28, p. 462].

The 802.11 MAC layer also has a number of management/control fields to handle mobility, registration, power, and security. Management and control frames are often the target of wireless attacks. Wireless attacks on ad-hoc networks at the MAC layer partially stem from the problem of negotiating access to and control of the channel with users or clients that are not necessarily listed or pre-accounted for.

Different types of jamming and attacks

Jamming causes a disruption of communication between clients either by denying access or corrupting information. Several types of attacks exist against the 802.11 framework. Those pertaining to this experiment are divided into PHY and MAC categories and listed according to the general amount of intelligence required in Figure 34. Most PHY layer jamming is an effect of raising the background (thermal) noise such that it effectively disrupts synchronization, tracking, and transmissions between clients [31].

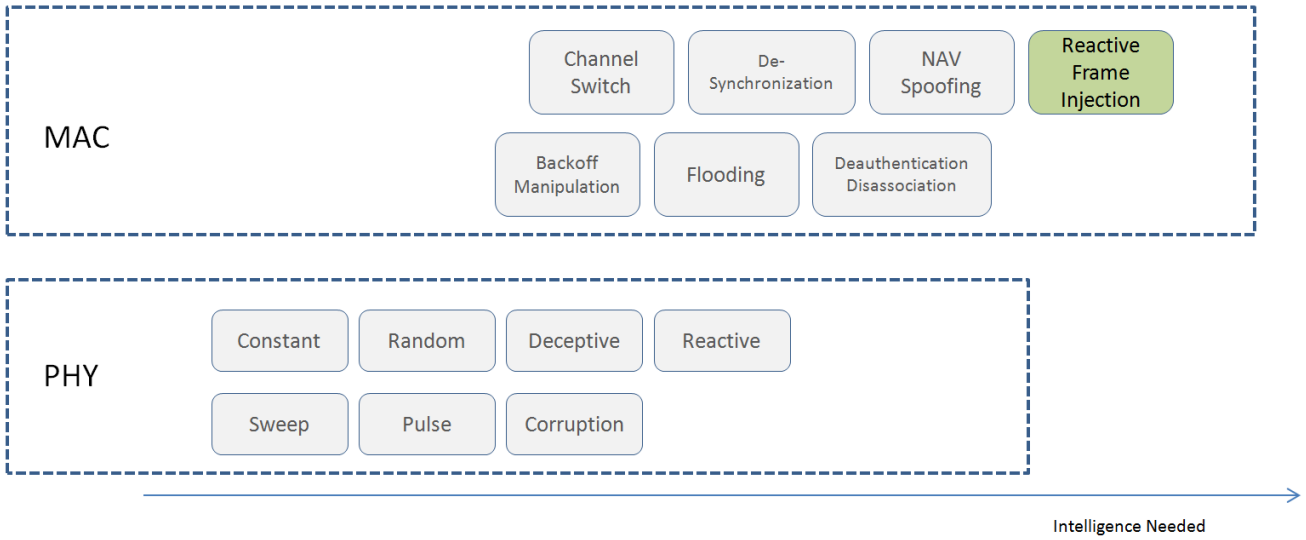


Figure 34: Jamming Attacks at MAC & PHY Layer. Techniques are listed by intelligence required.

A short list of PHY layer attacks (Table 4) consists of RF Jamming using noise (typically Additive White Gaussian Noise [AWGN]) as a sweep, random bursts or pulses, or even modulated data using Differential Binary Phase Shift Keying (DBPSK). Modulated (deceptive) noise imitates a signal that contains information, often forcing the receiver to spend time and energy decoding the signal. MAC layer attacks, listed in Table 5, are more complex and require some knowledge of the network. Jamming methods at higher layers (MAC and above) typically require intelligence gathering before commencing an attack.

Table 4: PHY Layer Jamming Definitions.

Name	Definition
Constant	Continuous jamming with AWGN.
Sweep	Continually jamming, typically with a single carrier tone, in a sweep pattern across a range of frequencies.
Deceptive	Modulating noise to appear as though it contains information.
Random/Pulse	Transmitting signals at random intervals to save power and avoid detection.
Reactive/Corruption	Jamming for short durations to destroy packets when a transmission is detected.

Each technique in Table 4 has its own advantages and disadvantages. For example, constant jamming requires the most power, but will completely prevent communication in the target area, especially when using directed antennas. Most PHY layer attacks do not discriminate between friends and foes, but MAC layer attacks have the potential to selectively target clients. A short list of attacks relative to this report is defined in Table 5.

Table 5: MAC Layer Jamming Definitions.

Name	Definition
Deauthentication/Disassociation	Spoof (fake) frames that force clients to disconnect from each other.
Backoff Manipulation	Fooling a receiver to increase the time spent waiting to avoid collisions.
NAV Spoofing	Cause other clients to wait until the channel is busy by sending fake CTS/RTS messages.
Channel Switch	Fooling or causing a transmitter to switch channels unnecessarily.
De-synchronization	Altering time stamps in management frames in order to cause de-synchronization at the receiver.
Flooding	Sending many (thousands or more) of beacons or association requests in order to overflow the association table.
Reactive Frame Injection	Injecting malicious information into management frames on rate, encryption, channel, and association, immediately after the target's frame.

Unlike PHY layer jamming, the effectiveness and efficiency of MAC attacks vary depending on the protocol used by the target. The techniques in Table 5 are specific to 802.11b/g, but can occasionally be applied to other existing protocols, which is why some ‘intelligence gathering’ is necessary with higher layer attacks. One of the most effective techniques is a deauthentication or disassociation attack, which constantly spoofs frames that disconnect you from other nodes, making communication near impossible. However, effectiveness does not always imply

efficiency, an important parameter in ad-hoc networks, as they are usually mobile and rely on battery power. A chart which categorizes several of the above listed attacks is shown in Figure 35. Note that this chart is subjective generalized; any PHY jammer can be made 100% effective with enough power, and any MAC layer attack can prove more effective depending on the protocol and hardware used in the network.

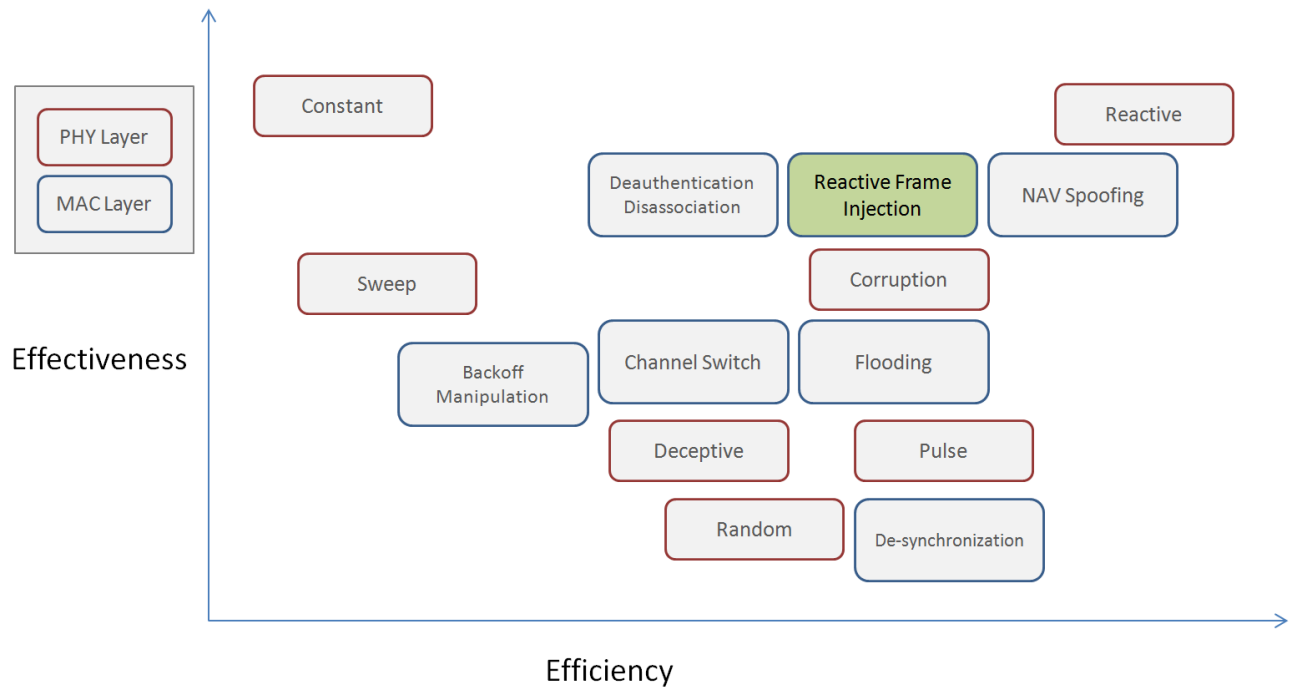


Figure 35: Chart of Effectiveness vs. Efficiency of PHY (RED) and MAC (BLUE) layer attacks. Note: All attacks are subjective.

PHY layer attacks are inherently more effective, as they prevent the most basic use of a medium, but are typically less efficient. Constant jamming is the least efficient as it consumes the most power and involves unceasing transmission. An exception is reactive jamming, which involves transmitting a small burst of noise when an on-going transmission has been detected, and is considered one of the most efficient methods of RF jamming. Unlike some naïve PHY jamming techniques which are not very efficient (constant, sweep, random, pulse), MAC attacks have the potential to substantially decrease effective throughput using far less energy.

NAV spoofing is slightly less efficient and effective since it has to repeatedly spoof CTS/RTS frames, and cannot destroy other packets. We propose that the reactive frame injection method will be of the same efficiency of NAV spoofing, since it will transmit with similar periodicity.

However, reactive frame injection could prove more effective than NAV spoofing, since it has the power to selectively silence communications, whereas NAV spoofing can only silence all clients in the area except one node.

3 Methods

As previously discussed, this project is composed of two distinct, but closely related, parts: testbed construction and a Wi-Fi denial of service attack on that testbed. Both components are equally important and dependent on each other. The testbed provides a mechanism to test the team's proposed MAC layer Wi-Fi attack while the well known PHY layer jamming attacks provide the team with a way to validate the testbed. In this chapter, the team will explain the process of developing, executing, and testing/validating the different key components of this project. This will include a description of the testbed design process and the techniques use to perform preliminary testing. The team will also cover the techniques used to perform PHY layer jamming, starting off the testbed to create a point of comparison and then moving to the testbed to confirm testbed functionality. Lastly, the team will discuss the development and execution of the MAC layer attack performed on the testbed.

3.1 Channel Emulator Design Process

Before settling on a final design for the channel emulator portion of the testbed, the team explored some preliminary ideas. Ideas were based upon the original specifications provided to the team by mentors at MIT Lincoln Laboratory. These specifications included:

- Wideband (30MHz – 8GHz)
- Support for 6 radio nodes
- Isolation no less than 20dB between fingers of splitters
- No more than 45dB of loss throughout the system
- No more than 2dB of variation in loss between the different paths through the system
- Attenuators switch within 1ms timing

Although the original design ideas were not ultimately the chosen solutions, they played an important role in the design process. Evaluating the pros and cons of these initial designs led the team to the final channel emulator design that best met specifications.

Original Design Ideas and Assessment

Prior to commencing any detailed design, the team constructed a very basic outline of the channel emulator and its key components. Figure 36 below is a visual summary of the basic channel emulator structure with its most fundamental components.

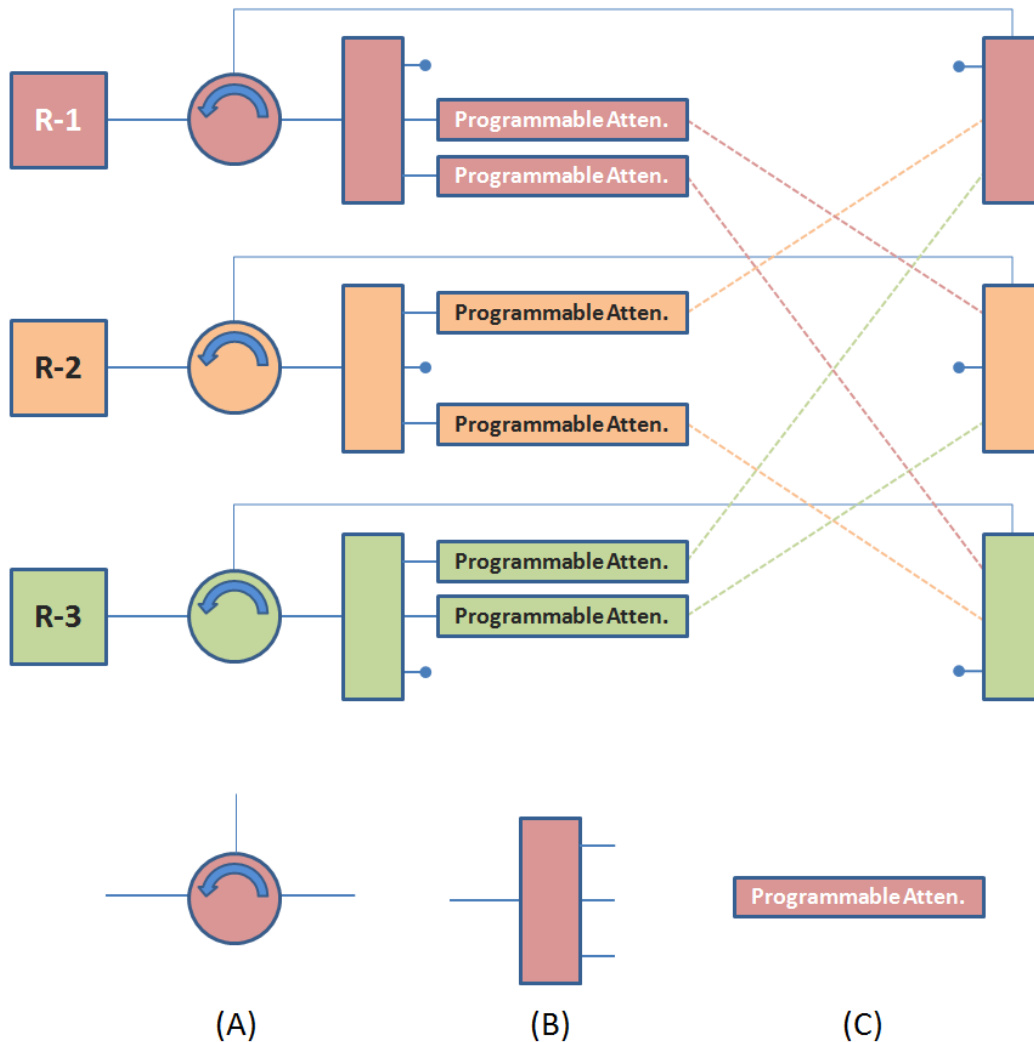


Figure 36: Basic structure of analog channel emulator with key parts (A) Circulator (B) Power Splitter/Combiner and (C) Programmable Attenuator. This diagram shows a channel emulator that supports only three radio nodes.

This design schematic is a scaled down channel emulator that supports three radios, although the same concepts in this design can be scaled up to support more nodes. In the schematic, each of the three radios is connected to a circulator, Figure 36 (a), which allows the radio to transmit and receive simultaneously. The transmit path connects to a power splitter, Figure 36 (b), which divides the power from each radio three ways. Two of the three RF paths created by the splitter

connect to a programmable attenuator, Figure 36 (c), which allows the user to control the magnitude of the signal sent from each radio to all of the other radios. The remaining RF path, which does not connect to an attenuator, can either be terminated with a 50Ω load or can be sent to an oscilloscope or spectrum analyzer.

A second set of three-way splitters recombine signal power from two of the radios and send it back to the receiving port of the circulator. In summary, the fundamental channel emulator design was found to need three important key parts or functions: circulators to provide isolation between TX and RX, splitters/combiners, and programmable attenuation.

With the important functions of the channel emulator determined, specific parts to perform these key functions were selected. Because the specifications are for a six radio channel emulator, the splitters need to be six-way, unlike in Figure 36, where the splitters were three-way to support a three radio channel emulator. Considering the specifications, the team put together two different lists of parts for two different design schemes. Both designs use a Hittite Microwave programmable attenuator (HMC-C018) that works from DC to 13GHz and provides attenuation from 0 to 31.5dB in steps of 0.5dB.

When programmed to the 0dB attenuation state, this attenuator has an insertion loss of 4dB. Both designs also involved a more narrowband circulator, on hand in the laboratory, which could be switched out for a more permanent wideband solution later on. The design ideas differed in their implementation of the six-way splitter.

The first design scheme creates the six way splitters out of one two-way resistive power splitter (Mini-Circuits ZFRSC-123+) cascaded with two three way splitters (Mini-Circuits SF3RSC-542+). A diagram of the composite six-way splitter is shown below in Figure 37.

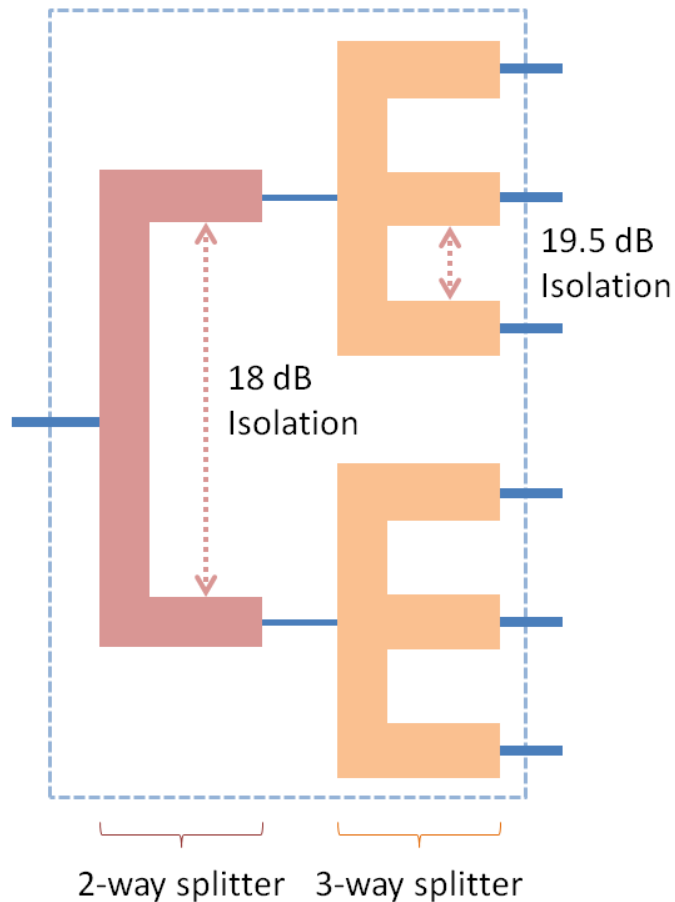


Figure 37: Six-way splitter composed of cascaded two and three-way splitters. This design was not ultimately used because it was too lossy.

Isolation between the fingers of the different splitters, as described on the data sheet, is shown in Figure 37. The two-way splitter has an isolation of 18dB between fingers of the splitter while the three way splitter has isolation of 19.5dB. While the isolation in this splitter is relatively close to the specifications, it is extremely lossy, with 10dB in each two-way splitter and 20dB in each three way splitter. When a radio transmits, the power goes through the circulator, the cascaded splitters, back through a different set of cascaded splitters, and finally back through the circulator again. The total loss due to travelling through the six way splitters alone is 60dB. This is far above the given 45dB specification for loss throughout the system. In addition, the 6 way splitter only supports a bandwidth of DC - 5.4GHz which falls short of the bandwidth specification.

The second design idea involved cascading five two-way power splitters (Mini-Circuits ZX10R-14+) to create the six way splitter/combiner. These splitters have less loss, specifically 7.5dB per two-way splitter and 45dB total for the two six-way splitters created by cascading them, but this is still too much.

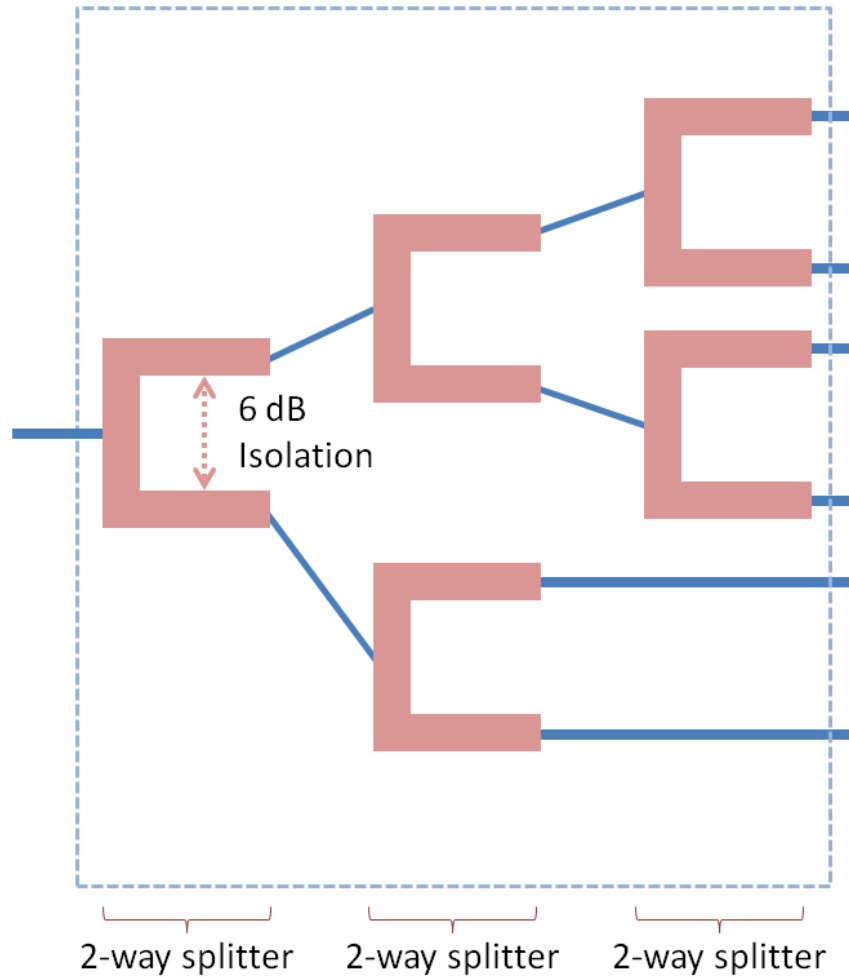


Figure 38: Five two-way splitters cascaded to create a six-way splitter. This design was not ultimately used because it did not provide enough isolation.

While the second design idea supports the full specified band, the two way splitters only have 6dB of isolation between the fingers of the splitters, as shown in Figure 38. This is substantially lower than the specified isolation. The limitations of these two original design ideas are summarized in Table 6.

Table 6: Design attempts for RF channel emulator. The two original design attempts did not meet specifications.

	Specifications	Design Attempt 1	Design Attempt 2
Parts		<ol style="list-style-type: none"> 1. Programmable attenuator (Hittite HMC-C018) 2. Two-way power splitter (Mini-Circuits ZFRSC-123+) 3. Three-way power splitter (Mini-Circuits ZF3RSC-542+) 4. Circulator (RFLC-301-4) 	<ol style="list-style-type: none"> 1. Programmable attenuator (Hittite HMC-C018) 2. Two-way power splitter (Mini-Circuits ZX10R-14+) 3. Circulator (RFLC-301-4)
Bandwidth	30MHz – 8GHz	DC – 5.4GHz	DC – 10GHz
Isolation	20dB	18dB (minimum)	6dB
Total System Loss	45dB	65dB	50dB

In summary, the original ideas both failed to meet specifications. The first design attempt had almost enough isolation but too much loss and did not cover the desired bandwidth. The second design attempt contained less loss than the first plan but still too much, and, while it covered the full band, it had far too little isolation. Learning from these first passes at the problem helped the team produce the final design.

Final Design

Due to the difficulty meeting the system specifications for such a wide bandwidth, the team decided to employ band breaks in the system. Distinct sets of parts are used to support the lower and upper portions of the frequency band. Based upon a review of available parts, the team decided to have the lower frequency band support 30MHz to 3GHz and the higher frequency band support 2 to 8GHz, with an overlap from 2 to 3GHz. Diplexers could be used to direct signal of different frequency content through the two different channels of the channel emulator. Due to the early difficulties finding resistive power dividers that could provide the desired isolation and frequency coverage without too much loss, the team decided to use cascaded

directional couplers to perform the same function. A diagram showing the design of the four-way splitter formed by cascading three couplers is shown in Figure 39.

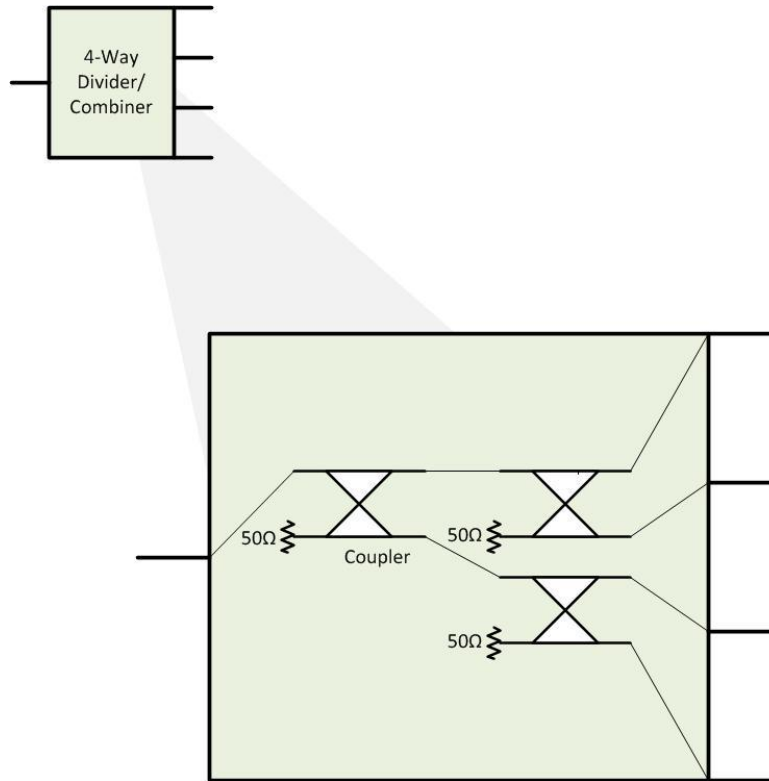


Figure 39: Four-way splitter created from three cascaded couplers. This design is not very lossy and provides enough isolation between paths.

Couplers typically have much higher isolation with less loss and the team was able to find two different couplers to support the two frequency bands. The team selected a circulator by DiTom Inc. to support the 2 to 8GHz band with an amplifier followed by an attenuator pad to provide isolation for the 30MHz to 3GHz band. The same Hittite attenuator is used in the final design.

Table 7 shows the parts selected for each of the two frequency bands.

Table 7: The channel emulator was channelized into two separate frequency bands, 30MHz - 3GHz and 2 - 8GHz, with two separate sets of parts.

Frequency Range	Splitter	Circulator	Programmable attenuator
30MHz – 3GHz	180° hybrid coupler (MACOM H-183-4)	Amplifier (unselected)	0 – 31.5dB (Hittite HMC-C018)
2GHz – 8GHz	180° Hybrid Coupler (Krytar model 4020080)	Circulator (DiTom D3C2080)	Same as above

Because the couplers that support the 30MHz to 3GHz frequency band have a 12 week lead time and the duration of the MQP is only nine weeks, the team chose to focus on building the 2 to 8GHz portion while providing plans for later implementation of the lower frequency band. The design shown in Figure 40 is the 2 to 8GHz 4 radio channel emulator that the team decided to focus on during the seven week MQP.

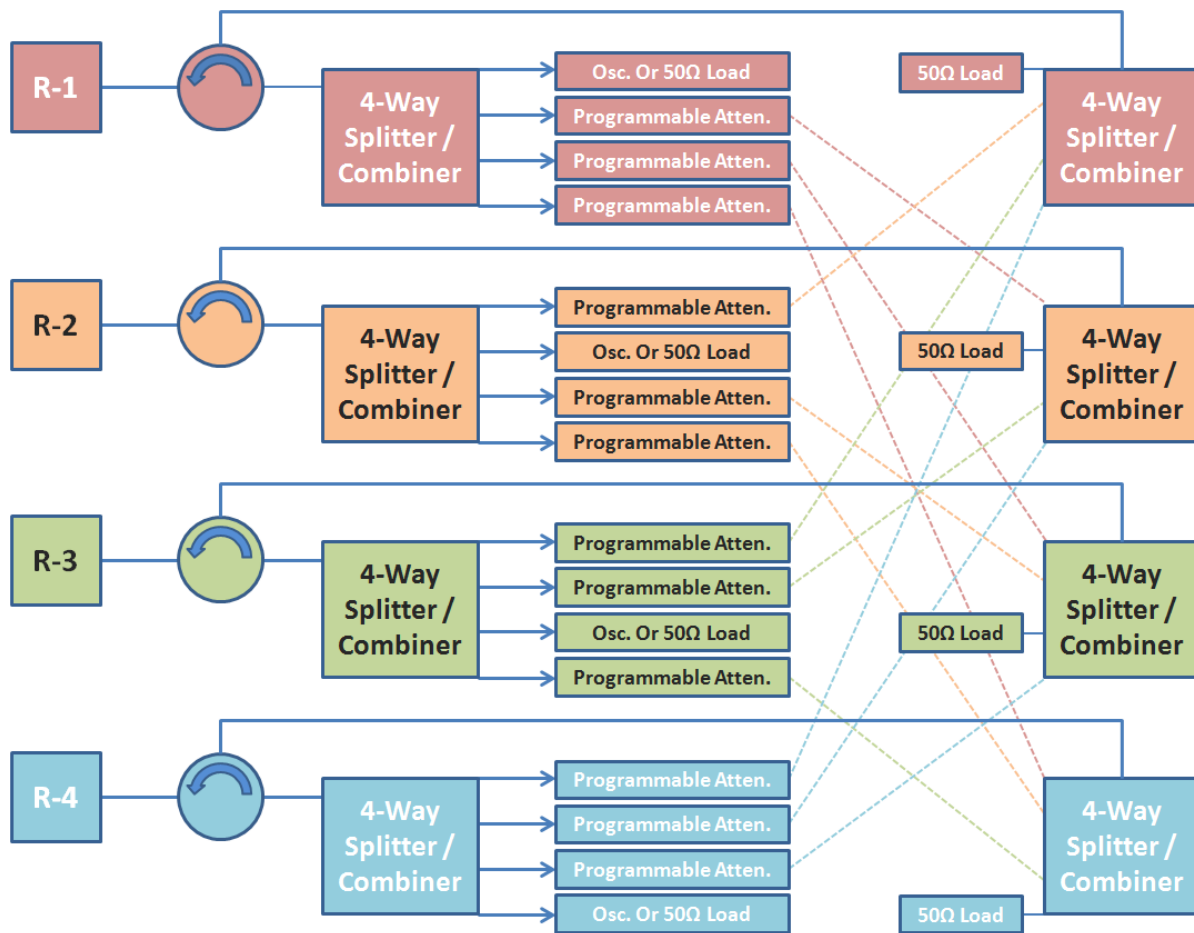


Figure 40: The team decided to focus on a four node channel emulator that works from 2 to 8GHz. Each 4-way splitter/combiner is composed of three cascaded couplers.

In addition, the team chose to start by ordering enough parts for a four radio channel emulator. Time allowing, this channel emulator could be scaled up to support more nodes.

3.2 Attenuator Control

Controlling attenuators in the channel emulator in order to emulate changing radio geometries was an important aspect of the channel emulator design. Design specifications call for

attenuators to be able to switch, as a group, within a millisecond or less. The chosen attenuator, Hittite's HMC-C018, is capable of switching at this speed or faster. This specific attenuator has four digital inputs (clock, reset, serial input, and latch) and requires a negative five volt power rail and ground. Due to availability, a National Instruments PCI card (NI 6601) with digital I/O was selected to serve as the control interface. Digital signals from the card were routed through a National Instruments SCB-68 breakout board and to a breadboard where the attenuators were connected. Originally, the team planned to control the cards using MATLAB. During assembly and testing of the attenuator control circuit, a number of problems arose and were addressed, ultimately leading to the final design.

In order to emulate a moving configuration of radio nodes, radio separation is represented with meaningful attenuation values. A MATLAB function was written to calculate attenuation values between all node pairs at certain time intervals based upon the start location of each radio, the stop location of each radio, and the duration of the experiment in seconds. The attenuation values calculated by this function are converted to a bit pattern to be written to the PCI card. Originally the team intended to use MATLAB to write digital words to the card but this method was found to be too slow for the speed specification. To address the speed concern, the bit pattern produced in MATLAB was written to a text file. A C program reads the text file line by line and writes each line to the PCI card.

While the PCI card was able to write values to the attenuators at an adequate speed (approximately 40KHz), voltage overshoot on the different lines was found to be substantial. The clock line had ringing as much as three volts above the five volt logic high and as much as 2 volts below zero on the falling edge. These values exceed maximum ratings for the data pins of the attenuators. In order to address ringing, a ringing suppressant circuit was added at the end of each data line on the bread board. This circuit is shown in Figure 41 below.

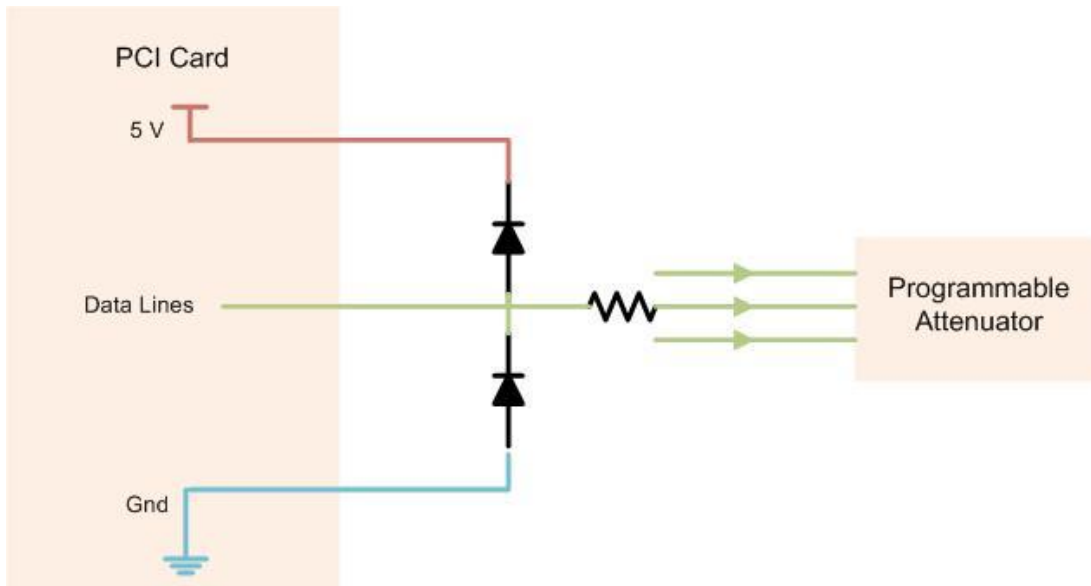


Figure 41: Original ringing suppressing circuit with PCI Card (Left) and Programmable Attenuator (Right). This circuit worked well enough when there were fewer attenuators.

When the data line goes high, the lower diode goes into reverse bias and the drop across the upper diode goes to approximately zero. The diodes help to clamp down on overshoots in the digital signal and the resistor dampens the ringing even further. While this circuit slows the rise and fall times, it did not appear to negatively impact the functionality of the attenuator.

Further challenges were encountered in scaling up the setup to support additional attenuators. Initially, the design involved supporting multiple attenuators with a shared clock, latch, and reset pin because these pins are the same for all of the attenuators. It is the serial input that determines each attenuator's unique value so every attenuator has a distinct serial line. However, a single clock, latch, and reset pin were found to be insufficient to support more than two attenuators reliably. This is most likely due to a considerable voltage drop across the large resistor used to dampen ringing. In response to this issue, more clock, reset, and latch lines were broken out from the card such that each line supports no more than two attenuators. The additional clock lines remedied the power issues but increased ringing in all of the other signal lines. Ringing in many of the latch lines occurred whenever the clock switched states, sometimes causing the attenuator to latch a new value. To resolve this problem, a new ringing suppressing circuit was designed. This circuit is shown in Figure 42.

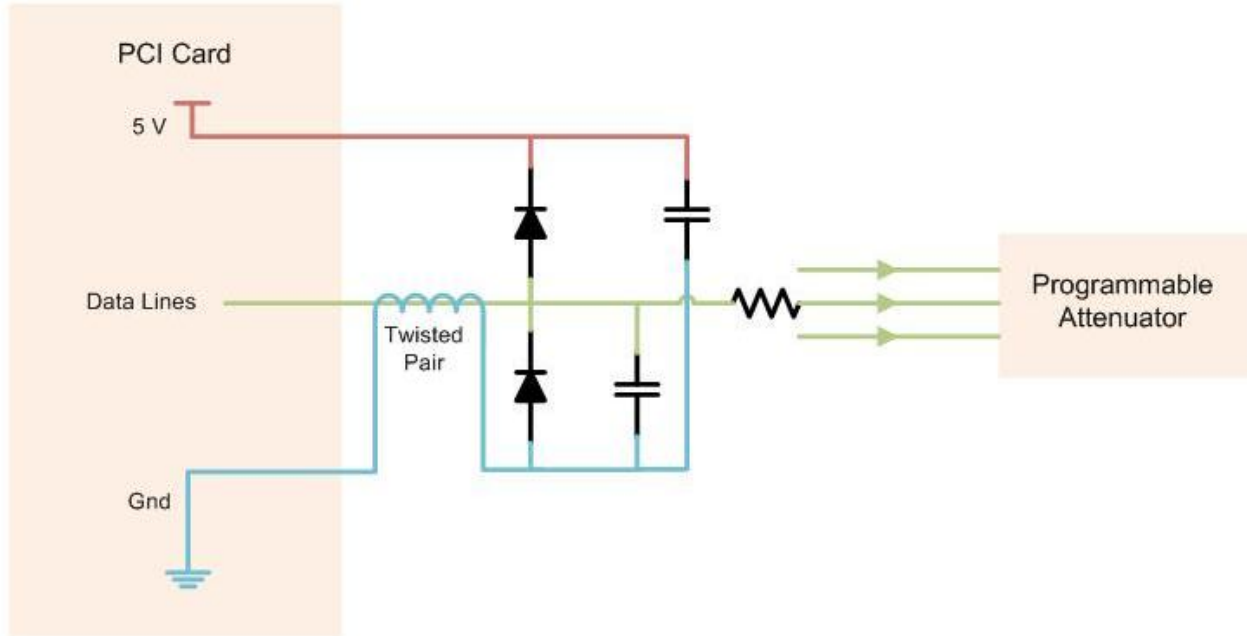


Figure 42: Final ringing suppressing circuit with added buffer capacitors placed within close proximity to data lines, and twisted pair cables (paired with GND) for each data signal. Note: Twisted Pair cable is not an inductor.

In addition to suppressing the ringing with the circuit shown in Figure 42, other precautions were taken to ensure the integrity of the digital lines. All alike lines were grouped together to minimize the exposure of lower frequency signals like the latch to ringing caused by higher frequency signals like the clock. Also, each signal line was twisted with a ground from the breakout board as suggested by the PCI card datasheet. These precautions in combination with the new ringing suppressing circuit worked well and are part of the final design. Once the system that drives the attenuators was completely designed, attenuators were added to the system one by one and tested individually to ensure functionality. With the final design of the channel emulator was determined, the team selected several techniques for testing individual parts and then the channel emulator as a whole. These methods will be discussed in the subsequent section.

3.3 Channel Emulator Construction and Preliminary Testing

In order to verify the functionality of each individual component in the channel emulator as well as the system as a whole, the team conducted a variety of tests. S-parameter measurements were collected for individual parts and for the assembled system. Two-tone testing was used to measure the linearity of attenuator and assembled channel emulator. Finally, the rise and fall

time of the attenuator transitioning between different attenuation states was measured. The techniques used to perform these various tests will be described below.

An Agilent E8364C PNA Network Analyzer was used to measure the s-parameters of all of the parts individually. In instances where many of the same part were used, with the exception of the attenuators, several parts were randomly selected and measured to assess the degree of variability across the parts. Measurements were saved as .s2p files and processed in MATLAB. These s-parameter measurements were used to produce graphs showing the insertion loss of each component across the 2 to 8GHz frequency band. Attention was also paid to the isolation between the -3dB ports of the coupler and the accuracy and flatness of the different attenuator states throughout the complete frequency range. In order to collect this data, each attenuation state was programmed into the device and then s-parameter data was collected. In addition, return loss (S11) was measured for all of the different components and then for the system as a complete unit. System gain was also measured.

Additional tests were performed on the assembled system beyond just those performed using the network analyzer, including a two tone test and a measurement of rise and fall time in the attenuator. One of these tests was a two tone test to measure the third-order intercept point of the device. This is a measurement to determine the degree of nonlinearity in a system. In a two-tone test, two sinusoids of equal power, approximately a megahertz apart, are fed into a system. The setup we used is shown below in Figure 43.

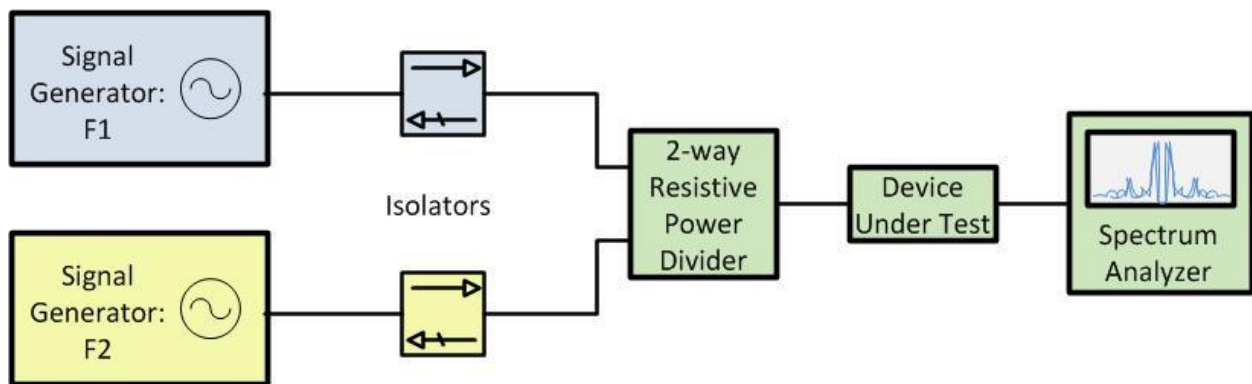


Figure 43: Two-tone test setup. From left to right: Signal Generators, Isolators, Power Divider, Device Under Test (DUT), Spectrum Analyzer. The two-tone test helps to identify third order nonlinearities of a RF device.

The circulators shown in the diagram, with the third port terminated in a fifty ohm load, are used to increase isolation between the two branches of the power splitter. The splitter combines the two sinusoids and feeds them into the device under test, the attenuator. The output of the attenuator is fed to a spectrum analyzer which is used to measure the third-order intermodulation products of the two sinusoids. Care was taken to ensure that the intermodulation products originated in the attenuator rather than in the front end of the spectrum analyzer itself. If the first fundamental tone is at frequency F_1 and the second tone is at frequency F_2 then the two third-order intermodulation products are at:

$$F_{3o1} = 2F_2 - F_1 \quad [Hz] \quad (3.1)$$

$$F_{3o2} = 2F_1 - F_2 \quad [Hz] \quad (3.2)$$

If the test is set up properly, the third-order intermodulation products should be approximately the same. In order to calculate the third-order intermodulation distortion IMD_3 , the power measured at the third-order intermodulation products P_{o3} is subtracted from the power P_o at one of the fundamental tones [34]:

$$IMD_3 = P_o - P_{o3} \quad [dB] \quad (3.3)$$

The output third-order intercept point is defined as

$$OIP_3 = \frac{IMD_3}{2} + P_o \quad [dB] \quad (3.4)$$

The input third-order intercept point IIP_3 is simply the output third-order intercept point OIP_3 minus the gain G in the device.

$$IIP_3 = OIP_3 - G \quad [dB] \quad (3.5)$$

The results of this test were used to confirm the values provided on the attenuator data sheet. After testing each individual part and the testbed system as a whole, the team further validated the testbed by executing a series of known PHY layer attacks using the testbed.

3.4 PHY layer jamming

PHY layer jamming involves creating RF noise, pulses, or tones, with enough power to cause errors in transmission at the receiver. A logical approach to recreating and validating proven PHY layer jamming techniques involved replicating and comparing results to other, repeatable experiments in literature. Available resources limited the selection of these experiments, and although exact replication was not possible, similar procedures and equipment were used. A list of the equipment used is shown in Table 8.

Table 8: List of equipment used in PHY layer attacks by name, model, and specifications.

Device	Model	Specifications
Signal Generator (Jammer)	HP 83622A – HP Synthesized Sweeper	2 – 20GHz
USRP (Jammer)	USRPN210	2.4 – 2.5GHz
Gumstix Computer/Radio	Gumstix Overo Fire COM	Wi-Fi 802.11b/g
Circulator	D3C2080 – DITOM SMA Circulator	2-8GHz
Power Meter	E4419B – Agilent EPM Series	
Signal Analyzer	N9010A – Agilent EXA Signal Analyzer	9KHz – 26.5GHz
DC Power Supply	E3610A – HP DC Power Supply	0-15 V, 0-3 A
Attenuator Pad	(Various) Weinshel Engineering	3-20dB
RF Cables		SMA

Most jamming methods are aimed at the receiver; hence this experiment will focus primarily on the receiver’s ability to maintain throughput despite interference. The parameters used with each type of jamming signal are described in the following section.

The signals listed below are created primarily with a USRP using GNURadio. Due to the hardware limitations of the USRP (mainly, speed and bandwidth), a noise or signal generator was used in creating large bandwidth signals and pulsed noise.

- **Digital** Noise Jamming
 - BPSK modulated pseudorandom data at 20 M samples/second using USRP & GNURadio
- **Pulse** Noise Jamming
 - AWGN Noise pulsed with pulse lengths of 100 μ S – 1000 μ S and pulse intervals of 1 mS to 10 mS.
- **Sweep** Tone Jamming
 - A single sine wave swept across the 2.4GHz Wi-Fi band (100MHz) in 0.5 to 20 seconds.

Validating the Testbed against Previous Experiments

Conducting experiments on a two-radio network allowed efficient use of time while waiting for equipment to arrive (digital attenuators and couplers) while partially validating the procedure and equipment against previous experiments in the literature [7], [35]. This also helped to prepare and refine any methods used for the final experiment involving mobility, described in section 3.3.2. After all equipment had been prepared and assembled, our team implemented identical tests on a three-radio (four nodes total) network before proceeding to mobile scenarios.

The two-radio network included two radio nodes, a jammer node, and a signal analyzer, shown in Figure 44. The radio nodes consist of individual Gumstix computers, each with their own Wi-Fi enabled 802.11b/g radio with external u.FL connectors (miniature coaxial RF connectors). Special u.FL adapters were required to connect each radio to the SMA cables used in the experiment. The jammer node was either a USRP or a signal generator depending on the experiment. A signal analyzer measured the power level of the signal from the transmitter compared to the signal from the jammer, also known as the *Signal to Jammer Ratio* (SJR).

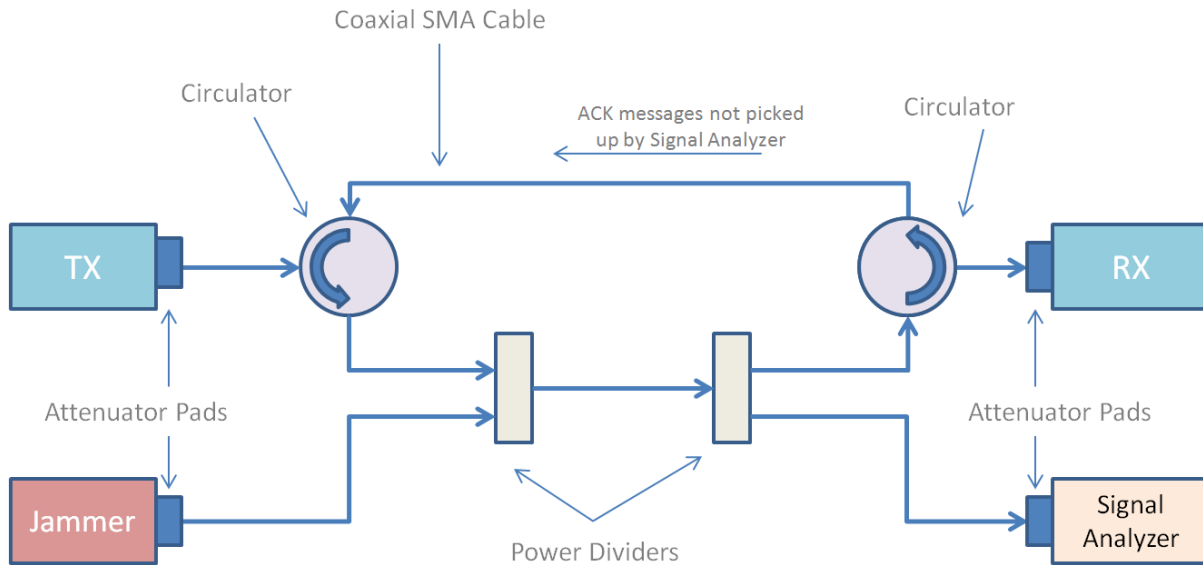


Figure 44: Two Radio Network consisting of Attenuators, Circulators, and Power Dividers. Radios are Gumstix computers with Wi-Fi 802.11b/g. Jammers used are: USRPN210, Signal Generators, or Noise Generators.

Circulators prevented ACK message interference at the signal analyzer. Otherwise, the signal analyzer would report high signal levels that originate from the *receiver*, inadvertently affecting perceived SJR. Coaxial SMA (Sub-Miniature Version A) RF connectors were used to connect each device. Software control of each radio’s transmit power was not possible, thus Attenuator pads were used to achieve desired signal levels in the receiver (-45 to -50dBm).

One power divider (left) combined the transmit signal and the jammer signal. The other power divider (right) separated the signal, one path leading to the signal analyzer and one path leading to the receiver radio. Attenuation for each device was recorded, in addition to verifying frequency response in the desired 2.4GHz band.

Mobile PHY Layer Jamming on the RF Channel Emulator

One of the more important criteria to an analog channel emulator is realism. For the same purpose, this project includes a mobile scenario where all nodes can vary their (virtual) distance between each other. Their connections to the RF channel emulator are simplified in Figure 45.

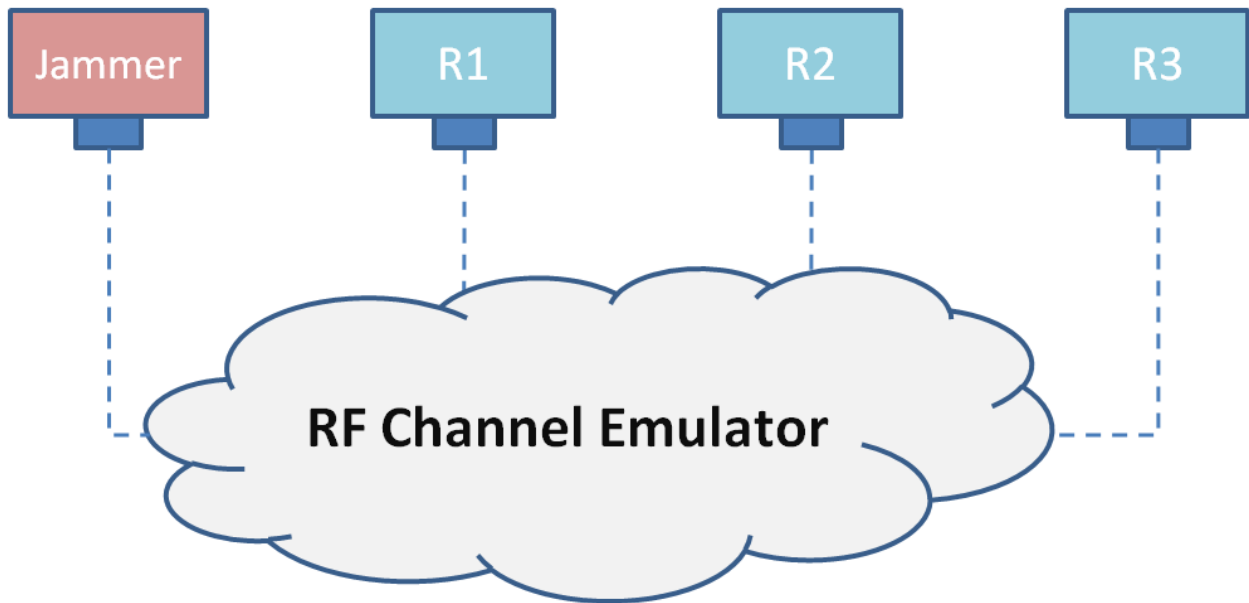


Figure 45: Simplified diagram of connections between radio nodes and RF Channel Emulator. Each node can vary their distance between every other node.

The “RF Cloud” is a layer of abstraction controlled by digital attenuators that emulate distance, allowing the experiment to demonstrate the effectiveness of a denial of service attack in a mobile scenario. This layer of mobility allows the testbed to take one step closer to real-life. There are a number of interesting mobile scenarios that are useful demonstrations of how well the DoS attack would work, although only three are chosen for this report.

Listed in the following section are three mobile scenarios where the jammer is moving towards or away from the network. In each experiment, the jammer node moves toward the network at a rate of approximately 2 meters/second, passes within 3 meters of the closest radio node, and continues through towards the end point. Iperf is used to exchange traffic at 11 Mbit/s using 802.11b (DSSS).

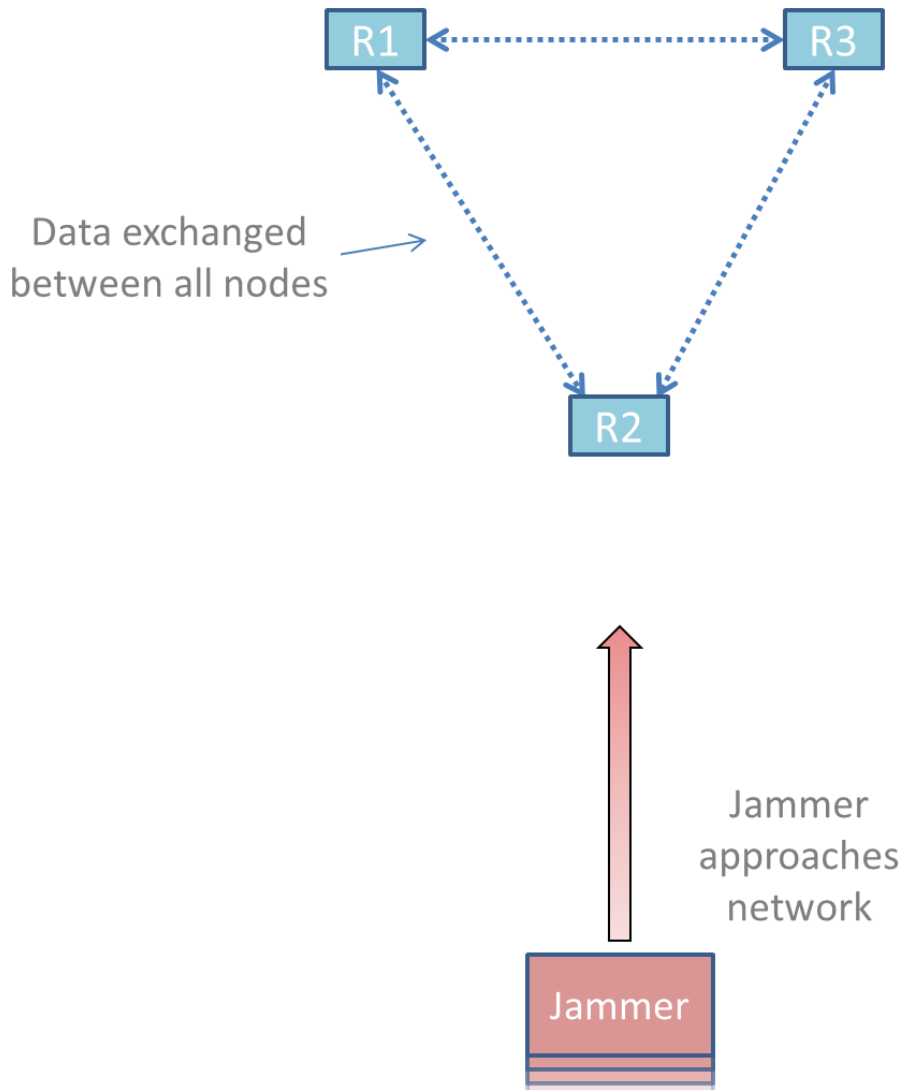


Figure 46: Equidistant node topology. All nodes are the same distance from each other and can exchange data with all other nodes. The jammer will approach the network at a rate of 2 meter/sec.

All nodes in this experiment are stationary and can exchange data at the same rate. A jammer moving toward this network would mimic a scenario in which there are local, neglected Wi-Fi emitters (R1, R2, and R3) in an uninhibited, equidistant topology. Figure 47 depicts a realistic scenario of this situation.

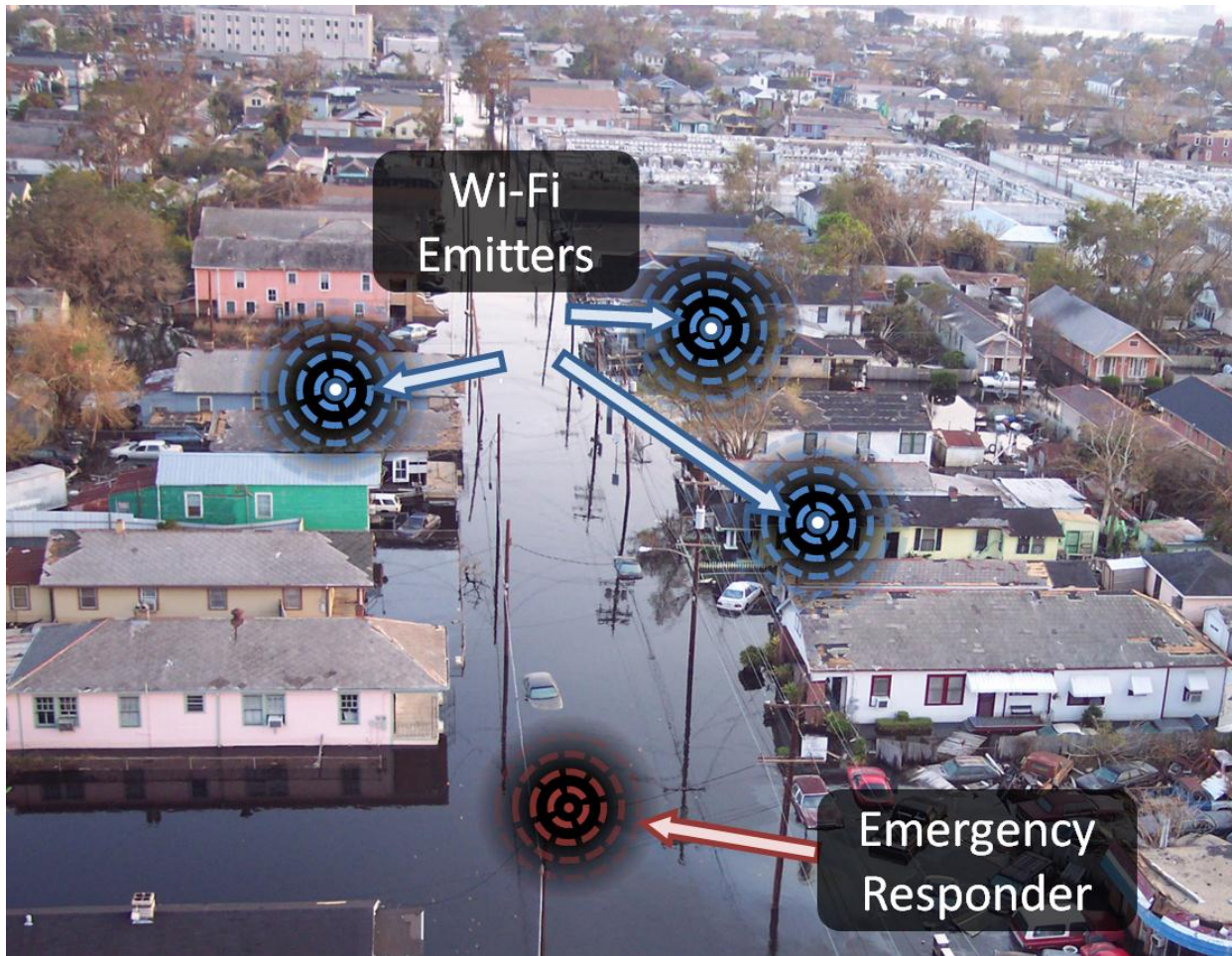


Figure 47: Realistic picture of Wi-Fi scenario. Three Wi-Fi emitters (Blue) within 15 meters of another. All (Blue) nodes can exchange data at the same rate. The Emergency Responder (Red) approaches the network and passes through while attempting to regain spectrum. Note: not to scale.

Figure 47 is a picture taken immediately after Hurricane Katrina passed through in New Orleans. A hypothetical emergency responder would drive through on a boat and attempt to regain network resources from the Wi-Fi emitters. Note that this picture does not indicate exact distance, nor does it represent the maximum effective distance of the Wi-Fi signals. For a more specific geometric reference, refer to Figure 48.

The attenuation associated with the RF channel emulator, in addition to insertion loss, has a dynamic range of 20dB to 51.5dB. With respect to FSPL, this translates into a distance of 1-3 meters that the network can emulate. To represent realistic scenarios, attenuator pads were added to each radio, contributing to a range of 50dB to 81.5dB, or a distance of 3-120 meters

(range varies with each antenna, but the maximum range of Wi-Fi 802.11b/g in indoor environments is typically less than 100 m [36]).

In other words, each radio cannot “move” (programmable attenuators emulate mobility) further than 120 meters or closer than 3 meters from another node. Figure 48 uses Google Maps to illustrate the Equidistant node scenario shown previously, where the emergency responder is at most 100 meters away from the furthest node, and at least 3 meters from the closest node, at any one time.

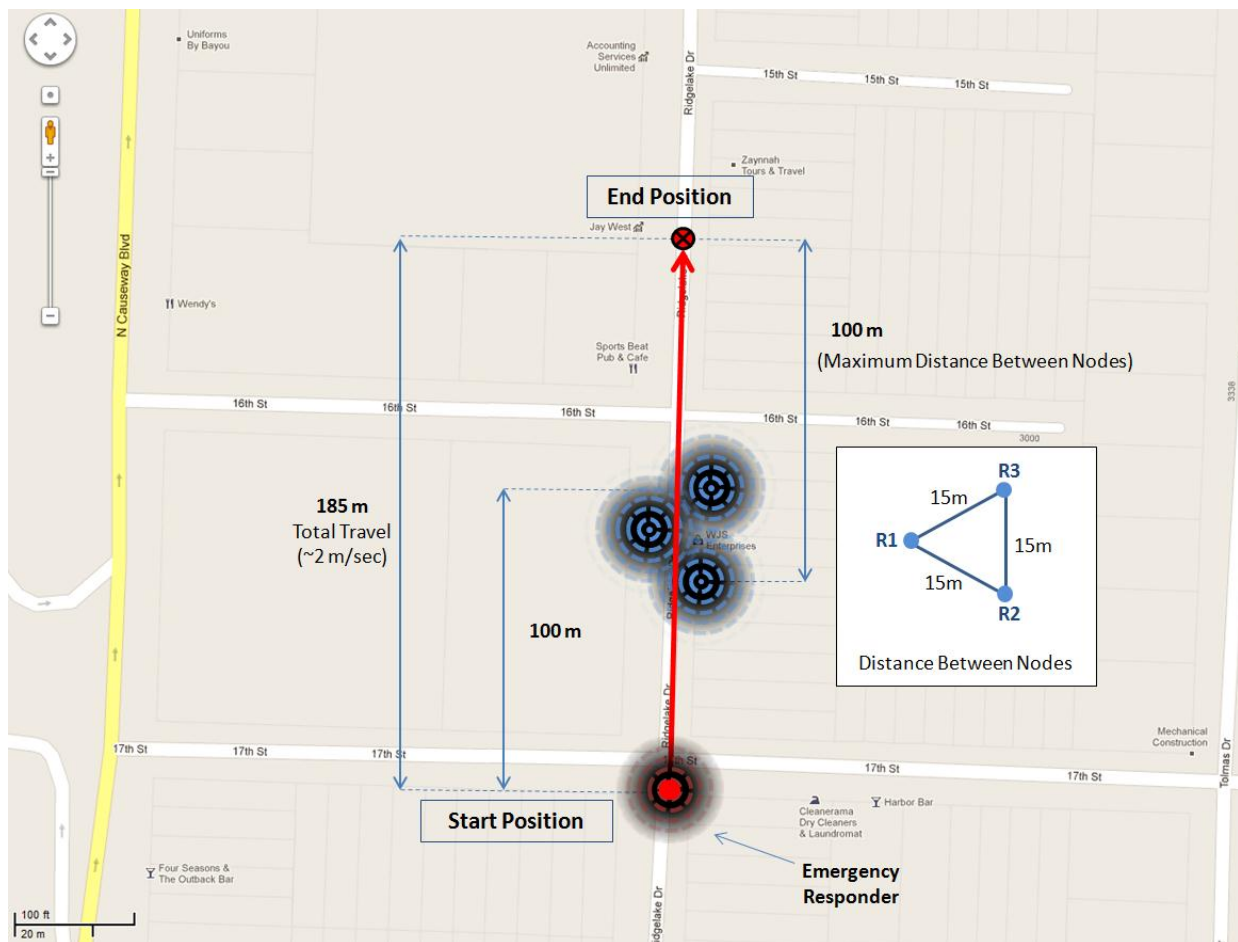


Figure 48: Map of Equidistance Node scenario. Three Wi-Fi emitters (Blue) within 15 meters of another; each can exchange data at the same rate. The Emergency Responder (Red) approaches the network and passes through while attempting to regain spectrum. Note: not to scale.

For simplicity, the mobile scenario involves only one moving node: the emergency responder. Radio nodes R1, R2, and R3 are approximately 15 m apart in an equilateral triangle. The main purpose of these positions is to allow each node to transmit and receive at the same rate. The

emergency responder begins 100 m from R3, and passes through the network at a rate of 2 m/s until it is 100 m from R2. The values of attenuation between each node is generated using a script in Matlab, and then passed to a program written in C that controls the signals sent to the NI-PCI card, which controls the attenuators.

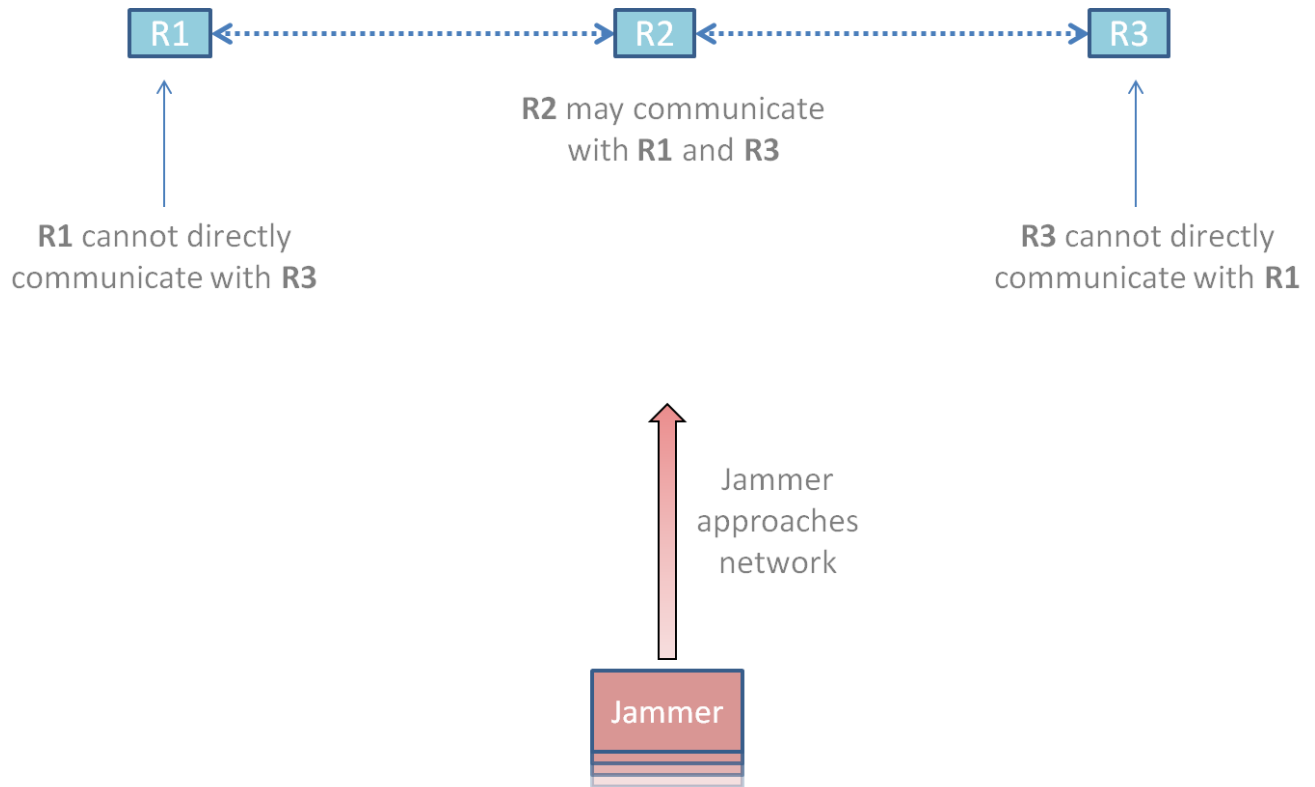


Figure 49: Hidden Node topology. R1 (Left) and R3 (Right) cannot communicate directly with each other. R2 can communicate with both nodes. The jammer moves toward this network at a rate of ~2 meters/sec.

This topology was briefly introduced as the Hidden Node problem in the Background section. The scenario will demonstrate the effectiveness of a jammer moving towards a network that relies on the RTS/CTS mechanism.

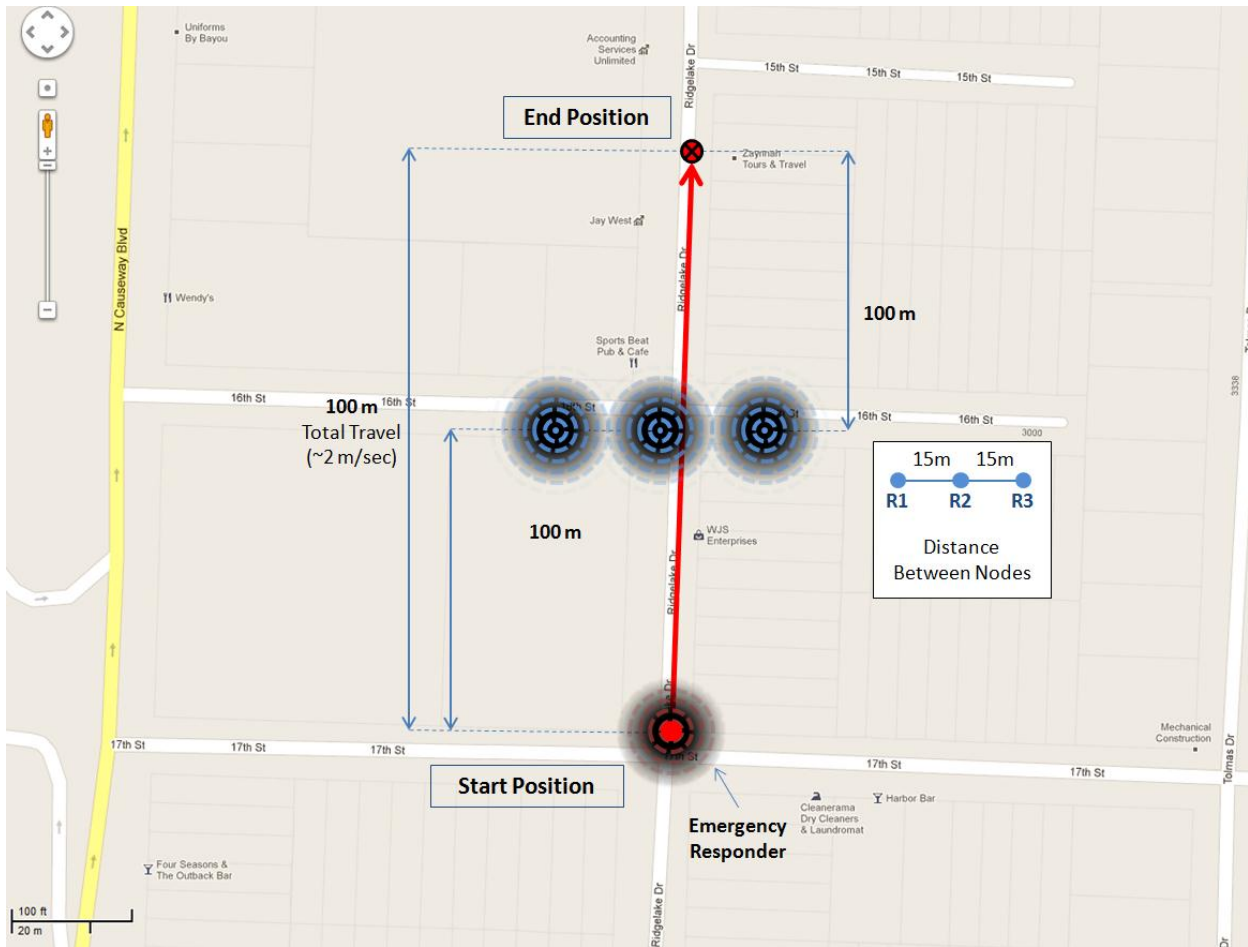


Figure 50: Map of Hidden Node topology. Three Wi-Fi emitters (blue, R1, R2, and R3, from left to right). R1 cannot communicate with R3 and vice versa. The Emergency Responder (Red) approaches the network and passes through, attempting to regain spectrum. Note: not to scale.

Figure 50 shows a map of the hidden node scenario. The total travel distance is only 100 meters in this experiment. Since the run time of each experiment is not directly controllable and is typically 90 seconds, the jammer is actually moving more slowly (1.1 m/s) through this topology.

Due to time limitations of this course, flow control of the attenuator program is beyond the scope of this project. Our team was not able to program the control script to provide accurate timing and execution, thus the difference in speed of the jammer will remain a small discrepancy among the results.

A distant node topology is described in Figure 51. The distant node is R3 and is approximately 50 m away from R2, and 70 m away from R1. Since R1 and R3 are normally able to

communicate from a distance of 70 m, their connection within the RF testbed will be terminated with a 50 Ω load.

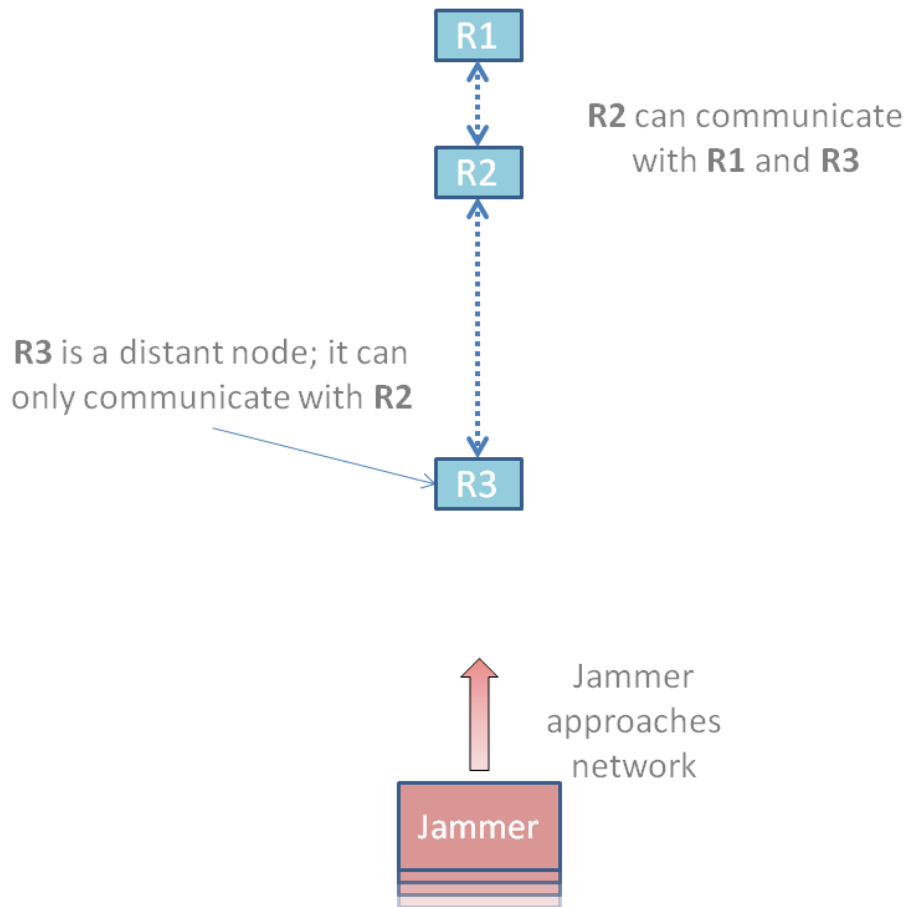


Figure 51: Distant Node topology. Each node starts equidistant from other nodes and moves away from the network in the opposite direction. The jammer approaches the network at a rate of 2 meters/sec.

A distant node topology is similar to hidden node topology except that one node is at a greater distance away from the other two nodes. It is assumed that this node is not able to achieve the same data rate and contend for resources at the same capacity as a closer node.

This could be an insightful subject in future research regarding optimal jamming methods, as the ability to jam nodes that reach to distant networks is highly valuable, and any network topology is likely to have a distant node at some location.

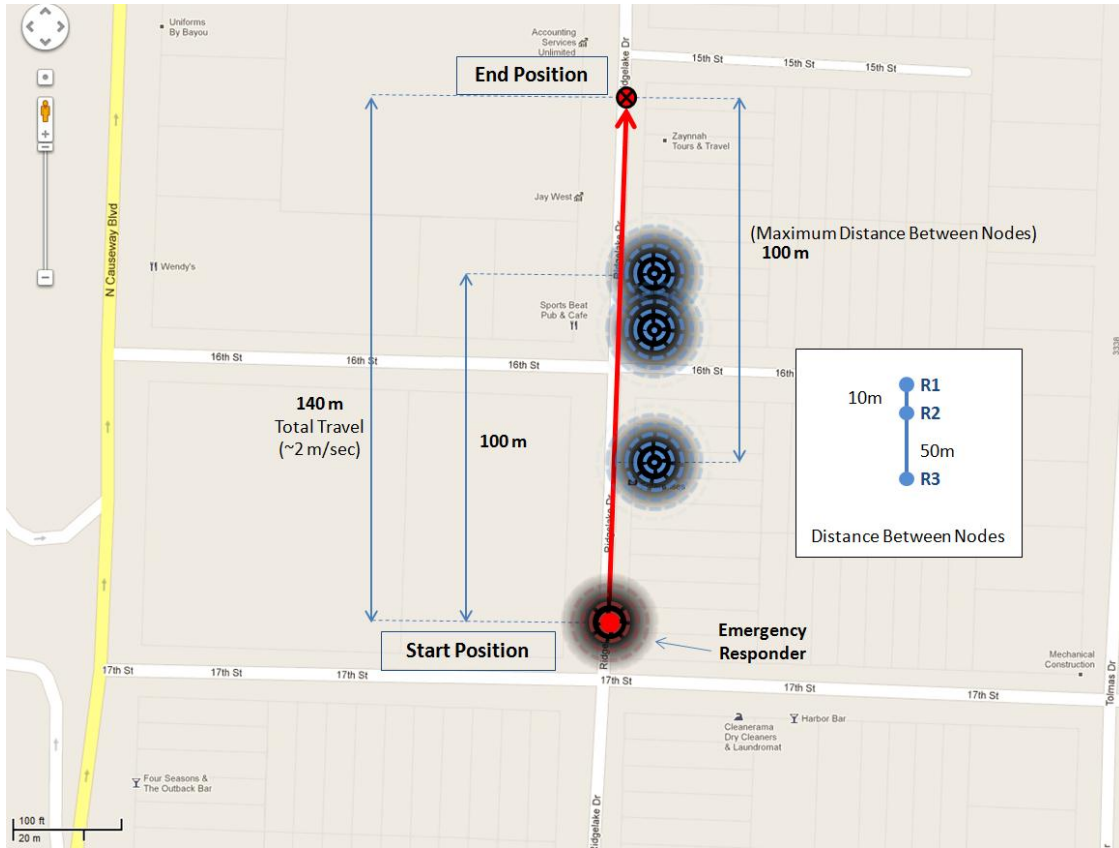


Figure 52: Map of Distant Node topology. Three Wi-Fi emitters. R1 cannot communicate with R3 and vice versa. The Emergency Responder (Red) approaches the network and passes through, attempting to regain spectrum. Note: not to scale.

Figure 52 helps to illustrate the distances between each node and the start and end position of the jammer. For the purposes of this experiment, the link between R1 and R3 is disconnected manually. This is due to the dynamic range limitation of the attenuators, which can only emulate 0-31.5dB of attenuation.

3.5 MAC Layer Jamming

An important aspect to jamming is not only physical jamming, but *protocol* jamming. The techniques listed in the next section target the MAC protocol of the Data Link layer in IEEE 802.11b/g. Upper protocols require more knowledge about the network and a higher degree of sophistication, but can prove to be much more efficient than RF jamming at the PHY layer.

Original Idea: Reactive Beacon Frame Injection

A literature review of the current state of the art in MAC jamming produced some ideas of possible new attacks that may be able to target management of the network. Similar attacks that

target management frames are Disassociation or Deauthentication attacks which attempt to spoof (fake) frames that tell others a client has left the network, forcing the target to continuously rejoin the network before being able to transmit. Flooding attacks are also related; they spoof management frames (beacon or authentication/association frames), typically thousands at a time, in order to cause the client to overflow a buffer and crash, fill its association table, or to waste its resources by continuously connecting with fake clients.

We propose a method called “Reactive Beacon Frame Injection,” based on manipulating the exchange of network parameters such as data rate, encryption, synchronization, modulation, and channel specification. This attack spoofs frames directly after (or immediately before) the target user sends its own beacon, notifying all clients that the user wishes to use incorrect network parameters (low data rates, weak encryption or none at all, unspecified modulation schemes, etc.). It is suspected that this technique will force other clients to disregard the original beacon frame and use the spoofed (manipulated) frame instead. This would cause other clients to use the manipulated network parameters when sending packets to the target, forcing the target to drop those packets. Figure 53 shows this procedure in action.

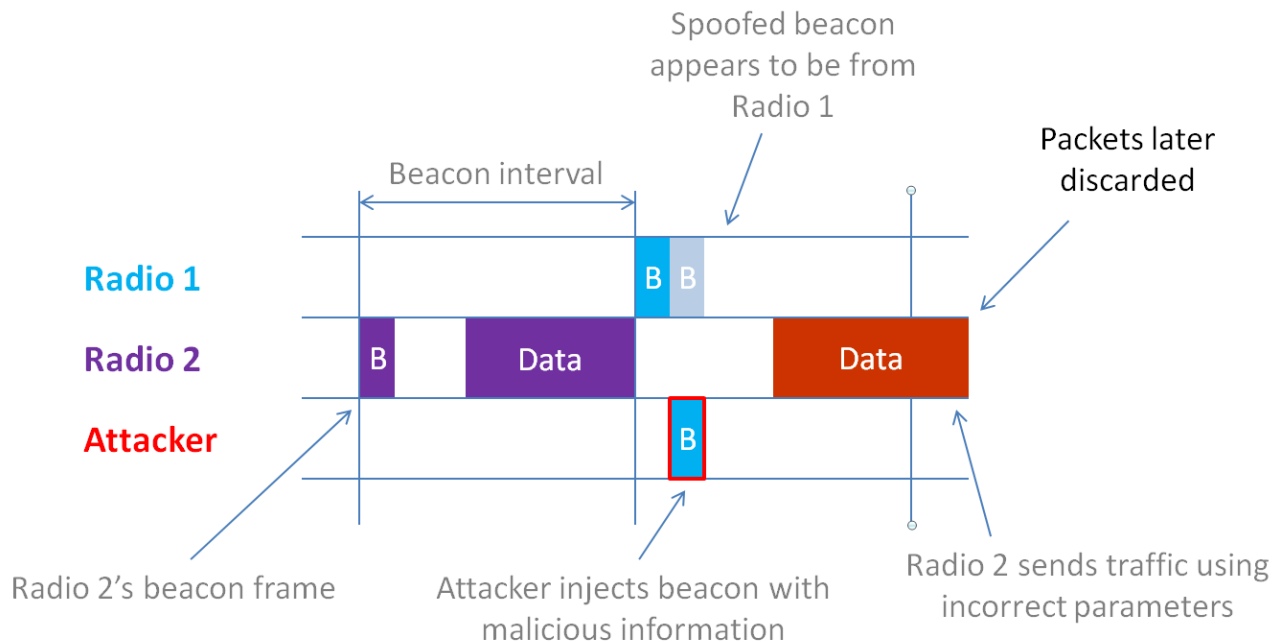


Figure 53: Reactive Beacon Frame Injection attack on IEEE 802.11b/g. The attack injects a manipulated beacon frame that seems as though it came from the target client. Subsequent packets sent to that client are then using the wrong network parameters, resulting in dropped packets and/or weakened security.

The ideal location to inject a fake beacon frame is not particularly known, although it is suspected to be either immediately before or after the target's beacon frame. The USRP used in this experiment can respond on the order of milliseconds, but this is too slow of a reaction to effectively replace beacon frames as they are sent. On the other hand, nodes in Ad-hoc mode will typically alternate sending beacons every 10 mS; therefore the attacker only has to synchronize to this interval to be effective. However, if the target notices the attacker's fake beacon frame, it may attempt to retransmit its beacon directly after, which may inadvertently shift the beacon interval. In this case the attacker will have to detect and react to this shift in the interval.

Implementing the Attack

Demonstrating a proof of concept may be possible by simply testing the theory using the USRP to record and play back beacon frames. However, the effectiveness and efficiency of the attack may be greatly enhanced by using specialized tools and hardware, such as those provided with the Linux distribution "Backtrack."

Typically, Gumstix radios are equipped with standard, basic tools which only allow the operator to view signal levels, transmitted/received packets, and change a few parameters such as modulation (between b or g), Ad-hoc or AP mode, and encryption (WEP or WPA). In order to manipulate and inject MAC frames, a highly configurable wireless card was used, along with a wireless penetration operating system called Backtrack. Backtrack contains tools and drivers that provide users with specialized access to certain wireless hardware. The AWUS036H wireless card was chosen based upon its known compatibility with Backtrack.

Before attempting this method using specialized hardware, our team conducted a quick test of the theory behind the attack with a USRP and GNURadio. A network of two radios was prepared using the four node testbed. As previously mentioned, in Ad-hoc mode, radios will alternate sending beacon frames approximately every 10 mS. This transmission was recorded using a USRP. The radios kept the same IP addresses, but the configuration of encryption, data rate, and modulation was altered. While using Iperf to generate traffic between the two nodes and record throughput, the recorded transmission of beacon frames was played back into the network. If the theory is correct, this playback of old beacon frames would affect the network in

two ways: (1) the beacon frames may cause collisions in the transfer of packets, (2) the clients will accept the recorded (false) beacon information and change their data rate, encryption and modulation, and a subsequent drop in throughput should be observed.

A sophisticated attack could similarly be executed using tools found in Backtrack. The attack begins with “Wireshark,” which captures beacon packets and uses the time stamps to specify the beacon interval. The time-stamp, IP and MAC addresses are relayed to “aireplay,” a program that can inject falsified beacon frames into the network. If successful, a script that can utilize these programs will be able to implement the same beacon frame attack described above.

4 Results

Throughout the duration of the project, a variety of results and measurements were collected. The team compiled several different types of data to verify the functionality of the testbed. Before assembly, measurements were taken to characterize the performance of different channel emulator components across the band. Once constructed, additional measurements were taken and known PHY layer experiments were repeated on the complete testbed for validation and verification. After the functionality of the testbed was characterized, three different types of PHY layer jamming were implemented using the channel emulator mobility feature. Results from all of these different measurements and experiments will be presented in the following chapter.

4.1 Channel Emulator: Testing and Validation

A number of different measurements were taken to validate and characterize the channel emulator components and the system as a whole. S-parameters were collected for all of the individual components as well as for the assembled channel emulator. Basic PHY layer jamming techniques were performed using different RF hardware and then repeated on the testbed to check performance. Channel emulator related results are below; starting with tests performed on the individual components, followed by images of the assembled system and tests on the complete testbed.

Hittite Attenuator

Results that describe the insertion loss and flatness of major attenuation states are shown below in Figure 54. The measurement was taken on the network analyzer from DC to 8GHz. Insertion loss is shown in blue. Major attenuation states, including 0.5dB, 1dB, 2dB, 4dB, 8dB, and 16dB, are shown in red. These states are adjusted to be relative to the insertion loss state of the device.

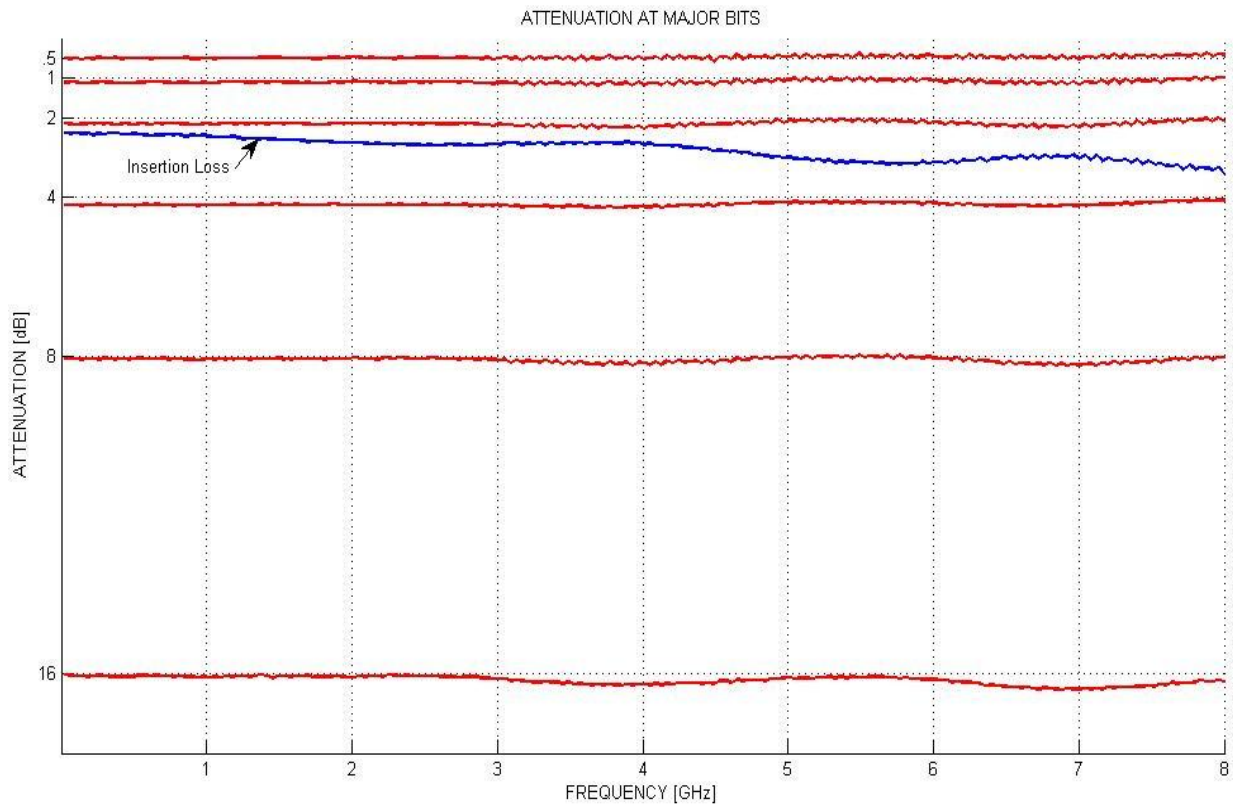


Figure 54: Major attenuation states, adjusted to insertion loss, DC to 8GHz. Insertion loss is shown in blue. Attenuation states are relatively flat across the band.

Figure 54 shows that attenuation remains relatively flat across the band. Furthermore, across the narrower Wi-Fi band (2.4GHz to 2.425GHz), variation is extremely low. The team also looked into the maximum switching speed of the attenuator in the channel emulator setup to determine if the 1 ms specification had been met.

An oscilloscope screen shot of the attenuator stepping through its different attenuation states is shown in Figure 55. The setting at the far left of the screenshot, where the waveform has the largest amplitude, corresponds to the zero attenuation state. This state is the result of insertion loss alone. At the lowest amplitude, the attenuator is programmed to maximum attenuation, or 31.5dB.

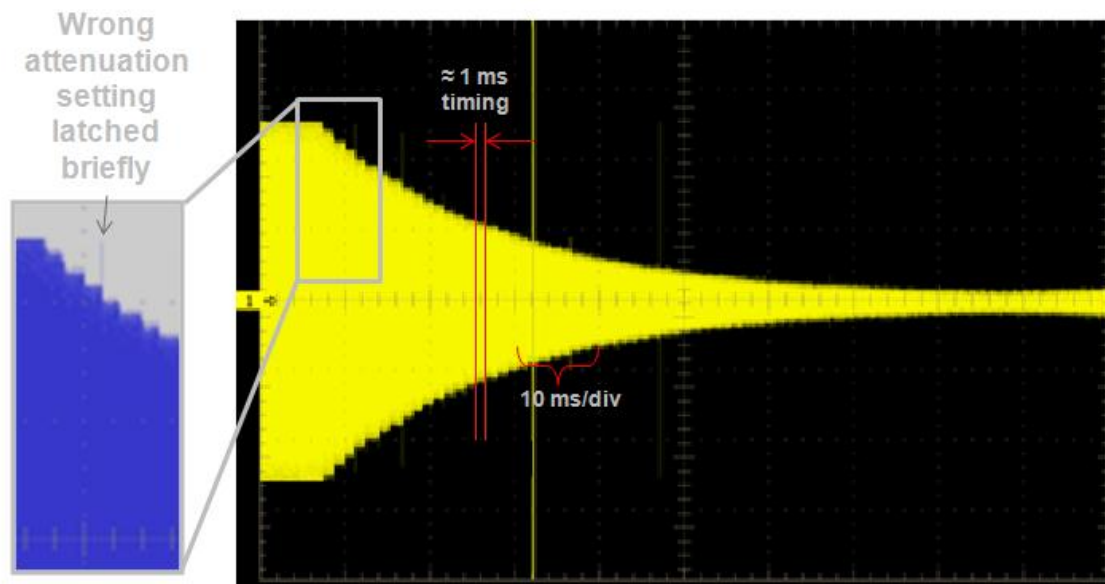


Figure 55: A tone being fed through the attenuator while it steps through different attenuation settings. The blue image on the left shows an instance of the attenuator latching the wrong state. Note: blue/grey portion of image have been inverted to improve visibility.

Based upon Figure 55, the attenuator switches within approximately 1 millisecond. On occasion, it takes slightly more or less time. This is likely due to the asynchronous nature of the clock driven by non-real-time controlling computer. For the purpose of this project, this was not a problem. The inset to the left of Figure 55 also demonstrates that every once in a while for a very brief amount of time, generally less than 100 us, the attenuator latches the wrong value. This is most apparent in the blue box on the left of the plot, where a lower attenuation state is briefly latched.

This discrepancy is less than 100 us and was determined to have a minimal impact on the metrics for network performance. This might happen when one of the high density pin connectors used to interface the data lines to the attenuators shifts or moves possibly causing the attenuator to latch at the wrong time. To minimize the likelihood of interference, the controller continually re-latches the current setting. This way, even if the attenuation state suddenly changes, it is very quickly reset back to the desired state.

Krytar Coupler

Several performance metrics of the couplers were important to verify, including isolation between -3dB ports, return loss looking into all three ports of interest, and the insertion loss of

the device. Measurements to characterize isolation between the two -3dB ports of the couplers were conducted on the network analyzer. Isolation was measured across a 2 to 8GHz band for two different couplers. Results for the first coupler are shown in red and the second coupler is shown in blue in Figure 56.

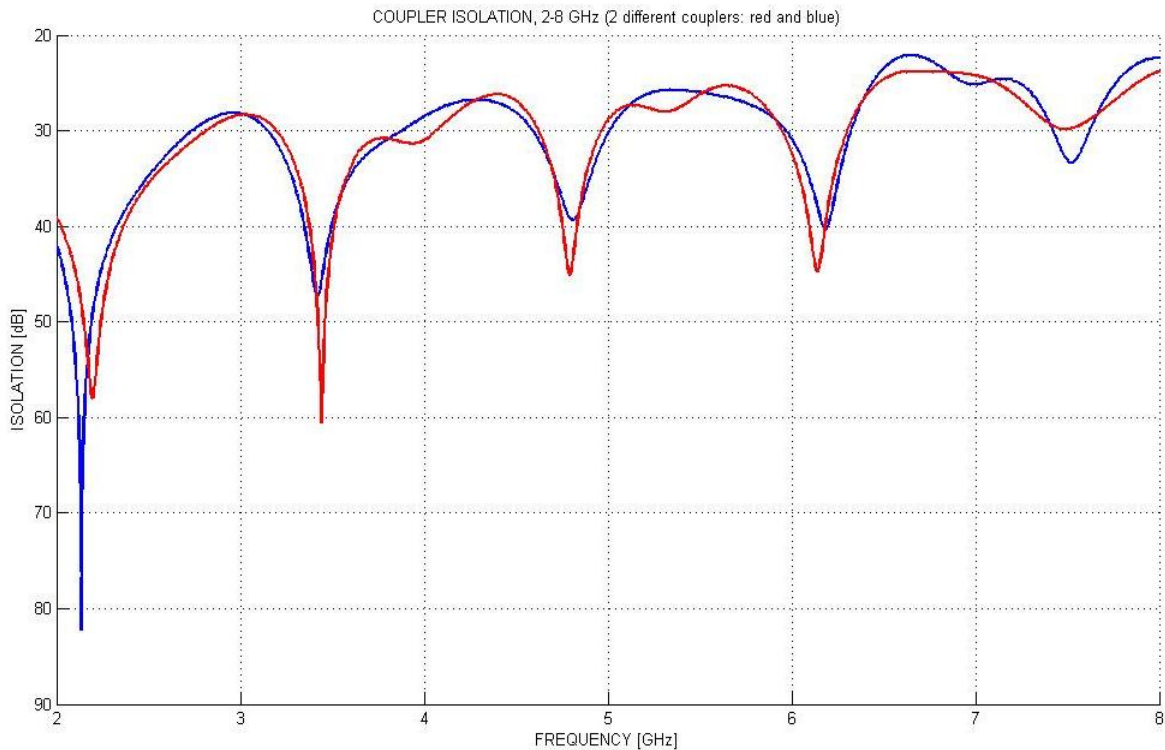


Figure 56: Isolation between -3dB ports of two different couplers. This measurement was taken from 2 to 8GHz with the vector network analyzer.

The datasheet for the coupler specifies that isolation should be greater than 18dB. From Figure 55Figure 56: Isolation between -3dB ports of two different couplers. This measurement was taken from 2 to 8GHz with the vector network analyzer, the isolation between ports is well above this. In fact, across the 2GHz to 8GHz band, the isolation is consistently above 20dB. In the Wi-Fi band, where the team did the majority of the experiments, the isolation is greater than 30dB. The specification for the channel emulator required isolation greater than 20dB between the two -3dB ports; from these measurements it was determined that this specification had been satisfied.

Return loss was also measured on both -3dB ports and the sum port of the coupler. Results of this measurement from 2 to 8GHz are shown below in Figure 59. The red and blue lines are the return loss at the two -3dB ports. The black line is the return loss measured at the sum port. While the datasheet does not specify a return loss for any ports of the coupler, all three ports are better than 15dB. In the Wi-Fi band, return loss is greater than 25dB at all ports.

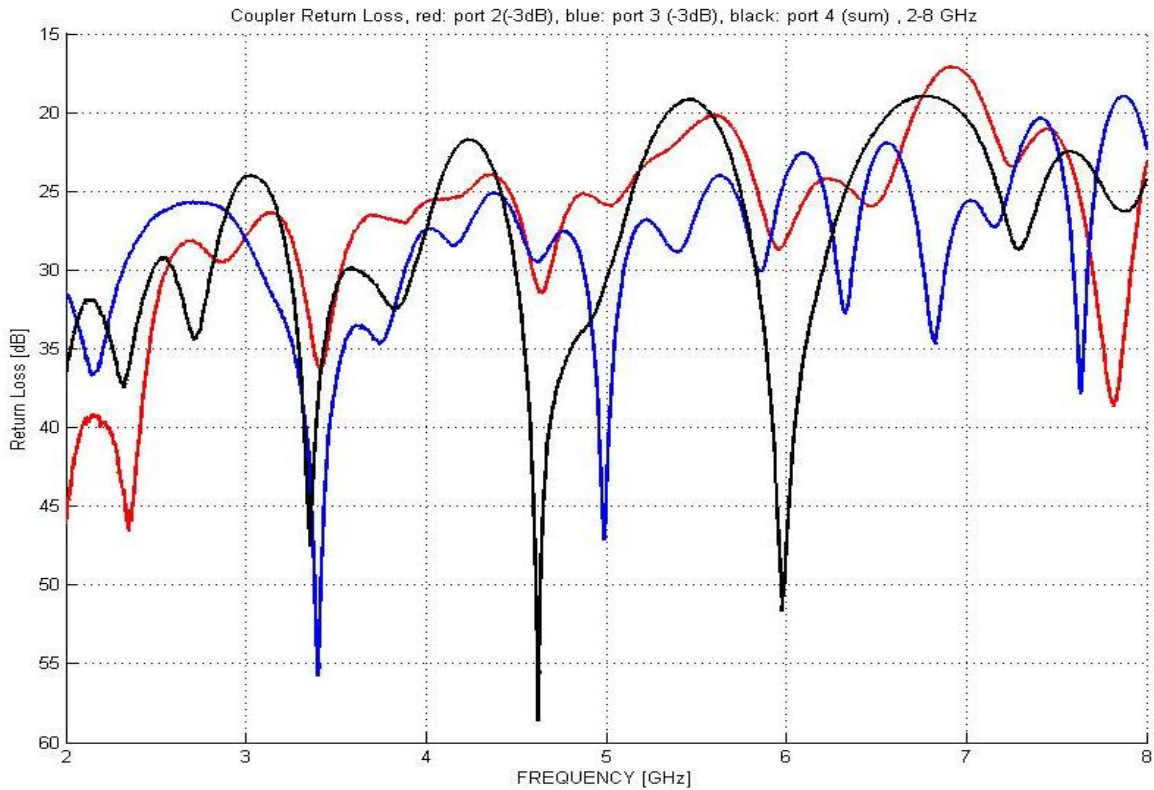


Figure 57: Coupler return loss, measured from 2 to 8GHz. Return loss for each of the -3dB ports shown in red and blue. Return loss for sum port shown in black.

Coupler insertion loss was measured using the network analyzer for two different couplers. The results for this measurement are shown in Figure 58. For each of the two couplers measured, insertion loss was measured between the sum port and both of the -3dB ports. The first coupler measured is shown in red, the second coupler measured is shown in blue.

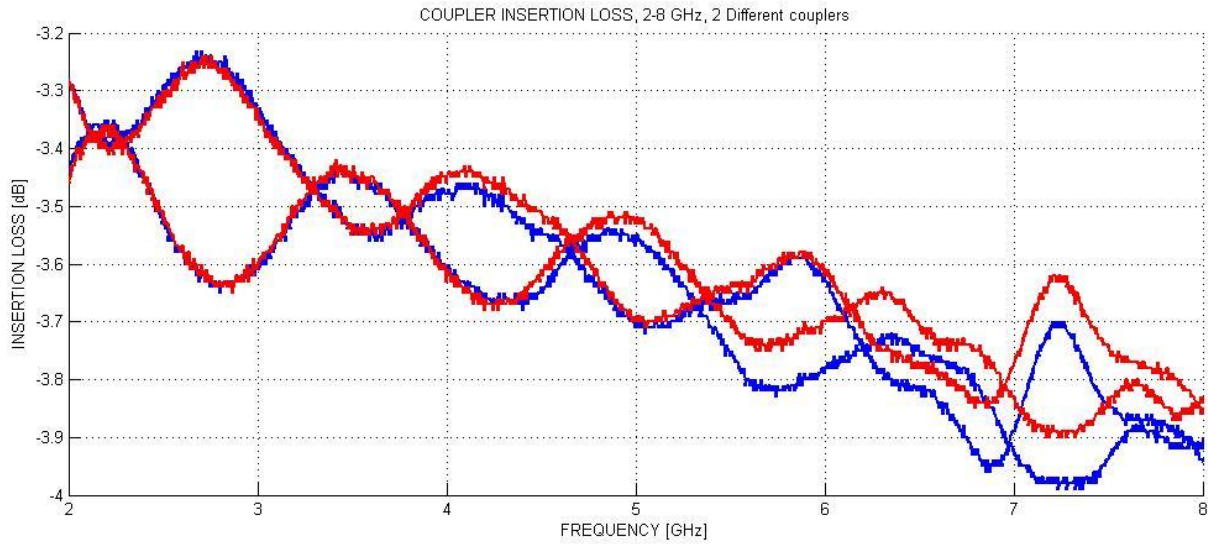


Figure 58: Coupler insertion loss from sum port to both -3dB ports for two different couplers. Each of the two blue lines correspond to the loss measurement between the sum port and one of the -3dB ports while the two red lines are the same for the other coupler measured. This measurement was taken from 2 to 8GHz.

From Figure 58, it is clear that there is little variation between the two couplers measured. The datasheet for this device specifies insertion loss to be less than 1.1dB across the 2 to 8GHz bandwidth. In addition to that 1.1dB loss, we would expect another 3dB loss due to the fact that the power at the sum port is being divided two ways. In total, the loss from the sum port to each -3dB port should be no more than 4.1dB. This is verified in the results shown in Figure 58. For the 2 to 8GHz range, the loss remains below 4dB. In the Wi-Fi band, loss is below 3.6dB. For the channel emulator to function properly it is important to have relatively flat loss across the band and this was confirmed to be the case for the coupler in these particular measurements.

DiTom Circulator

Measurements on the DiTom circulator included a measurement of insertion loss between two ports as well as a measurement of the reverse isolation between the same two ports. Results were collected for all three port pairs for one of the circulators and are shown in Figure 59. Each pair of ports is shown in red, blue, or black. Insertion loss is generally between 1 and 3dB while isolation between the ports is typically between 9 and 13dB across the band.

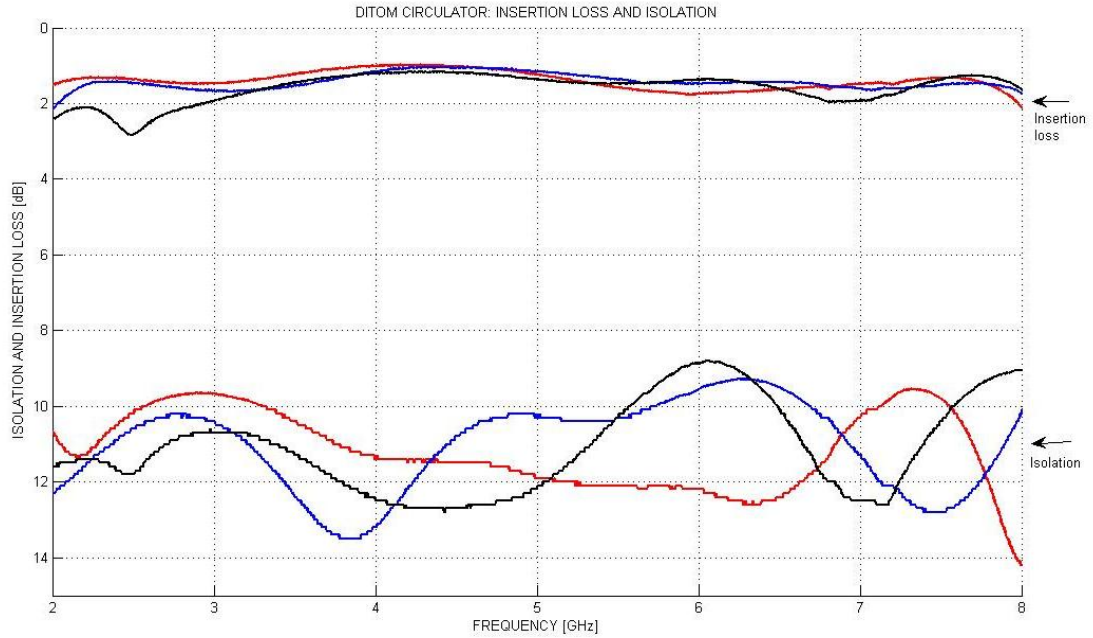


Figure 59: Circulator insertion loss (top) and isolation (bottom), measured from 2 to 8GHz with network analyzer.

The insertion loss in the circulator is consistently below 3dB but not below the 1.5dB specified on the datasheet. The datasheet also claims isolation provided is 10dB minimum in the 2 to 8GHz range. This doesn't seem to be the case in Figure 59, although in the Wi-Fi band, isolation is no lower than 10dB.

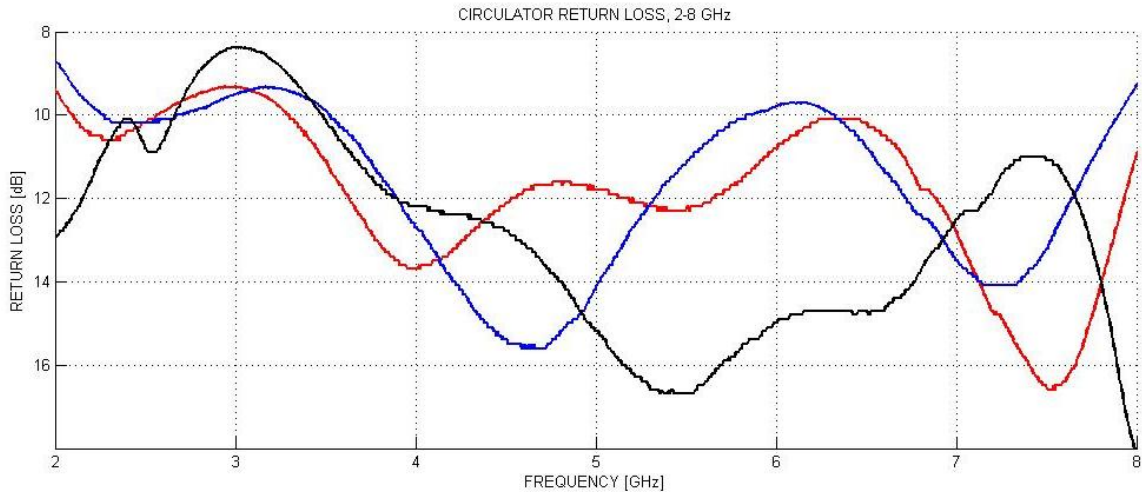


Figure 60: Return loss of DiTom circulator, measured from 2 to 8GHz with network analyzer. Each different color represents one of the three different ports of the device.

The return loss from each of the three ports of the circulator was measured and the results are shown in Figure 60. The three ports are shown in red, blue, and black. Return loss is generally between 8 and 17dB, and is acceptable for the channel emulator design.

Assembled RF Testbed

The final assembled testbed, including the channel emulator component and complete with radio hardware is shown below in Figure 61. Key components of the setup are labeled, including radio hardware, circulators, couplers, programmable attenuators, and the control circuitry for the attenuators.

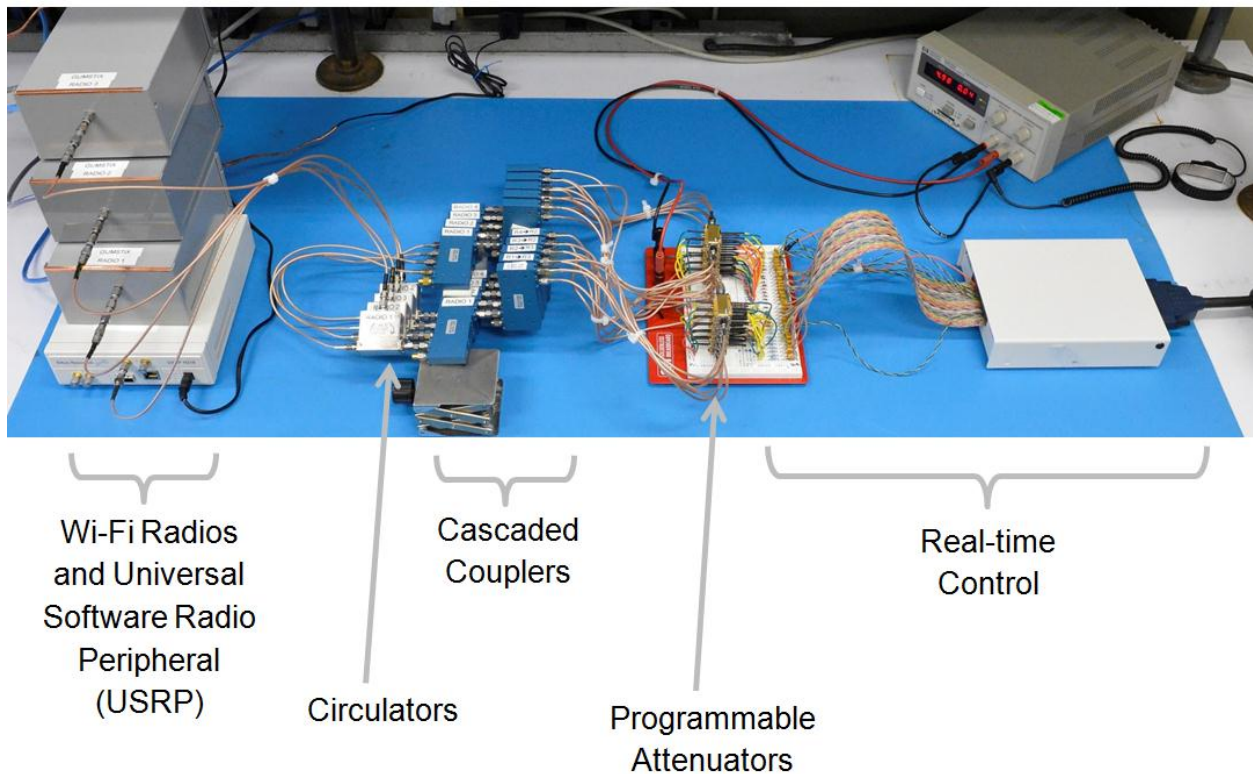


Figure 61: Assembled RF Analog Testbed. Radio hardware is on the far left, with circulators and couplers towards the middle. Attenuators are on the breadboard with the PCI breakout board on the far right.

The transmitting and receiving cascaded couplers connected to the circulators are shown towards the middle of Figure 61. A close-up photograph of this part of the setup is labeled in Figure 62.

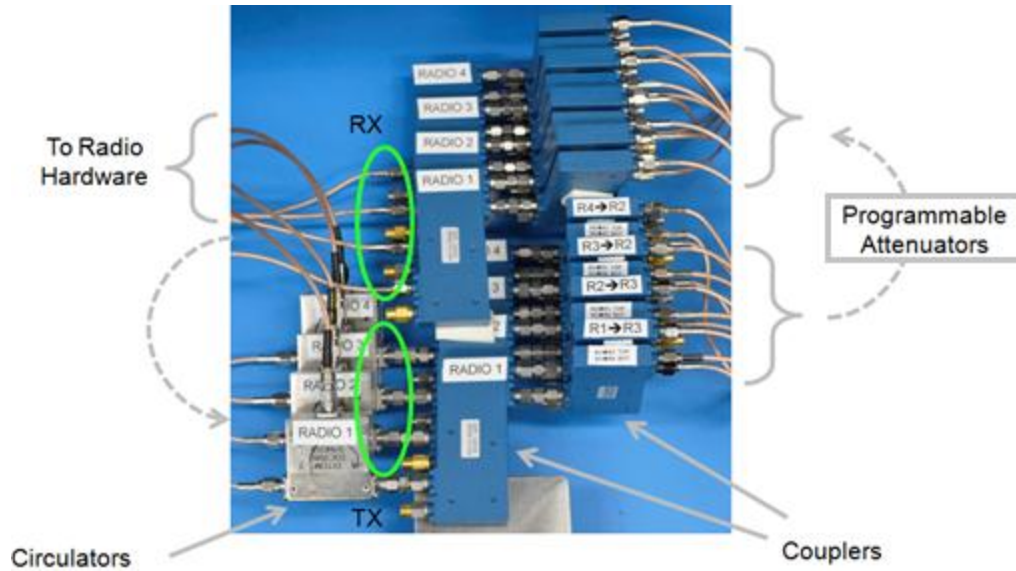


Figure 62: Circulators and cascaded couplers in final channel emulator configuration. The transmit and receive sides of the circulators are circled in green.

Circulators are shown in grey on the far left with the transmitting and receiving sides labeled. The transmit side feeds into a series of cascaded couplers. The output from these couplers goes to the receiving set of couplers through the twelve programmable attenuators. Figure 63 shows these programmable attenuators with the control circuitry, including the ringing suppression circuit.

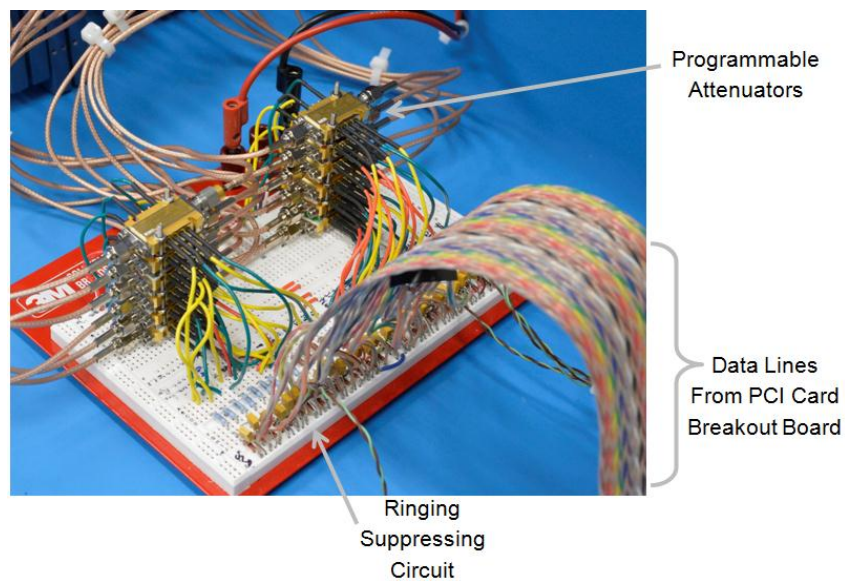


Figure 63: Programmable attenuators with ringing suppression circuit on breadboard

The programmable attenuators are in two stacks of six, towards the left of Figure 63. The data lines from the PCI controller card are in the bottom right of the image, each twisted with a ground return. The breakout board for the PCI controller is depicted in Figure 64, both closed (top) and open (bottom).

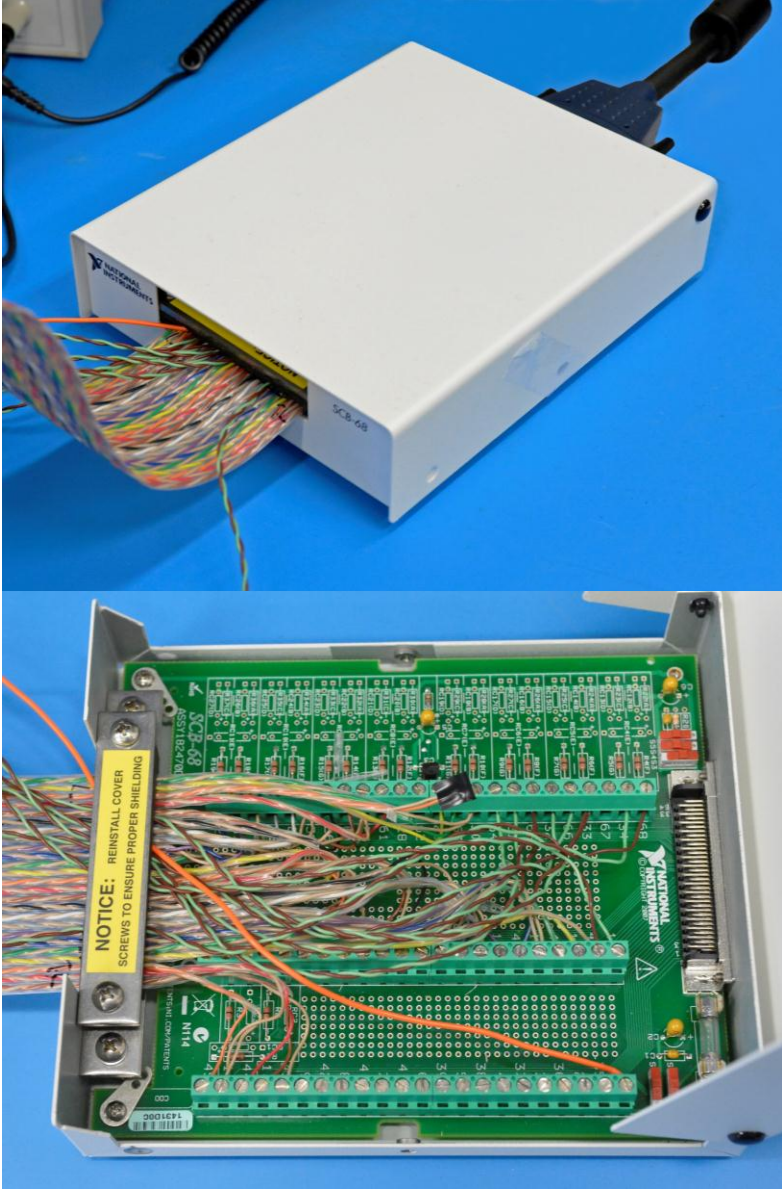


Figure 64: SCB-68 NI breakout board closed (top) and open (bottom). Wires from this board are each twisted with a ground wire and connected to the attenuators on the breadboard.

Testing and measurements on the assembled system

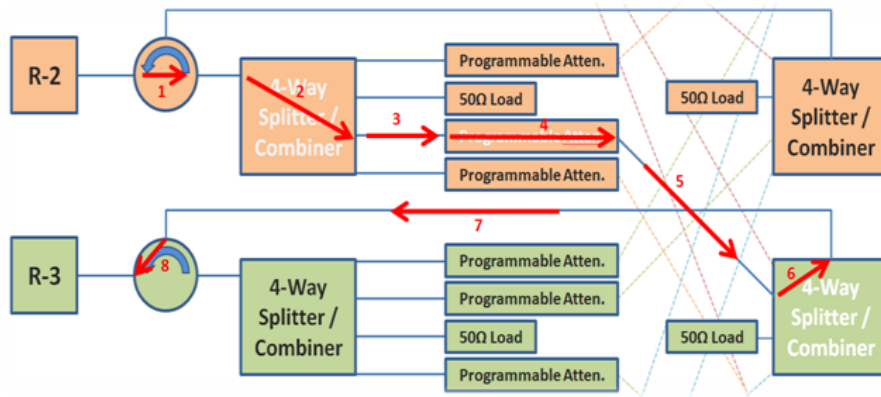
S-parameters were measured for each of the twelve channel paths to verify that loss from channel to channel was sufficiently uniform in all of the channels. As mentioned before, the twelve paths each have a unique attenuator. Every radio pair has two paths between them to accommodate full duplex communication. For example, path 1 and path 4 both go between radio 1 and radio 2. However, path 1 allows radio 1 to transmit to radio 2 while path 4 allows communications from radio 2 back to radio 1. The twelve different paths are summarized in Table 9.

Table 9: The twelve 'paths' in the channel emulator. Each path has its own programmable attenuator.

Path Number	Transmitting Radio	Receiving Radio
1	1	2
2	1	3
3	1	4
4	2	1
5	2	3
6	2	4
7	3	1
8	3	2
9	3	4
10	4	1
11	4	2
12	4	3

It is important that the loss throughout the system does not vary more than 2dB between each of the paths. Beyond this, calibration can be done in the software as necessary. Based on measured component values, path loss was to be around 21dB. This number is the sum of the loss

measured in each individual part, as shown in Figure 65. Parts are listed in the table in the order that they appear in the system, from transmit to receive.



Arrow	Part	Loss [dB]
1	Circulator (TX)	1.5
2	4-Way Splitter/Combiner (2 Cascaded Couplers)	7
3	Coax Cable	0.5
4	Attenuator (Insertion Loss)	2.5
5	Coax Cable	0.5
6	4-Way Splitter/Combiner (2 Cascaded Couplers)	7
7	Coax Cable	0.5
8	Circulator (RX)	1.5
	SUM	21

Figure 65: analysis throughout the system, based upon measured loss in each individual part at 2.4GHz. Expected loss through the system is 21dB.

The loss each path, as measured using the network analyzer before calibrating the system, is shown on the left of Figure 66. As expected, the total loss is approximately 21dB throughout the system.

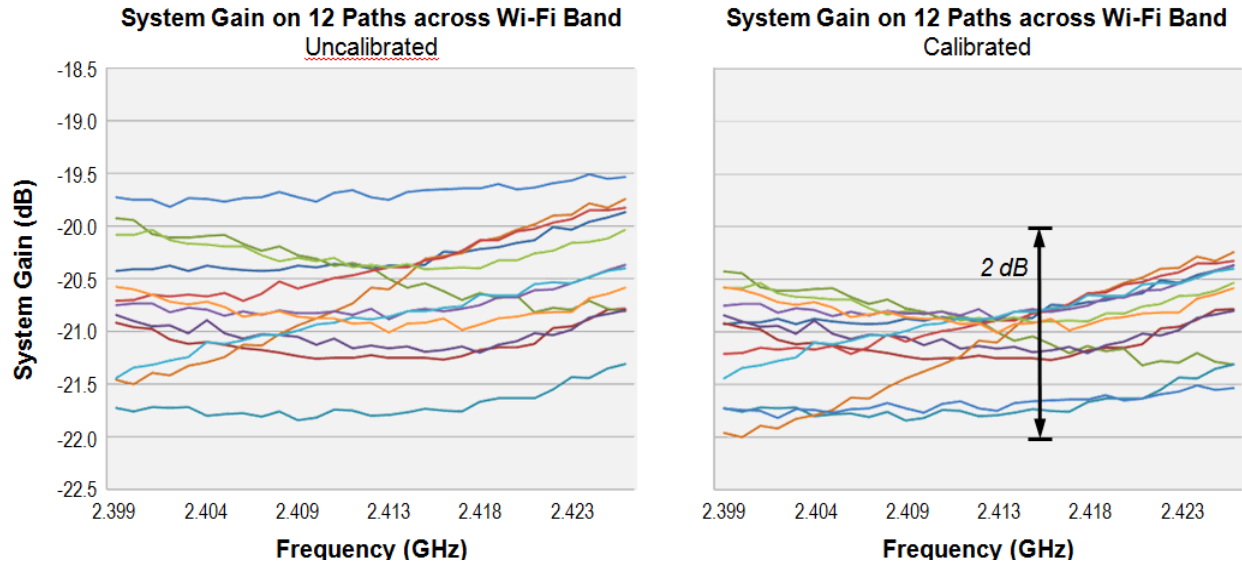


Figure 66: Gain through the system on all twelve paths, before (left) and after calibration (right). Colored lines correspond to 12 distinct paths through emulator.

While the loss across the different channels is similar, it is not within 2dB of variation between paths at any given frequency as specified for the channel emulator. By adding attenuator pads to some of the paths with the least loss, the specification can be achieved. The result of adding attenuator pads is shown on the right of Figure 66, where the variation in loss between paths is below 2dB.

Once the system was calibrated, a two tone test was conducted to determine the power limitations of the system. The tones were set at 2.44GHz and 2.441GHz, one megahertz apart. Based upon these frequencies, the third order intermodulation products would be expected at 2.439GHz and 2.442GHz. As shown in Figure 43, the two RF tones were fed into a resistive power combiner with circulators at the input for additional isolation. Prior to feeding the combined tones into the channel emulator, they were fed directly into the spectrum analyzer. The spectrum of the combined tones before going into channel emulator is shown in Figure 67.

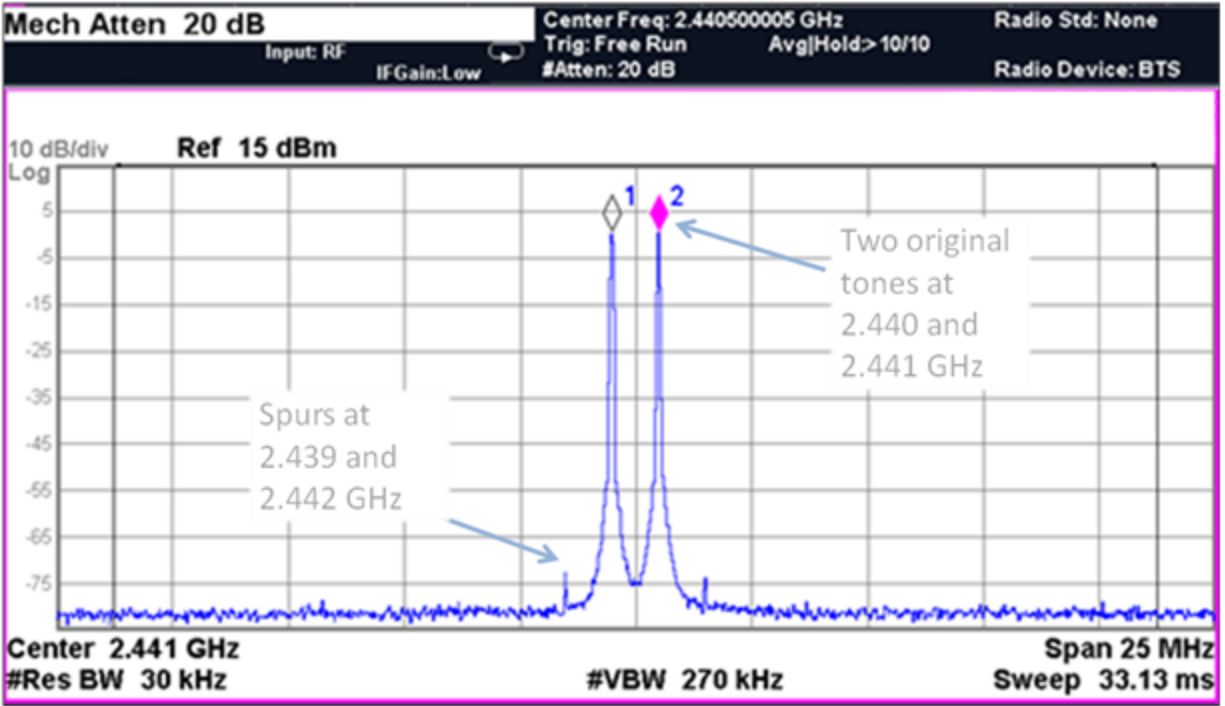


Figure 67: Spectrum of two tones combined, before entering the channel emulator

The power of the two tones measured by the spectrum analyzer is 5dBm. The coax cables used to connect the combined signals to the spectrum analyzer had a loss of about 8dB so the strength of the tones when connected directly to the channel emulator would be approximately 13dBm each. The spurs seen at 2.439GHz and at 2.442GHz are at -77dBc, that is 77dB below the input tones, and are probably due to either the front end of the spectrum analyzer or nonlinearities in other components such as the circulators. The 77dB spur range is sufficient for measuring nonlinearities in the switches.

After characterizing the spectrum of the combined tones, they were fed into one of the ports of the channel emulator. A different port was connected to the spectrum analyzer to visualize the resulting spectrum. The result of this measurement is shown in Figure 68 for attenuators set at the zero attenuation state, Figure 69 for attenuators programmed to 16dB, and Figure 70 for an attenuation setting of 31.5dB.

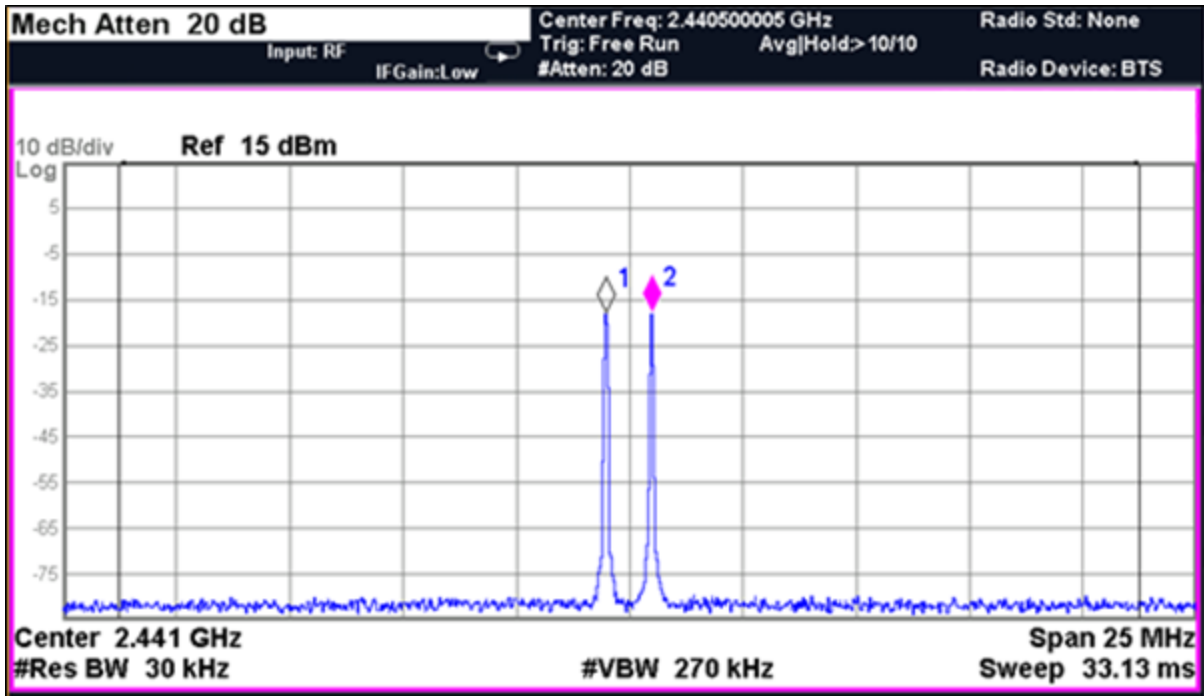


Figure 68: Two tones through the system, attenuators set to insertion loss

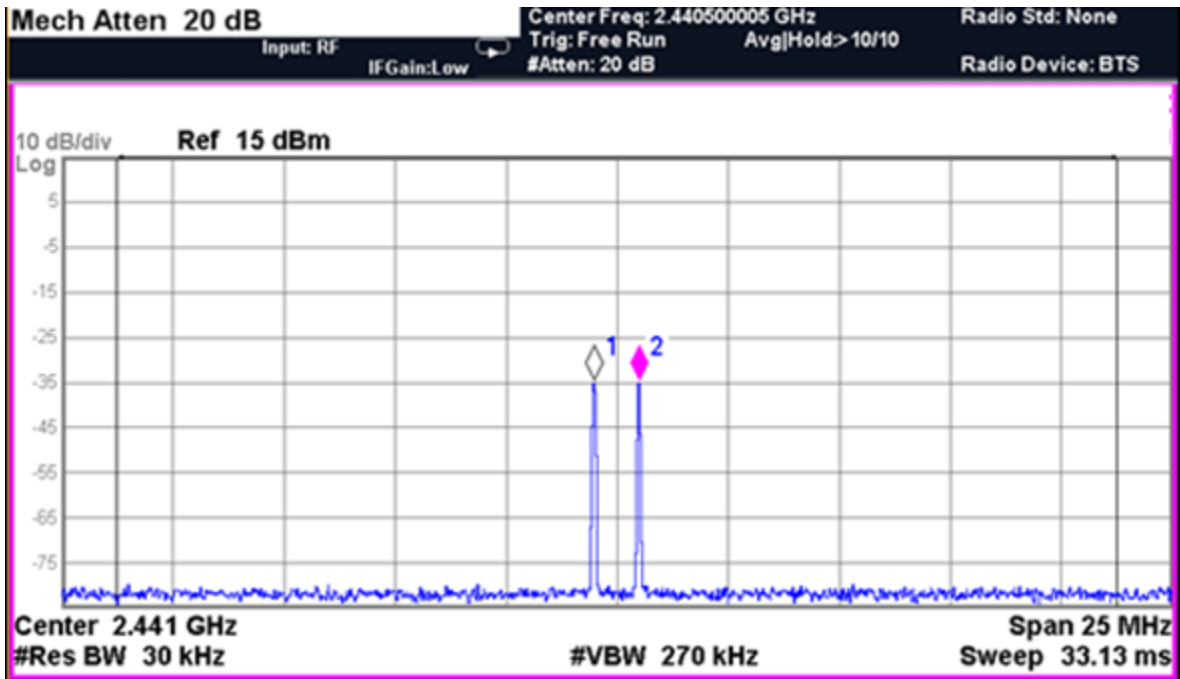


Figure 69: Two tones through the system, attenuators set to 16dB setting

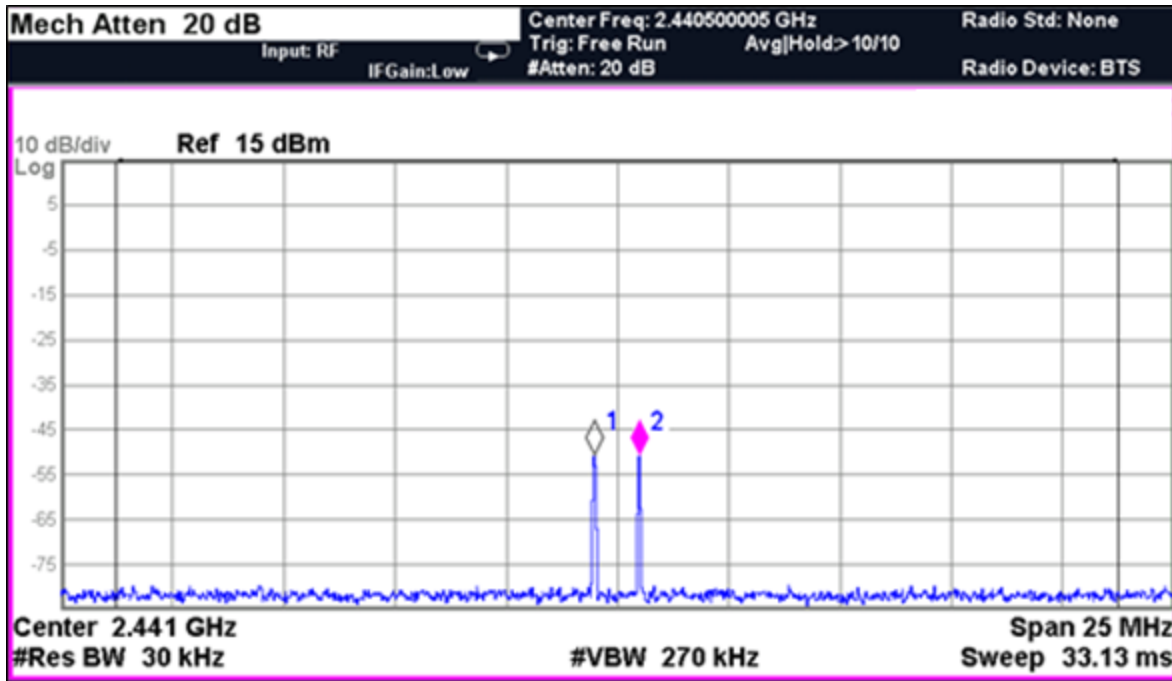


Figure 70: Two tones through the system, attenuators set to 31.5dB setting

In this test, the power in the signal generators was turned up to the maximum allowable strength, and we did not observe any spurs. In order to verify that this is a reasonable result, the team used the third order input intercept point provided on the datasheet to back-calculate for the power expected at the third order intercept products, assuming the attenuator is the primary source of intermodulation distortion. Based upon this calculation, the team found that the power expected at the third order intercept points would be well below the noise floor, so the measured results make sense.

The purpose of this experiment was to verify that any intermodulation products were suitably below the threshold for our experiment. Since the radios used in this experiment can operate at an SNR as low as 20dB, the team does not expect any problems. To better describe this system, more powerful tones might be fed into the channel emulator so that the intermodulation products might be observed above the noise floor. Also, the measurement was spur free for greater than 50dB at the highest attenuation setting which is more than sufficient for the channel emulator needs.

The team also repeated a published PHY layer DoS attack on a two radio network similar to the one described in the literature [7]. Results of the repeated two radio network are shown in Figure

94, Figure 95, and Figure 96 in the Appendix. Once results similar to the paper were obtained on the two radio network, the same tests were repeated on the four radio channel emulator to ensure functionality. None of these tests use the mobility aspect of the channel emulator. These tests confirmed that our testing parameters were acceptable measures of network operability. Results of these experiments are below, including pulse, sweep, and digital jamming.

There were some differences between the two and four radio networks but these can be explained due to the differences in equipment, hardware, and software. We begin with comparing pulse jamming tests with the two radio testbed, and then the four radio testbed in Figure 71.

Two Radio Testbed

Transmit: 11Mbit/s DSSS
Period

Length	10 ms	5 ms	3 ms	1 ms
100 us	5.78	5.75	5.73	5.68
300 us	5.71	5.57	5.52	5.4
500 us	5.63	5.35	5.16	4.73
700 us	5.54	5.08	4.67	2.89
900 us	5.41	4.69	3.91	0.4
1000 us	5.38	4.55	3.67	0

Values in Mbit/sec

Transmit: 9Mbit/s OFDM
Period

Length	10 ms	5 ms	3 ms	1 ms
100 us	5.74	5.7	5.67	5.61
300 us	5.69	5.55	5.48	5.14
500 us	5.65	5.32	5.14	3.94
700 us	5.6	5	4.6	2.18
900 us	5.55	4.53	3.67	0.3
1000 us	5.39	4.35	3.32	0

Values in Mbit/sec

A.)

Four Radio Testbed

Transmit: 11Mbit/s DSSS
Period

Length	10 ms	5 ms	3 ms	1 ms
100 us	5.82	5.81	5.80	5.76
300 us	5.79	5.75	5.72	5.56
500 us	5.78	5.67	5.62	5.04
700 us	5.76	5.54	5.40	3.83
900 us	5.73	5.15	4.71	1.04
1000 us	5.72	4.87	4.18	0.00

Values in Mbit/sec

Transmit: 9Mbit/s OFDM
Period

Length	10 ms	5 ms	3 ms	1 ms
100 us	5.77	5.76	5.75	5.69
300 us	5.74	5.67	5.63	5.42
500 us	5.74	5.60	5.53	4.99
700 us	5.72	5.46	5.29	3.85
900 us	5.69	5.01	4.51	0.40
1000 us	5.66	4.76	4.07	0.00

Values in Mbit/sec

B.)

Figure 71: Pulse Jamming tests: Throughput vs. Pulse length & period in Two Radio (A) testbed at 11Mbit/sec (DSSS), 9Mbit/sec (OFDM), and on the Four Radio testbed (B) at 11Mbit/sec (DSSS), 9Mbit/sec (OFDM).

The two radio testbed provides verification and validation of the procedure, equipment, and analysis of the listed jamming techniques. Each experiment is a direct replication of peer-reviewed research obtained from reputable sources [7], using similar software and hardware.

Shown in Figure 71, the pulse lengths (left column) are varied between 100 μ S to 1000 μ S, and pulse periods are varied between 1 mS and 10 mS. If the pulse length and period are equal, the jammer is continuous (bottom right corner).

When comparing Figure 71 (A) with (B) we notice that the results between the tests beds are similar, although the four radio testbed shows an overall 7% increase in throughput compared with the previous testbed. This is displayed clearly in Figure 73 which examines the differences in performance observed between the two and four radio testbed. Sweep jamming results are shown in Figure 72.

Two Radio Testbed

Transmit: 11Mbit/s DSSS
SJR (dB)

Sweep Time (sec)	10	0	-10	-15
0.5	3.50	2.95	2.91	2.90
0.66	3.50	2.94	2.89	2.87
1	3.50	2.90	2.86	2.84
2	3.50	2.88	2.84	2.80
10	3.50	2.84	2.79	2.77
20	3.50	2.85	2.80	2.78

Values in Mbit/sec

Transmit: 9Mbit/s OFDM
SJR (dB)

Sweep Time (sec)	10	0	-10	-15
0.5	3.50	2.97	2.91	2.89
0.66	3.50	2.94	2.89	2.87
1	3.50	2.91	2.86	2.84
2	3.50	2.88	2.83	2.81
10	3.50	2.85	2.79	2.77
20	3.50	2.85	2.77	2.77

Values in Mbit/sec

A.)

Four Radio Testbed

Transmit: 11Mbit/s DSSS
SJR (dB)

Sweep Time (sec)	10	0	-10	-15
0.5	2.93	2.89	2.89	2.90
0.66	2.90	2.87	2.86	2.87
1	2.87	2.84	2.83	2.84
2	2.84	2.80	2.81	2.80
10	2.81	2.83	2.78	2.78
20	2.82	2.77	2.73	2.78

Values in Mbit/sec

Transmit: 9Mbit/s OFDM
SJR (dB)

Sweep Time (sec)	10	0	-10	-15
0.5	2.93	2.89	2.90	2.90
0.66	2.90	2.87	2.87	2.87
1	2.87	2.84	2.85	2.83
2	2.84	2.82	2.83	2.81
10	2.81	2.77	2.78	2.78
20	2.81	2.78	2.78	2.75

Values in Mbit/sec

B.)

Figure 72: Sweep Jamming tests: Throughput vs. SJR & Sweep time in Two Radio testbed (A) at 11Mbit/sec (DSSS), 9Mbit/sec (OFDM), and on the Four Radio testbed (B) at 11Mbit/sec (DSSS), 9Mbit/sec (OFDM). Results are in Mbit/sec. Signal to Jammer Ratio (SJR) and sweep time are varied.

Figure 72 shows the effects when introducing a single sine wave swept across the entire Wi-Fi band (100MHz) in 0.5 to 20 seconds. This is accomplished using the HP Synthesized Sweeper listed in Table 8. Figure 72 lists sweep times (left column) along with the signal to jammer ratio (SJR). The four radio testbed shows a slight decrease in jammer performance compared to the

two radio testbed. An SJR of 10dB in the two radio testbed shows almost no effect on throughput, while the four radio testbed shows 17% reduction in throughput.

Differences in Performance

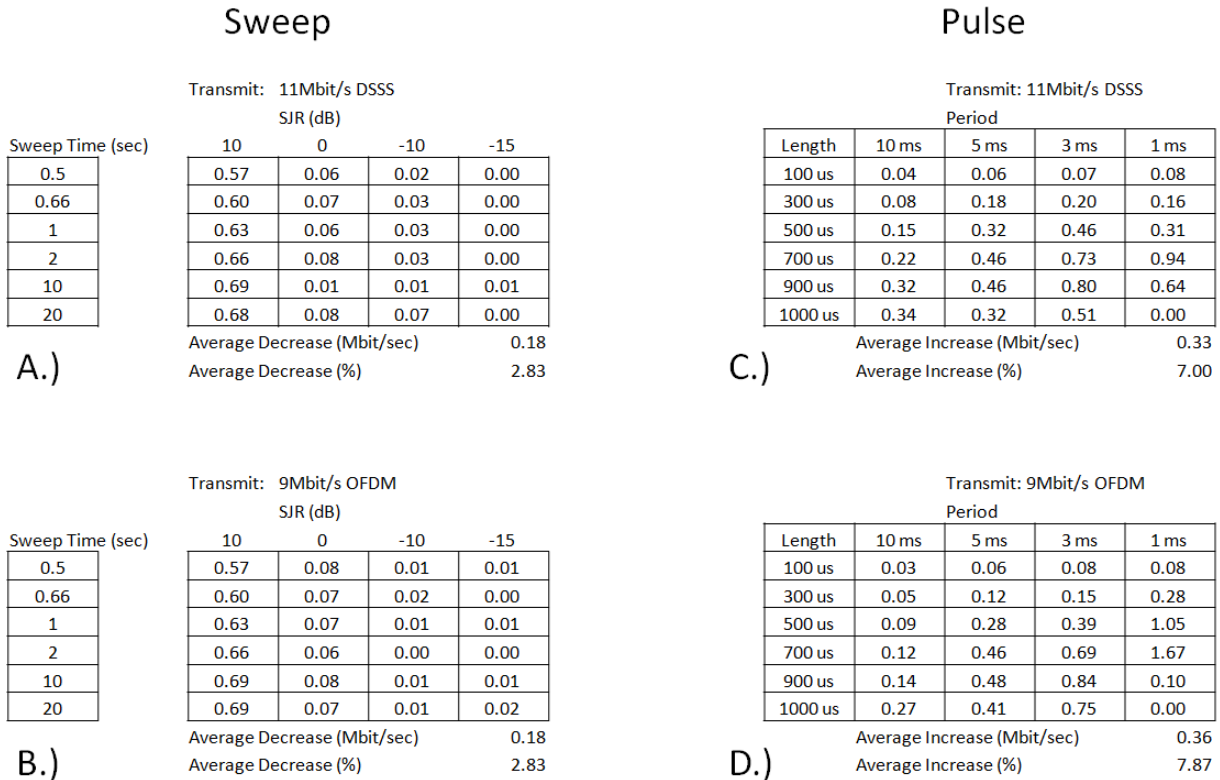


Figure 73: Differences in performance of Two Radio Testbed vs. Four Radio Testbed when subject to Sweep and Pulse waveforms.

To help compare these results, Figure 73 displays the absolute differences between the two testbeds. The sweep waveform in Figure 73 (A), (B), shows a decrease in throughput compared to the two radio testbed (note that this translates to an increase in performance of the emergency responder). It is suspected that the shielded boxes encased around the Gumstix in the four radio testbed may help prevent Wi-Fi radiation, which would prevent transmissions from bypassing RF cables and the sweep jammer. However, this conflicts with the previous pulse jamming experiment where the performance of the jammer had decreased by approximately 7 percent. The maximum effect on throughput in Figure 72 evens out at approximately 2.78 Mbit/sec with an SJR of -15dB; very similar to the two radio testbed. Overall, the new testbed shows a 2.8%

decrease in throughput using sweep tone jamming and a 7.87% increase in throughput using pulse jamming.

Digital jamming on the two radio testbed was implemented using MATLAB Simulink and its UHD toolbox. Due to a loss of software during a computer crash, the digital jamming technique was implemented on a readily available version of GNURadio. This may help to explain some differences in the results, in particular the SJR at which throughput reaches zero, shown in Figure 74.

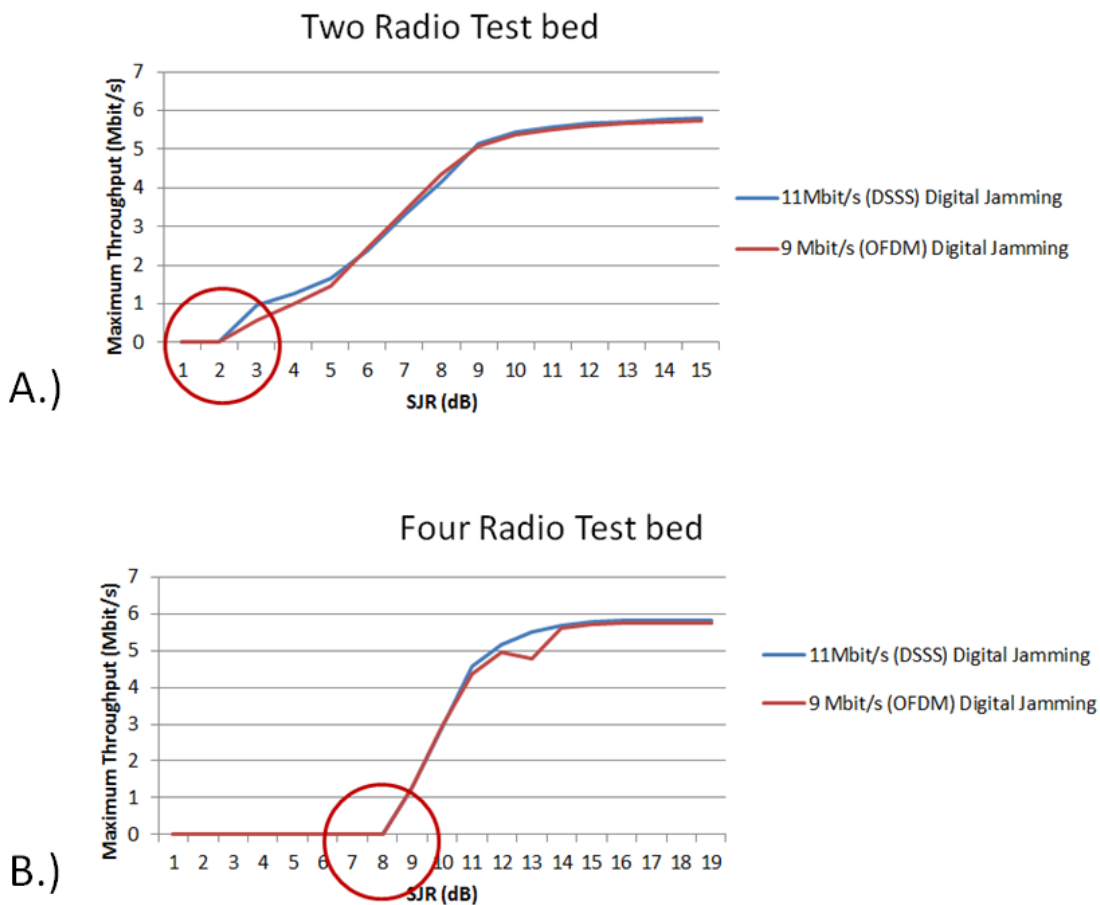


Figure 74: Digital Jamming tests: Throughput vs. SJR on the Two Radio testbed using MATLAB (A) and Four Radio testbed using GNURadio (B) using 11 Mbit/sec DSSS and 9 Mbit/sec OFDM.

Figure 74 shows digital jamming (pseudo random DBPSK at 2.4GHz) against DSSS (Blue) and OFDM (Red). The previous testbed shows zero throughput at an SJR of 2dB (Figure 74 (A), circled in Red), while the new testbed shows zero throughput at an SJR of 8dB (Figure 74 B, circled in Red). When first attempting the experiment, we found that transmissions would cease

at an unexpected SJR of 20dB. After altering excess bandwidth settings on GNURadio, this point changed to 8dB. This may suggest that the excess bandwidth or power produced using GNURadio is enough to drop throughput at a much lower SJR than when using MATLAB.

Nearing the end of the project an opportunity arose that enabled us to test this theory. The experiment was repeated using MATLAB with the emergency responder. Results are displayed in Figure 75.

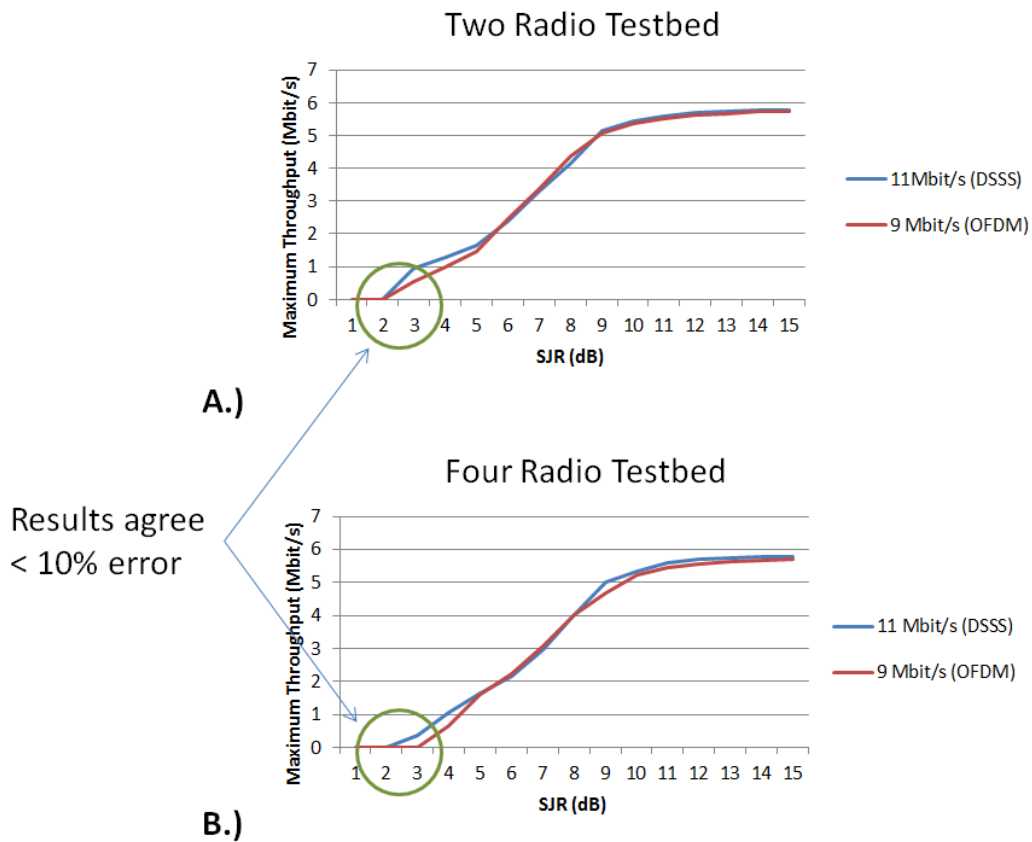


Figure 75: Digital Jamming tests (Corrected): Throughput vs. SJR on the Two Radio testbed using MATLAB (A) and Four Radio testbed using MATLAB (B) using 11 Mbit/sec DSSS and 9 Mbit/sec OFDM.

After repeating the Digital jamming test in Figure 74 using MATLAB with the emergency responder in the four channel testbed, we found the results between the two testbeds to be within 10% error. A slight increase in the performance of the jammer is observed as throughput halts at a higher SJR in Figure 75 (B) than (A). Additionally, the power spectrum density (PSD) was recorded ~6dB less when using MATLAB compared to GNURadio. This confirms our

hypothesis stated earlier that the increase in performance in Figure 74 (B) was a direct result of the substitution of GNURadio for MATLAB.

According to work by Harjula et. al., [7], there should exist some difference in performance against digital jamming between DSSS and OFDM, as OFDM resembles a digital-like signal and would be more susceptible to digital jamming than DSSS, which slightly resembles noise. The lack of separation between DSSS and OFDM suggests that the Gumstix Wi-Fi radios may be changing modulation schemes. In other words, the Wi-Fi radio may be selecting whether to use 802.11b or 802.11g depending on signal conditions, even though they are strictly configured by the user. We explore this question in Figure 76.

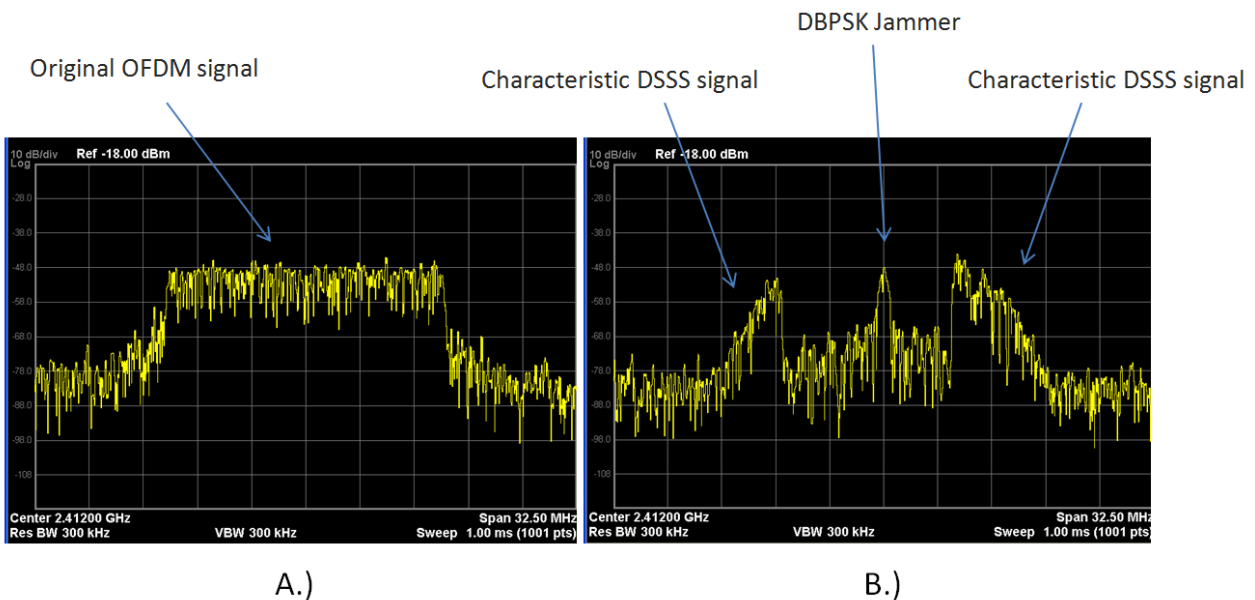


Figure 76: Spectrum of OFDM (9 Mbit/sec, 802.11g) signal (A) and with the addition of a Digital jammer (B). The graph in (A) shows a typical flat, OFDM signal modulation. The graph in (B) shows the OFDM modulation changing to a DSSS-like signal when a Digital jammer is introduced.

This experiment examines the spectrum of Wi-Fi signals using the signal analyzer listed in Table 8 before and after a Digital jammer is introduced in the network. Each Wi-Fi radio is set to use 802.11g at 9 Mbit/s using the *iwconfig* utility. Figure 76 (A) shows a typical Wi-Fi transmission; the spectrum is semi-flat at its peak, a characteristic of OFDM and 802.11g. A Digital jammer is introduced with equal power (0 SJR), and begins to interfere with communication between the two radios. What we notice is a drop in throughput and occasionally, the spectrum of the signal changes to a round shape, a characteristic of 802.11b. Occasionally, ‘clipping’ effects may

appear when viewing the spectrum as in Figure 76 (B); this is likely an effect caused by the slow sweep pattern of the signal analyzer. Our team made attempts to minimize this effect, but in the interest of showing the best possible explanation some clipping was acceptable.

We propose two possible explanations; the jammer effectively breaks communication between both nodes, and each node subsequently and repeatedly sends beacon packets (which look similar to 802.11b signals). Or, the Gumstix radios are self-configuring their own modulation, using 802.11b or 802.11g when it deems necessary. However, combined with the information obtained from Figure 77, it is likely that the radio is self-configuring its modulation.

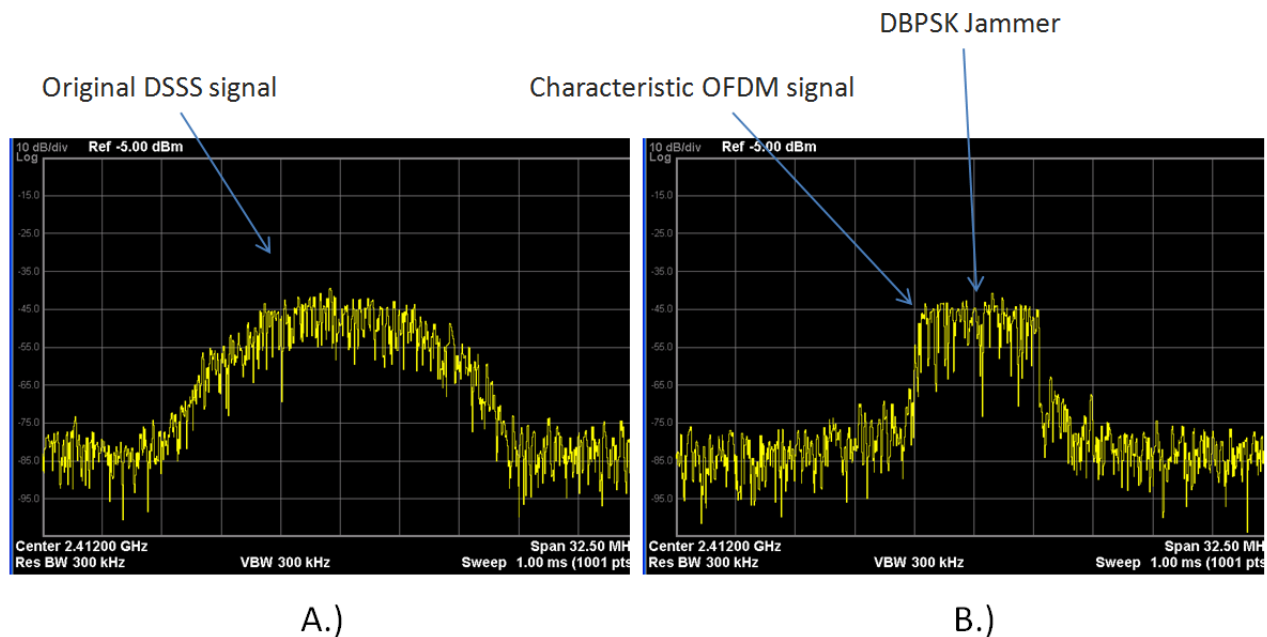


Figure 77: Spectrum of DSSS (11 Mbit/sec, 802.11b) signal (A) and with the addition of a Digital jammer (B). The graph in (A) shows a typical DSSS signal modulation. The graph in (B) shows the DSSS modulation changing to an OFDM-like signal when a Digital jammer is introduced.

This experiment is similar to the previous except we first transmit data using 802.11b at 11 Mbit/sec (DSSS) (set using the *iwconfig* utility). Figure 77 (A) shows a typical 802.11b spectrum. Then, we introduce a Digital jammer in Figure 77 (B). Notice how the spectrum changes shape this time to a flat, OFDM shaped spectrum. It is worth noting that after taking several samples, the flat-shaped spectrum samples were only a small percentage of the 802.11b shaped samples. In other words, the radio primarily relies on 802.11b, but occasionally we can see the 802.11g modulation being used. This behavior was observed only with the addition of an interferer, suggesting that it may be switching modulation to increase performance against

interference. Again, these results imply that the differences noted in the testbed when compared to previously published research (Figure 94, found the Appendix), are due to the self-configuring adaptation of the Gumstix' Wi-Fi radios when subject to interference.

4.2 Wi-Fi mobile jamming experiments

This section is primarily focused on the ability to accurately emulate distance between radio nodes over time. Mobility is demonstrated by the results of the following experiments. Additionally, we examined the differences between digital, pulse, and sweep jamming techniques in equidistant, hidden, and distant node mobile scenarios. To further understand the results, note the flow of traffic shown in Figure 78.

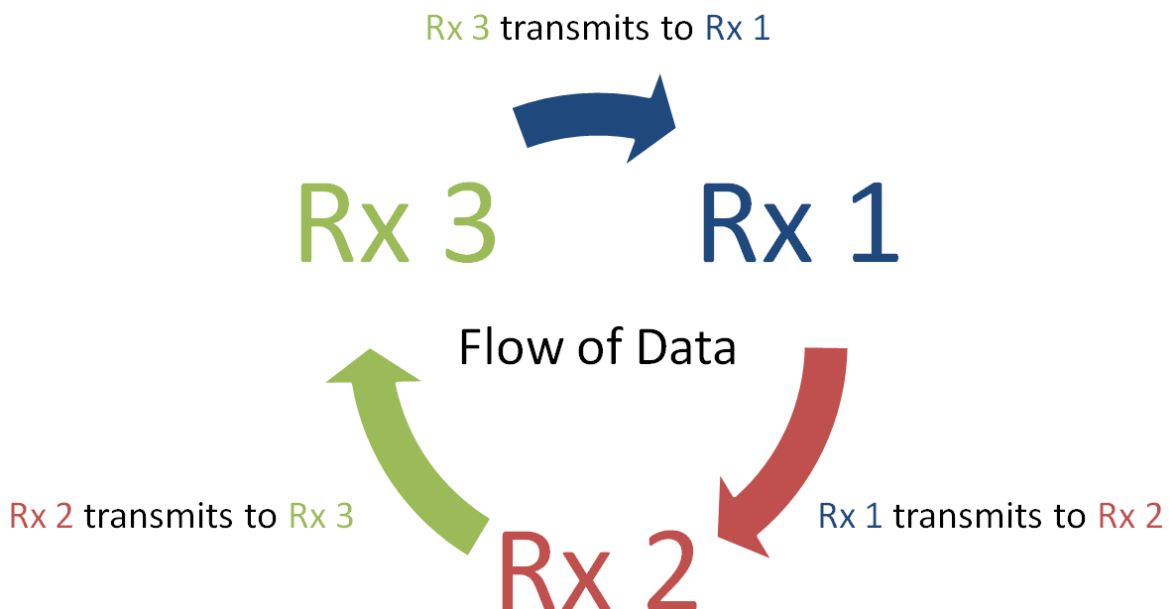


Figure 78: Flow of data in mobile experiments. All mobile data shown in graphs are transmitted in one direction by the prior node.

It is possible to transmit between every node, however this is difficult with Iperf as there is no way to discern where the traffic originates. Therefore, we decided to use one direction of traffic through each node. Radio 1 will transmit data to Radio 2 (Red), Radio 2 transmits to Radio 3 (Green), and Radio 3 transmits to Radio 1 (Blue). All nodes will use the same standard of color throughout the following figures. Using this method the throughput between each radio link can be measured. Note that the following Digital jamming experiments are shown using GNURadio

not MATLAB, and reflect the gain in power when using GNURadio, discussed in earlier in Figure 74 and Figure 75.

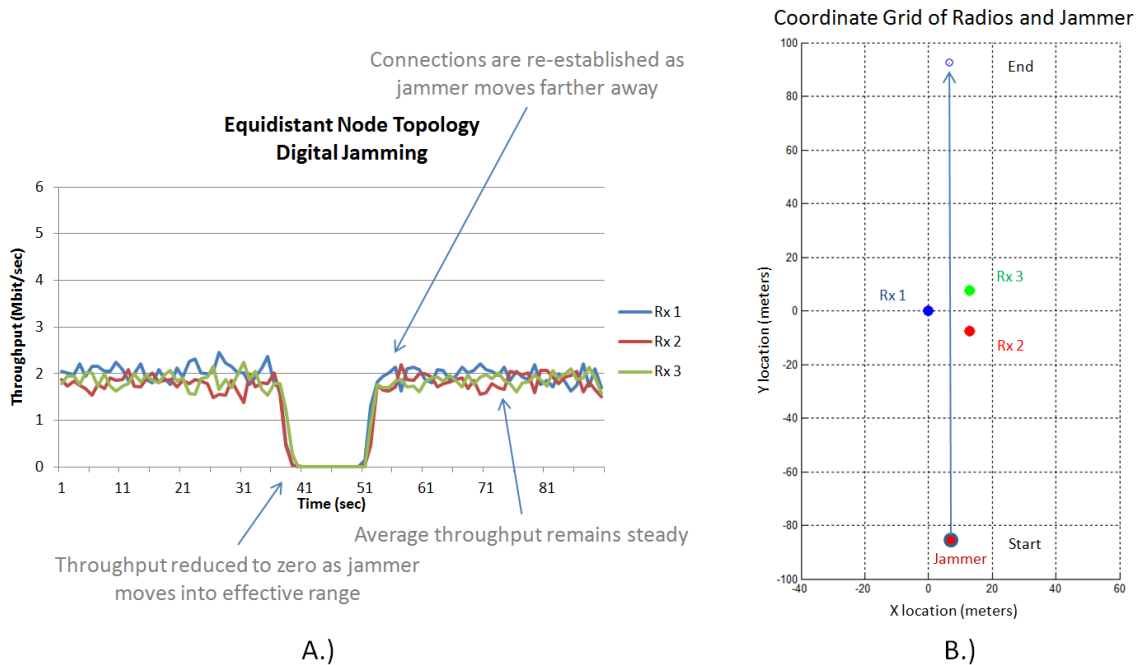


Figure 79: Equidistant node topology in a mobile environment: Throughput vs. Time (A), and Coordinate Grid of Radios and Jammer (B). A Digital jamming node passes between three clients (Rx 1, 2, 3) that are equally spaced (15 meters from each node).

Figure 79 (A, left) shows one run of this scenario. Normally, each scenario is run multiple times in order to acquire three quality samples. A coordinate grid is displayed to the right (B) to help illustrate the location of each node as well as the start and end point of the jammer. Note that only the jammer is mobile. Since there is no flow control within the attenuator control program, each time the scenario is run it can last between 85-90 seconds. Therefore, each scenario was executed multiple times in order to provide at least three quality samples with similar elapsed run times (less than 3 seconds variation).

Notice that as the throughput between one link (two radios) decreases, the throughput between another link will increase. This indicates contention between each node as they compete for resources on the channel. Noted on Figure 79 (A) at 40 seconds is a drop in throughput between all radios. This indicates the effective range of the jammer. In order to validate that the nodes are within this range, consider the following explanation. At 40 seconds, the jammer has moved $40/90 \text{ seconds} = 44\%$ of the total distance of 185 m, which is around 82 m from the starting

point. This location is 7-10 m from Rx 1 and Rx 2. When factoring in FSPL, these distances translate to 57 to 60dB. Since the signal power at each receiver is approximately -50dBm, the SJR at these locations is 7dB to 10dB. Refer to Figure 80 for a more precise, graphical explanation.

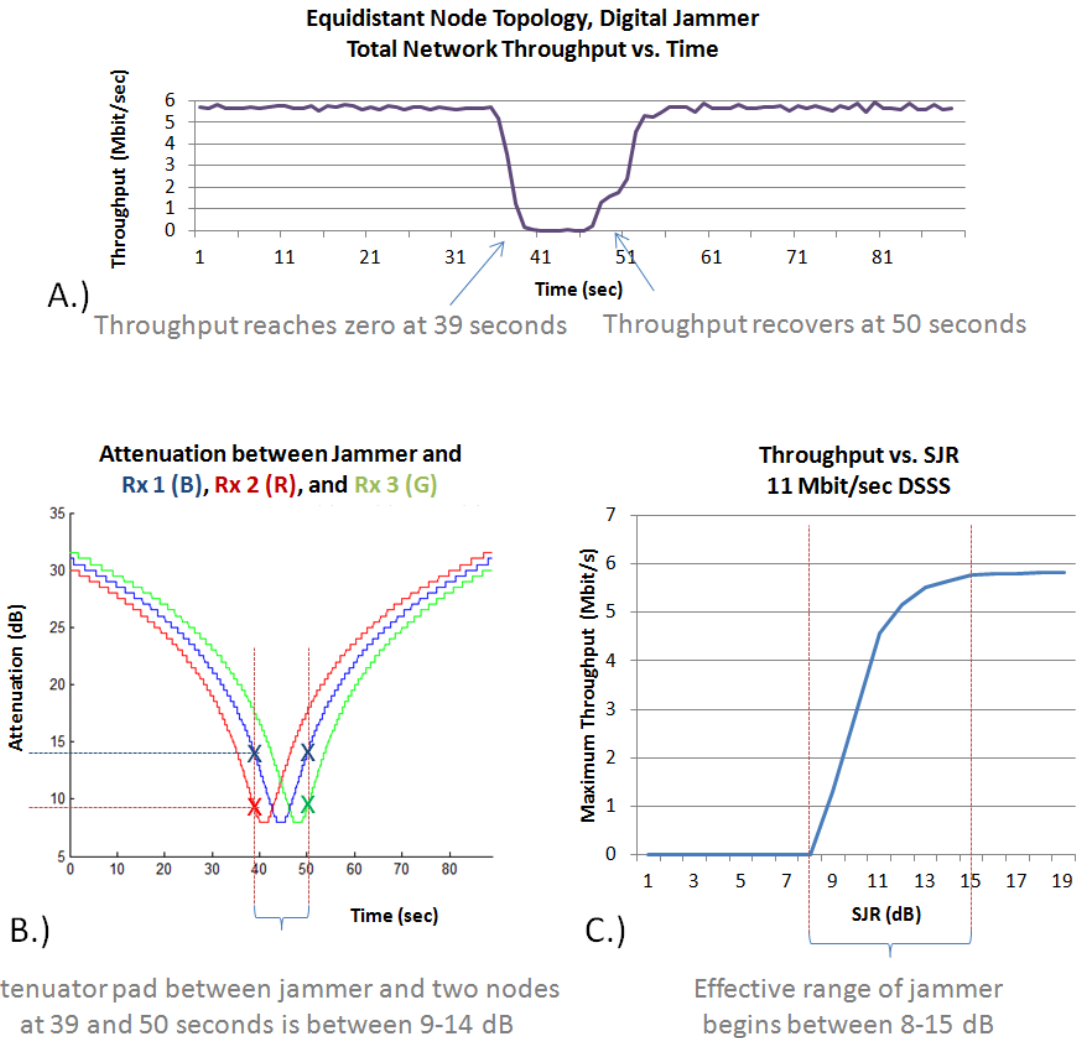


Figure 80: Correlation between Jammer attenuation (distance) and Throughput between nodes for Digital Jammer in Equidistant Node Topology. Total Network Throughput vs. Time (A), Attenuation vs. Time of programmable attenuators (B), Throughput vs. SJR of Digital Jammer in previous PHY layer experiment (C).

Figure 80 (A) shows the sum of throughput between each radio over time (Purple). Note that throughput declines around 39 seconds and recovers around 50 seconds. Figure 80 (B) displays the programmable attenuator values over time between each radio and the jammer. The attenuation at 39 and 50 seconds are marked at 9 and 14dB respectively. Only the lowest two

attenuator values are marked; this is because if two radios are jammed, the total network is considered unavailable. During this 11 second period, the jammer is considered to be $< 15\text{dB}$ from the radio nodes. According to previous PHY layer results in Figure 74, total throughput during this period is expected to be from 0 to 5 Mbit/sec. When comparing these values to Figure 80 (C), it is easy to see at 39 - 50 seconds the jammer has reached its effective range of 0-15dB, and throughput has ceased. Figure 81 displays the same Equidistant scenario with a pulse jammer.

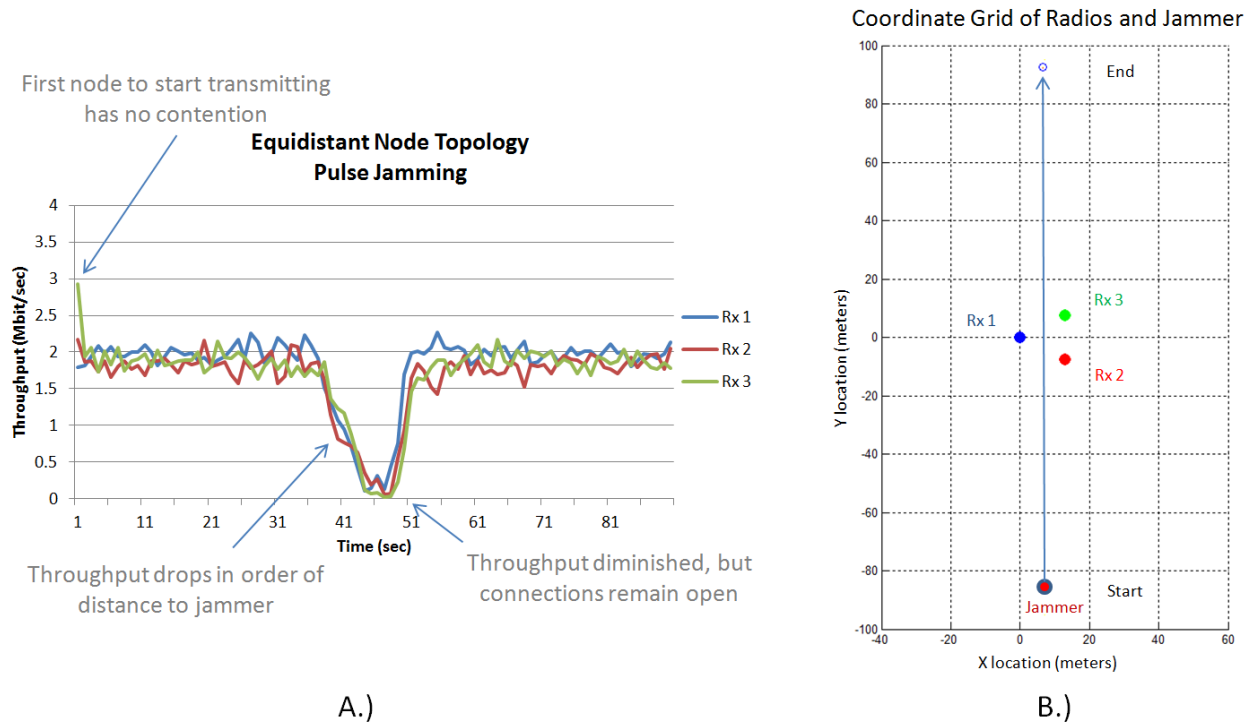
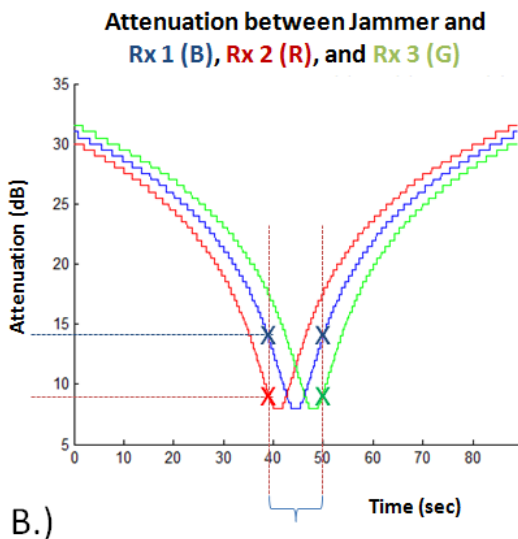
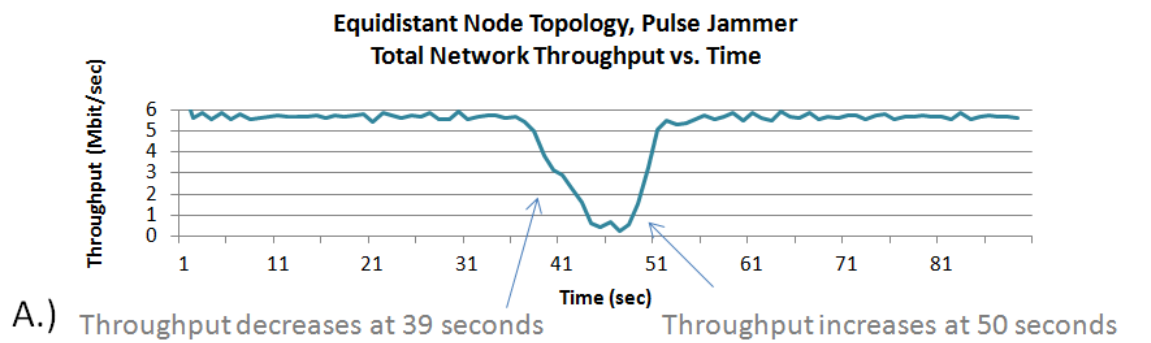


Figure 81: Equidistant node topology in a mobile environment: Throughput vs. Time (A), and Coordinate Grid of Radios and Jammer (B). A Pulse jamming node passes between three clients (Rx 1, 2, 3) that are equally spaced (15 meters from each node).

The only variation in this experiment is the substitution for a Pulse jammer. The first data point in Figure 81 (A) indicates high throughput from Rx 2 to Rx 3 (Green). When starting the experiment, the first node will attempt to transmit while no other clients are on the network. This contention free period allows high throughput, but is short-lived. In Figure 81 (A) throughput decreases in the following order: Rx 2, Rx 1, Rx 3. This has a correlation to the proximity of the jammer as it reaches these nodes in the same order. Nodes recover in a similar

pattern as the jammer leaves the vicinity with Rx 1 receiving the first transmission, although one would expect Rx 2 to recover first.

To show an effective drop in network throughput the pulse jammer had been modified to transmit approximately 75% of the time. The exact value in Mbit/sec was not previously recorded in the PHY layer experiments; however the expected value is between 1.0 - 3.8 Mbit/sec at 0 SJR. In Figure 82 we examine the correlation between the total network throughput and the jammer's effective range.



Attenuation between jammer and two nodes at 39 and 50 seconds is between 9-14 dB

Throughput vs. Pulse Length vs. Pulse Period

Throughput measured in Mbit/sec

Length	Period			
	10ms	5ms	3ms	1ms
100us	5.82	5.81	5.80	5.76
300us	5.79	5.75	5.72	5.56
500us	5.78	5.67	5.62	5.04
700us	5.76	5.54	5.40	3.83
900us	5.73	5.15	4.71	1.04
1000us	5.72	4.87	4.18	0.00

C.)

Pulse jammer is active approximately $\frac{3}{4}$ of total time

Figure 82: Correlation between Jammer attenuation (distance) and Throughput between nodes for Pulse Jammer in Equidistant Node Topology. Total Network Throughput vs. Time (A), Attenuation vs. Time of programmable attenuators (B), Throughput vs. Pulse Length vs. Pulse Period of Pulse Jammer in previous PHY layer experiment (C).

In terms of throughput over time the pulse jammer in Figure 82 (A) shows similar behavior to the Digital jammer, although throughput (Teal) never totally reaches zero. Noticeable declines in throughput are marked starting at 39 seconds, ending at 50 seconds. Figure 82 (B) indicates the attenuation settings for these two points: 9 and 14dB respectively. Although no tests were conducted to measure the SJR range of pulse jamming, the results are within expectations; total network throughput briefly touches below 1 Mbit/sec.

A single sine wave swept across the entire Wi-Fi band (100MHz) every two seconds acts as the jammer in the following experiment. Two second sweeps were selected against the more successful 20 second sweeps due to the short duration of the mobile scenarios; 20 second sweeps could miss the effective range of each radio node entirely. In the same topology and SJR as the previous experiment, a swept jammer has moderate impact on throughput. Figure 83 (A) shows throughput over time, and (B) indicates node and jammer positions on a grid.

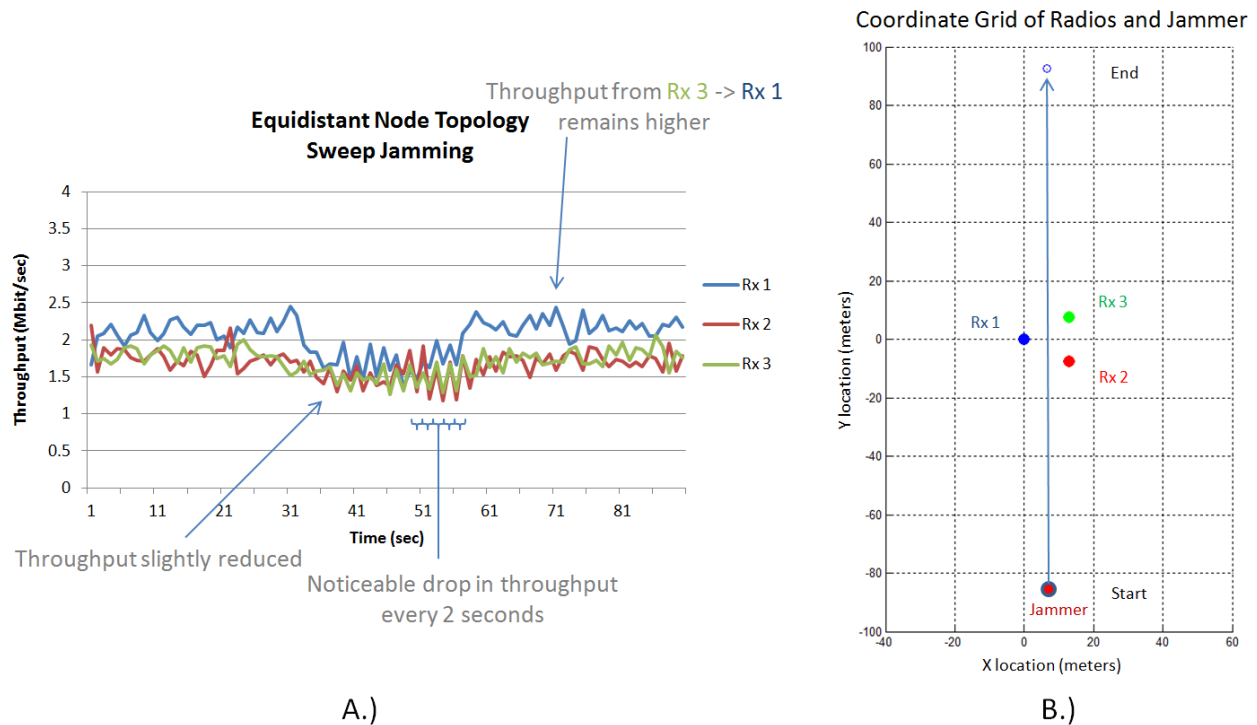


Figure 83: Equidistant node topology in a mobile environment: Throughput vs. Time (A), and Coordinate Grid of Radios and Jammer (B). A Sweep jamming node passes between three clients (Rx 1, 2, 3) that are equally spaced (15 meters from each node).

Although the sweep jammer is not as effective as digital or pulse signals, there is a noticeable decrease in throughput every two seconds. A peculiar result is shown in Figure 83 (A), where

the throughput from Rx 3 to Rx 1 (Blue) remains higher for most of the test period, despite the jammer's proximity to those nodes. Yet, this increase is not reflected among other scenarios and suggests that the problem is not likely an error with path-loss calibration, but perhaps simply a temporary increase in throughput.

Figure 84 (A) demonstrates the correlation between expected throughput when the jammer is closest to each node. At first glance, Figure 84 (A) does not match the throughput shown in (C); previous experiments show that the maximum throughput between 0 and 10dB SJR is between 2.8 – 2.84 Mbit/sec. However, the previous experiment in Figure 72 used a transmit rate of 3.5 Mbit/sec, whereas the current mobile experiment transmits at 11 Mbit/sec. To account for this change, the previous experiment was repeated between two radios at the desired 0-10dB SJR. The results are in agreement; throughput between two radios was averaged to 4.72 – 4.66 Mbit/sec [Figure 84 (C)], and the total network throughput in Figure 84 (A) hover around these values between 33 and 57 seconds.

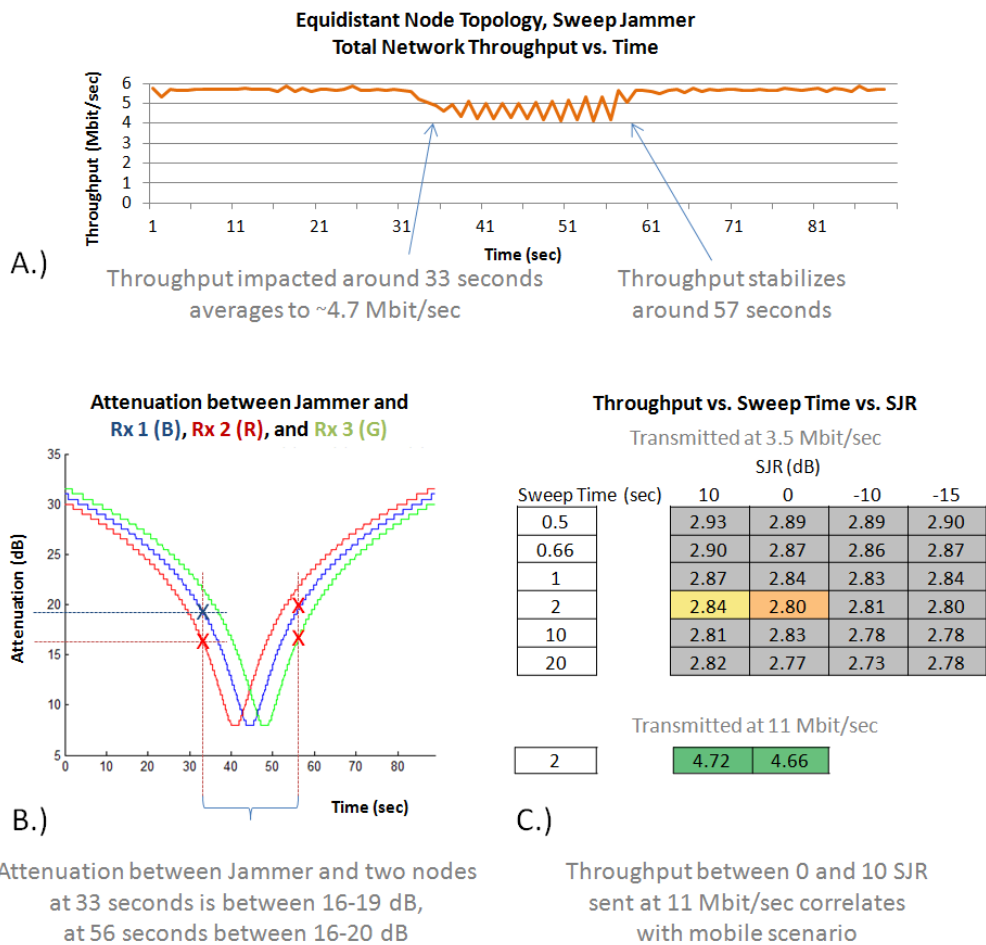
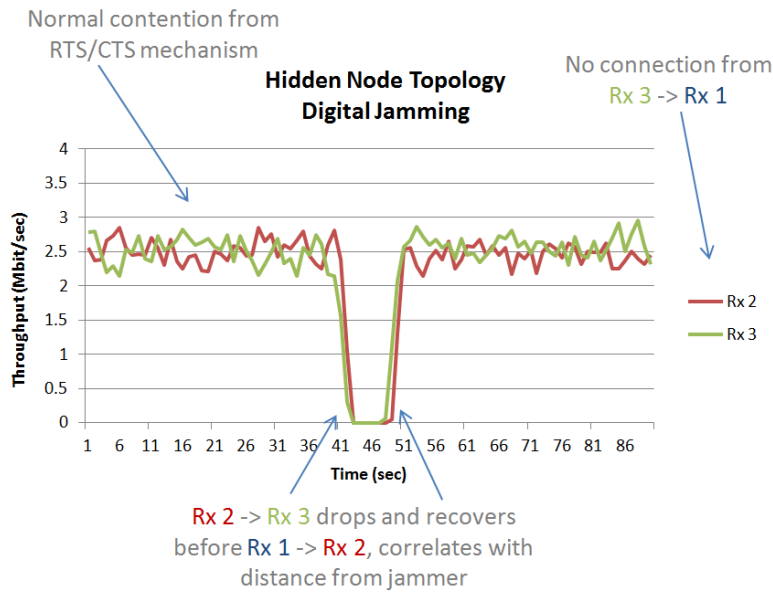


Figure 84: Correlation between Jammer attenuation (distance) and Throughput between nodes for Sweep Jammer in Equidistant Node Topology. Total Network Throughput vs. Time (A), Attenuation vs. Time of programmable attenuators (B), Throughput vs. Sweep Time vs. SJR of Sweep Jammer in previous PHY layer experiment (C).

The sweep jammer seems to affect the network at a much higher SJR (in other words, from a larger distance) than the digital and pulse jammer. Previous tests indicate this difference as well. The experiment in Figure 72 (A) shows no direct impact on throughput (Orange) at 10dB SJR, yet the experiment in Figure 72 (B) shows a modest 17% reduction in throughput. This reduction is congruent in the mobile scenario, where the average throughput without a jammer is ~ 5.7 Mbit/sec, and in close proximity to the jammer the throughput is ~ 4.7 Mbit/sec. These results confirm expected values when introducing the mobile platform.

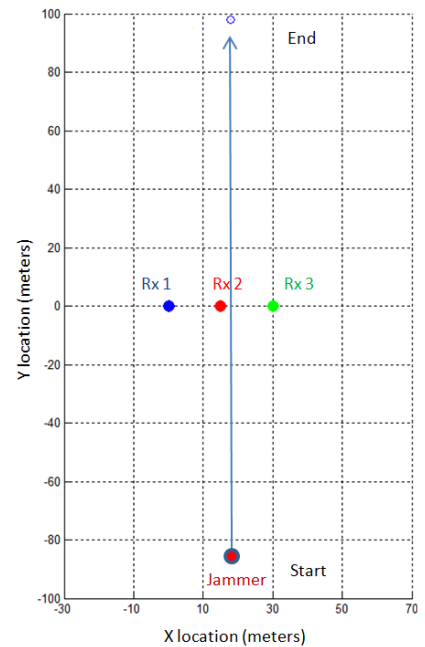
The hidden node topology was chosen as a scenario to examine the impacts of jamming a network that relies on the CSMA/CA protocol. To create a hidden node, the most distant nodes must not be able to communicate. Keeping the signal levels at the receiver within the -50dBm target range required a virtual separation of each node by 15 m. Normally, Rx 1 and Rx 3 can communicate with each other at a distance of 30 m, thus their link was separated manually. This is accomplished by disconnecting the cables between the attenuators and couplers of Rx 1 and Rx 3, and terminating those connections with 50 Ω . With this method, each receiver maintains the target signal level of approximately -50dBm, but Rx 1 and Rx 3 must rely on RTS/CTS handshakes to establish a connection with Rx 2.

Additionally, we used the wireless configuration utility in the Gumstix radio to confirm Rx 1 could not communicate with Rx 3. The Gumstix occasionally reported a signal level of -80dBm, and other times did not report any signal at all. The appearance of a signal when the connections are terminated may indicate a leak of Wi-Fi radiation through the shielded boxes or by coupling through the power cables.



A.)

Coordinate Grid of Radios and Jammer



B.)

Figure 85: Hidden node topology in a mobile environment: Throughput vs. Time (A), and Coordinate Grid of Radios and Jammer (B). A Digital jamming node passes between three clients (Rx 1, 2, 3) that are spaced apart laterally as to emulate a hidden node (Rx 1 and Rx 3 cannot communicate with each other).

Since Rx 3 cannot communicate with Rx 1, their throughput is not shown in Figure 85 (A). We observed normal behavior of RTS/CTS contention on the network. The jammer affects throughput at roughly the same time intervals as the equidistant node experiment (39 to 50 seconds). It is also shown that the link between Rx 2 to Rx 3 breaks and recovers before Rx 1 to Rx 3, which agrees with expectations that the jammer will first affect nodes closest to it, and those nodes will also be the first to recover as the jammer moves further away.

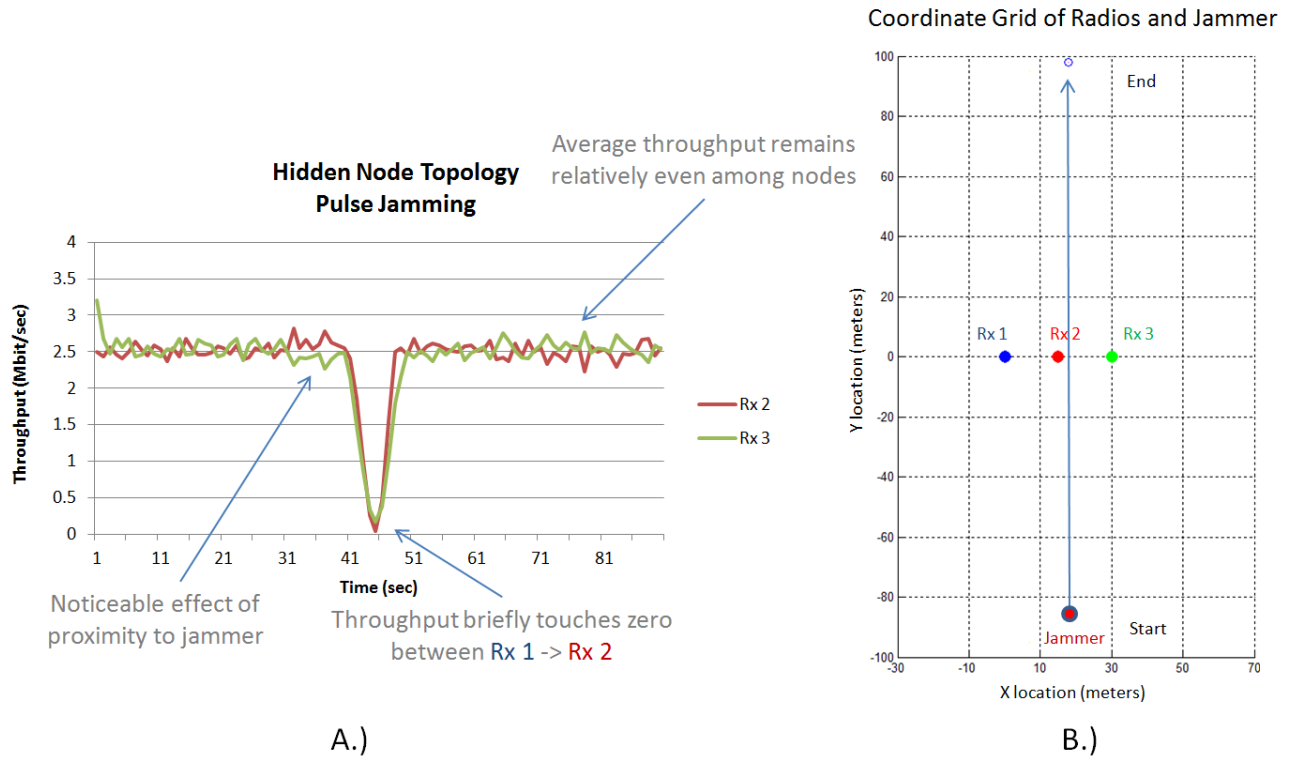


Figure 86: Hidden node topology in a mobile environment: Throughput vs. Time (A), and Coordinate Grid of Radios and Jammer (B). A Pulse jamming node passes between three clients (Rx 1, 2, 3) that are spaced apart laterally as to emulate a hidden node (Rx 1 and Rx 3 cannot communicate with each other).

This experiment exhibits a shorter jamming duration, with throughput recovering more quickly than with digital jamming. As the jammer approaches around 36 seconds, there is a noticeable separation in throughput between Rx 2 to Rx 3 (Green) compared to the link from Rx 1 to Rx 2 (Red). This effect is seen in all hidden node scenarios and shows that even though the jammer is only 3 meters closer to Rx 3 than Rx 1, it appears to have an impact on the network.

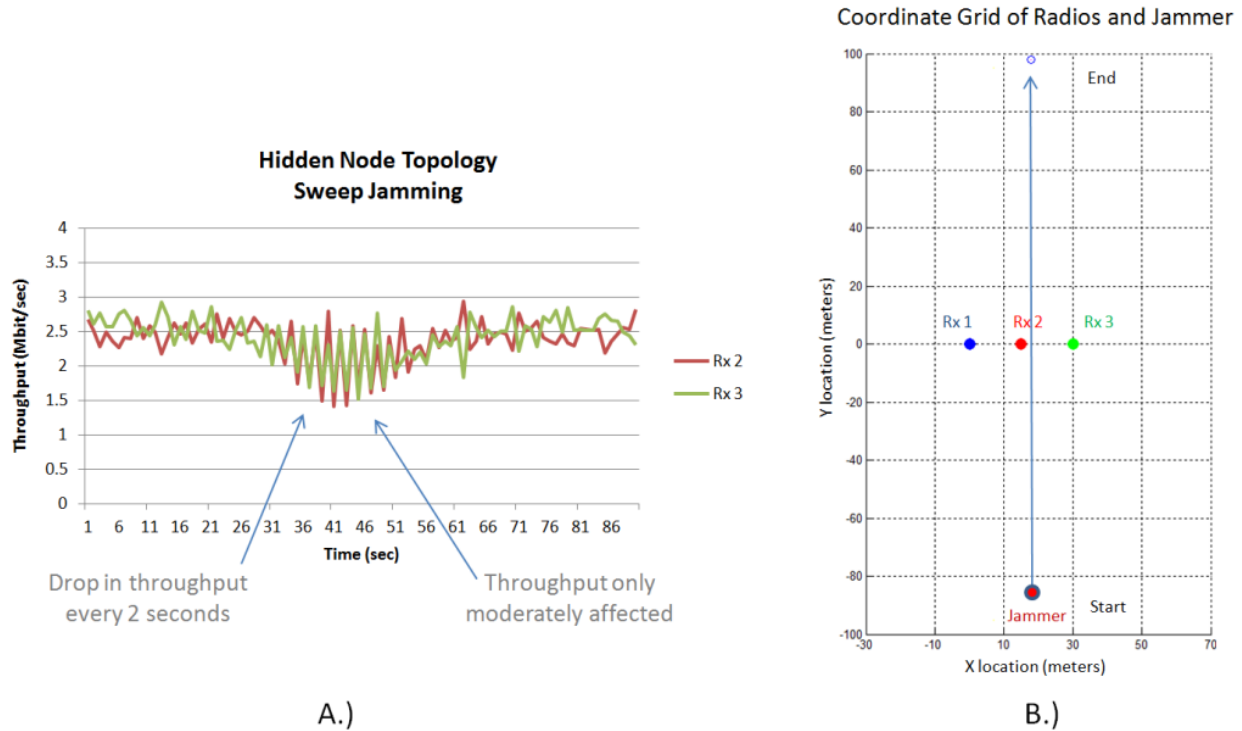


Figure 87: Hidden node topology in a mobile environment: Throughput vs. Time (A), and Coordinate Grid of Radios and Jammer (B). A Sweep jamming node passes between three clients (Rx 1, 2, 3) that are spaced apart laterally as to emulate a hidden node (Rx 1 and Rx 3 cannot communicate with each other).

We observed an increased range of performance when using a Sweep waveform; notice the periodic drop in throughput in Figure 87 (A) is evident beginning around 30 seconds, which is around 10 seconds earlier (~20 m ahead), where the link is also slow to recover. The sweep jammer may be able to disturb MAC layer protocols more effectively than other waveforms, which would explain its ability to affect throughput at a greater distance.

Preparation for a distant node scenario is similar to the hidden node experiment in that the link between the two furthest nodes is broken; in this case, Rx 3 to Rx 1. The connection between the programmable attenuators and couplers between Rx 1 and Rx 3 were left untouched with a 50 Ω termination from the hidden node experiment.

In Figure 88 (A) it is clear that the jammer affects Rx 3 (Green) within the first 10 seconds. The throughput received at Rx 2 (Red) reaches only 5 Mbit/sec of the typical maximum 5.8 Mbit/sec. This virtual ceiling may be due to the overhead of attempted retransmissions of Rx 2 while Rx 3 is unavailable, in combination with a longer distance (thus, smaller data rate). Figure 93

indicates a reduced maximum throughput between all hidden and distant node scenarios, which seem to support this theory.

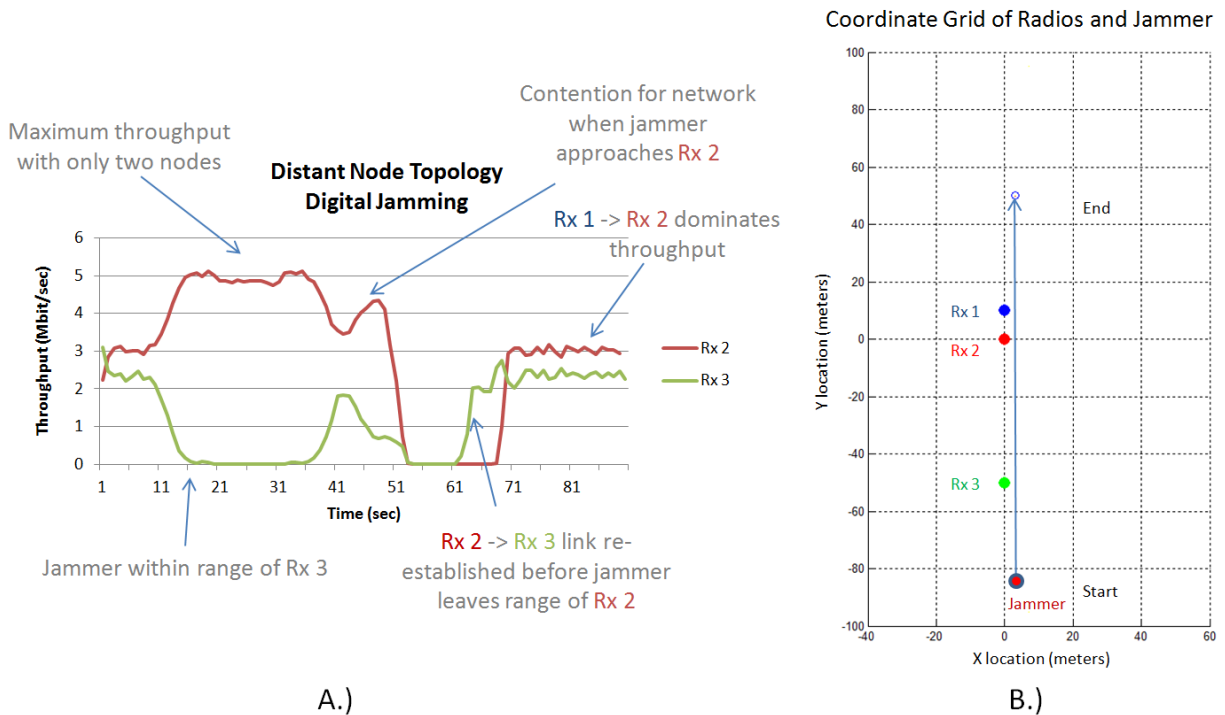


Figure 88: Distant node topology in a mobile environment: Throughput vs. Time (A), and Coordinate Grid of Radios and Jammer (B). A Digital jamming node passes between three clients (Rx 1, 2, 3); Rx 3 is isolated and can only communicate with Rx 2 from a longer distance.

There is a noticeable loss in throughput between Rx 1 to Rx 2 (Red), and an increase in throughput between Rx 2 to Rx 3 (Green). This is likely due to the sudden availability of Rx 3 as the jammer is not within effective range of any node, followed by a loss in throughput at node Rx 2. As expected, the link between Rx 2 to Rx 3 recovers before the link between Rx 1 to Rx 2 (at approximately 61 seconds).

Figure 88 (A) shows that the maximum throughput achieved by Rx 2 to Rx 3 is less than the throughput achieved by Rx 1 to Rx 2, which is also expected since throughput decreases with distance. However, the results of the next experiment conflict with this theory; the data rate between both links average out towards the end of the test, shown in Figure 89 (A).

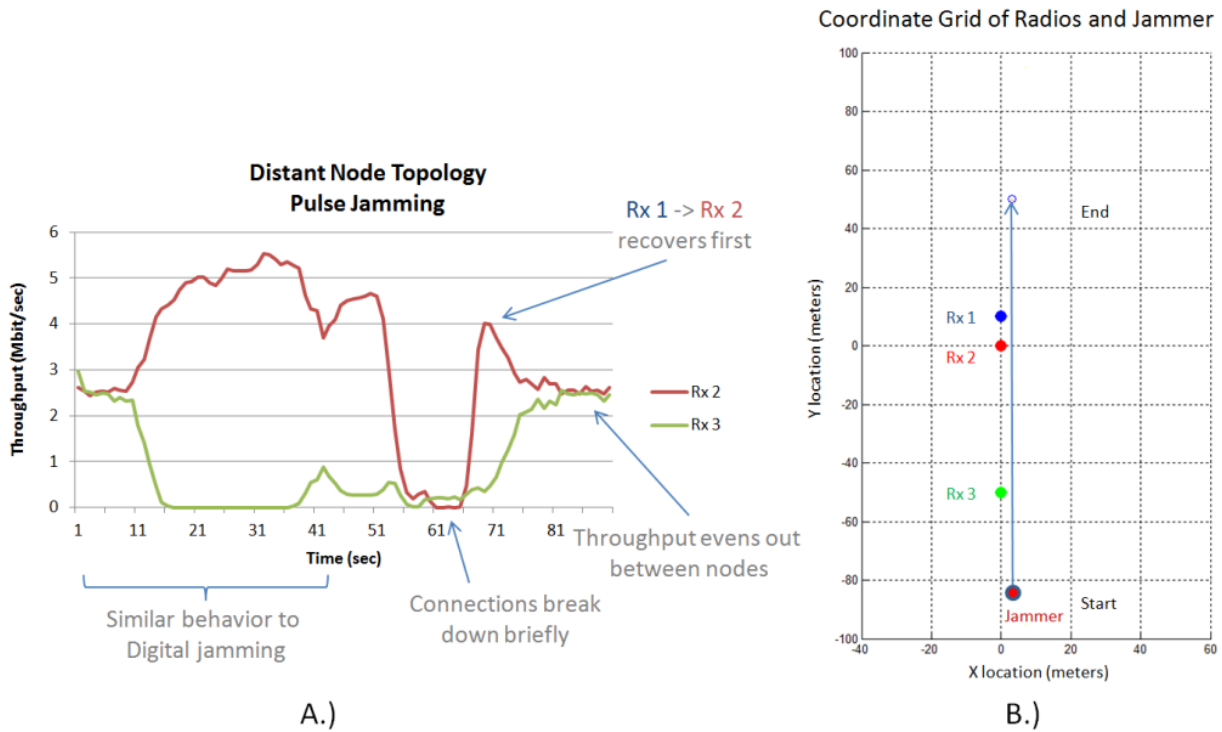
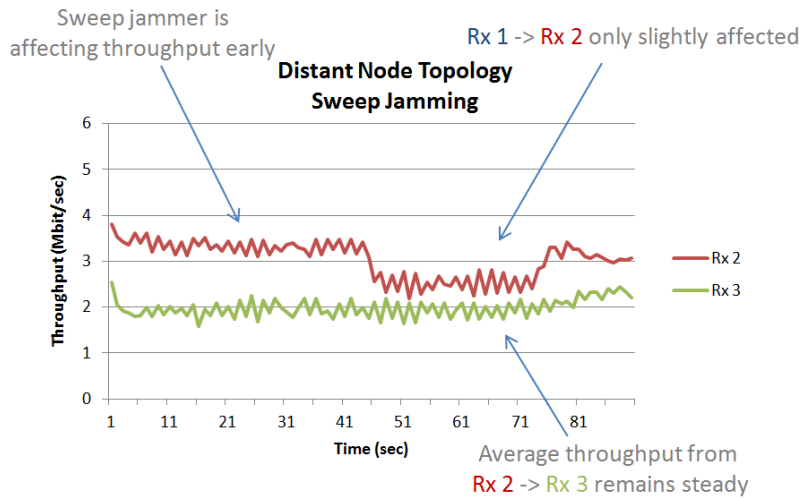


Figure 89: Distant node topology in a mobile environment: Throughput vs. Time (A), and Coordinate Grid of Radios and Jammer (B). A Pulse jamming node passes between three clients (Rx 1, 2, 3); Rx 3 is isolated and can only communicate with Rx 2 from a longer distance.

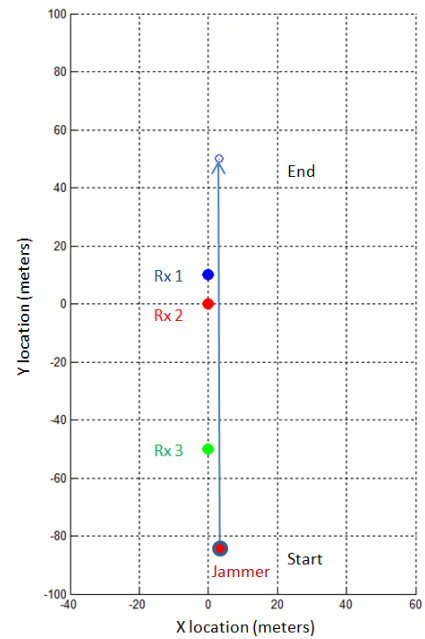
Figure 89 (A) shows different behavior from the beginning of the experiment. These differences are subtle; refer to Figure 93 for a clearer comparison between jamming techniques. We observed a similar contention point at 41 seconds, although it appears as though the signal from Rx 1 to Rx 2 (Red) is strong enough to dominate the spectrum. At about 60 seconds, we notice that the link from Rx 1 to Rx 2 breaks down, but quickly recovers while the link from Rx 2 to Rx 3 is delayed, unlike the digital jammer in Figure 88 (A). This may be due to the weakness of the pulse jammer to effectively prevent Rx 1 from communicating with Rx 2.

Additionally, throughput averages out between both links to the same value of 2.5 Mbit/sec after 75 seconds, unlike Figure 88. The fact that both links can achieve equal throughput suggests that Rx 3 is not far away enough to lose a contention for resources. The next experiment involves a sweep jammer in the same distant node topology.



A.)

Coordinate Grid of Radios and Jammer



B.)

Figure 90: Distant node topology in a mobile environment: Throughput vs. Time (A), and Coordinate Grid of Radios and Jammer (B). A Sweep jamming node passes between three clients (Rx 1, 2, 3); Rx 3 is isolated and can only communicate with Rx 2 from a longer distance.

The effectiveness of a sweep jammer at these specifications is questionable (100MHz sweep range of a 22MHz channel). However, we do notice some effect from the sweep jammer at a very early stage. This is in agreement with our experimental results, as the sweep jammer achieves a 15% reduction in throughput from only 10dB SJR, it is likely to have a smaller effect from 15-20dB SJR.

An interesting point of this graph is the reduction in throughput at the receiver of Rx 2, yet no reduction at Rx 3. Even though the jammer reaches the same proximity to all nodes, it is not powerful enough to decrease throughput beyond 2.5 Mbit/sec, and since Rx 3 is already limited in throughput (from a distance), the jammer has little effect on this node. Compared to other techniques, each jammer's performance is varied, as shown in Figure 91.

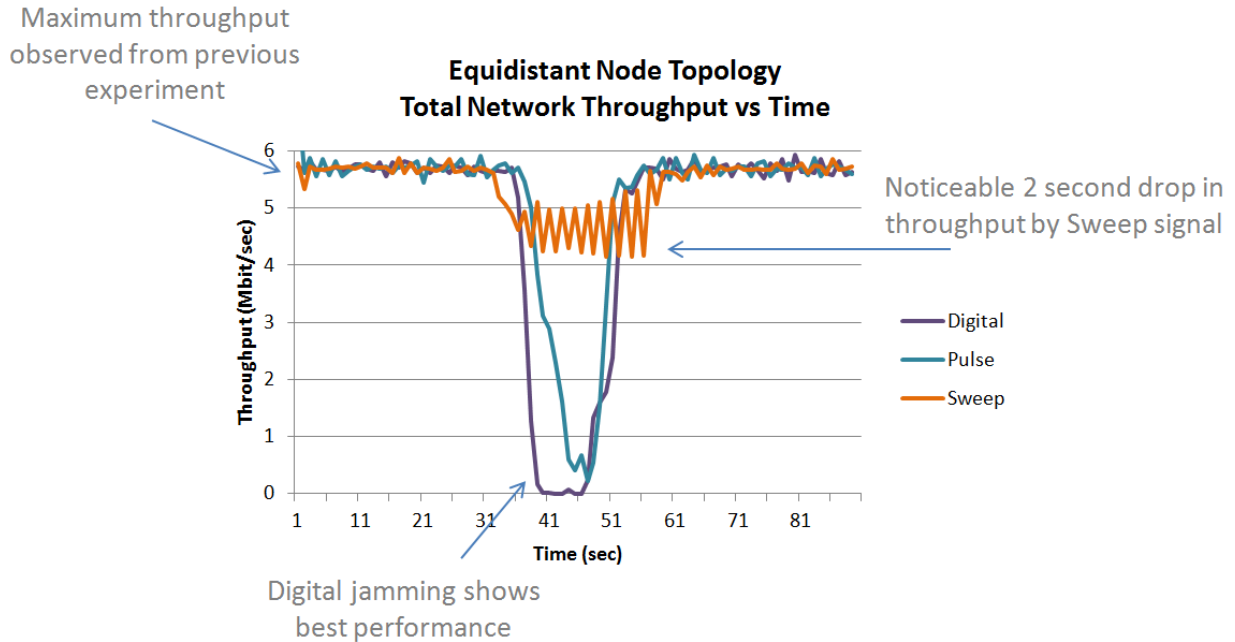


Figure 91: Comparison of performance among different jamming techniques in a mobile, Equidistant node topology. Graph of Total Network Throughput vs. Time of Digital, Pulse, and Sweep jamming.

Digital jamming (Purple) clearly shows improved performance over the Pulse (Teal) and Sweep (Orange) methods. Maximum throughput matches results from previous experiments: around 5.7-5.8 Mbit/sec average without presence of a jammer. Pulse jamming results also agree with results taken from previous experiments: nearly 1 Mbit/sec at close range of the jammer. A sweep tone with a range only across channel 1 of Wi-Fi 802.11b/g may show increased performance and perhaps the ability to interfere with enough packets to cause a disconnection or disassociation between nodes.

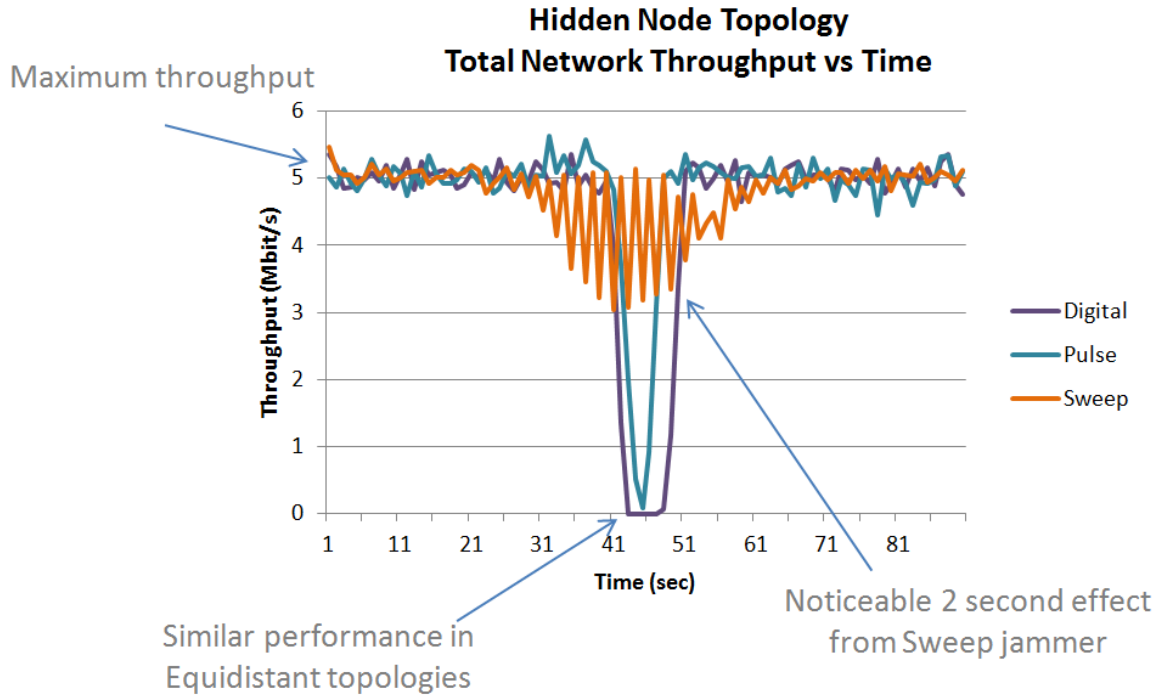


Figure 92: Comparison of performance among different jamming techniques in a mobile, Hidden node topology. Graph of Total Network Throughput vs. Time of Digital, Pulse, and Sweep jamming.

Total throughput in Figure 92 is approximately 5 Mbit/sec, compared to 5.8 Mbit/sec in the Equidistant node topology. The reduction in throughput may be due to the added overhead when relying on a middle node. The sweep jammer seems to have less of an effect, but a wider range of variability; another indication of its ability to affect communications with high SJR, most likely by affecting the MAC layer.

However, since the two radio testbed results of sweep tone jamming are similar to results produced by Harjula et. al., indicating an effect with an SJR < 10dB, the values shown in Figure 92 remain an undefined anomaly of the four radio testbed as it suggests a range of SJR > 10dB.

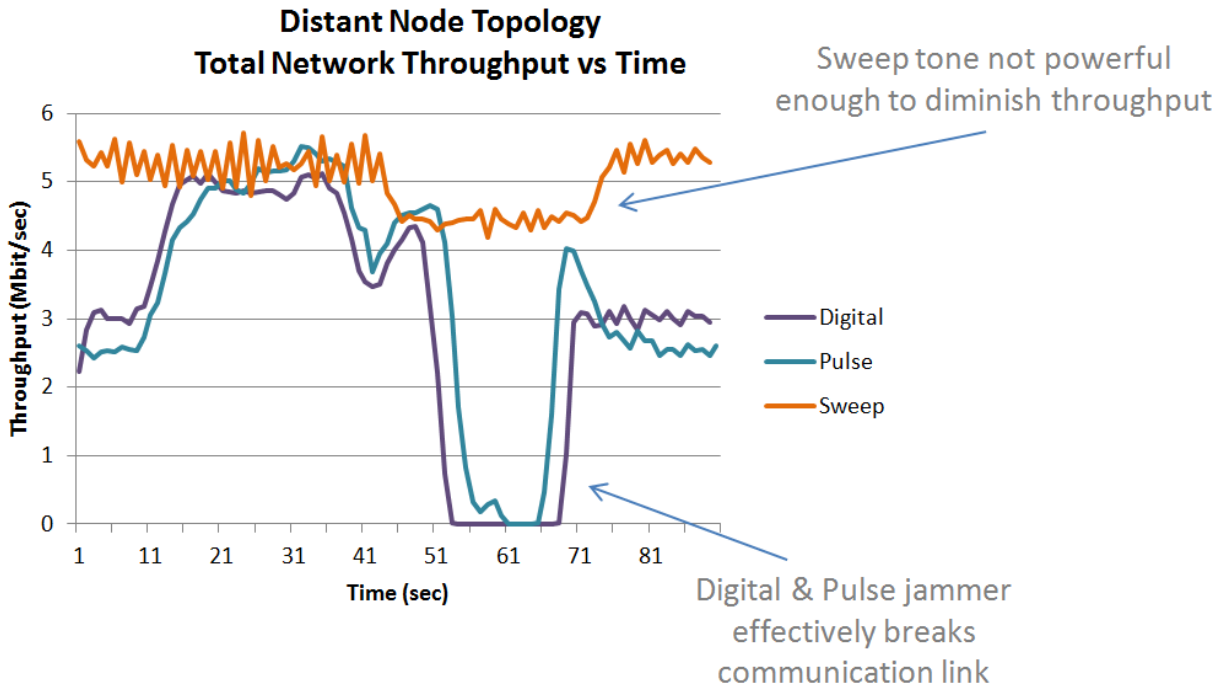


Figure 93: Comparison of performance among different jamming techniques in a mobile, Distant node topology. Graph of Total Network Throughput vs. Time of Digital, Pulse, and Sweep jamming.

From Figure 93, we see a definitive separate in performance from sweep jamming, but the digital and pulse techniques show a split in performance at two intervals. At 21 seconds and 73 seconds the effectiveness of the digital and pulse jammers alternate, implying that a Pulse jammer is more effective against distant nodes from greater than 10 meters, but a Digital jammer is more effective at closer ranges.

Overall we observed mostly predictable behavior with a few discrepancies. It was predicted and later verified that the mobile jammer would affect the radio nodes according to its effective range derived from the PHY layer experiments. However, even though we used different software (substituted GNURadio for MATLAB) in the digital jamming experiment, we did not expect such a dramatic increase in effective range (6-7dB). This was explained and confirmed in Figure 74 and Figure 75 by the increase in bandwidth of signals produced by GNURadio as opposed to MATLAB.

It was unexpected to see a slight increase in performance of sweep and digital jamming. Although, these gains could be explained by the addition of shielded boxes and the placement of copper tape along power cables in the four radio testbed (the previous two radio testbed had no

shielding over the Gumstix) which help to reduce Wi-Fi radiation and consequently prevent signals from bypassing the jammer, but this does not explain the decreased performance of pulse jamming.

4.2.1 MAC Layer Mobile Jamming

We began testing the theory that repeated beacons would have an impact on network throughput. Approximately four seconds of typical beacon traffic between three nodes was captured using GNURadio and the USRP. This data was then played back into a wireless card connected to a computer with Linux: Backtrack. A tool called “horst” (Highly Optimized Radio Spectrum Tool) confirmed that the packets being transmitted were legitimate. Additionally, we observed the iwconfig utility on one single wireless node (unconnected to any network) which reported a valid connection. This means that the process of recording and play-back of the wireless beacon traffic was being correctly received.

Traffic was recorded when all three nodes were using WEP encryption and a 1 Mbit/s data rate. Then, the network was modified to use no encryption and a 54 Mbit/s rate. We observed an impact on throughput when this recording was played back into the network within a maximum range of 15-20dB SJR. However, we also transmitted pulsed noise designed to mimic the wireless traffic but did not contain any useful information, and this had the same impact on throughput. This means that the replayed beacons had the same impact as pulsed noise, and suggest that the network is not affected by malicious beacon traffic.

On the contrary, it may be that the wireless nodes are rejecting these beacon packets as they are not properly synced with their own beacons. Unfortunately, due to time constraints our team was not able to completely explore the “reactive” portion of this experiment. We did find that the Wireshark tool was not able to display management frames, and was not fast enough to support reliable predictions of beacon traffic. In the future we would suggest aligning fake beacon traffic to occur directly before or after the target’s beacon, at which time the target would be more likely to accept the new information as it aligns with other beacons. This could be implemented using UHD tools instead of GNURadio, which would offer a much faster response time.

5 Conclusions and Future Work

The RF channel emulator designed, built, and tested in this project provided a suitable testing platform for PHY layer jamming techniques on a mobile configuration of radios. Results from testing and validation indicate that the testbed is functional and representative of a simplified RF channel. In addition, results from the mobile PHY layer jamming experiments suggest that the testbed is a viable platform for investigating jamming methods and techniques. Its mid-range price tag achieves an economical balance between the high fidelity of hardware systems and the repeatability of wireless channel emulators. The demonstration of the MAC layer attack was unsuccessful; a repeated beacon signal did not seem to have an effect on network performance, however this topic was not fully explored. Finally, while the testbed served the purposes and scope of the project, the team has identified several improvements and alterations that could increase accuracy and robustness. In this chapter, key conclusions will be described followed by areas identified for additional work and development.

The tests on various components and the system as a whole indicated that the testbed designed and built over the course of this project meets specifications and is fully functional. As originally defined, key specifications for the testbed included attenuator switching speed less than 1 ms, isolation greater than 20dB between different paths, less than 45dB loss through the system, and no greater than 2dB of variation in loss between those paths. As shown in the results and discussion chapter, these specifications have been met.

In general, the channel emulator performed to specification based upon testing. It also performed well in the validation testing done. In order to verify the functionality of the channel emulator, the team repeated some stationary PHY layer experiments from a publication by Harjula et al [7] and compared results. When results were compared with this published research, the team findings contained an acceptable amount of error which could otherwise be explained by the substitution of equipment and software. This served as a validation of the channel emulator, confirmed testing procedure, and provided a benchmark for future mobile scenarios.

Our research into the performance and effects of various jamming techniques in a mobile environment produced expected results; in most scenarios, digital jamming remains the most effective against 802.11 receivers, compared to pulse and sweep jamming. Yet, these findings

are preliminary. Additional research using wireless cards that offer enhanced control and flexibility (for instance the ability to definitively control modulation, data rate, transmit power, and MAC layer controls) would allow for selective tests that target specific layers of the 802.11 protocol and could help to answer *how* each technique affects communications while moving.

While the team did not ultimately have enough time for any conclusive testing on the MAC layer beacon frame attack, some preliminary testing was completed. The 'reactive' portion of the technique was found to be challenging due to timing limitations, so beacons were instead replicated without precise timing. The team found that replicating a client's beacon frame using false encryption and data rates did not severely affect network performance. A noticeable drop in throughput was observed, but this is likely correlated to collisions from transmitting beacon packets. It is possible that other nodes on the network are rejecting these false packets. Future work in this area could implement a truly reactive beacon to confirm this theory.

Although the channel emulator met testing requirements for this project, there are several steps that could be taken to improve its utility as a long term test asset. For example, although the channel emulator is designed to support testing from 2 to 8GHz, it is only calibrated for the Wi-Fi band. Extending calibration over the entire band would make the channel emulator useful for a wider variety of testing scenarios. An even larger bandwidth could be supported if the 30MHz to 3GHz parts are added to the system as discussed in the methodology. Some enhancements might also be added that could improve the range of mobile situations that can be represented on the channel emulator. Currently, the channel emulator supports changing geometries where each node starts and ends at a specified location and moves between those two locations during the simulation in a straight line at a constant rate over a specified run time. A more complicated scenario might involve motion beyond just a straight line. More sophisticated MATLAB code would enable this type of experiment. A GUI which prompts users for information regarding node placement and then generates corresponding graphic depicting the moving nodes might also improve the usability of the channel emulator.

In addition to increasing the number of testing scenarios supported by the channel emulator, system durability and robustness could be improved with further work. One potential area for improvement involves the attenuator driving mechanism. In the current setup, the attenuators are

driven by an NI PCI card connected to a breadboard through a breakout board. An FPGA might offer cleaner signals and more flexibility. The breadboard itself is not the best long term setup. Replacing that with a more permanent structure with soldered connections might reduce any problems due to the temporary nature of the high density pin connectors.

In summary, the team constructed a functional, four node, 2 – 8GHz channel emulator calibrated over the Wi-Fi band. This channel emulator was used to test a series of mobile jamming techniques in three different scenarios. The team found that digital jamming shows an increased ability to negatively affect network performance when compared with pulse and sweep techniques, except in distant node topologies where pulse jamming displays better performance at a distance greater than 10 meters.

Our increased reliance on wireless communications, especially in crowded public safety bands, underlies the importance of spectrum reallocation for use by emergency responders during a crisis. The ability to utilize a calibrated, wireless, mobile test environment is critical to those who wish to alleviate the problem of congested networks. We hope that continued development of flexible test platforms, such as the channel emulator described in this report, will contribute to effective re-establishment of communications by emergency responders and authorized personnel in the event of a natural disaster.

6 References

- [1] The Guardian, "Tsunami report criticises relief effort," 5 10 2005. [Online]. Available: <http://www.guardian.co.uk/world/2005/oct/05/internationalaidanddevelopment.tsunami2004>. [Accessed 2 10 2012].
- [2] T. W. House, "The Federal Reponse to Hurricane Katrina: Lessons Learned," 2006.
- [3] Satellite Today, "Proactive Measures Needed When it Comes to Communications," 3 10 2005. [Online]. Available: http://www.satellitetoday.com/via/features/Proactive-Measures-Needed-When-It-Comes-To-Communications_278.html. [Accessed 2 10 2012].
- [4] A. M. Townsend and M. L. Moss, "Telecommunications Infrastructure in Disasters," New York University: Center for Catasrophe Preparedness and Response, 2005.
- [5] A. Bogan, "DHS Official Says Cell Phone Emergency Service Failed During Eastern Quake," ExecutiveGov, 29 Nov 2011. [Online]. Available: www.executivegov.com/2011/11/dhs-official-says-cell-phone-emergency-service-failed-during-eastern-quake/. [Accessed 3 September 2012].
- [6] F. C. Commission, "Public Safety/Private Partnership," Public Safety and Homeland Security Bureau, [Online]. Available: transition.fcc.gov/pshs/public-safety-spectrum/700-MHz/partnership.html. [Accessed 3 September 2012].
- [7] I. Harjula, J. Pinola and J. Prokkola, "Performance of IEEE 802.11 Based WLAN Devices Under Various Jamming Signals," VTT Technical Research Centre of Finland, Oulu, 2011.
- [8] R. Vaidya, C. Yadav, J. Kunkumath and P. Yadati, "Network Congestion Control: Mechanisms for Congestion Avoidance and Recovery," Juniper Networks, Bangalore, 2011.
- [9] P. Hart, L. Heyse and A. Boin, "New Trends in Crisis Management Practice and Crisis Management Research: Setting the Agenda," *Journal of Contingencies and Crisis Management*, vol. 9, no. 4, p. 182, 2001.
- [10] T. W. Coombs, *Ongoing Crisis Communication*, Thousand Oaks: SAGE Publications, Inc., 2012.
- [11] R. Miller, "Hurricane Katrina: Communications & Infrastructure Impacts," 2006. [Online]. Available: www.carlisle.army.mil/DIME/documents/Hurricane%20Katrina%20Communications%20&%20Infrastructure%20Impacts.pdf. [Accessed 3 9 2012].

- [12] A. Kwasinski, "Effects of Notable Natural Disasters from 2005 to 2011 on Telecommunications Infrastructure," University of Texas at Austin, Austin, 2011.
- [13] R. C. Johnson, S. A. William and A. G. Klein, *Software Receiver Design*, Cambridge, UK: Cambridge University Press, 2011.
- [14] W. Stallings, *Data and Computer Communications*, Upper Saddle River, NJ: Prentice Hall, 2011.
- [15] ADC Telecommunications Inc., "Modern Technology vs. HFC Ingress Noise," 1 March 2001. [Online]. Available: www.adc.com/us/en/Library/Literature/100327EC.pdf.
- [16] P. De, S. Sharma and T. Chiueh, "Design considerations for a multihop wireless network testbed," *Communications Magazine, IEEE*, pp. 102-109, 2005.
- [17] T. Krop, M. Hollick, P. S. Mogre and R. Steinmetz, "A survey on real world and emulation testbeds for mobile ad hoc networks," in *Testbeds and REsearch Infrastructures for the Development of Networks and Communities*, Barcelona, 2006.
- [18] S. Sanghani, T. Brown, S. Bhandare and S. Doshi, "EWANT: the emulated wireless ad hoc network testbed," in *Wireless Communications and Networking*, New Orleans, 2003.
- [19] K. Bialkowski and M. Portmann, "Design of testbed for wireless mesh networks," in *Antennas and Propagation Society International Symposium*, Toronto, 2010.
- [20] T. Clancy and B. Walker, "MeshTest: laboratory-based wireless testbed for large topologies," in *TridentCom 2007*, Lake Buena, 2007.
- [21] Rutgers University, "ORBIT - Wireless Network Testbed," 2012. [Online]. Available: www.winlab.rutgers.edu/docs/focus/ORBIT.html.
- [22] JFW Industries, "RF Matrix Switch Application Note," [Online]. Available: http://www.jfwindustries.com/catalog/RF_Matrix_Switch_App_Note-111-1.html.
- [23] G. Judd, D. D. Stancil and P. Steenkiste, "FPGA-Based Channel Simulator for a Wireless Network Emulator," in *Vehicular Technology Conference*, Barcelona, 2009.
- [24] Elektrobit, [Online]. Available: <https://www.elektrobit.com/file.php?id=3038>. [Accessed 20 September 2012].
- [25] W. A. Arbaugh, N. Shankar and Y. J. Wan, "Your 802.11 Wireless Network has No Clothes*," Department of Computer Science, University of Maryland, 2001.
- [26] IEEE, "The IEEE Standards Association - 802.11i-2004," 2004. [Online]. Available:

- <http://standards.ieee.org/getieee802/download/802.11i-2004.pdf>. [Accessed 23 8 2012].
- [27] W. Chou, "Architecture Lecture Notes," 2004. [Online]. Available: <http://www4.ncsu.edu/~chou/course/LectureNotes/architecture.htm>.
- [28] K. Pahlavan and P. Krishnamurth, Principles of Wireless Networks, Prentice Hall, 2002.
- [29] Agilent, "RF Testing of WLAN Products - Application Note 1380-1," 2007.
- [30] J. Fakatselis and M. Belkerdid, "Processing Gain for Direct Sequence Spread Spectrum Communication Systems and PRISMTM," Harris Semiconductor, 1996.
- [31] R. A. Poisel, Modern Communications Jamming: Principles and Techniques, Norwood: Artech House, 2011.
- [32] Wi-Fi Alliance, "WiFi CERTIFIED n: Longer-Range, Faster-Throughput, Multimedia-Grade WiFi Networks," 2009.
- [33] J. DiMascio, "Jammers Causing Interference in Iraq," *InsideDefense.com*, 2006.
- [34] National Instruments, "Two-Tone Third-Order Intermodulation Distortion Measurement," National Instruments, 15 March 2010. [Online]. Available: <http://www.ni.com/white-paper/4384/en>. [Accessed 31 August 2012].
- [35] E. Bayraktaroglu, C. King, X. Liu, G. Noubir, R. Rajaraman and B. Thapa, "Performance of IEEE 802.11 under Jamming," 2010.
- [36] P. Romano, "The Range vs. Rate Dilemma of WLANs," *EE Times*, 2004.
- [37] B. Walker, I. Vo, M. Beecher and C. Clancy, "A demonstration of the MeshTest wireless testbed," in *TridentCom*, Washington, DC, 2009.
- [38] D. Raychaudhuri, I. Seskar, M. Ott, S. Ganu, K. Ramachandran, H. Kremo, R. Siracusa, H. Liu and M. Singh, "Overview of the ORBIT radio grid testbed for evaluation of next-generation wireless network protocols," in *Wireless Communications and Networking Conference, 2005 IEEE*, 2005.
- [39] National Severe Storms Laboratory, "Questions and Answers about Lightning," 20 July 2009. [Online]. Available: http://www.nssl.noaa.gov/primer/lightning/lgt_climatology.html.
- [40] National Instruments, "Testing Wireless Receivers with Recorded RF Spectrum," 2012. [Online]. Available: image from <http://zone.ni.com/devzone/cda/pub/p/id/197>.
- [41] Agilent Technologies, "Cascaded Noise Analysis," 2012. [Online]. Available:

<http://edocs.soco.agilent.com/display/sv201001/Advanced+Spectrasys>.

- [42] M. Debbah, "Short Introduction to OFDM," Mobile Communications Group, 2004.
- [43] "Gumstix," 2012. [Online]. Available: www.gumstix.com.
- [44] R. C. Johnson, W. Sethares and A. G. Klein, *Software Receiver Design*, Cambridge, UK: Cambridge University Press, 2011.
- [45] D. M. Pozar, *Microwave and RF Design of Wireless Systems*, New York: John Wiley and Sons, Inc., 2001.
- [46] R. B. Ertel, P. Cadieri, K. W. Sowerby, T. S. Rappaport and J. H. Reed, "Overview of Spatial Channel Models for Antenna Array Communication Systems," *Personal Communications, IEEE*, vol. 5, no. 1, pp. 10-22, 1998.

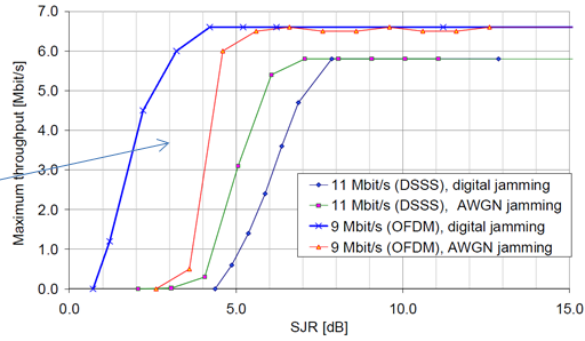
7 Appendix

Table 10: List of 802.11 Standards [14].

Standard	Scope
IEEE 802.11	Medium access control (MAC): One common MAC for WLAN applications
	Physical layer: Infrared at 1 and 2 Mbps
	Physical layer: 2.4-GHz FHSS at 1 and 2 Mbps
	Physical layer: 2.4-GHz DSSS at 1 and 2 Mbps
IEEE 802.11a	Physical layer: 5-GHz OFDM at rates from 6 to 54 Mbps
IEEE 802.11b	Physical layer: 2.4-GHz DSSS at 5.5 and 11 Mbps
IEEE 802.11c	Bridge operation at 802.11 MAC layer
IEEE 802.11d	Physical layer: Extend operation of 802.11 WLANs to new regulatory domains (countries)
IEEE 802.11e	MAC: Enhance to improve quality of service and enhance security mechanisms
IEEE 802.11f	Recommended practices for multivendor access point interoperability
IEEE 802.11g	Physical layer: Extend 802.11b to data rates >20 Mbps
IEEE 802.11h	Physical/MAC: Enhance IEEE 802.11a to add indoor and outdoor channel selection and to improve spectrum and transmit power management
IEEE 802.11i	MAC: Enhance security and authentication mechanisms
IEEE 802.11j	Physical: Enhance IEEE 802.11a to conform to Japanese requirements
IEEE 802.11k	Radio resource measurement enhancements to provide interface to higher layers for radio and network measurements
IEEE 802.11m	Maintenance of IEEE 802.11-1999 standard with technical and editorial corrections
IEEE 802.11n	Physical/MAC: Enhancements to enable higher throughput
IEEE 802.11p	Physical/MAC: Wireless access in vehicular environments
IEEE 802.11r	Physical/MAC: Fast roaming (fast BSS transition)
IEEE 802.11s	Physical/MAC: ESS mesh networking
IEEE 802.11,2	Recommended practice for the Evaluation of 802.11 wireless performance
IEEE 802.11u	Physical/MAC: Interworking with external networks

Results from Report

Clear benefit of OFDM vs. DSSS Against certain noise



Experimental Results

No benefit from OFDM vs. DSSS against modulated noise

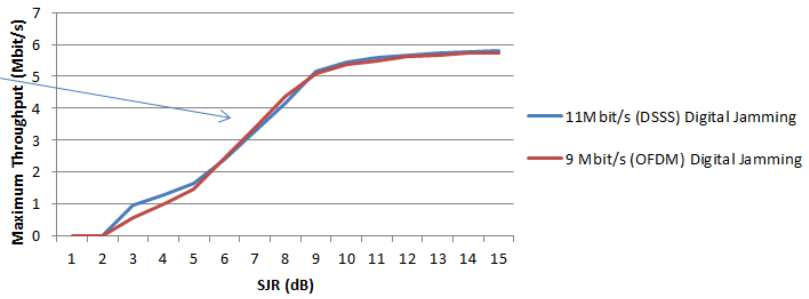


Figure 94: Effects on throughput from Digital Jamming. Results from published work [7] (top), results from two node testbed (bottom).

TABLE II. THROUGHPUT FOR 11 MBIT/S DSSS, PULSED JAMMING

Pulse length [μs]	Pulse period [μs]			
	10000	5000	3000	1000
1	-	-	3.5	3.5
10	-	3.5	3.4	2.8
30	-	N/A	N/A	1.4
100	-	3.4	2.9	0.3
300	3.5	3.3	2.6	0.1
500	3.4	3.1	2.1	0
700	3.3	2.9	1.5	0
900	3.2	2.8	0.9	0
1000	3.2	2.6	0.3	0

TABLE III. THROUGHPUT FOR 9 MBIT/S OFDM, PULSED JAMMING

Pulse length [μs]	Pulse period [μs]			
	10000	5000	3000	1000
1	-	-	-	-
3	-	-	3.5	3.5
10	-	-	3.4	2.1
30	-	-	3.0	0.2
100	-	-	2.8	0.1
300	-	-	2.6	0
500	-	3.5	2.0	0
700	-	3.3	0.6	0
900	-	3.1	0.1	0
1000	3.5	3.0	0.3	0

Results obtained from report

11M DSSS sent @ 11Mbit/s
Period

Length	10ms	5ms	3ms	1ms
100us	5.78	5.75	5.73	5.68
300us	5.71	5.57	5.52	5.4
500us	5.63	5.35	5.16	4.73
700us	5.54	5.08	4.67	2.89
900us	5.41	4.69	3.91	0.4
1000us	5.38	4.55	3.67	0

9M OFDM sent @ 9Mbit/s
Period

Length	10ms	5ms	3ms	1ms
100us	5.74	5.7	5.67	5.61
300us	5.69	5.55	5.48	5.14
500us	5.65	5.32	5.14	3.94
700us	5.6	5	4.6	2.18
900us	5.55	4.53	3.67	0.3
1000us	5.39	4.35	3.32	0

Results obtained from experiment

Figure 95: Effects on throughput from Pulse Jamming. Results from published work [7] (left), results from two node testbed (right).

TABLE VI. THROUGHPUT FOR 11 MBIT/S DSSS, SWEEPED JAMMING

Frequency separation [MHz]	Sweep time [s]	SJR [dB]			
		10	0	-10	-15
2	0.5	3.5	2.7	2.7	2.7
1.5	0.66	3.5	2.9	2.9	2.8
1	1	3.5	3.2	2.8	2.8
0.5	2	3.5	3.2	3	2.8
0.1	10	3.5	3.2	3	2.9
0.05	20	3.5	2.24	0.9483	1.9575
Jamming at f_c		0.3	0	0	0
Jamming at 5 MHz from f_c		3.5	0	0	0

TABLE VII. THROUGHPUT FOR 9 MBIT/S OFDM, SWEEPED JAMMING

Frequency separation [MHz]	Sweep time [s]	SJR [dB]			
		10	0	-10	-15
2	0.5	3.45	2.4	2.2	1.8
1.5	0.66	3.5	2.6	2.2	1.8
1	1	3.5	2.5	1.9	1.7
0.5	2	3.45	2.55	2.2	1.9
0.1	10	3.2	2.5	1.59	0.39
0.05	20	3.1	0.47	0.63	0.53
Jamming at f_c		0.3	0	0	0
Jamming at 5 MHz from f_c		3.5	0	0	0

11Mbit/s DSSS
SJR (dB)

Sweep Time (sec)	10	0	-10	-15
0.5	3.50	2.95	2.91	2.90
0.66	3.50	2.94	2.89	2.87
1	3.50	2.90	2.86	2.84
2	3.50	2.88	2.84	2.80
10	3.50	2.84	2.79	2.77
20	3.50	2.85	2.80	2.78

9Mbit/s OFDM
SJR (dB)

Sweep Time (sec)	10	0	-10	-15
0.5	3.50	2.97	2.91	2.89
0.66	3.50	2.94	2.89	2.87
1	3.50	2.91	2.86	2.84
2	3.50	2.88	2.83	2.81
10	3.50	2.85	2.79	2.77
20	3.50	2.85	2.77	2.77

Figure 96: Effects on throughput from Sweep Jamming. Results from published work [34] (left), results from two node testbed (right).

MATLAB Code: Calculate Programmable Attenuator Values

```
function [ attenuation_values ] = calc_att(start_vector,...
    stop_vector, duration_s )

%CALC_ATT This function consumes a start_vector(4,1) with imaginary number
%components where the real part is the x location and the imaginary part is
%the y location. Stop vector is the same. Duration is the number of ms the
%experiment is meant to be run.

duration_ms = (1.6667*duration_s)*1000;
% figure out timing
num_ms = round(duration_ms);
time_vector = 0:1:(num_ms); %[ms]
time_vector = rot90(fliplr(time_vector));
att_pad_dB = 50.5;%SUBJECT TO CHANGE, this is the value of the additional
% attenuator pads in the system

delta = stop_vector - start_vector; %[meters]
velocity = delta./num_ms; %[meters/ms]
freq = 2.4; %[GHZ]
position = ones(num_ms+1,4); %initialize
for a = 1:1:4

    position(:,a) = rot90( real(velocity(a))*time_vector +real(start_vector(a))...
        + j* ( imag (velocity(a))*time_vector +imag(start_vector(a))));
end

distance = ones(num_ms+1, 6);
mult = [2 3 4 3 4 4; 1 1 1 2 2 3];
for b = 1:1:(num_ms+1) %rows-- num_ms

    for c = 1:1:6 %columns-- specifies which column of mult to use
        radioa = mult(1,c);
        radiob = mult(2,c);
        distance(b,c) = abs( position(b, radioa) - position( b, radiob) );
    end

end

distance;

%attenuation_values = ones(num_ms, 6); %initialize
attenuation_values6 = 20*log10(distance/1000) + 20*log10(freq) + 94.45;
attenuation_values = ones(num_ms+1, 12);

%fill matrix
attenuation_values(:,1:3) = attenuation_values6(:,1:3);
attenuation_values(:,4) = attenuation_values6(:,1);
attenuation_values(:,5:6) = attenuation_values6(:,4:5);
attenuation_values(:,7) = attenuation_values6(:,2);
```

```

attenuation_values(:,8) = attenuation_values6(:,4);
attenuation_values(:,9) = attenuation_values6(:,6);
attenuation_values(:,10) = attenuation_values6(:,3);
attenuation_values(:,11) = attenuation_values6(:,5);
attenuation_values(:,12) = attenuation_values6(:,6);

attenuation_values = round((attenuation_values-att_pad_dB)*2)/2;

%Plotting the changing geometry and attenuation settings:
figure
subplot(1,2,2)

hold on
grid on

x = 0:1:1667;
plot(x,(attenuation_values(:,3)), 'b')
plot(x,(attenuation_values(:,6)), 'r')
plot(x,(attenuation_values(:,9)), 'g')
plot(x,(attenuation_values(:,1)), 'c')
plot(x,(attenuation_values(:,2)), 'k')
plot(x,(attenuation_values(:,5)), 'm')
title('Att. setting btwn jammer & radios 1(b) 2(r) and 3(g)')
ylabel('Attenuation between nodes [dB]');
xlabel('Time [s]');
set(gca, 'XTick', 0:187.4668:1668)
set(gca, 'XTickLabel', {'0','10','20','30', '40', '50',...
    '60', '70', '80', '90'})
xlim([0 1667]);
hold off

subplot(1,2,1)
grid on
xlabel('X Location [meters]');
ylabel('Y Location [meters]');
title('Radio1 (b) Radio2 (r) Radio 3 (g) Jammer (moving)')
set(gca, 'YTick', -100:20:100)
set(gca, 'YTickLabel', {'-100','-80','-60','-40','-20','0','20', '40', '60', '80' '100'})

% hidden node
% xlim([-30 70])
% set(gca, 'XTick', -30:20:70)
% set(gca, 'XTickLabel', {'-30','-10','10','30','50','70'})

% equidistant & distant node
xlim([-40 60])
set(gca, 'XTick', -40:20:60)
set(gca, 'XTickLabel', {'-40','-20','0','20','40','60'})

hold on
scatter(7, 95, 1, 'y')

```

```

scatter(7, -95, 1, 'y')
hold on
scatter(real(position(:,1)),imag(position(:,1)), 100, 'b', 'filled')
hold on
scatter(real(position(:,2)),imag(position(:,2)), 100, 'r', 'filled');
hold on
scatter(real(position(:,3)),imag(position(:,3)), 100, 'g', 'filled');
comet(real(position(:,4)),imag(position(:,4)))

end

```

MATLAB Code: Generate ASCII Characters

```

function [] = gen_ascii3( attenuation_values )
%GEN_ASCII2 This function generates a matrix of ones and zeros to be sent
%to 12 attenuators and writes to a txt file named 'writefile.txt'

num_ms = length(attenuation_values(:,1));
% structure output matrix q
% each att value takes up 24 rows of a four column matrix.Att val switches
% every ms so:
q = ones((24*num_ms),15);

% initialize attenuation matrix, columns: C,R,L,S(12). Each attenuation
% matrix sets one set of values for all twelve attenuators
matrix = ones(24,15);
    for n = 1:2:23
        matrix(n,1)=0;
    end
matrix(1:20,3) = 0;
matrix(3:4,2) = 0;

%This loop sets up the matrix for each value and puts it into q at the
%appropriate location
for i = 1:1:num_ms

    %intitialize att bits
    attenuation_bits = ones(12,12);
    for j = 1:1:12 %this loop sets the attenuation bits,goes down x axis
        a = round(attenuation_values(i,j)*2);
        binary_rep = dec2bin(a,6);
        %binary_rep = str2num(dec2bin( round(attenuation_values(i,j)*2) , 6 ))
        for k = 1:1:6 %goes down the y axis of matrix filling in
            l = 7-k;
            b = not(str2num(binary_rep(l)));
            attenuation_bits( ((2*k)-1):(2*k), j )= b;
        end
    end
end

```

```

end

matrix(9:20,4:15) = attenuation_bits;

offset = ((i-1)*24)+1;
offset2 = offset+23;

q(offset:offset2,:) = matrix;

end
% below are modifications for the problems we had scaling up to support...
% more attenuators, i.e. more clock, reset, and latch lines

% out is new output[c c c r r r l l l s1-->s6 c c c r r r l l l s7-->s12]
c = q(:,1); % clock
r = q(:,2); % reset
l = q(:,3); % latch
filler = 0*1; % zeroes for pins that we don't use
s16 = q(:,4:9); % serial lines for attenuators 1 through 6
s712 = q(:,10:15); % serial lines for attenuators 7 through 12

out = [c,c,c,r,r,r,l,l,l,s16,c,c,c,r,r,r,l,l,filler, s712,filler,1];
%writes 'out' to writefile.txt
dlmwrite('writefile.txt',out, ' ')

end

```

C Code: Write to NI-PCI Card

```

#include <stdio.h>
#include <NIDAQmx.h>
#include <sys/stat.h>
#include <time.h>
#define DAQmxErrChk(functionCall) if( DAQmxFailed(error=(functionCall)) ) goto Error;
else
#define Start_Delay 1

char *load_buffer(char *argv[]); //This function creates a buffer of information
// read from the text file

char *load_buffer(char *argv[])
{
    FILE * pFile;
    long lSize;
    static char *buffer;
    size_t result;
    int i=0;
    pFile = fopen ( argv[1], "rb" );
    if (pFile==NULL) {fputs ("File error",stderr); exit (1);}

    // obtain file size:
    fseek (pFile , 0 , SEEK_END);
    lSize = ftell (pFile);
    rewind (pFile);

```

```

    // allocate memory to contain the whole file:
    buffer = (char*) malloc (sizeof(char)*lSize);
    if (buffer == NULL) {fputs ("Memory error",stderr); exit (2);}

    // copy the file into the buffer:
    result = fread (buffer,1,lSize,pFile);
    if (result != lSize) {fputs ("Reading error",stderr); exit (3);}
    /* the whole file is now loaded in the memory buffer. */
    return buffer;
}

int main(int argc, char *argv[]) // loops through the different lines of data writing
them
    // to the card one line at a time

    // To use this program, type:
    // ./WriteDigChan_jeff file2write.txt -r
    // include -r if you want to write the file to the card on repeat
{
    int32      error=0;
    TaskHandle taskHandle=0;
    char      errBuff[2048]='\0';
    char Devstr[32] ;
    int i;
    int option_index = 0;
    char str1[]="Dev2/port0/line0:31";
    strncpy(Devstr, str1, 32);
    char *buf = load_buffer(argv);
    sleep(Start_Delay);
    DAQmxErrChk (DAQmxCreateTask("",&taskHandle));
    DAQmxErrChk (DAQmxCreateDOChan(taskHandle,Devstr,"",DAQmx_Val_ChanForAllLines));
    DAQmxErrChk (DAQmxStartTask(taskHandle));

    /******
    // DAQmx Write Code
    /******
    uInt8 output[32];
    do
    {
        char* ptr = &buf[0];
        int temp_buffer[32];
        while(*ptr != '\0')
        {
            for (i=0;i<=31;i++)
            {
                temp_buffer[i]=(int)(*ptr)-48;
                ptr++; ptr++;
                output[i]=(uInt8)temp_buffer[i];
                // printf("%i ", output[i]);
            }
            //printf("\n");
            DAQmxErrChk
            (DAQmxWriteDigitalLines(taskHandle,1,1,10.0,DAQmx_Val_GroupByChannel,output,NULL,NULL));
        }
        int z; for (z=0;z<1000;z++){z=z;} // seems to suppress clock delay problems
    } while(argc==3 && strcmp(argv[2],"-r") == 0);
}

```


Error:

```
    if( DAQmxFailed(error) )
        DAQmxGetExtendedErrorInfo(errBuff,2048);
    if( taskHandle!=0 )
        DAQmxStopTask(taskHandle);
    if( DAQmxFailed(error) )
        printf("DAQmx Error: %s\n",errBuff);

    return 0;
}
```

=====

Datasheet: Krytar Coupler



**MODEL 4020080
DOUBLE ARROW**

2-8 GHz 180° HYBRID COUPLER

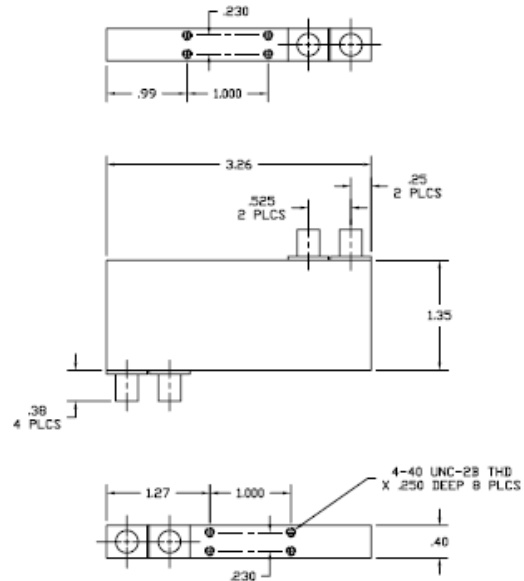


SPECIFICATIONS

FREQUENCY RANGE	2-8 GHz
COUPLING	3 dB
AMPLITUDE IMBALANCE	± 0.3 dB
PHASE IMBALANCE *	± 8 Degrees
ISOLATION	> 18 dB
MAXIMUM VSWR	1.4
INSERTION LOSS	< 1.1 dB
POWER RATING	
Average	20 W
Peak	3 KW
STANDARD CONNECTORS	SMA Female
WEIGHT (ounces)	3.0
OPERATING TEMPERATURE	-54° to +85° C

* Units with a tighter phase imbalance specification can be supplied.

DIMENSIONS



1288 Anvilwood Ave. • Sunnyvale, CA 94089 • (408) 734-5999 • FAX: (408) 734-3017
Toll Free 1 (877) 734-5999 • www.krytar.com



0.5dB LSB GaAs MMIC 6-BIT DIGITAL SERIAL CONTROL ATTENUATOR MODULE, DC - 13 GHz



Features

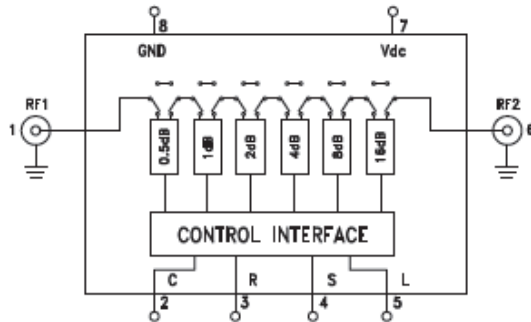
- 0.5 dB LSB Steps to 31.5 dB
- CMOS Compatible Serial Data Interface
- Typical Bit Error: ± 0.3 dB
- Hermetically Sealed Module
- Field Replaceable SMA Connectors
- 55 °C to +85 °C Operating Temperature

Typical Applications

The HMC-C018 is ideal for:

- Telecom Infrastructure
- Military Radio, Radar & ECM
- Space Systems
- Test Instrumentation

Functional Diagram



General Description

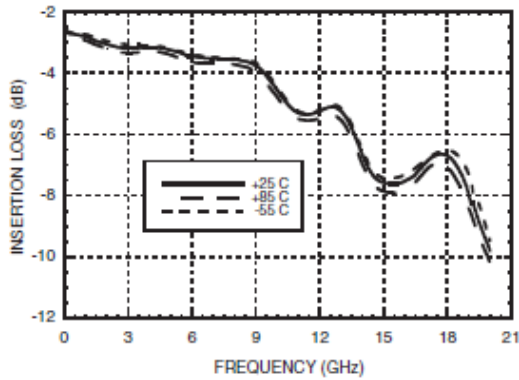
The HMC-C018 is a DC to 13 GHz 6-bit GaAs IC Digital Serial Control Attenuator housed in a miniature hermetic module. This wideband attenuator features 3.6 dB typical insertion loss, +38 dBm input IP3, and bit values of 0.5 (LSB), 1, 2, 4, 8, and 16 dB for a total attenuation of 31.5 dB. Attenuation accuracy is excellent with ± 0.3 dB typical step error. A six bit CMOS compatible serial control word is used to select each attenuation state and a single Vdc bias of -5V allows operation at frequencies down to DC. Removable SMA connectors can be detached to allow direct connection of the module's I/O pins to a microstrip or coplanar circuit.

Electrical Specifications, $T_A = +25$ °C, with Vdc = -5V and 0/+5V CMOS Control

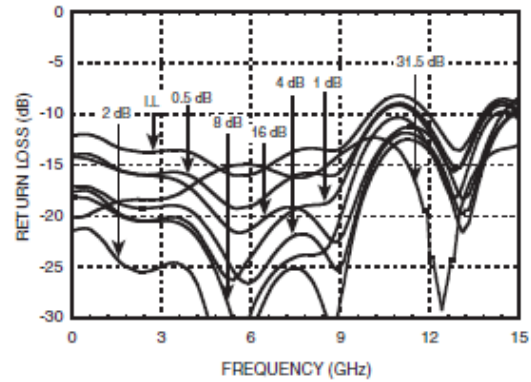
Parameter	Frequency (GHz)	Min.	Typ.	Max.	Units
Insertion Loss	DC - 4.0 GHz		3.2	3.7	dB
	4.0 - 8.0 GHz		3.6	4.1	dB
	8.0 - 13.0 GHz		5.0	6.0	dB
Attenuation Range	DC - 13.0 GHz		31.5		dB
Return Loss (RF1 & RF2, All Atten. States)	DC - 8.0 GHz		15		dB
	8.0 - 13.0 GHz		10		dB
Attenuation Accuracy: (Referenced to Insertion Loss)	DC - 3.0 GHz	$\pm (0.2 + 3\% \text{ of Atten. Setting}) \text{ Max}$			dB
		$\pm (0.4 + 3\% \text{ of Atten. Setting}) \text{ Max}$			dB
	3.0 - 10.0 GHz	$\pm (0.5 + 6\% \text{ of Atten. Setting}) \text{ Max}$			dB
		$\pm (0.6 + 6\% \text{ of Atten. Setting}) \text{ Max}$			dB
Input Power for 0.1 dB Compression	1.0 - 13.0 GHz		22		dBm
Input Third Order Intercept Point (Two-Tone Input Power= 0 dBm Each Tone)	1.0 - 13.0 GHz	REF State	46		dBm
		All Other States	32		dBm
Switching Characteristics	DC - 13.0 GHz				
		tRISE, tFALL (10/90% RF)	600		ns
		tON/OFF (50% CTL to 10/90% RF)	700		ns



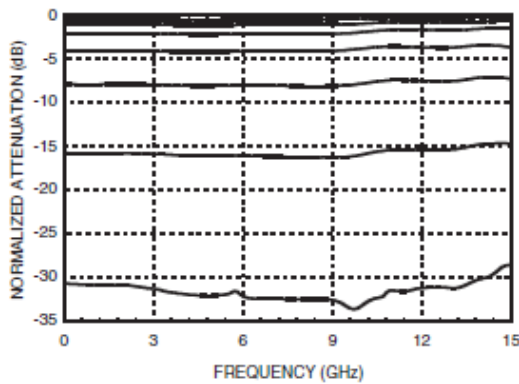
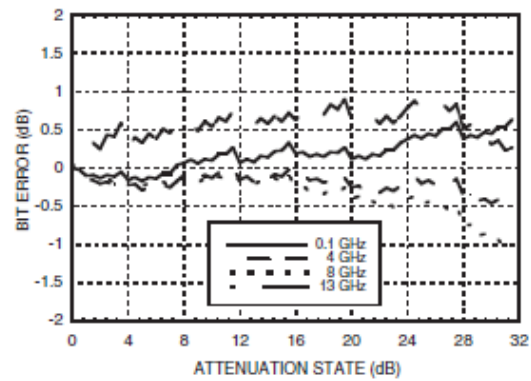
0.5dB LSB GaAs MMIC 6-BIT DIGITAL SERIAL CONTROL ATTENUATOR MODULE, DC - 13 GHz

Insertion Loss

Return Loss RF1, RF2

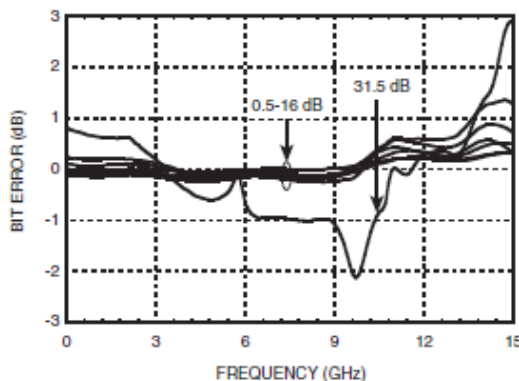
(Only Major States are Shown)


Normalized Attenuation

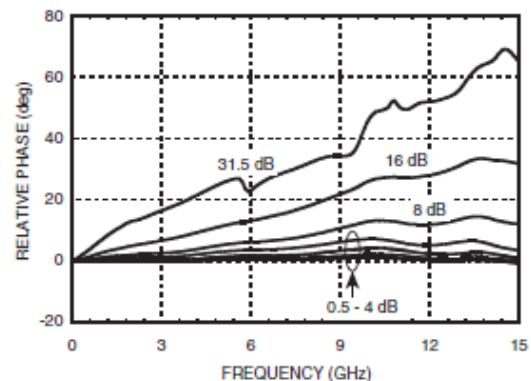
(Only Major States are Shown)


Bit Error vs. Attenuation State

Bit Error vs. Frequency

(Only Major States are Shown)


Relative Phase vs. Frequency

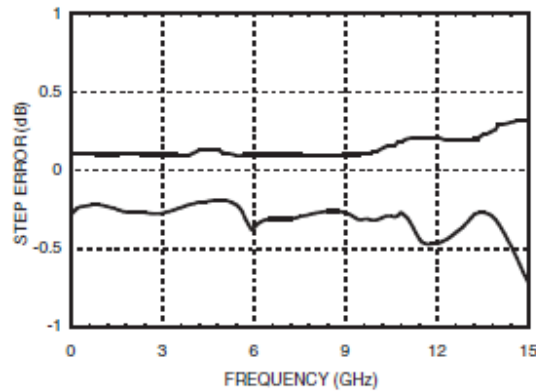
(Only Major States are Shown)





0.5dB LSB GaAs MMIC 6-BIT DIGITAL SERIAL CONTROL ATTENUATOR MODULE, DC - 13 GHz

Worst Case Step Error Between Successive Attenuation States



Absolute Maximum Ratings

Digital Inputs (Reset, Shift Clock, Latch Enable & Serial Input)	-0.5V to +5.5V
Bias Voltage (VDC)	-7.0 Vdc
Storage Temperature	-65 to + 150 °C
Operating Temperature	-55 to +85 °C
RF Input Power (0.5 - 13.0 GHz)	+25 dBm



**ELECTROSTATIC SENSITIVE DEVICE
OBSERVE HANDLING PRECAUTIONS**

Bias Voltage & Current

VDC Range= -5.0 Vdc ± 10%		
VDC	Idc (Typ.) (mA)	Idc (Max.) (mA)
-5.0	5	9

CMOS Control Voltages

State	Bias Condition
Low	0 to +1.3V
High	+3.5 to +5.0V

Serial Input Truth Table

Latch Enable	Shift Clock	Reset	Function
X	X	L	Shift register cleared
X	↑	H	Shift register clocked
↑	X	H	Contents of shift register transferred to Digital Attenuator

Truth Table

Serial Control Input						Attenuation Settings RF1 - RF2
C0.5	C1	C2	C4	C8	C16	
H	H	H	H	H	H	Reference I.L.
L	H	H	H	H	H	0.5 dB
H	L	H	H	H	H	1 dB
H	H	L	H	H	H	2 dB
H	H	H	L	H	H	4 dB
H	H	H	H	L	H	8 dB
H	H	H	H	H	L	16 dB
L	L	L	L	L	L	31.5 dB

Any combination of the above states will provide an attenuation approximately equal to the sum of the bits selected.



MICROWAVE CORPORATION v03.0310

HMC-C018



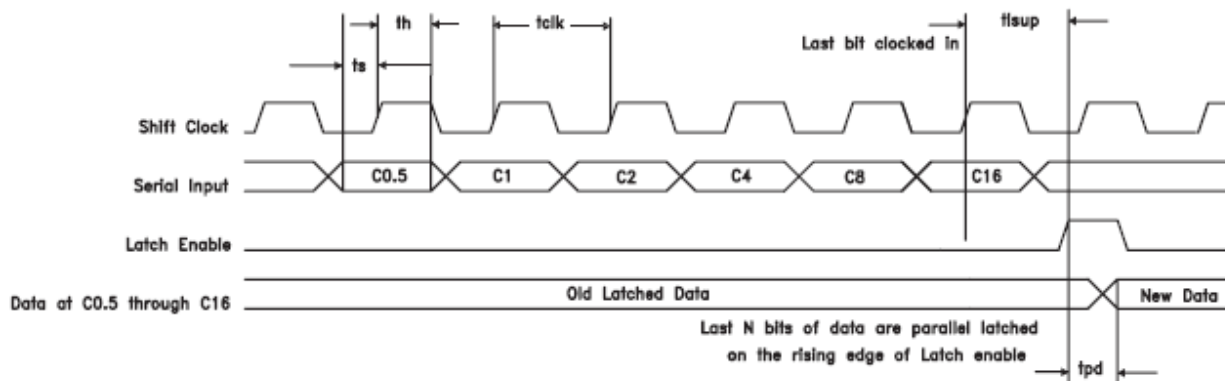
0.5dB LSB GaAs MMIC 6-BIT DIGITAL SERIAL CONTROL ATTENUATOR MODULE, DC - 13 GHz

Timing

Parameter	Symbol	Min.	Max.	Units
Serial Input Setup Time	ts	20	-	ns
Hold time from Serial Input to Shift Clock	th	0	-	ns
Setup time from Shift Clock to Latch Enable	tisup	40	-	ns
Propagation delay, Latch Enable to C0.5 through C8	tpd	-	30	ns
Setup time from Reset to Shift Clock	-	20	-	ns
Clock Frequency (1/tclk)	fclk	-	30	MHz

Timing Diagram

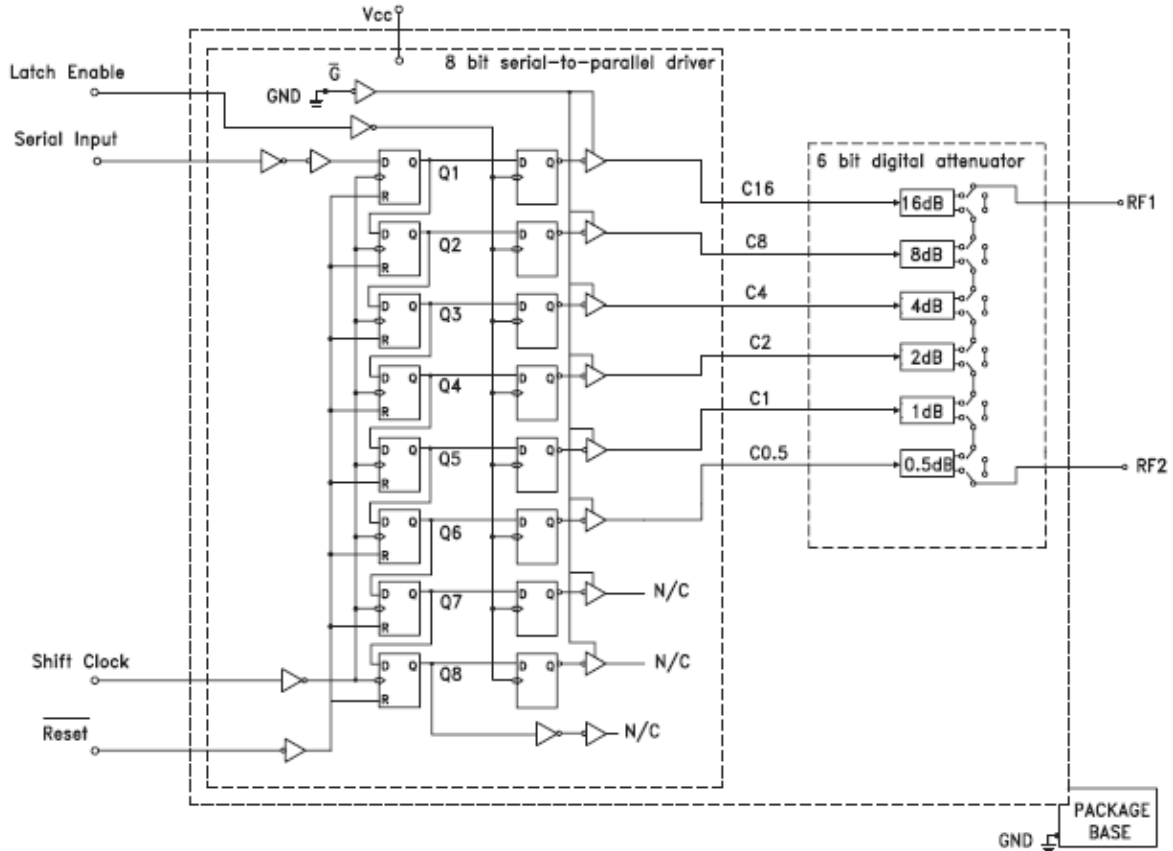
Serial data is shifted in on the rising edge of the Shift Clock, LSB first, and is latched on the rising edge of Latch Enable.





0.5dB LSB GaAs MMIC 6-BIT DIGITAL SERIAL CONTROL ATTENUATOR MODULE, DC - 13 GHz

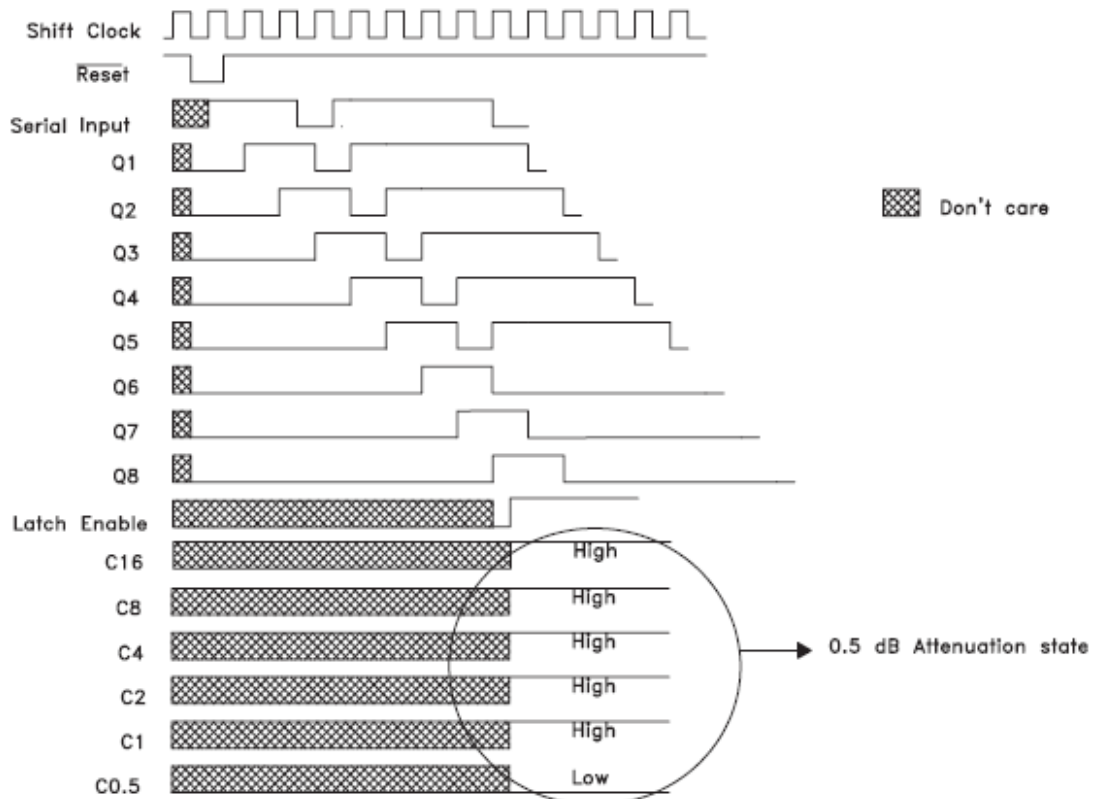
Logic / Functional Diagram





0.5dB LSB GaAs MMIC 6-BIT DIGITAL SERIAL CONTROL ATTENUATOR MODULE, DC - 13 GHz

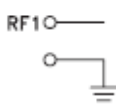
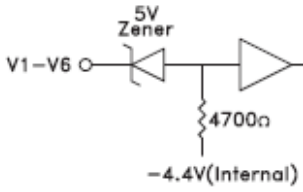
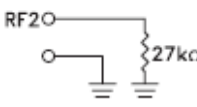
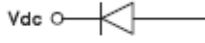
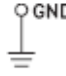
Programming Example to Select 0.5 dB Attenuation State





0.5dB LSB GaAs MMIC 6-BIT DIGITAL SERIAL CONTROL ATTENUATOR MODULE, DC - 13 GHz

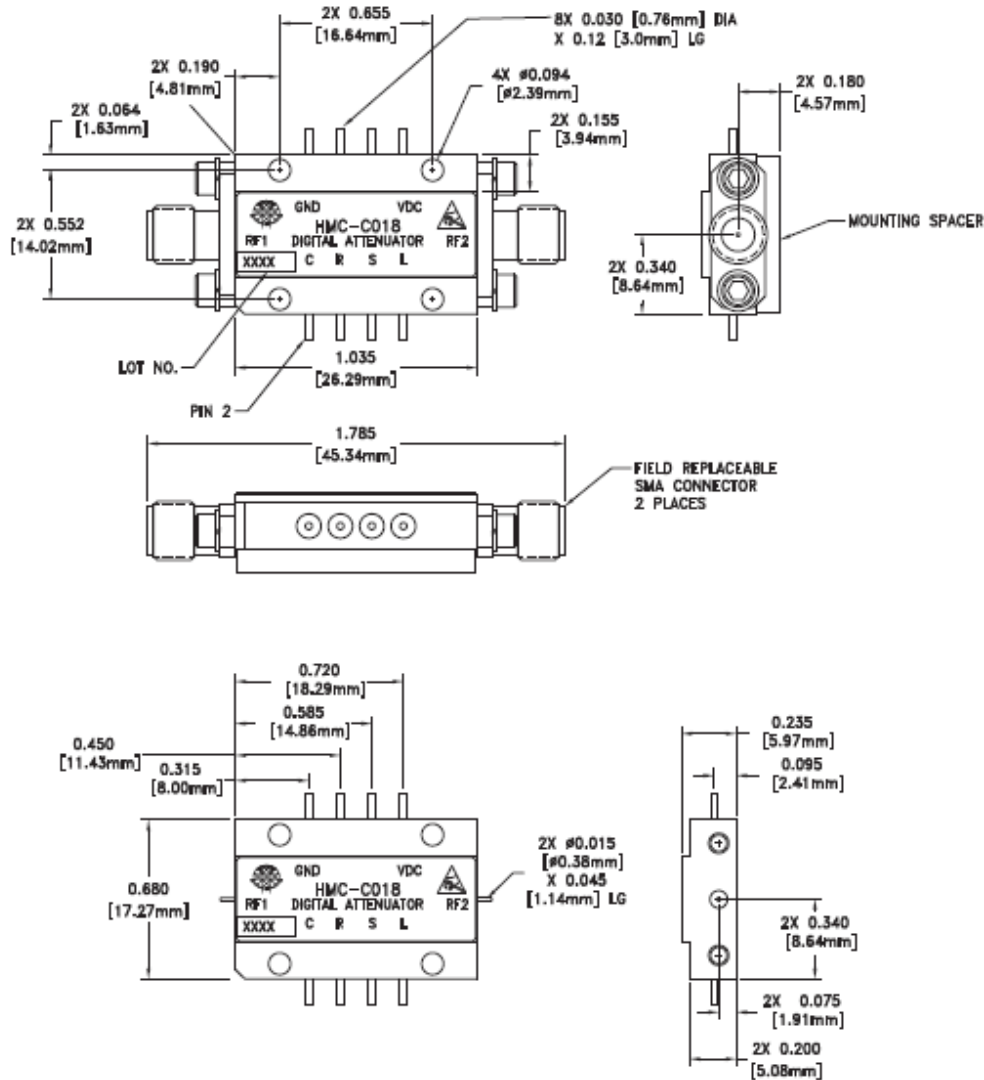
Pin Description

Pin Number	Function	Description	Interface Schematic
1	RF1	This pin is DC coupled and matched to 50 Ohms. Blocking capacitors are required if RF line potential is not equal to 0 Vdc.	
2	C	Shift Clock	
3	R	Reset	
4	S	Serial Input	
5	L	Latch Enable	
6	RF2	This pin is DC coupled and matched to 50 Ohms. Blocking capacitors are required if RF line potential is not equal to 0 Vdc.	
7	Vdc	Supply voltage: -5 Vdc ±10%. (Internal diode for reverse bias protection)	
8	GND	Power Supply Ground	



0.5dB LSB GaAs MMIC 6-BIT DIGITAL SERIAL CONTROL ATTENUATOR MODULE, DC - 13 GHz

Outline Drawing



VIEW SHOWN WITH CONNECTORS REMOVED

Package Information

Package Type	C-6
Package Weight ^[1]	17.4 gms [2]
Spacer Weight	3 gms [2]

[1] Includes the connectors

[2] ±1 gms Tolerance

NOTES:

1. PACKAGE, LEADS, COVER MATERIAL: KOVAR™
2. PLATING: ELECTROLYTIC GOLD 50 MICROINCHES MIN., OVER ELECTROLYTIC NICKEL 75 MICROINCHES MIN
3. MOUNTING SPACER: NICKEL PLATED ALUMINUM
4. ALL DIMENSIONS ARE IN INCHES [MILLIMETERS]
5. TOLERANCES ±0.010 [0.25] UNLESS OTHERWISE SPECIFIED
6. FIELD REPLACEABLE SMA CONNECTORS TENSOLITE 5602 - 5CCSF OR EQUIVALENT
7. TO MOUNT MODULE TO SYSTEM PLATFORM REPLACE 0 - 80 HARDWARE WITH DESIRED MOUNTING SCREWS

H-183-4



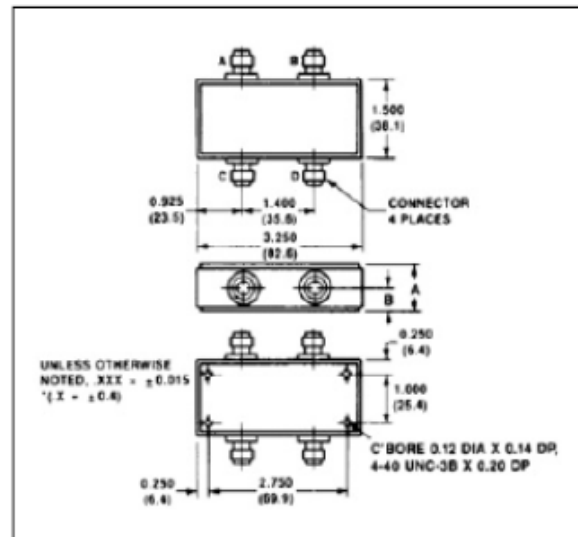
Microwave Hybrid Junction, 30 MHz - 3 GHz

Rev. V2

Features

- 0° - 180° Hybrid
- Seven Octave Frequency Range

C-11



Guaranteed Specifications*: From -55°C to +85°C

Frequency Range		30-3000 MHz
Insertion Loss (less coupling)	30-100 MHz 100-1500 MHz 1500-3000 MHz	1.2 dB Max 1.5 dB Max 2.5 dB Max
Isolation	30-100 MHz 100-1500 MHz 1500-3000 MHz	25 dB Min 20 dB Min 20 dB Min
Amplitude Balance	2-2000 MHz	0.4 dB Max
VSWR	30-100 MHz 100-1500 MHz 1500-3000 MHz	1.6:1 Max 1.6:1 Max 2.5:1 Max
Phase Balance	30-100 MHz 100-1500 MHz 1500-3000 MHz	2° Max 7.5° Max 15° Max

Operating Characteristics

	A	B
H-183-4	1.207 ± 0.020 (30.6 ± 0.5)	0.592 ± 0.020 (15.03 ± 0.5)

Parameter	Absolute Maximum
Impedance	50 Ohms Nominal
Input Power	5.0 Watt Max
Environmental	MIL-STD-883 screening available.

* All specifications apply with 50 ohm source and load impedance. This product contains elements protected by United States Patent Number 3,508,171.

ADVANCED: Data Sheets contain information regarding a product M/A-COM Technology Solutions is considering for development. Performance is based on target specifications, simulated results, and/or prototype measurements. Commitment to develop is not guaranteed.
PRELIMINARY: Data Sheets contain information regarding a product M/A-COM Technology Solutions has under development. Performance is based on engineering tests. Specifications are typical. Mechanical outline has been fixed. Engineering samples and/or test data may be available. Commitment to produce in volume is not guaranteed.

• North America Tel: 800.368.2266 • Europe Tel: +353.21.244.6400
• India Tel: +91.80.4155721 • China Tel: +86.21.2407.1588
Visit www.maacointech.com for additional data sheets and product information.

M/A-COM Technology Solutions Inc. and its affiliates reserve the right to make changes to the product(s) or information contained herein without notice.

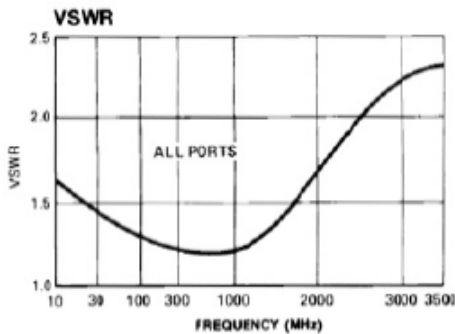
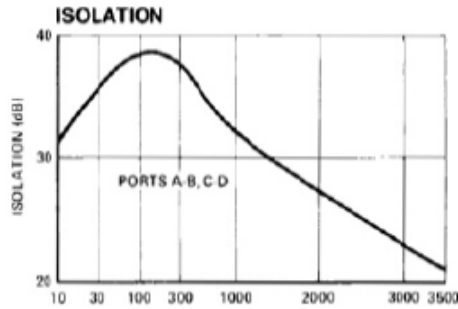
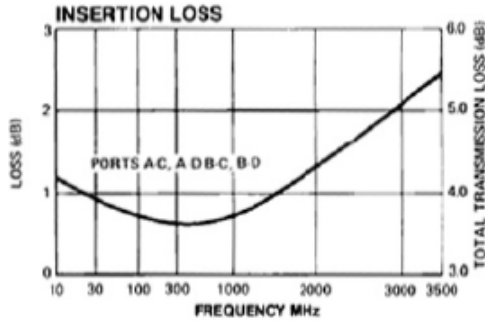
H-183-4



Microwave Hybrid Junction, 30 MHz - 3 GHz

Rev. V2

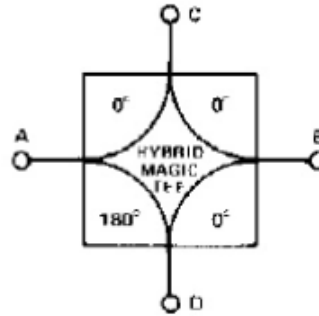
Typical Performance Curves



Ordering Information

Part Number	Package
H-183-4 SMA	Connectorized

Functional Diagram



ADVANCED: Data Sheets contain information regarding a product M/A-COM Technology Solutions is considering for development. Performance is based on target specifications, simulated results, and/or prototype measurements. Commitment to develop is not guaranteed.
 PRELIMINARY: Data Sheets contain information regarding a product M/A-COM Technology Solutions has under development. Performance is based on engineering tests. Specifications are typical. Mechanical outline has been fixed. Engineering samples and/or test data may be available. Commitment to produce in volume is not guaranteed.

• North America Tel: 800.368.2266 • Europe Tel: +353.21.244.6400
 • India Tel: +91.80.4155721 • China Tel: +86.21.2407.1588
 Visit www.macomtech.com for additional data sheets and product information.

M/A-COM Technology Solutions Inc. and its affiliates reserve the right to make changes to the product(s) or information contained herein without notice.